

Universidad Autónoma de
Madrid



Facultad de Ciencias
Departamento de Física Teórica

Consejo Superior de
Investigaciones Científicas



Instituto de Física Teórica
IFT UAM-CSIC

Unitarity of the Leptonic Mixing Matrix

Jacobo López Pavón

Madrid, Mayo 2010.

Universidad Autónoma de
Madrid



Facultad de Ciencias
Departamento de Física Teórica

Consejo Superior de
Investigaciones Científicas



Instituto de Física Teórica
IFT UAM-CSIC

Unitarity of the Leptonic Mixing Matrix

Memoria de Tesis doctoral realizada por
Jacobo López Pavón
presentada ante el Departamento de Física Teórica
de la Universidad Autónoma de Madrid
para la obtención del Doctorado.

Proyecto dirigido por
Andrea Donini
Científico Titular del Instituto de Física Teórica (UAM/CSIC)
y **M. Belén Gavela Legazpi**
Catedrática del Departamento de Física Teórica de la UAM

Madrid, Mayo 2010.

Contents

Motivaciones y objetivos	6
Motivations and goals	12
1 Theory of Massive Neutrinos	18
1.1 Neutrinos in the Standard Model	18
1.2 The neutrino mass problem	20
1.2.1 The paradigmatic neutrino mass model: The Seesaw	22
1.3 Neutrino Oscillations	27
1.3.1 In Vacuum	29
1.3.2 In Matter	33
1.4 Experimental constraints on the three neutrino standard approach . . .	37
1.4.1 Searching the absolute neutrino mass scale	40
1.4.2 Future neutrino oscillation facilities	42
2 Minimal Unitarity Violation	46
2.1 The effective lagrangian	48
2.2 Neutrino oscillations without unitarity	52
2.2.1 Vacuum oscillations	52
2.2.2 Matter effects	56
2.3 Matrix elements from neutrino oscillations	57
2.3.1 Constraints on the e -row	59
2.3.2 Constraints on the μ -row	61
2.3.3 Constraints on non-unitarity from near detectors	62
2.4 Constraints on non-unitarity from electroweak decays	62

	3
2.4.1	W decays 63
2.4.2	Invisible Z decay 63
2.4.3	Universality tests 63
2.4.4	Rare charged lepton decays 64
2.4.5	Summary of constraints on non-unitarity from decays 65
2.5	The mixing matrix 66
2.6	Future experiments 67
3	CP-violation from non-unitarity leptonic mixing 70
3.1	Parametrization of N 71
3.2	New CP-asymmetries 72
3.3	Sensitivity to the new CP-odd phases. A tuned Neutrino Factory set-up. 74
3.3.1	The $\nu_\mu \rightarrow \nu_\tau$ channel 75
3.3.2	The $\nu_e \rightarrow \nu_\tau$ channel 77
3.4	IDS Neutrino Factory sensitivity to non-unitary leptonic mixing 78
3.4.1	Sensitivity to $\eta_{\mu\tau}$ 81
3.4.2	Sensitivity to $\eta_{e\tau}$ 83
3.5	MUV vs NSI 84
4	Sterile Neutrinos, a low energy source of three flavour unitarity violation 88
4.1	Four neutrino schemes 91
4.1.1	(2+2)-schemes 91
4.1.2	(3+1)-schemes with the LSND constraint 92
4.1.3	(3+1)-schemes without the LSND constraint 92
4.1.4	Oscillation probabilities at the Neutrino Factory in the (3+1)- scheme 94
4.2	Sensitivity to (3 + 1) sterile neutrinos at the Neutrino Factory 96
4.2.1	Sensitivity to $(\theta_{13}, \theta_{14})$ 97
4.2.2	Sensitivity to $U_{e4}U_{\mu4}$ and $U_{e4}U_{\tau4}$ 103
4.2.3	Sensitivity to $(\theta_{24}, \theta_{34})$ 104
4.2.4	CP-violating sterile neutrino signals 110
	Summary and conclusions 116

Resultados y conclusiones	120
Agradecimientos	124
A Oscillation probabilities in presence of unitarity violation	126
A.1 Short baseline limit	128
A.2 More on oscillation probabilities in presence of unitarity violation . . .	129
B Sterile Neutrinos	134
B.1 The mixing matrix elements $U_{\alpha j}$	134
B.2 The Neutrino Factory and the Hybrid-MIND detector	135
B.2.1 The MIND detector: $\nu_e \rightarrow \nu_\mu$ and $\nu_\mu \rightarrow \nu_\mu$	137
B.2.2 The MECC detector: $\nu_e \rightarrow \nu_\tau$ and $\nu_\mu \rightarrow \nu_\tau$	138
B.3 Simulation details	141
B.3.1 Section 4.2.1	141
B.3.2 Section 4.2.2	142
B.3.3 Section 4.2.3	143
B.3.4 Section 4.2.4	143
B.4 Dependence of sensitivity on the systematic errors	144
B.5 Oscillation probabilities by the KTY formalism	146
B.6 Discrimination of the four neutrino schemes	149

Motivaciones y objetivos

El Modelo Estándar de física de partícula (ME) ha sido hasta ahora una teoría realmente predictiva [1], que ha permitido comprender el universo de la física de partículas con un nivel de precisión nunca antes alcanzado. Sin embargo, existen evidencias experimentales que nos indican que el ME no es la teoría definitiva que describe la física de partículas, como sugiere por ejemplo la existencia de materia oscura no bariónica (no incluida en el ME). La diferencia entre las curvas de rotación de galaxias observadas y las que se predicen teóricamente teniendo en cuenta materia bariónica luminosa, supuso el primer indicio de la presencia de materia oscura en nuestro universo. Este primer indicio fue posteriormente confirmado y reforzado por múltiples medidas, como las basadas en el efecto de lentes gravitacionales, o el análisis detallado del fondo cósmico de la microondas en experimentos tales como WMAP. Dado que la solución más convincente a este problema implica la existencia de nuevas partículas y/o interacciones, se puede considerar como una de las señales de física más allá del ME más robustas. Por otro lado, el ME fue formulado de tal manera que el contenido de materia conservara, accidentalmente, la simetría global $B - L$ (en el momento en que fue formulado nada indicaba que los neutrinos tuvieran masa), de modo que las masas de los neutrinos son cero a todos los órdenes en teoría de perturbaciones. Ahora, dado que los experimentos de oscilaciones de neutrinos nos revelan que estos tienen masa, el ME debe ser extendido con nuevos campos y, por tanto la masa no nula de los neutrinos puede ser considerada a su vez como una nueva señal de física más allá del ME.

Además, dentro del marco del ME surgen una serie de importantes cuestiones que todavía no entendemos en profundidad así como ciertos problemas que, desde el punto de vista teórico, parecen indicar que probablemente el ME es sólo una (muy) buena descripción de bajas energías de una teoría más fundamental.

En primer lugar, debemos comentar que quizá el problema más importante de la física no procede estrictamente de física de partículas, se trata del problema de la constante cosmológica. En realidad, sólo entendemos alrededor del 5% del contenido de materia de nuestro universo, el 20% está formado por materia oscura, y alrededor de un 75% corresponde a un fluido conocido como energía oscura que permite explicar la expansión acelerada del universo. Sin embargo, no tenemos idea de qué son realmente estas componentes. En particular la energía oscura podría ser, por ejemplo, el resultado de la contribución de una constante cosmológica o simplemente la energía de vacío que permea el universo observado. Del mismo modo, este desconocimiento de la estructura

del vacío aparece reflejado en física de partículas a través del *problema de CP fuerte* (vacío de QCD) y del origen de las masas de las partículas.

En el SM, las masas de los bosones “gauge” se generan a través del mecanismo de Higgs. Es más, las masas de quarks y leptones cargados se generan también gracias a los acoplos (de Yukawa) de dichas partículas con el mismo campo escalar, conocido como Higgs, que por tanto juega un papel fundamental en la teoría. En realidad, este mecanismo se introdujo *ad hoc* en la teoría como la solución más simple a la generación de masas. Por ejemplo, en otros modelos no es sólo un campo escalar el responsable de dar masas a bosones y fermiones. En este mismo espíritu minimalista, en el ME el potencial escalar es elegido como el más simple que garantiza la existencia de un mínimo no trivial, un valor esperado en el vacío no nulo para el campo escalar v . Esta es la clave para la generación de las masas dentro del ME. Sin embargo, este potencial sufre el conocido *problema de la trivialidad* [2–4]: el valor renormalizado de los parámetros del potencial escalar evita la aparición del mencionado mínimo no trivial. Sólo si existe un “cut-off” en la teoría, dichos valores renormalizados podrían garantizar la esencial existencia de un mínimo de potencial distinto de cero, lo cuál implicaría que el ME es un teoría efectiva de bajas energías correspondiente a otra más completa de altas energías. Parece evidente pues que no comprendemos en profundidad el vacío de la teoría.

Aún más, el Higgs todavía no ha sido detectado y sólo disponemos de cotas experimentales sobre su masa así como ciertos prejuicios teóricos. Estas cotas indican que la masa del Higgs debería encontrarse alrededor de la escala electrodébil, lo cuál resulta poco “natural” ya que dicha masa no está protegida por las simetrías gauge del ME. Esto es, si consideramos el ME como una teoría efectiva de bajas energías, su masa sería cuadráticamente sensible al “cut-off” natural del modelo Λ a través de correcciones radiativas. Si $\Lambda \gg v$ este comportamiento radiativo requeriría un fuerte ajuste fino de los parámetros de cara a estabilizar la masa alrededor de la escala electrodébil v . Por otro lado, si Λ no es tan grande ($\Lambda \sim \text{TeV}$) este incomodo problema de ajuste fino, aunque todavía presente, se suavizaría. Este problema es conocido como el *problema de la jerarquía* [5, 6].

De nuevo relacionado con la generación de masas en el ME aparece el llamado *problema del “flavour”*. ¿Por qué esos valores de las masas de quarks y leptones? Las matrices de Yukawa tienen autovalores muy diferentes fijados por el valor experimental de las masas, sin embargo no existe una explicación teórica que justifique dichos valores. ¿Por qué existen tres familias de fermiones, con idénticas propiedades gauge pero un espectro de masas jerárquico? La gran diferencia entre las masas de los quarks “top” y “up”, $m_t \sim 10^6 m_u$, hace está cuestión particularmente llamativa. ¿Por qué precisamente esos valores de los parámetros en el sector de mezcla de los quarks? Todas estas cuestiones conforman el *problema del “flavour”* en el ME. Pero además, la evidencia experimental de que los neutrinos tienen masa ha empeorado aún más si cabe este problema, dando lugar a la mezcla en el sector leptónico al igual que ocurre en el de los quarks.

Finalmente, la asimetría materia-antimateria del universo observado supone otra evidencia observacional que parece necesitar de una explicación teórica. Teniendo en cuenta que la anchura de desintegración es la misma para partículas y antipartículas según nos dicen las medidas en aceleradores de partículas, ¿Por qué no encontramos antimateria a nuestro alrededor? Si asumimos que en el inicio del Big-Bang esta simetría si existía, lo cuál es una suposición bastante natural (y a su vez predicha por inflación) es esencial entender cuál es el mecanismo mediante el que se alcanzó esta ausencia de antimateria en la actualidad. La explicación más sencilla, *Bariogénesis*, requiere que se cumplan tres condiciones: a) violación del número bariónico B , b) violación de C y CP , y c) que debe ocurrir fuera del equilibrio térmico. El ME cumple en principio todos los requisitos, sin embargo la magnitud de violación de CP no sería suficiente para dar resultados cuantitativos, siendo necesarias nuevas fuentes de violación de CP no contempladas en el ME.

Junto con la existencia de materia oscura no bariónica y masas no nulas de los neutrinos, todas estas cuestiones y problemas abiertos comentados nos llevan a pensar que el ME no es la teoría definitiva que describe la naturaleza, sino una teoría efectiva de bajas energías correspondiente a otra teoría más completa capaz de responder a todo esto. En este mismo sentido, el hecho de que las masas de los neutrinos sean mucho menores que las de los fermiones del ME, sugiere que hay Nueva Física (NF) a altas energías. El mecanismo de seesaw [7–10] es, por ejemplo, un mecanismo capaz de explicar el origen de las masas de los neutrinos de un modo “natural” gracias a la introducción de singletes pesados (o tripletes de $SU_L(2)$), apuntando a escalas de energía mucho mayores que la electrodébil. Dichos modelos podrían ser capaces, a su vez, de proporcionar una posible explicación a la asimetría materia-antimateria a través del mecanismo de *Leptogénesis* [11].

Varias teorías de física más allá del ME que podrían explicar tanto el *problema de la jerarquía* como el de la materia oscura están a punto de ser testadas en el LHC. De forma complementaria, los experimentos de oscilaciones de neutrinos están viviendo un impresionante desarrollo de cara a obtener medidas precisas de las diferencias de masa, las fases de violación de CP y los ángulos de mezcla del sector leptónico. La escala absoluta de las masas de los neutrinos así como su naturaleza -Dirac o Majorana- son cuestiones que también necesitan una respuesta experimental. Los experimentos de “ β -decay” y “neutrinoless double beta decay” son responsables de esta ardua tarea. Estamos entrando en una nueva era en la física de neutrinos, con varios proyectos experimentales nuevos actualmente en proceso de discusión, que podrían dar lugar a medidas de alta precisión en el futuro próximo. Por tanto, la búsqueda de señales de NF de más altas energías motivada por el hecho de que las masas de los neutrinos son muy ligeras, parece también más que pertinente. Un efecto típico a bajas energías de esta NF es la generación de desviaciones de la unitariedad de la matriz de mezcla leptónica. En general, este tipo de efectos se esperan si los neutrinos del ME se mezclan con fermiones pesados como, por ejemplo, en modelos tales como los “seesaws” tipo I y tipo III. En realidad, incluso si sólo los leptones cargados se mezclaran con nuevos fermiones aparecerían también este tipo de efectos, surgiendo matrices de mezcla (unitarias) de

dimensión mayor que 3 pero con una submatriz no necesariamente unitaria para los campos ligeros. La observación de desviaciones de unitariedad podría implicar pues la existencia de nueva física a altas energías.

La no unitariedad de la matriz de mezcla CKM asociada al sector de los quarks es considerada genéricamente como una buena ventana a la NF y ha sido ampliamente estudiada. En la búsqueda experimental de estos nuevos efectos, tanto en el sector de los quarks como en el leptónico, se asume que las matrices de mezcla son unitarias a la hora de analizar los datos. Nosotros partiremos aquí de un marco teórico genérico que permite que la matriz de mezcla leptónica no sea unitaria, haciendo después un análisis coherente con esta hipótesis.

Por ahora sólo hemos mencionado desviaciones de unitariedad de la matriz de mezcla leptónica 3×3 procedentes de NF de altas energías. Sin embargo, existe otra posible fuente de desviaciones de unitariedad que podría proceder de nueva física a bajas energías: la existencia de los llamados neutrinos estériles, simplemente fermiones ligeros que son singletes bajo los grupos gauge del ME. Muchas teorías de NF comprenden estos singletes fermiónicos en el espectro de bajas energías, como por ejemplo, en modelos de dimensiones extra o super simetría. Los mencionados neutrinos estériles no interaccionarían directamente con el resto de partículas, sin embargo, dado que estarían involucrados en la generación de masas para los neutrinos, a través de la mezcla leptónica podrían dar lugar a efectos medibles en oscilaciones de neutrinos. Completaremos por tanto este trabajo estudiando también este tipo de NF.

Estructura del documento

Los contenidos de esta tesis se organizan en los siguientes capítulos:

- En el capítulo 1, ponemos en contexto nuestro trabajo. Repasamos el problema de las masas de los neutrinos en el contexto del ME, discutiendo cómo podrían ser incluidas en el ME a través de extensiones mínimas del lagrangiano. Siguiendo esta línea, revisamos el mecanismo de "seesaw" recordando por qué supone una manera natural de dar masas a los neutrinos, pero también apuntando sus puntos débiles. Además, estudiamos el formalismo asociado a las oscilaciones de neutrinos, tanto en vacío como en materia, con la habitual hipótesis de unitariedad en tres familias. Al final del capítulo repasamos la actual información sobre los parámetros de mezcla leptónica que se pueden extraer de los experimentos de neutrinos. Prestamos especial atención a las cotas sobre la escala absoluta de las masas de los neutrinos. Finalmente, presentamos brevemente los futuros experimentos de oscilaciones actualmente bajo discusión.
- En el capítulo 2, introducimos el MUV. Un esquema minimal que puede contemplar la existencia de una matriz de mezcla leptónica no unitaria de una manera consistente, considerando sólo tres neutrinos ligeros y, básicamente, sustituyendo la habitual matriz de mezcla unitaria U_{PMNS} por una más general N que no tiene por qué serlo. Se trata de manera independiente del modelo de introducir violaciones de unitariedad en tres familias de la matriz de mezcla PMNS, principalmente debido a la mezcla con fermiones pesados. En primer lugar, discutimos hasta que punto este análisis independiente del modelo puede contemplar distintos modelos de nueva física. Más tarde, aclaramos el formalismo necesario para estudiar las oscilaciones de neutrinos dentro de esta nueva hipótesis y calculamos las cotas sobre N que se pueden extraer de experimentos de oscilaciones de neutrinos y desintegraciones leptónicas. Al final del capítulo, echamos un vistazo a las futuras perspectivas de mejorar dichas cotas.
- El capítulo 3 está dedicado al estudio de las nuevas fases de CP asociadas a la no unitariedad dentro del MUV. En primer lugar introducimos una conveniente parametrización de la matriz de mezcla no unitaria N . Posteriormente, analizamos dos diferentes propuestas de "Neutrino Factory" que podrían ser sensibles a estas nuevas fases en el futuro. La primera, una "Neutrino Factory" de $\mathcal{O}(20\text{GeV})$ con una distancia fuente-detector bastante corta ~ 100 km, está optimizada de cara a la observación de las nuevas fases que surgen en el MUV. Pero también estudiamos hasta que punto la segunda opción, diseñada de cara a la física de neutrinos estándar, podría acotar los parámetros del MUV poniendo especial atención a las nuevas fases de CP. Además, estudiamos como incluir detectores cercanos podría ayudar a la hora de medir o acotar dichos parámetros.

- En el capítulo 4, investigamos una fuente diferente de violación de unitariedad en tres familias: la existencia de neutrinos estériles en el espectro de bajas energías. En particular, analizamos el potencial de una “Neutrino Factory”, similar a la última mencionada, para medir los nuevos parámetros del modelo de neutrinos estériles $3+1$. Una vez los resultados de LSND (no confirmados por MiniBooNE) no son considerados, el $3+1$ es el modelo fenomenológico más simple no excluido experimentalmente. De nuevo, ponemos especial atención a la posibilidad de medir las nuevas fases de CP, esta vez asociadas a la presencia de neutrinos estériles.

Motivations and goals

The Standard Model of particle physics (SM) has been so far a highly predictive theory [1]. It has provided understanding of a great part of particle physics with a level of precision never reached before. Nevertheless, there are some observational evidences which tell us that the SM is not the ultimate theory able to describe particle physics, as the existence of non-baryonic (not included in the SM) Dark Matter indicates. The difference between the observed galaxy rotation curves and the theoretically predicted ones, computed taking into account luminous baryonic matter, was the first hint for the presence of Dark Matter in our Universe. This first indication was later reinforced by multitude of different measurements, as those based on “Gravitational Lensing”, or the detailed analysis of the Cosmic Microwave Background, with experiments such as WMAP. Since the most convincing solution to this problem implies new particles and/or new interactions, this can be considered a robust signal of the existence of Physics Beyond the SM (BSM). Besides, the SM was formulated in such a way that the matter content would accidentally conserve the global symmetry $B - L$ (at the time of its formulation there was no evidence for non-zero masses for neutrinos) and hence neutrinos would remain massless to all orders in perturbation theory. Since neutrino oscillation experiments tell us that neutrinos have non-vanishing masses, the SM has to be extended with new fields and, thus, it can be considered as a signal of BSM physics as well.

Moreover, the SM contains several important questions that are not yet understood, and some theoretical problems which indicate that probably the SM is only a (very) good low-energy description of a more fundamental underlying theory.

First of all, we have to say that probably the most important question does not come strictly from particle physics: the cosmological constant problem. Actually we only understand around the 5% of the matter content of the universe. A 20% is made of the already mentioned Dark Matter, and about a 75% is a Dark energy fluid which allows us to explain the observation of the accelerated expansion of the universe. However, we have no idea about what these two components are. In particular, Dark Energy could be the contribution of a cosmological constant (a constant in a curved space-time background matters, since it gravitates) or only the vacuum energy. This lack of knowledge of the structure of vacuum is also reflected in the “*strong CP problem*” (QCD vacuum) as well as in the origin of masses in the context of particle physics.

In the SM, the gauge boson masses are generated through the Higgs mechanism.

Furthermore, the masses of quarks and charged leptons are also generated through (Yukawa) couplings of these particles with the same scalar field, so-called Higgs, which therefore plays a fundamental role in the theory. In fact, this mechanism has been introduced *ad hoc* in the theory as the simplest solution to the problem of generating masses. For instance, in other models no unique scalar field gives masses to bosons and fermions at the same time. In the same minimal spirit, in the SM the scalar potential is chosen as the simplest one with a shape that guarantees a non-trivial minimum, a non-zero vacuum expectation value for the scalar field, v . This is the key that allows us for mass generation. However, this potential suffers of the so-called *triviality problem* [2–4]: the renormalized value of the scalar potential parameters gives as a result a potential without non trivial minimum. Only if there is a physical cut-off in the theory, the renormalized values of these parameters can guarantee the essential presence of a scalar potential minimum different from zero, which would imply that the SM is a low-energy effective theory of a more complete high energy one. It seems, thus, clear that we do not fully understand the vacuum of the theory.

Moreover, the Higgs has not been detected so far. We only have indirect limits on its mass and some theoretical prejudices as well. These limits indicate that the Higgs mass should be of the order of the electroweak scale, which appears to be “non-natural”, since it is not protected by the Gauge Symmetry of the SM. That is, if we consider the SM as an effective theory, the Higgs mass is quadratically sensitive through radiative corrections to the “natural” “cut-off” of the model, Λ . If $\Lambda \gg v$ this running behaviour would require a strong fine tuning of the parameters in order to stabilize the mass at the order of the electroweak scale v . On the other hand, if Λ is not so big, $\Lambda \sim \text{TeV}$, this fine uncomfortable tuning problem would be softened but still present. This fundamental problem is known as *hierarchy problem* [5, 6]

Again related with the mass generation in the SM appears the so-called *Flavour Problem*. Why these values for quarks and charged leptons masses? Yukawa matrices have very different eigenvalues, fixed by the experimental values of masses. There is no theoretical explanation to justify them. Why are there three fermionic families, with identical gauge properties but with hierarchical mass spectra? This question becomes particularly striking when one realises the huge difference between the top and the up quark masses: $m_t \sim 10^6 m_u$. Why those parameter values in the quark mixing sector? All these questions constitute the *Flavour Problem* in the SM. Moreover, this problem has been worsened with the experimental evidence of the existence of light neutrino masses. The fact that neutrinos have masses gives rise to lepton mixing as well as in the quark sector, increasing the *Flavour Problem*.

Finally, another observational evidence which calls for a theoretical explanation is the matter-antimatter asymmetry in the Universe. Why don’t we find antimatter surrounding us, given that measurements in particle accelerators tell us that the decay width is the same for both particle and antiparticle production? Assuming that at the beginning of the Big-Bang this symmetry did exist, which is a quite natural assumption (and it is, besides, predicted by Inflation), it is necessary to understand the mechanism by which the observed absence of antimatter is reached. The simplest

explanation, *Baryogenesis*, requires that three conditions are satisfied: a) violation of baryonic number B , b) violation of both C and CP and, c) that must happen out of thermal equilibrium. In principle, the SM can fulfill the required conditions, but the amount of CP violation does not seem to be enough to give quantitative results, being necessary new sources of CP violation not contemplated in the SM.

Besides the evidence of the existence of non-baryonic Dark Matter and neutrino masses, all these open questions lead to think that the SM is not the definitive theory that describes Nature, but a low-energy theory, underlying some other one capable of answering all these questions. In the same sense, the lightness of the neutrino masses compared with the fermions of the SM, suggests again the existence of New Physics (NP) at high energies. The seesaw mechanism [7–10] is, for instance, a mechanism that can explain neutrino masses in a “natural” way by the introduction of heavy singlets (or $SU(2)_L$ triplets), pointing to energy scales much higher than the electroweak one. This model could also provide a possible explanation for the matter-antimatter asymmetry via the *Leptogenesis* mechanism [11].

Several theories of Physics Beyond the Standard Model proposed to explain both the Higgs mass *hierarchy problem* and the problem of non-baryonic dark matter are about to be tested at the LHC. Complementarily, neutrino oscillation experiments are experiencing an impressive development in order to obtain accurate measurements of the mass differences, the CP -violating phase and the mixing angles in the leptonic sector. The absolute mass of neutrinos and their nature -Dirac or Majorana- are questions that also need an experimental answer. Experiments of β -decay and neutrinoless double beta decay have this hard task. We are entering in a new era of neutrino physics, with new facilities now under discussion which will give rise to high precision measurements in the near future. Thus, the search for signals of NP at higher energies, motivated by the fact that neutrino masses are light, also seems to be pertinent. A low-energy effect typical of this NP concerning neutrinos is the deviation from unitarity of the leptonic mixing matrix. Generically, this sort of effects is expected whenever heavy fermions mix with the SM neutrinos as, for instance, in theories like the type-I and type-III seesaws. Indeed, even if only charged leptons mix with other new fermions this kind of effects would appear as well: the mixing would lead to unitary mixing matrices of dimension larger than 3 while the submatrix for the light fields needs not be unitary. Observation of deviation from unitarity would imply thus a powerful indication of new physics at high energies.

Non-unitarity of the CKM mixing matrix in the quark sector is considered a good window to NP and has been widely studied. Usually, when experimentally searching these deviations, both in the quark and leptonic sector, unitarity of the mixing matrix is assumed when fitting the data. We will start from a generic theoretical frame that allows non-unitarity of the leptonic mixing matrix, making later a data analysis coherent with this hypothesis.

We have only mentioned so far deviations from the 3×3 unitarity of the leptonic mixing matrix coming from higher energy NP. However, there is another possible source

of non-unitarity which could come from low-energy NP: the existence of the so-called sterile neutrinos, nothing but light fermionic singlets under the SM gauge group. Many theories of NP have fermionic singlets in their low-energy spectrum such as, for instance, in extra-dimensions models or in supersymmetric models (as the MSSM). These sterile neutrinos do not interact directly with the rest of the particle content but, since they would be involved in the neutrino mass generation, they could give a sizeable effect in neutrino oscillations through the leptonic mixing. We will complete, thus, our work studying this kind of NP as well.

Outline of the write-up

The contents of the present thesis are organised in the following chapters:

- In chapter 1, we put into context our work. We review the problem of neutrino masses in the context of the SM, discussing how these masses can be included considering minimal extensions of the SM lagrangian. Following this line, we revisit the seesaw mechanism recalling why it supposes a natural way to give masses to the neutrinos, but also pointing out its weak points. In addition, we study the neutrino oscillation formalism, both in vacuum and matter, within the usual assumption of three flavour unitarity. At the end of the chapter we review the present information about the lepton mixing parameters which can be extracted from neutrino experiments. We pay special attention to the constraints on the absolute scale of neutrino masses. Finally, we briefly present the future oscillation facilities currently under discussion.
- In chapter 2, we introduce the MUV scheme. A minimal scheme which can contain a non-unitary leptonic mixing matrix consistently, considering only three light neutrino species and with the usual unitary matrix U_{PMNS} basically replaced by the most general non-unitary one N . It consists in a model-independent way to introduce unitarity violation of the three-family PMNS matrix, mainly due to the mixing with heavy fermions. We first discuss to what extent this model-independent approach can apply to different new physics models. Afterwards, we clarify the formalism for studying neutrino oscillations in this scheme and then compute the bounds to the N matrix elements from present oscillation and weak decay experiments. At the end of the chapter we take a look to the future prospects in the improvement of unitarity constraints.
- Chapter 3 is devoted to the study of the new CP-phases associated to non-unitarity in the MUV scheme. We first introduce a convenient parametrization of the non-unitary mixing matrix N . Afterwards, we analyse two different Neutrino Factory setups which could be sensitive to the new CP-phases in the future. The first one, a $\mathcal{O}(20\text{GeV})$ Neutrino Factory with a short-baseline ~ 100 km, is tuned in order to see the new CP violation effects arising in the MUV scheme. We also study to what extent a second setup, designed to look for the last unknown parameters in the standard approach (assuming three neutrinos and unitarity), could constrain the MUV parameters focusing in the new CP-phases. In addition, we look into how adding small near detectors to the experimental configuration could help to constrain these parameters.
- In chapter 4, we investigate a different source of three flavour unitarity violation: the presence of sterile neutrinos in the low-energy spectrum. Particularly,

we analyse the potential of a Neutrino Factory setup, similar to the last one mentioned, to measure or constrain the parameters of the $3 + 1$ sterile neutrino model. Once LSND results (not confirmed by MiniBooNE) are not considered, the $3 + 1$ model is the simplest phenomenological sterile neutrino model allowed by oscillation experiments. Again, we pay special attention to the possibility of measuring new CP-phases, this time arising in the $3 + 1$ sterile neutrino model.

Chapter 1

Theory of Massive Neutrinos

1.1 Neutrinos in the Standard Model

The Standard Model (SM) is a renormalizable quantum field theory that, so far, has been able to describe the strong and electroweak interactions present in nature. The gauge symmetry group, $SU(3) \times SU(2)_L \times U_Y(1)$, determines the number and general properties of the gauge fields which mediate those interactions.

The fermionic matter is chosen in order to accommodate experimental data. Three generations of leptons and quarks, different in mass but with identical gauge properties are included¹:

<i>SM fermion</i>	$U_Y(1)$	$SU(2)_L$	$SU(3)$
$q_{\alpha L} = (u_{\alpha L}, d_{\alpha L})$	1/6	2	3
$L_{\alpha} = (\nu_{\alpha L}, l_{\alpha L})$	-1/2	2	1
$l_{\alpha R}$	-1	1	1
$u_{\alpha R}$	2/3	1	3
$d_{\alpha R}$	-1/3	1	3

Table 1.1: *Gauge charges of the SM fermions*

The numbers in Table 1.1 indicate the fermion representation under the corresponding group. The subindex L and R denotes left-handed and right-handed chirality respectively, while the subindex α denotes the flavour².

In addition to these fields, the SM includes a scalar field Φ , the Higgs, which is a singlet under $SU(3)$, doublet under $SU(2)_L$, and has hypercharge 1/2. This field gives rise to spontaneous electroweak symmetry breaking (EWSB)

$$SU(3) \times SU(2)_L \times U_Y(1) \longrightarrow SU(3) \times U_Q(1), \quad (1.1)$$

¹We are considering the convention $Q = T_3 + Y$.

² $\alpha = e, \mu, \tau$ for leptons; $\alpha = u, c, t$ for u-quarks and $\alpha = d, s, b$ for t-quarks.

when the Higgs acquires a vacuum expectation value (vev)

$$\langle \phi^\dagger \phi \rangle = v^2/2, \quad (1.2)$$

resulting in two massive gauge bosons, W_μ^\pm and Z_μ^0 , and a massless photon A_μ . This mechanism allows, as well, to generate the masses and mixture of fermions, as we will see in the next section.

Neutrinos are electrically neutral particles of spin 1/2 which only interact via weak processes. These weak interactions are due to the coupling of neutrinos and charged leptons with the gauge W and Z vector bosons, described by the charged-current (CC) and neutral-current (NC) interaction Lagrangians:

$$\mathcal{L}_{CC} = -\frac{g}{\sqrt{2}} (J_\mu^{CC} W^{+\mu} + J_\mu^{+CC} W^{-\mu}) , \quad (1.3)$$

$$(\mathcal{L}_{NC})_\nu = -\frac{g}{\cos \theta_W} (J_\mu^{NC})_\nu Z^{0\mu} , \quad (1.4)$$

where g is the $SU(2)_L$ gauge coupling constant, θ_W is the weak angle and the charged and neutral currents J_μ^{CC} and $(J_\mu^{NC})_\nu$ are given by the expressions

$$J_\mu^{CC} = \overline{l_{\alpha L}} \gamma^\mu \nu_{\alpha L} , \quad (1.5)$$

$$(J_\mu^{NC})_\nu = \frac{1}{2} \overline{\nu_{\alpha L}} \gamma^\mu \nu_{\alpha L} . \quad (1.6)$$

We have written explicitly only the weak interaction terms containing the neutrino fields. The subindex $\alpha = e, \mu, \tau$ denotes the flavour of both the neutrinos (ν_α) and the charged leptons (l_α). The three charged lepton weak eigenstates, by convention, are also defined as the mass eigenstates. The corresponding neutrino flavour ν_e, ν_μ and ν_τ are those coupled to the charged lepton fields through CC weak interactions: for example, the ν_μ is the ‘‘particle’’ produced in the decay $\pi^+ \rightarrow \mu^+ + \nu_\mu$ and so on.

The number of light active neutrinos is given by the invisible width of the Z boson, which was measured at LEP for the first time. A recent experimental value of the number of light neutrino flavours is 2.984 ± 0.008 [12] in reasonable agreement with the three flavours associated to the CC.

Notice that CC and NC interactions only contain the neutrino and lepton left-handed part, and conserve the electron, muon and tau lepton numbers (L_e, L_μ and L_τ respectively). In all the observed processes so far the total lepton number $L = L_e + L_\mu + L_\tau$ and the baryon number B are conserved. The most general renormalizable, Lorentz and gauge invariant (under $SU(3) \times SU(2)_L \times U_Y(1)$) lagrangian that we can construct with the SM fields, does not violate these global symmetries. However, this B and L invariance can be considered only as an accidental consequence of the particular choice of matter content and the requirement of the 4-D renormalizability. On the other hand, non-perturbative effects break these global symmetries at one loop, leaving only $U(1)_{B-L}$ as non-anomalous global symmetry.

1.2 The neutrino mass problem

Since the gauge symmetry forbids the existence of $SU(3) \times SU(2)_L \times U_Y(1)$ invariant fermion mass terms, in order to generate their Dirac masses the Higgs boson is introduced. Once the Higgs is included in the model, the gauge principle tells us that all terms compatible with the SM gauge symmetries have to be taken into account in the lagrangian. Therefore, the SM also contains the Yukawa-type interactions of the fermions with the Higgs scalar field:

$$-\mathcal{L}_{\text{Yukawa}} = Y_{\alpha\beta}^d \overline{q_{\alpha L}} \phi d_{\beta R} + Y_{\alpha\beta}^u \overline{q_{\alpha L}} \tilde{\phi} u_{\beta R} + Y_{\alpha\beta}^l \overline{L_{\alpha}} \phi l_{\beta R} + \text{h.c.} , \quad (1.7)$$

with $\tilde{\phi} = i\tau_2 \phi^*$. The matrices $Y^{d,u,l}$, generically non-diagonal, contain the Yukawa couplings for the up-quarks, down-quarks and for the charged leptons, respectively. After EWSB, Dirac mass terms are generated for all charged fermions:

$$\frac{1}{\sqrt{2}} Y^f v \overline{f_L} f_R + \text{h.c.} = m^f \overline{f_L} f_R + \text{h.c.} \quad (1.8)$$

All the masses in the SM, thus, are generated ‘‘spontaneously’’ thanks to their couplings to the Higgs: those of the electroweak gauge bosons, as well as those of the charged fermions. The SM in its minimal version, however, does not include fields that are singlets under the gauge group, which will be called ν_R along this work. This implies that there are no Yukawa terms such as $\overline{L_{\alpha}} \tilde{\phi} Y_{\alpha i}^{\nu} \nu_{Ri}$ giving rise to a Dirac mass $\sim Y_{\alpha i}^{\nu} v \overline{\nu_{\alpha L}} \nu_{Ri}$ for neutrinos in the SM.

Is it possible to obtain a neutrino Majorana mass term for left-handed neutrinos in the SM ³? The answer is no. With the SM minimal field content (only one Higgs doublet), the unique possibility is through $m_{\nu} \overline{\nu_{\alpha L}} \nu_{\alpha L}^c + \text{h.c.}$, but this term is forbidden by the $SU(2)_L \times U_Y(1)$ gauge symmetry.

In order to contemplate the neutrino masses in the model, there are two options:

- The most evident one is to extend the particle content of the SM with ν_R , generating neutrino masses through the same mechanism as the rest of the fermions of the SM. The main drawback of this option is that the smallness of the neutrino masses would not be explained in a ‘‘natural’’ way, as we will see in the next subsection.

- The second possibility is considering the SM as an effective low-energy theory of a higher energy one able to explain neutrino masses. This new physics too heavy for being directly studied (and, in general, new physics from higher energies) would manifest at low energy as non renormalizable operators made out of the SM fields, invariant under the SM gauge group, and weighted by inverse powers of the heavy scale Λ :

$$\mathcal{L}^{eff} = \mathcal{L}_{SM} + \delta\mathcal{L}^{d=5} + \delta\mathcal{L}^{d=6} + \dots , \text{ with } \delta\mathcal{L}^d \propto 1/\Lambda^{d-4}, \quad (1.9)$$

³In the sense of a 4-D renormalizable theory with the minimal field content.

where \mathcal{L}_{SM} is the SM lagrangian which contains all $SU(3) \times SU(2)_L \times U_Y(1)$ invariant operators of dimension $d \leq 4$. If we consider $B - L$ as a fundamental symmetry of the SM, its conservation would also forbid a neutrino Majorana mass term. However, unlike the gauge symmetry which protects the photon or gluon masses, the $B - L$ symmetry does not seem to be a building block of the theory: as we have already commented above it can be considered just an accidental consequence of the SM matter content and the renormalizability demand. Therefore, it is plausible that it may be broken if some extension of the SM is required to fit the data. On the other hand, this violation should be soft because experimentally we have not seen any $B - L$ violating process yet.

Then let us not impose $B - L$ conservation. Within the SM field content, the easiest way to give mass to the neutrinos is adding the following dimension 5 operator [13]:

$$\frac{c_{\alpha\beta}}{\Lambda} \left(\overline{L_\alpha \tilde{\phi}} \right) \left(\tilde{\phi}^T L_\beta^c \right), \quad (1.10)$$

where c is a dimensionless coefficient. Inserting the Higgs vev v , this operator gives a Majorana neutrino mass term

$$m_{\alpha\beta}^\nu \overline{\nu_{\alpha L}^c} \nu_{\beta L} / 2 \quad \text{with} \quad m^\nu = v^2 c / \Lambda. \quad (1.11)$$

In fact, this operator is the unique gauge invariant dimension 5 operator we can build with SM fields that gives rise to neutrino masses.

More generically, after EWSB, the operators with $d > 4$ in (1.9) give small corrections suppressed by powers of $1/\Lambda$ to the physics at low energy⁴. In the case of the Weinberg operator, given in Eq. (1.10), $m_\nu = c v^2 / \Lambda \sim 0.1 \text{ eV}$ would naively imply $\Lambda \sim 10^{14-15} \text{ GeV}$, which suggestively points to the scale of Grand Unified Theories [14, 15]. Namely, neutrino masses might be the first manifestation of a new energy scale Λ in nature.

The NP, manifested at low energies by these tower of non-renormalizable operators, can be searched experimentally in several ways, for instance:

1. going to higher energies;
2. searching for small effects in precision experiments at low energies;
3. studying rare processes;
4. searching processes that cannot be generated by renormalizable operators.

Later on, we will search for generic NP associated to the generation of neutrino masses focusing on the second and third possibilities.

⁴Modifying the couplings present in the SM lagrangian *and/or* producing new exotic couplings among the SM fields.

1.2.1 The paradigmatic neutrino mass model: The Seesaw

The minimal SM extension which can contemplate weakly interacting neutrino masses involves the enlarging of the field content with n fermionic singlets⁵ (right-handed neutrinos ν_R), adding to the SM lagrangian all the new terms allowed by the SM gauge symmetry, but imposing $B - L$ and preserving the renormalizability of the theory. In other words, adding only the following new Yukawa coupling:

$$\overline{L}_\alpha \tilde{\phi} Y_{\alpha j}^\nu \nu_{Rj} + h.c. \quad (1.12)$$

In this way, neutrinos would obtain Dirac masses as the rest of the SM fermions: $m^\nu = Y^\nu v / \sqrt{2}$. On the other hand, this simple and, in some sense, reasonable extension of the SM (the neutrinos would get masses in the same way as the rest of the SM fermions) suffers from “theoretical” problems: $m^\nu = Y^\nu v \approx 0.1 eV$ would imply, barring fine-tuned cancellations, $Y^\nu \sim 10^{-12}$. This value can be considered very unnatural (in the ‘t Hooft sense [16]) and additionally, it is many orders of magnitude smaller than those corresponding to charged leptons. Then, in addition to the *ad hoc* assumption of $B - L$ conservation, we would not be able to explain the mass hierarchy between neutrinos and the other fermions within this model, which suggests that there could be another origin for the tiny neutrino masses. At the end of this section we will come back over the theoretical problems just mentioned and the naturalness criterium.

At this point, we can thus relax the assumption of the $B - L$ conservation, which can be seen as an accidental symmetry as we have already explained. Without assuming $B - L$ conservation the Majorana mass terms for the ν_R are no longer forbidden due to any symmetry. Then, following the gauge principle, the most general lagrangian in this framework would be:

$$\mathcal{L} = \mathcal{L}_{SM} + \mathcal{L}_{\nu_R}, \quad (1.13)$$

where \mathcal{L}_{SM} is the SM lagrangian, while

$$\mathcal{L}_{\nu_R} = i \overline{\nu_{Ri}} \not{\partial} \nu_{Ri} - \left(\overline{L}_\alpha \tilde{\phi} Y_{\alpha i}^\nu \nu_{Ri} - \frac{1}{2} \overline{\nu_{Ri}^c} M_{ii} \nu_{Ri} \right) + h.c. . \quad (1.14)$$

\mathcal{L}_{ν_R} contains the kinetic energy⁶, the Majorana mass term M for the right-handed neutrinos as well as the neutrino Yukawa couplings Y^ν . Take into account that we have chosen, without loss of generality, a diagonal Majorana mass matrix for the fermionic singlets. Notice also that, since we are allowing $B - L$ violation, the right-handed neutrino Majorana mass M in Eq. (1.14) is not protected from becoming much larger than the electroweak scale v through loop corrections. If the elements of the Majorana mass matrix, M_{ii} , are much larger than the electroweak scale v the above lagrangian

⁵Actually, two fermionic singlets would be enough to explain neutrino oscillation phenomena.

⁶Notice that, since the ν_R are $SU(3) \times SU(2)_L \times U_Y(1)$ singlets, the covariant derivative reduces to $D_\mu = \partial_\mu$ in the kinetic energy terms.

corresponds to the so-called (type-I) *seesaw model*, which will be considered in the following.

Upon EWSB, the mass terms in Eq. (1.14) take the form

$$\begin{aligned} -\mathcal{L}_{mass} &= \sum_{i=1}^n Y_{\alpha i} \frac{v}{\sqrt{2}} \overline{\nu_{\alpha L}} \nu_{Ri} + h.c. + \frac{1}{2} \sum_{i=1}^n M_{ii} \overline{\nu_{Ri}^c} \nu_{Ri} + h.c. = \\ &= \frac{1}{2} \overline{\vec{\nu}_L^c} M_\nu \vec{\nu}_L + h.c., \end{aligned} \quad (1.15)$$

where

$$\vec{\nu}_L = (\nu_{eL}, \nu_{\mu L}, \nu_{\tau L}, \nu_{R1}^c, \dots, \nu_{Rn}^c) \quad (1.16)$$

and

$$M_\nu = \begin{pmatrix} 0 & Y^{\nu*} v / \sqrt{2} \\ Y^{\nu\dagger} v / \sqrt{2} & \text{diag} \{M_{11}, M_{22}, \dots, M_{nn}\} \end{pmatrix}. \quad (1.17)$$

For three leptonic generations, M_ν is a $(3+n) \times (3+n)$ matrix, where Y^ν is the $3 \times n$ complex matrix containing the Yukawa neutrino couplings. The number of physical parameters in the model is [17]: $n(3+1)$ moduli and $3(n-1)$ phases.

As an illustration, consider the simplest case with only one generation. In this particular case, M_ν is a real 2×2 matrix while M and Y^ν are constants. Upon diagonalization, the following eigenvalues are found:

$$m_{1,2} = \frac{M}{2} \mp \sqrt{\left(\frac{M}{2}\right)^2 + \left(Y^\nu \frac{v}{\sqrt{2}}\right)^2}. \quad (1.18)$$

Within the seesaw hypothesis $M \gg v$, the eigenvalues simplify to

$$m_1 \simeq \frac{v^2 (Y^\nu)^2}{2M} + \mathcal{O}(1/M^2), \quad (1.19)$$

$$m_2 \simeq M(1 + \mathcal{O}(1/M^2)), \quad (1.20)$$

For $n > 1$ the light neutrino masses are given by

$$m_\nu = \frac{v^2}{2} Y^{\nu*} M^{-1} Y^{\nu\dagger} \quad (1.21)$$

which reduces to Eq. (1.19) in the one generation case. In the case of three leptonic generations and three heavy singlets, due to $M \gg v$, the full 6×6 mass matrix \mathcal{M} gives rise to 3 (almost) pure right-handed neutrinos with heavy Majorana masses, and to 3 (almost) pure left-handed neutrinos with light Majorana masses. It is interesting to redo the parameter counting for this low-energy mass matrix [17]. At low energies we have the following number of physical parameters: 6 moduli and 3 phases⁷.

For values of the Yukawa couplings $Y^\nu \sim \mathcal{O}(1)$, barring fine-tuned cancellations, roughly speaking the light neutrino masses are given by

$$m_\nu \simeq \frac{v^2}{M}. \quad (1.22)$$

Then, assuming $M \gg v$, the smallness of neutrino masses is explained in a “natural” way, without any fine-tuning. For instance, for $m_\nu < 0.58$ eV (see Eq. (1.74)) we would get the following NP scale:

$$M \gtrsim 10^{14} \text{ GeV}. \quad (1.23)$$

It is surprising and very suggesting that, simply by allowing $B - L$ to be broken, present neutrino data naively point to the scale of GUT’s. What is even more interesting is that, as it has mentioned in the motivations, this violation of lepton number together with the increased number of CP-violating phases present in the high energy lagrangian might explain the matter-antimatter asymmetry observed in the universe via the leptogenesis mechanism.

Of course, we can re-derive the same result in terms of the dimension 5 effective operator presented before. Integrating out the heavy neutrinos gives a non-renormalizable effective lagrangian that only contains the observable low-energy fields (see [17] and refs. therein). Fig. 1.1 left shows that ν_R exchange generates the dimension 5 effective operator $(\overline{L}\widetilde{\phi}) (\widetilde{\phi}^T L^c)$ with coefficient $Y_\nu^* \frac{1}{M} Y_\nu^\dagger$, one Y_ν associated to each ν_R Yukawa coupling and the $\frac{1}{M}$ from the ν_R propagator.

It is important to remark that this is not the unique realization of the seesaw model. The same dimension 5 operator responsible of Majorana masses can be mediated not only by fermionic singlets but also by other heavy fields, as it is shown in Fig. 1.1 extracted from Ref. [18]. We have three possible realizations:

1. Type-I seesaw. The SM field content is extended with fermionic singlets. This is the case studied in detail in this section and the first seesaw model proposed.

⁷Notice that, for this parameter counting, we are “only” considering the SM plus the effect of the dimension 5 Weinberg operator (see Eq. (1.10)). But we are not taking into account the effect of other higher dimension effective operators as the dimension 6 one, responsible of deviations from unitarity of the leptonic mixing matrix, as we will see in the next chapter.

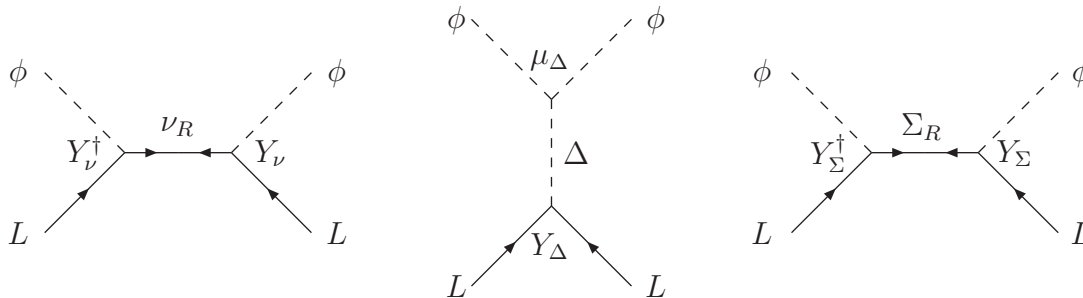


Figure 1.1: *The three generic realizations of the seesaw mechanism, depending on the nature of the heavy fields exchanged: SM singlet fermions (type I Seesaw) on the left, SM triplet scalars (type II Seesaw) and SM triplet fermions (type III Seesaw) on the right.*

2. Type-II seesaw. The SM field content is enlarged adding a scalar triplet of $SU_L(2)$ [19–23].
3. Type-III seesaw. In this case, the extension is made with the minimal introduction of a triplet fermion of $SU_L(2)$ [24].

These three extensions of the SM explain the smallness of neutrino masses exactly in the same way after the heavy fields involved have been integrated out. In this sense, there is no fundamental reason to think that one of these realizations is more probable than the others. Traditionally, in the neutrino literature more attention has been paid to the type-I seesaw, mainly because of historical reasons since it was the first seesaw model proposed. On the other hand, once the next effective operator (the dimension 6 one) is considered in the low energy analysis, the phenomenology is no longer the same in the three models [18]. In any case, in this section we keep on studying the type I seesaw model, but similar qualitative conclusions can be extracted for the rest of the options.

A remarkable warning is pertinent here. Although the seesaw model provides a simple and “natural” explanation for the smallness of neutrino masses, it gives rise to a new manifestation of the Higgs mass hierarchy problem. Due to the Yukawa couplings of the Higgs field with the heavy neutrinos, the Higgs mass is sensitive quadratically to the new scale characteristic of the seesaw model⁸. The one-loop corrections to Higgs mass due to the heavy ν_R are [25, 26]:

$$\delta m_H^2 |_{\nu_R} \propto \left[\Lambda^2 - M^2 \log \left(\frac{M^2}{\Lambda^2} \right) \right], \quad (1.24)$$

where Λ is the regulator cutoff. Therefore, for “natural” values of the seesaw scale, much larger than v , the tree level Higgs mass $(m_H^0)^2 = m_H^2 + \delta m_H^2$ would have to be highly fine-tuned in order to get the Higgs mass at the electroweak scale, worsening the *hierarchy problem* (we will come back to this point below). Hence, in the context

⁸The three realizations of the seesaw model just commented present this quadratic dependence of the new scale.

of the SM, the seesaw model suffers an important fine tuning problem which can be interpreted as a call for the existence of additional NP, besides right-handed neutrinos. This is a subject under active investigation. For instance, a possible framework to accommodate the seesaw mechanism could be SUSY where the electroweak fine tuning problem could be much softened.

On the other hand, the naturalness criteria is something which can be a bit subtle. We can use naturalness criteria, also in the 't Hooft sense, to justify that considering small values of Majorana masses is also natural. Following the renormalization group analysis, the Majorana masses⁹ M_{ii} , run with the renormalization scale as:

$$\Lambda \frac{dM_{ii}}{d\Lambda} \propto M_{ii} \sum_{\alpha} |Y_{\alpha i}|^2 \quad (1.25)$$

since they are protected by the chiral symmetry, exactly in the same sense as the Dirac masses after the electroweak symmetry breaking. Thus, the renormalization group analysis tells us that, in principle, M_{ii} can be anything. If M_{ii} is small, $B - L$ is partially conserved in the lagrangian. Thus, considering small values of this parameter enlarges the lagrangian symmetries: this should be compared with the analogous 't Hooft argument applied to the quark masses in QCD.

Concerning the SM Higgs hierarchy problem, scalar masses are not protected by the chiral symmetry and thus, at one loop, in the SM generically:

$$\delta m_H^2 \sim \frac{1}{v^2} (4 m_t^2 - 2 M_W^2 - M_Z^2 - m_H^2) \Lambda^2, \quad (1.26)$$

which points to a huge value of the Higgs mass, unless an uncomfortable fine tuning would be invoked. Notice that the running mass equation for the scalar fields would be not proportional to their masses, contrary to the fermion case. If one adds right-handed neutrinos and a Majorana mass term to the SM lagrangian, as we have seen in Eq. (1.24), the Higgs mass is sensitive to the Majorana masses M_{ii} in such a way that for large values of the seesaw scale $M \gg v$, the tree level Higgs mass would have to be even highly fine-tuned than in the SM in order to stabilize the Higgs mass around the electroweak scale. However, if one assumes that M is small this extra problem does not appear, again because the Majorana mass term would be protected by the chiral symmetry, and the calling for additional NP would not be necessary in this sense.

Finally, notice that the running behaviour of the Majorana masses is the same as the Dirac masses one. In fact, one could think that there is no fundamental reason to distinguish between Majorana and Dirac fermions in the SM: both are fermions with their masses protected by chiral symmetry. In this context, it seems also convenient to study models with light Majorana neutrinos and not only the seesaw case. Notice that light Majorana neutrinos would be a particular case of what is called *sterile neutrinos* [27] in the literature. In Chap. 4, we will analyze a pure phenomenological model which contemplates the presence of these light sterile neutrinos.

⁹This result has been calculated at one loop.

1.3 Neutrino Oscillations

The experimental observation of neutrino oscillations in solar [28–31, 31–35], atmospheric [36–38], reactor [39–42] and accelerator [43–46] neutrino experiments regimes constitutes a robust evidence for neutrino masses. Oscillations are quantum mechanics interference phenomena which basically consist in the transition of a neutrino of flavour α into a neutrino of a different flavour β during its evolution after travelling a distance L . The idea was suggested long ago, before gauge theories became popular [47]. We will now discuss neutrino oscillations in vacuum and matter, assuming that neutrinos are *stable* and *ultrarelativistic*. Both assumptions are reasonable with light neutrinos. In anycase, if instability is assumed then decay widths should be included in Eq. (1.42).

If neutrinos are massive, then weak interaction (or flavour) ν_α ($\alpha = e, \mu, \tau, s_1, s_2, \dots$) and mass eigenstates ν_i ($i = 1, 2, \dots, n$) do not generally coincide¹⁰, leading to the phenomenon of flavour transition. The left-handed components of the neutrino flavour fields are superpositions of the left-handed components of the (Dirac or Majorana) neutrino fields with definite masses m_i :

$$\nu_{\alpha L} = \sum_{i=1}^n V_{\alpha i} \nu_{iL} \quad (\alpha = e, \mu, \tau), \quad (1.27)$$

where V is a unitary mixing matrix which comes from diagonalization of the neutrino mass matrix. The number of massive neutrino fields n could be equal or more than 3. If n is larger than 3 there are sterile neutrinos¹¹ that do not take part in the standard weak interactions given by Eq. (1.5) and Eq. (1.6). So in the most general case, although the whole matrix V is unitary, in the mixing Eq. (1.27) only a submatrix of V appears, which, in general is not squared. In any case, we will suppose in this section that there are no sterile neutrinos.

Let us rewrite the neutrino weak currents, Eq. (1.5) and Eq. (1.6) in the mass basis, defined in Eq. (1.27) as

$$J_\mu^{-CC} = \sum_{i=1}^3 \bar{l}_{\alpha L} \gamma^\mu \left(\tilde{V}^\dagger V \right)_{\alpha i} \nu_{iL}, \quad (1.28)$$

$$(J_\mu^{NC})_\nu = \sum_{i=1}^3 \frac{1}{2} \bar{\nu}_{iL} \gamma^\mu \nu_{iL}, \quad (1.29)$$

where \tilde{V} is a unitary mixing matrix which comes from diagonalization of the charged lepton mass matrix. By convention, all the mixing is included in the neutrinos so that

¹⁰In what follows, we shall use Latin indices for the mass eigenstates and Greek indices for the flavour basis defined in Eq. (1.5)

¹¹LSND [48–50] could have found an evidence of the existence of sterile neutrinos. However similar experiments have not confirmed the LSND result so far (See Chap. 4).

charged lepton weak eigenstates are also defined as the mass eigenstates. Hence, the leptonic mixing matrix is given as $\tilde{V}^\dagger V$. On the other hand, it is usual (and useful) to redefine the mixing matrix by reabsorbing the unphysical phases in $\tilde{V}V$ into the charged lepton (and neutrino if they are Dirac) fields. Then, the CC becomes

$$J_\mu^{-CC} = \sum_{i=1}^3 \bar{l}_{\alpha L} \gamma^\mu U_{\alpha i} \nu_{iL}, \quad (1.30)$$

where U is the *Pontecorvo-Maki-Nakagawa-Sakata* mixing matrix [27, 47, 51, 52], which is related to the matrices \tilde{V} and V by

$$U \equiv \Omega_l \tilde{V} V (\Omega_\nu), \quad (1.31)$$

where Ω_l is a diagonal 3×3 phase matrix, that is used to redefine 3 phases in U . Ω_ν is a diagonal matrix with additional phases, chosen to reduce by 2 the number of phases in U , only if neutrinos are Dirac fermions (for Majorana neutrinos Ω_ν is the unit matrix). Then, taking into account that $\tilde{V}V$ is unitary, if there are three Majorana (Dirac) neutrinos U is a 3×3 matrix which depends on 6 (4) independent parameters: 3 mixing angles and 3 (1) phases. Finally, with these redefinitions the following relation between mass and flavour fields is obtained

$$\nu_{\alpha L} = \sum_{i=1}^3 U_{\alpha i} \nu_{iL} \quad (\alpha = e, \mu, \tau). \quad (1.32)$$

Since neutrino mass differences are small, a state of a flavour neutrino $|\nu_\alpha\rangle$ produced in a weak process (as the $\pi^+ \rightarrow \mu^+ \nu_\mu$ decay, nuclear beta-decays, etc.) is described by the coherent superposition of mass eigenstates in agreement with ¹²

$$|\nu_\alpha\rangle = \sum_{i=1}^3 U_{\alpha i}^* |\nu_i\rangle. \quad (1.34)$$

Here $|\nu_i\rangle$ is the state of a neutrino with negative helicity, mass m_i , momentum p_i , and with energy $E = \sqrt{m_i^2 + p_i^2}$.

¹²By convention, a field operator creates anti-particles while an anti-field operator creates particles. As a consequence one must be careful in distinguishing fields from quantum states (U from U^*). The correct relations between mass basis and flavour basis are:

$$\begin{array}{lll} \text{Field operators } \nu: & \nu_\alpha = U_{\alpha i} \nu_i, & \bar{\nu}_\alpha = U_{\alpha i}^* \bar{\nu}_i \\ \text{One-particle states } |\nu\rangle: & |\nu_\alpha\rangle = U_{\alpha i}^* |\nu_i\rangle & |\bar{\nu}_\alpha\rangle = U_{\alpha i} |\bar{\nu}_i\rangle \\ \text{Wave-functions } \nu(x) \equiv \langle x|\nu\rangle & \nu_\alpha(x) = U_{\alpha i}^* \nu_i(x), & \bar{\nu}_\alpha(x) = U_{\alpha i} \bar{\nu}_i(x) \end{array} \quad (1.33)$$

1.3.1 In Vacuum

The particles that propagate from the neutrino source to the detector are the ν_i , and the contributions of the different ν_i must be added coherently. Thus, using Eq. (1.34), the amplitude of a flavour transition $\nu_\alpha \rightarrow \nu_\beta$ after a time t and a distance L is given by

$$A_{\nu_\alpha \rightarrow \nu_\beta} = \langle \nu_\beta | \nu_\alpha(t, L) \rangle = \sum_i U_{\alpha i}^* T_i(t, L) U_{\beta i} . \quad (1.35)$$

This formula has a very simple interpretation. $U_{\alpha i}^*$ is the amplitude to find the neutrino mass eigenstate $|\nu_i\rangle$ in the state of the flavour neutrino $|\nu_\alpha\rangle$; the factor $T_i(t, L)$ gives the evolution of the mass eigenstate and, finally, the term $U_{\beta i}$ gives the amplitude to find the flavour neutrino state $|\nu_\beta\rangle$ in the mass eigenstate $|\nu_i\rangle$.

Let us see which is the form of $T_i(t, L)$ by studying the evolution equation of the massive states. If ν_i has rest mass m_i , then in its rest frame its corresponding state obeys the Schrödinger equation

$$i \frac{\partial}{\partial \tau_i} |\nu_i(\tau_i)\rangle = m_i |\nu_i(\tau_i)\rangle , \quad (1.36)$$

where τ_i is the proper time associated to the rest frame of the ν_i . So,

$$|\nu_i(\tau_i)\rangle = e^{-im_i\tau_i} |\nu_i(0)\rangle . \quad (1.37)$$

Thus, the amplitude $\langle \nu_i(0) | \nu_i(\tau_i) \rangle$ for finding the original ν_i state $|\nu_i(0)\rangle$ in the time evolved state $|\nu_i(\tau_i)\rangle$, is simply $T_i(t, L) = \exp[-im_i\tau_i]$. With τ_i being the proper time taken by ν_i to travel from the neutrino source to the detector.

By Lorentz invariance, the phase $m_i\tau_i$ in the ν_i propagator $T_i(t, L)$ is given in terms of the laboratory-frame variables (E_i, p_i, t and L) by

$$m_i\tau_i = E_i t - p_i L . \quad (1.38)$$

A proper description of the neutrino behaviour should be given in terms of wave-packets characterized by certain energy and momentum spreads (ΔE) and (Δp). In practice, the experimental uncertainties of the present experiments are such that $(\Delta E) \ll (\Delta p)^{13}$. It is then a very good approximation to describe the initial flavour eigenstate as a mixture of mass eigenstates ν_i with sharp energy E and different momenta [53].

At energy E , a mass eigenstate $|\nu_i\rangle$, with mass m_i , has a momentum p_i given by

$$p_i = \sqrt{E^2 - m_i^2} \cong E - \frac{m_i^2}{2E} . \quad (1.39)$$

¹³This also means that we know with good precision the distance L travelled by neutrinos, but we do not know precisely the time of which they were created.

From Eqs. (1.38) and (1.39), we see that at energy E the phase $m_i\tau_i$ in $T_i(t, L)$ is given by

$$m_i\tau_i \cong E(t - L) + \frac{m_i^2}{2E}L. \quad (1.40)$$

In this expression, the phase $E(t - L)$ is irrelevant since it is common to all the interfering mass eigenstates and it will cancel when computing the modulus square. Thus, we may take

$$T_i(L) = \exp[-im_i^2\frac{L}{2E}] . \quad (1.41)$$

Using this result, it follows from Eq. (1.35) that the amplitude for a neutrino to change from a ν_α into a ν_β while travelling a distance L through vacuum with energy E is given by

$$A_{\nu_\alpha \rightarrow \nu_\beta} = \sum_i U_{\alpha i}^* e^{-im_i^2\frac{L}{2E}} U_{\beta i} . \quad (1.42)$$

Squaring it and considering the unitarity of U , we find that the probability $P(\nu_\alpha \rightarrow \nu_\beta)$ for $\nu_\alpha \rightarrow \nu_\beta$ is given by

$$\begin{aligned} P_{\nu_\alpha \rightarrow \nu_\beta} &= |A_{\nu_\alpha \rightarrow \nu_\beta}|^2 \\ &= \delta_{\alpha\beta} - 4 \sum_{i>j} \text{Re}(U_{\alpha i}^* U_{\beta i} U_{\alpha j} U_{\beta j}^*) \sin^2\left(\frac{\Delta m_{ij}^2 L}{4E}\right) \\ &\quad + 2 \sum_{i>j} \text{Im}(U_{\alpha i}^* U_{\beta i} U_{\alpha j} U_{\beta j}^*) \sin\left(\frac{\Delta m_{ij}^2 L}{2E}\right) , \end{aligned} \quad (1.43)$$

where

$$\Delta m_{ij}^2 \equiv m_i^2 - m_j^2 . \quad (1.44)$$

From the relation Eq. (1.32) it follows that the state describing a flavour antineutrino $\bar{\nu}_\alpha$ is given by

$$|\bar{\nu}_\alpha\rangle = \sum_{i=1}^n U_{\alpha i} |\bar{\nu}_i\rangle . \quad (1.45)$$

Thus the amplitude of $\bar{\nu}_\alpha \rightarrow \bar{\nu}_\beta$ transitions is given by

$$A_{\bar{\nu}_\alpha \rightarrow \bar{\nu}_\beta} = \langle \bar{\nu}_\beta | \bar{\nu}_\alpha(t, L) \rangle = \sum_i U_{\alpha i} T_i(t, L) U_{\beta i}^* . \quad (1.46)$$

Notice that the amplitude for antineutrino transitions differs from the corresponding amplitude Eq. (1.35) for neutrinos only by the exchange $U \rightarrow U^*$. Then it follows that

$$P_{\bar{\nu}_\alpha \rightarrow \bar{\nu}_\beta}(U) = P_{\nu_\alpha \rightarrow \nu_\beta}(U^*) \quad , \quad (1.47)$$

so that, the antineutrino transitions probability in vacuum is simply obtained by the exchange $U \rightarrow U^*$ in the probability expression given in Eq. (1.43). So,

$$\begin{aligned} P_{\bar{\nu}_\alpha \rightarrow \bar{\nu}_\beta} &= \delta_{\alpha\beta} - 4 \sum_{i>j} \text{Re}(U_{\alpha i}^* U_{\beta i} U_{\alpha j} U_{\beta j}^*) \sin^2 \left(\frac{\Delta m_{ij}^2 L}{4E} \right) \\ &\quad + 2 \sum_{i>j} \text{Im}(U_{\alpha i}^* U_{\beta i} U_{\alpha j} U_{\beta j}^*) \sin \left(\frac{\Delta m_{ij}^2 L}{2E} \right) \quad . \quad (1.48) \end{aligned}$$

It can be seen from the above expression that if all neutrinos are massless, and consequently all the splittings Δm_{ij}^2 vanish, then $P_{\bar{\nu}_\alpha \rightarrow \bar{\nu}_\beta} = \delta_{\alpha\beta}$. Thus, the oscillation in vacuum of ν_α into a *different* flavour ν_β implies that neutrinos have non-zero masses. Notice that at least two neutrinos have to be non-degenerated in order to have $P_{\nu_\alpha \rightarrow \nu_\beta} \neq \delta_{\alpha\beta}$. From Eq. (1.42), we see that this change of flavour also implies neutrino mixing: in the absence of mixing, the U matrix is diagonal, so that $A_{\nu_\alpha \rightarrow \nu_\beta}$ vanishes if $\beta \neq \alpha$. Finally, as Eq. (1.48) shows, the probability of flavour change in vacuum is a periodic function of L/E . Due to this behavior this flavour change is called ‘‘neutrino oscillations’’.

Comparing the expressions in Eq. (1.48) for the transition probabilities of neutrinos and antineutrinos we see that

$$P_{\nu_\alpha \rightarrow \nu_\beta} = P_{\bar{\nu}_\beta \rightarrow \bar{\nu}_\alpha} \quad . \quad (1.49)$$

This relation is a consequence of CPT invariance. From Eq. (1.48) (or from the above equation as well), it follows that the neutrino and antineutrino survival probabilities are equal:

$$P_{\nu_\alpha \rightarrow \nu_\alpha} = P_{\bar{\nu}_\alpha \rightarrow \bar{\nu}_\alpha} \quad . \quad (1.50)$$

However, as Eq. (1.48) shows, if the mixing matrix U is complex, $P_{\nu_\alpha \rightarrow \nu_\beta}$ and $P_{\bar{\nu}_\alpha \rightarrow \bar{\nu}_\beta}$ are different. They are equal only if there is CP invariance in the lepton sector. So, the observation of $P_{\nu_\alpha \rightarrow \nu_\beta} \neq P_{\bar{\nu}_\alpha \rightarrow \bar{\nu}_\beta}$ would indicate CP violation which, so far, has been observed only in the quark sector¹⁴. This CP violation in the leptonic sector would be very interesting for leptogenesis where plays a fundamental role.

¹⁴In any case, these relations are not valid when neutrinos propagate in matter. When interactions with matter affect the neutrino propagation they may no longer hold because the medium itself is generally not symmetric under CP and CPT (see next subsection).

On the other hand, we can also see in Eq. (1.48) that the oscillation probabilities are invariant under the phase transformation

$$U_{\alpha j} \rightarrow e^{-i\varphi_\alpha} U_{\alpha j} e^{i\phi_j} \quad (1.51)$$

Therefore, it is clear that the oscillation probabilities do not depend on the Majorana CP-violating phases and it is not possible to distinguish the Dirac and Majorana cases by the observation of neutrino oscillations.

Finally, the unitarity of U implies the probability conservation relation:

$$P_{\nu_\alpha \rightarrow \nu_\alpha} = 1 - \sum_{\beta \neq \alpha} P_{\nu_\alpha \rightarrow \nu_\beta}. \quad (1.52)$$

It is useful to include the so-far-omitted constants \hbar and c (we was using natural units) in the probability expression. So the argument of the oscillatory terms is given by

$$\Delta m_{ij}^2 \frac{L}{4E} = 1.27 \Delta m_{ij}^2 (\text{eV}^2) \frac{L (\text{km})}{E (\text{GeV})}. \quad (1.53)$$

Hence, in order for $\sin[1.27 \Delta m_{ij}^2 (\text{eV}^2) \frac{L (\text{km})}{E (\text{GeV})}]^2$ to be appreciable, it should be satisfied the condition

$$\Delta m_{ij}^2 (\text{eV}^2) \gtrsim \frac{E (\text{GeV})}{L (\text{km})} \quad (1.54)$$

Thus, the larger the value of the parameter L/E , the smaller are the values of Δm^2 which can be probed in the experiments. For example, an experiment with $L \sim 10^4$ km, the diameter of the Earth, and $E \sim 1$ GeV is sensitive to Δm_{ij}^2 down to $\sim 10^{-4}$ eV². As this illustrates, neutrino oscillation provides experimental access to very tiny neutrino mass difference. The above condition can be rewritten in terms of the oscillation length, $L^{osc} = \frac{4\pi E}{\Delta m_{ij}^2} \simeq 2.48 \frac{E (\text{GeV})}{\Delta m_{ij}^2 (\text{eV}^2)}$ km, in the form

$$L^{osc} \lesssim L. \quad (1.55)$$

Neutrino oscillations can be observed if the oscillation length is not much larger than the source – detector distance L . The opposite limit corresponds to $L^{osc} \ll L$. In this case due to the fact that in the experiment we have to average over the energies (the beam is not monochromatic) the information on the oscillation phase is lost since $\langle \sin(\Delta m_{ij}^2 \frac{L}{2E}) \rangle \simeq \langle \cos(\Delta m_{ij}^2 \frac{L}{2E}) \rangle \simeq 0$.

Also notice that the oscillation probability Eq. (1.48) is only sensitive to the squared mass difference Δm_{ij}^2 and not to the individual neutrino masses. Therefore, with neutrino oscillation experiments only mass squared differences can be measured, but not the absolute scale of neutrino masses.

As we have already mentioned, in the standard case of three families, if neutrinos are Majorana (Dirac) the mixing matrix U can be parametrized, after reabsorbing the unphysical phases into the charged lepton (and left handed neutrino) fields, with 3 mixing angles and 3 (1) phases. So U is usually written as:

$$U = \begin{array}{c} \text{Atmospheric} \\ \left[\begin{array}{ccc} 1 & 0 & 0 \\ 0 & c_{23} & s_{23} \\ 0 & -s_{23} & c_{23} \end{array} \right] \end{array} \begin{array}{c} \text{Cross-Mixing} \\ \left[\begin{array}{ccc} c_{13} & 0 & s_{13}e^{-i\delta} \\ 0 & 1 & 0 \\ -s_{13}e^{i\delta} & 0 & c_{13} \end{array} \right] \end{array} \begin{array}{c} \text{Solar} \\ \left[\begin{array}{ccc} c_{12} & s_{12} & 0 \\ -s_{12} & c_{12} & 0 \\ 0 & 0 & 1 \end{array} \right] \end{array} \begin{array}{c} \text{Majorana phases} \\ \left[\begin{array}{ccc} e^{i\phi_1/2} & 0 & 0 \\ 0 & e^{i\phi_2/2} & 0 \\ 0 & 0 & 1 \end{array} \right] \end{array} \quad (1.56)$$

We have defined $c_{ij} \equiv \cos \theta_{ij}$ and $s_{ij} \equiv \sin \theta_{ij}$, where θ_{ij} is a mixing angle, and δ , ϕ_1 , and ϕ_2 are CP-violating phases. As it has already been pointed out, neutrino oscillation experiments are not sensitive to the Majorana phases (ϕ_1 , and ϕ_2). Therefore, in this kind of experiments we could detect CP violation in the leptonic sector only through δ .

One important case is the two families one, because the results of neutrino oscillation experiments are usually analysed under this simple assumption. In any case, this approximation, where only two different neutrinos are important, is a quite good description of quite a lot of experiments. In this case the mixing matrix is simply given by

$$U = \begin{bmatrix} \cos \theta & \sin \theta \\ -\sin \theta & \cos \theta \end{bmatrix}. \quad (1.57)$$

Taking this into account in the probability expression given in Eq. (1.48) we obtain the following well known expressions

$$\begin{aligned} P_{(\bar{\nu})_{\alpha} \rightarrow (\bar{\nu})_{\beta}} &= \sin^2 2\theta \sin^2 \left(\frac{\Delta m^2 L}{4E} \right), \quad (\alpha \neq \beta) \\ P_{(\bar{\nu})_{\alpha} \rightarrow (\bar{\nu})_{\alpha}} &= 1 - P_{(\bar{\nu})_{\alpha} \rightarrow (\bar{\nu})_{\beta}} \end{aligned} \quad (1.58)$$

Thus, in the simplest case of transitions between two neutrino types the probability is determined only by one angle θ , one squared mass-difference Δm^2 and the relation L/E . From the above equations it is clear that in the two families case there is no CP violation.

1.3.2 In Matter

If neutrinos travel through matter then their evolution can be affected due to their interaction with the particles of the medium [54]. This will be reflected in the evolution

equation through a new effective term associated to the interaction.

Assuming that neutrino interactions are those described by the SM and because there are electrons in normal matter but not muons or taus¹⁵, a beam of ν_e would interact through CC and NC whereas one of ν_μ or ν_τ only through NC. For this reason, the ν_e interaction is different than the $\nu_{\mu,\tau}$ one, neutrino oscillations are affected by the presence of matter.

The CC interaction Hamiltonian density can be written as $\mathcal{H}_{\text{eff}}^{CC} = \frac{4G_F}{\sqrt{2}} J_\mu^{+CC} J^{CC\mu}$ (see Eq. (1.3) and Eq. (1.5)) for energies much lower than the W boson mass. After a Fierz rearrangement to write them as a product of charged currents, we get

$$\mathcal{H}_{\text{eff}}^{CC} = \frac{4G_F}{\sqrt{2}} (\bar{e}\gamma^\mu P_L e) (\bar{\nu}_e \gamma_\mu P_L \nu_e) \quad . \quad (1.59)$$

In order to obtain how the evolution equation in vacuum, Eq. (1.36), will be modified in presence of matter, we have to calculate the matrix elements of the interaction Hamiltonian¹⁶. Now, we should average the electron field bilinear over the background because the electrons in the medium have some distribution associated to some temperature. For a medium at rest composed by non-relativistic and non-polarized electrons and no positrons (e.g. the Earth, and to excellent level of approximation the sun) one has:

$$\langle \bar{e}\gamma_\mu \frac{1-\gamma_5}{2} e \rangle = \frac{n_e}{2} (1, 0, 0, 0)_\mu \quad \text{and therefore} \quad \langle \mathcal{H}_{\text{eff}}^{CC} \rangle = \sqrt{2} G_F n_e (\bar{\nu}_e \gamma_0 P_L \nu_e) \quad (1.60)$$

where n_e is the electron number density. Taking the matrix elements in the neutrino flavour basis, we obtain $(H_{\text{eff}}^{CC})_{\alpha\beta} = \sqrt{2} G_F n_e \delta_{\alpha e} \delta_{\beta e}$. Hence, an ‘effective’ potential energy $\langle H_{\text{eff}}^{CC} \rangle \equiv \langle e\nu_e | H_{\text{eff}}^{CC} | e\nu_e \rangle \simeq \sqrt{2} G_F n_e \equiv A$ will affect the propagation phase of the ν_e .

Then including also the NC-contribution, which can be calculated in a analogous way¹⁷, the effective interaction Hamiltonian density in ordinary matter is

$$\langle \mathcal{H}_{\text{eff}}^{\text{int}} \rangle = A \bar{\nu}_e \gamma_0 P_L \nu_e - A_n \sum_\alpha \bar{\nu}_\alpha \gamma_0 P_L \nu_\alpha \quad , \quad (1.61)$$

where $A_n = \frac{1}{\sqrt{2}} G_F n_n$ and n_n is the neutron number density. Finally, taking the neutrino matrix elements, one obtains that the matter effects modify the Schrödinger

¹⁵We consider neutral ordinary matter made up of electrons, protons and neutrons with densities n_e , $n_p = n_e$ and n_n respectively.

¹⁶Remember that the relation between the Hamiltonian density \mathcal{H} and the Hamiltonian H is: $H = \int d^3x \mathcal{H}$

¹⁷For neutral matter, the NC contribution of electrons and protons cancel each other, remaining only the contribution of neutrons through a n_n dependence.

equation, given in Eq. (1.36), in the following way

$$i \frac{\partial}{\partial t} |\nu_i(t)\rangle = H_{ij} |\nu_j(t)\rangle, \quad (1.62)$$

where

$$H = \begin{bmatrix} \frac{m_1^2}{2E} & 0 & 0 \\ 0 & \frac{m_2^2}{2E} & 0 \\ 0 & 0 & \frac{m_3^2}{2E} \end{bmatrix} + U^t \begin{bmatrix} A & 0 & 0 \\ 0 & 0 & 0 \\ 0 & 0 & 0 \end{bmatrix} U^* - U^t \begin{bmatrix} A_n & 0 & 0 \\ 0 & A_n & 0 \\ 0 & 0 & A_n \end{bmatrix} U^*. \quad (1.63)$$

As it can be seen in the above expression, the evolution equation is no longer diagonal in the mass eigenstates basis. The first term of H is diagonal and corresponds to the free evolution in vacuum. The second and the third ones represent the effect of the CC and NC interaction respectively. These effective potentials are diagonal in the flavour basis but not in the mass basis. Notice that the NC effect disappears from the probability because it is a global phase common to all the flavours $U^t \text{diag}(A_n, A_n, A_n) U^* = A_n \mathcal{I}$ ¹⁸.

For simplicity we will consider the case of mixing between two active neutrinos, ν_e and ν_β ($\beta = \mu$ or τ). Using the parametrization of the mixing matrix given in Eq. (1.57) one obtains

$$i \frac{d}{dt} \begin{pmatrix} \nu_e \\ \nu_\beta \end{pmatrix} = \begin{pmatrix} A - \frac{\Delta m^2}{4E} \cos 2\theta & \frac{\Delta m^2}{4E} \sin 2\theta \\ \frac{\Delta m^2}{4E} \sin 2\theta & \frac{\Delta m^2}{4E} \cos 2\theta \end{pmatrix} \begin{pmatrix} \nu_e \\ \nu_\beta \end{pmatrix} \quad (1.64)$$

In order to obtain the effective mass eigenstates in matter, the eigenstates of the Hamiltonian, we diagonalize the previous Hamiltonian by

$$\begin{pmatrix} \nu_e \\ \nu_\beta \end{pmatrix} = \tilde{U}_{2 \times 2} \begin{pmatrix} \tilde{\nu}_1 \\ \tilde{\nu}_2 \end{pmatrix} = \begin{pmatrix} \cos \tilde{\theta} & \sin \tilde{\theta} \\ -\sin \tilde{\theta} & \cos \tilde{\theta} \end{pmatrix} \begin{pmatrix} \tilde{\nu}_1 \\ \tilde{\nu}_2 \end{pmatrix}, \quad (1.65)$$

where $\tilde{\nu}_i$ are the effective mass eigenstates in matter and $\tilde{\theta}$ ¹⁹ is given by

$$\begin{aligned} \sin 2\tilde{\theta} &= \frac{\sin 2\theta}{\sqrt{\sin^2 2\theta + (x - \cos 2\theta)^2}}, \\ \cos 2\tilde{\theta} &= \frac{-x + \sin 2\theta}{\sqrt{\sin^2 2\theta + (x - \cos 2\theta)^2}}. \end{aligned} \quad (1.66)$$

Calculating the eigenvalues, one obtains the effective mass splitting in matter as

¹⁸However, NC would be relevant for oscillations into sterile neutrinos. Since for these neutrino species no NC interaction is present, the term associated to NC becomes a bigger diagonal matrix with all its 'sterile' elements vanish.

¹⁹The tilde indicates effective mixing parameters in matter, parameters in vacuum have no tilde

$$\Delta\tilde{m}^2 = \Delta m^2 \sqrt{\sin^2 2\theta + (x - \cos 2\theta)^2}, \quad (1.67)$$

where, as in Eq. (1.66) and in Eq. (1.67), x is given by

$$x \equiv \frac{A}{(\Delta m^2)/2E} = \frac{2\sqrt{2}G_F n_e E}{\Delta m^2} \quad (1.68)$$

As it can be seen in these expressions, x is a dimensionless parameter that tells us the relative importance of the matter effects in neutrino oscillations. So, the matter effects in oscillations are proportional to the beam energy and logically to the electron density of the medium. Basically, in present experiments the matter effects are relevant in two cases. The first one is for the most energetic neutrinos of the sun, namely the ^8B neutrinos. The second case is for the long-baseline accelerator experiments as well as the atmospheric neutrino ones. Let us consider, for instance, an accelerator-generated neutrino beam that travels ~ 1000 km between its source and its detector, the electron density n_e encountered will be that of the Earth's mantle. The splitting Δm^2 that will dominate the behavior of such a beam will be the ‘‘atmospheric’’ Δm^2 that also governs the behavior of atmospheric neutrinos, and whose size is approximately $2.5 \times 10^{-3} \text{eV}^2$. Then from Eq. (1.68) it can be deduced that $|x| \simeq \frac{E}{12 \text{GeV}}$. Thus, in a beam with $E = 2$ GeV, the matter effect is modest but not negligible, while in a beam with $E = 20$ GeV, the matter effect is quite large.

Eq. (1.66) shows that even if the vacuum mixing is very small, in principle, there could be an effective maximal mixing in matter ($\sin^2 2\tilde{\theta} = 1$) in the ‘resonance region’, corresponding to an electron density such that $x = \cos 2\theta$ (the so-called Mikheyev-Smirnov-Wolfenstein effect [54–57]). Also is important to note that if we consider antineutrinos instead of neutrinos then the sign of the interaction potential energy A changes in all the expressions ($x \rightarrow -x$). Thus, the effective mixing parameters would be different for antineutrinos than for neutrinos. This has relevant consequences, for instance: if the resonance takes place for neutrinos, then it would not appear for antineutrinos and the other way around. Hence, the matter effects result in very different oscillation patterns for neutrinos and antineutrinos that could help in the mixing parameter measurement.

The evolution equation for the effective massive eigenstates in matter is the following one

$$i \frac{d}{dt} \begin{pmatrix} \tilde{\nu}_1 \\ \tilde{\nu}_2 \end{pmatrix} = \begin{pmatrix} -\frac{\Delta\tilde{m}^2}{4E} & -i \frac{d\tilde{\theta}}{dt} \\ i \frac{d\tilde{\theta}}{dt} & \frac{\Delta\tilde{m}^2}{4E} \end{pmatrix} \begin{pmatrix} \tilde{\nu}_1 \\ \tilde{\nu}_2 \end{pmatrix}, \quad (1.69)$$

with

$$\frac{d\tilde{\theta}}{dt} = \frac{1}{2} \frac{\sin 2\theta}{\sqrt{\sin^2 2\theta + (x - \cos 2\theta)^2}} \frac{dx}{dt}. \quad (1.70)$$

If the electron density n_e is constant, then $\tilde{\theta}$ and $\Delta\tilde{m}^2$ will be constant as well during the neutrino evolution ($\dot{\tilde{\theta}} = 0$). Therefore, the $\tilde{\nu}_i$ would be authentic stationary eigenstates of the evolution. In that case, the transition probability is the same as the vacuum one Eq. (1.58) but with the exchange $\theta \rightarrow \tilde{\theta}$ and $\Delta m^2 \rightarrow \Delta\tilde{m}^2$

$$P_{\nu_e \rightarrow \nu_\beta} = \sin^2 2\tilde{\theta} \sin^2 \left(\frac{\Delta\tilde{m}^2 L}{4E} \right). \quad (1.71)$$

When the density of the medium changes along the neutrino path, the effective mass eigenstates are no longer evolution eigenstates and transitions between them are induced by a non-zero $d\tilde{\theta}/dt$. The transitions between matter mass eigenstates are usually negligible unless the neutrinos are near the resonance layer, for which the diagonal elements in Eq. (1.69) are minimum (see Eq. (1.67)) and $d\theta_m/dt$ is enhanced (see Eq. (1.70)).

If $\Delta\tilde{m}^2 \gg 4E\dot{\tilde{\theta}}$, the $\tilde{\nu}_i$ can be approximately considered as evolution eigenstates, having no transitions between them. This phenomenon is denoted as adiabaticity. What happens is simply that the off-diagonal elements in Eq. (1.69) can be neglected. This adiabaticity condition can be written as

$$\frac{\Delta m^2 \sin^2 2\theta}{2E \cos 2\theta} \gg \frac{1}{A} \frac{dA}{dt} \quad (1.72)$$

So, in the adiabatic regime, the natural frequency of the system is much higher than the potential change rate and therefore the $\tilde{\nu}_i$ almost do not feel the change. This is, for instance, the case for the most energetic neutrinos of the sun: the mentioned ^8B neutrinos.

1.4 Experimental constraints on the three neutrino standard approach

Thanks to the neutrino oscillation experiments we know that neutrinos have masses and, thus, that there is mixing in the lepton sector in the same way as in the quark sector. In the case of the lepton sector, as we have explained above, this mixing is given through the PMNS unitary mixing matrix presented in Eq. (1.56), always in the three family standard approach. The parametrization chosen is the most suitable one according to the results of the oscillation experiments. Basically, we can distinguish two different regimes depending on the oscillation frequency: the solar and the atmospheric ones. In practice, the two family approach (see Eq. (1.58)) works to fit the data in those regimes with some small corrections. Namely, solar experiments allow to measure θ_{12} and Δm_{21}^2 , while those experiments sensitive to the atmospheric regimen can measure θ_{23} and Δm_{31}^2 .

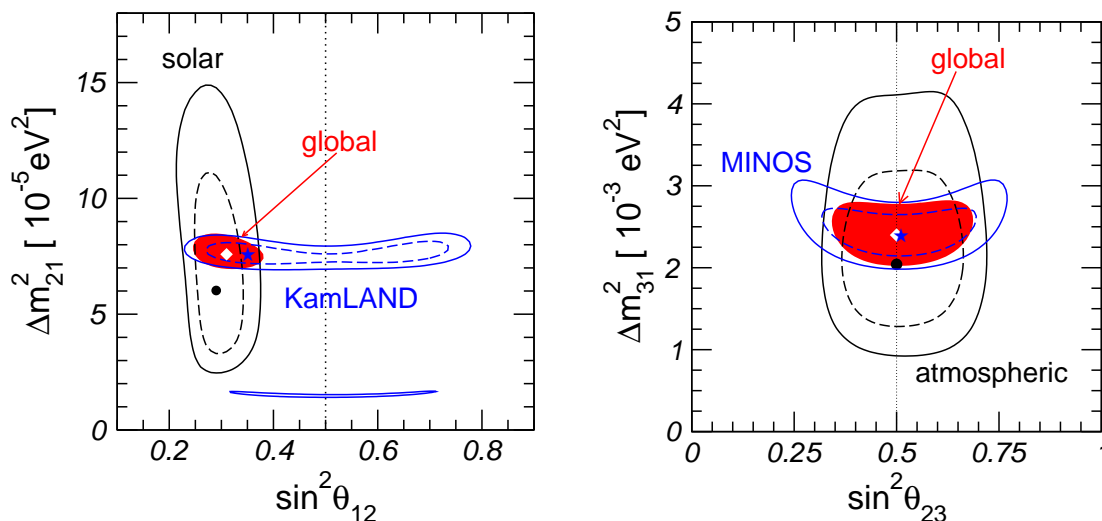


Figure 1.2: Determination of the leading “solar” and “atmospheric” oscillation parameters [61]. It is shown allowed regions at 90% and 99.73% CL (2 dof) for solar and KamLAND (left), and atmospheric and MINOS (right), as well as the 99.73% CL regions for the respective combined analysis.

Fig. 1.2, extracted from Ref [58], shows perfectly what we have just commented. Kamland [42, 59, 60] and the solar oscillation experiments (left panel), both mainly sensitive to the solar regime, give us a clean measurement of the solar parameters: θ_{12} and Δm_{21}^2 . While in the right panel we can see that MINOS [45, 46] and the atmospheric oscillation experiments (sensitive to the atmospheric regime) measure the atmospheric parameters: θ_{23} and Δm_{31}^2 .

The rest of the oscillation parameters are still unknown. In particular, there are upper bounds for θ_{13} but no information at all about the Dirac CP-phase δ . The lack of information on δ is directly related to our ignorance on θ_{13} : for $\theta_{13} = 0$, δ disappears from the oscillation probability (see Eqs. (1.56) and (1.48)) [62]. While, in principle, both atmospheric and solar data are sensitive to θ_{13} , this is only through subdominant terms in the probability. The dominant bound is given by the CHOOZ experiment [39, 40]. CHOOZ is a short baseline ($L \simeq 1$ km) reactor experiment ($E_{\nu_e} \sim$ few MeV) sensitive, thus, to Δm^2 down to 10^{-3} eV² (the atmospheric mass difference):

$$P_{ee} = 1 - \sin^2 2\theta_{13} \sin^2 \frac{\Delta_{31} L}{2} + \mathcal{O}(s_{13}^2 \Delta_{21} L) + \mathcal{O}((\Delta_{21} L)^2), \quad (1.73)$$

where $\Delta_{ij} \equiv \Delta m_{ij}^2 / 2E$. Since CHOOZ does not see atmospheric oscillations it gives an upper bound on θ_{13} , which is suppressing the oscillation as you can see in the probability expression above.

In anycase, the proper way to take into account all the experimental oscillation results is performing a global fit. Two recent global fits to the three family parameters are presented in Refs. [63] and [61]. For another recent analysis see Ref. [64] or, even more recent, [65]. The results are summarized in Table 1.2 [58]:

parameter	Ref. [61]		Ref. [63] (MINOS updated)	
	best fit $\pm 1\sigma$	3σ interval	best fit $\pm 1\sigma$	3σ interval
$\Delta m_{21}^2 [10^{-5}\text{eV}^2]$	$7.65^{+0.23}_{-0.20}$	7.05–8.34	$7.67^{+0.22}_{-0.21}$	7.07–8.34
$\Delta m_{31}^2 [10^{-3}\text{eV}^2]$	$\pm 2.40^{+0.12}_{-0.11}$	$\pm(2.07\text{--}2.75)$	-2.39 ± 0.12 $+2.49 \pm 0.12$	$-(2.02\text{--}2.79)$ $+(2.13\text{--}2.88)$
$\sin^2 \theta_{12}$	$0.304^{+0.022}_{-0.016}$	0.25–0.37	$0.321^{+0.023}_{-0.022}$	0.26–0.40
$\sin^2 \theta_{23}$	$0.50^{+0.07}_{-0.06}$	0.36–0.67	$0.47^{+0.07}_{-0.06}$	0.33–0.64
$\sin^2 \theta_{13}$	$0.01^{+0.016}_{-0.011}$	≤ 0.056	0.003 ± 0.015	≤ 0.049

Table 1.2: *Determination of three-flavour neutrino oscillation parameters from 2008 global data [61, 63].*

Let us summarize which is the still unknown information in the leptonic mixing matrix.

- The values of θ_{13} and the CP-violating Dirac phase δ remain unknown. To be precise, this is not exactly true: there are some hints for a non-zero value of θ_{13} . The statistical significance of this results is very low (around 1σ) as it can be seen in Tab 1.2. However we should remark that there is some tension between low and high energy solar neutrino data, as well as between solar and Kamland data, which points to this non-zero value of θ_{13} . A similar tension appears when one combines data from atmospheric neutrinos, CHOOZ and long baseline accelerator data (for a more detailed discussion see Ref. [65]). However there is still no information at all about δ . In any case, a clear observation of the three non-zero mixing angles is necessary to find CP violation. Therefore a precise measurement of θ_{13} is necessary in order to find a possible CP-violating phase.
- The ordering of the neutrino spectrum. Due to the present lack of knowledge on the sign of Δm_{31}^2 , the two possible patterns of neutrino masses compatible with $|\Delta m_{21}^2| \ll |\Delta m_{31}^2|$ cannot be distinguished.
 - *Normal hierarchy:* $m_3 \gg m_2 > m_1$
 - *Inverse hierarchy:* $m_2 > m_1 \gg m_3$

as illustrated in Fig. 1.3.

The matter effects present in future long baseline experiments will help to disentangle between the above patterns of neutrino masses.

- The absolute scale of neutrino masses. Notice that, if this scale is of the order of (or much larger than) the mass differences, then $m_1 \simeq m_2 \simeq m_3$ and the spectrum is called *quasi-degenerate*, while otherwise is called *hierarchical*.

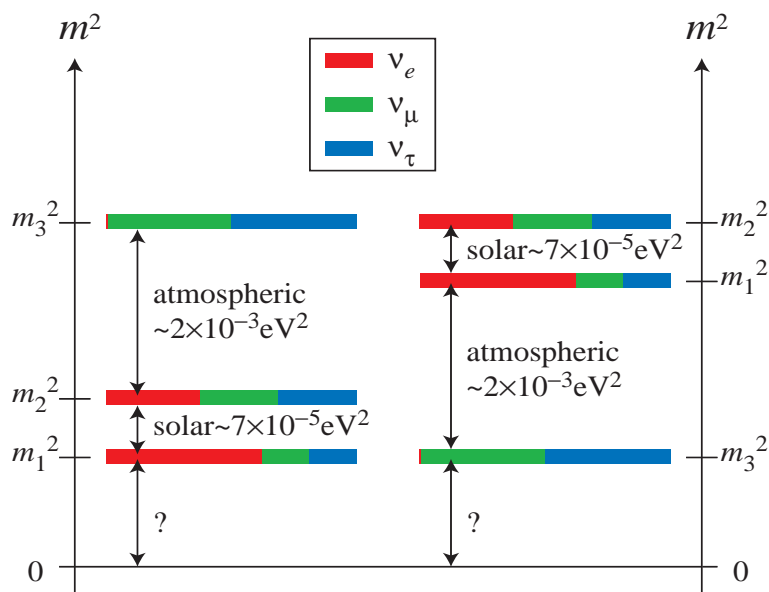


Figure 1.3: Neutrino mass patterns as indicated by the current data (figure extracted from [66]). The left hand diagram shows normal spectrum and the right hand side, an inverse spectrum.

- Finally, the fundamental question about whether neutrinos are Dirac or Majorana particles is still open. This is not an unknown parameter but is a fundamental question from the theoretical point of view. Most of the neutrino mass models work in the hypothesis that the neutrinos are Majorana particles.

1.4.1 Searching the absolute neutrino mass scale

The answer to the last two questions presented just above may also illuminate the origin of the neutrino masses. Nevertheless, as we have already pointed out, neutrino oscillation experiments cannot address these questions.

Upper bounds on the absolute neutrino masses can be inferred from cosmological analysis. The spectacular advance that the observational cosmology has lived in the last years has been translated into in more and more accurate constraints on the sum of the light neutrino masses. On the other hand, several cosmological analysis found different upper bounds on neutrino masses, since they depend on: the combination of cosmological data used; the assumed cosmological model (the number of parameters, related to the problem of parameter degeneracies); and the properties of relic neutrinos. A recent bound, assuming the Λ CDM model, combining the 7-year WMAP data with the latest distance measurements from the Baryon Acoustic Oscillations (BAO) and the Hubble constant (H_0) measurement gives [67]:

$$\sum_{light} m_i < 0.58 \text{ eV}. \quad (1.74)$$

Unfortunately we do not have an actual value yet. In any case, these cosmological bounds should be considered carefully. In addition to the dependence on the combination of data used and the assumed cosmological model, there are some general assumptions in the way in which bounds are obtained, for instance: neutrinos involved in Eq. (1.74) have to be in thermal equilibrium with the rest of the matter²⁰.

The *neutrinoless double beta decay* is also sensitive (through another parameter combination) to the absolute neutrino masses and, at the same time, the most promising way to determine if neutrinos have Dirac or Majorana nature. It consists of

$$(A, Z) \rightarrow (A, Z + 2) + e^- + e^- . \quad (1.75)$$

The process in Eq. (1.75) is interpreted as mediated by an Majorana neutrino, as illustrated in Fig. 1.4. This process has not been observed yet²¹ giving only upper bounds in the combination of parameters $|\sum_i U_{ei} m_i|$, as those presented in Ref. [71]:

$$|m_{ee}| = \left| \sum_i U_{ei} m_i \right| < (0.19 - 0.68) \text{ eV} \text{ (C.L. = 90\%)} . \quad (1.76)$$

Notice that this constraint does not always apply. For instance, a neutrino model as those described by the lagrangian given in Eq. (1.13), but with light Majorana masses (below ~ 100 MeV) would give a totally negligible contribution to this process [72]. In the literature the existence of NP at higher energies, as the different *seesaw* models case, is always implicitly assumed. New projects such as CUORE [73], EXO [74], NEXT [75], Super-NEMO [76] or MAJORANA [77] expect to improve the sensitivity up to $|m_{ee}| \simeq 10^{-2}$ eV.

In addition, there are other experiments which could help us in the search of the absolute neutrino mass. The “traditional way” to obtain constrains in the absolute neutrino masses is through kinematic studies of well known processes which involve charged particles emitted together with neutrinos -or antineutrinos. These analysis set an upper bound on the *effective flavour mass*:

$$m_{\nu_\alpha}^2 \equiv \sum_i |U_{\alpha i}|^2 m_i^2 , \quad (1.77)$$

The most sensitive limits to these *effective flavour masses* are:

²⁰For a review about how massive neutrinos affect the evolution of cosmological perturbations, a summary of the cosmological bounds on neutrino masses (not updated) and a discussion about how the future cosmological experiments are expected to be sensitive to them, see Ref. [68].

²¹We will ignore here the controversial claim of the discovery of neutrinoless double beta decay by the Moscow-Heidelberg collaboration [69, 70].

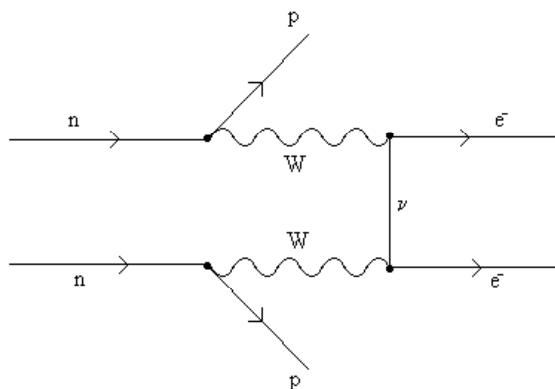


Figure 1.4: Feynman diagram of the neutrino-less double beta decay

$$\begin{array}{lll}
 m_{\nu_e} < & 2 \text{ eV} & \text{from } {}^3H \rightarrow {}^3He + e + \bar{\nu}_e \text{ [12] ,} \\
 m_{\nu_\mu} < & 0.190 \text{ MeV} & \text{from } \pi^+ \rightarrow \mu^+ \nu_\mu \text{ [12] ,} \\
 m_{\nu_\tau} < & 18.2 \text{ MeV} & \text{from } \tau^+ \rightarrow \pi^+ \nu_\tau \text{ [12] ,}
 \end{array}$$

1.4.2 Future neutrino oscillation facilities

On the other hand, in order to disentangle between normal and inverted mass orderings, to measure θ_{13} and search for CP violation in the leptonic sector, a new generation of neutrino oscillation experiments is needed. Different options are presently under study. Basically one can distinguish between the following future experiments, depending on the type of neutrino sources that they plan to use:

- **Reactors**

A new generation of reactor experiments is being planned, that will help to measure accurately the mixing parameters. In fact, reactor experiments generically study the $\bar{\nu}_e \rightarrow \bar{\nu}_e$ disappearance channel which is not sensitive to δ or the mass hierarchy, but it can give rise a clean measurement of θ_{13} free of degeneracy problems (see Eq. 1.73). Indeed, the present constraint on θ_{13} comes from the CHOOZ reactor experiment, which is basically limited by the systematic errors due to the flux uncertainties. So reducing the systematics (the flux uncertainties) a better upper bound can be obtained. For this purpose a near detector, identical to the far one, that would measure the neutrino flux coming from the reactor, will be built. Computing the ratio of the far and near rates many systematic uncertainties would cancel. That is the proposal of, for instance, Double-CHOOZ [78] which could improve the sensitivity of CHOOZ to $\sin^2 \theta_{13} < 0.006$.

- **Super-Beams**

The “Super-Beam” refers to (anti) muon-neutrino beam facilities, based on conventional neutrino beams from pion decays (such as MINOS) in conjunction with higher proton intensity (MWatt beam power) and large neutrino detector(s). In this case, $\nu_\mu \rightarrow \nu_\mu$ and $\nu_\mu \rightarrow \nu_e$ can be studied. In case of the golden channel $\nu_\mu \rightarrow \nu_e$ channel [79], the main one in order to study CP violation, the principal limitation is that it is difficult to achieve low electron neutrino contamination, mostly from muon and kaon decays, less than 0.5%. The advantages are that the technology and problems are well understood. Two options are wide band beam (on-axis beam) and narrow band beam (off-axis beam). The last one, which tilts the beam axis a few degrees with respect to the position of the far detector, is an interesting possibility because the beam is narrower, has lower energy and a smaller ν_e contamination, although the neutrino flux can be significantly smaller. Two examples of this kind of next generation experiments are T2K [80] at J-PARC (Japan Proton Accelerator Research Complex) and NO ν A [81] at Fermilab.

- **β -Beams**

The “ β -Beam” is a future neutrino facility proposed in Ref. [82] which would produce pure and intense (anti) electron neutrino beams, by accelerating radioactive ions and storing them in a km-scale decay ring in short enough bunches to suppress the atmospheric neutrino backgrounds. Then, the resulting β -Beam would be virtually background free and fluxes could be easily computed by the properties of the beta decay of the parent ion and by its Lorentz boost factor γ . Since the beam energy depends on this γ factor, the ion accelerator can be tuned to optimize the sensitivity of the experiment. The “standard” ion candidates so far are ^{18}Ne and ^6He for ν_e and $\bar{\nu}_e$ respectively [82–84]. However, there have been some recent studies [85–88] which propose to use other ions such as ^8Li and ^8B . In contrast with Super-Beams, β -Beam experiments basically search for $\nu_e \rightarrow \nu_\mu$ transitions, requiring a detector capable to identify muons from electrons. On the other hand, since the beam does not contain ν_μ or $\bar{\nu}_\mu$ in the initial state, magnetized detectors are not needed. This is in contrast with the neutrino factories (see below) where the determination of the muon sign is mandatory. A β -Beam Design Study appears as a part of EURISOL [89] Design Study (EURISOL is a project to aim a next-generation facility for on-line production of radioactive isotopes).

- **Neutrino Factory**

A Neutrino Factory (NF) [90,91] is a machine which would exploit muon decays ($\mu^+ \rightarrow e^+ \nu_e \bar{\nu}_\mu$ and $\mu^- \rightarrow e^- \bar{\nu}_e \nu_\mu$ with $E_\mu \sim 25 \text{ GeV}$) as source to obtain a neutrino beam²². The NF beam is produced by circulating μ^- or μ^+ beams in accumulators with large straight sections (the muon life time is quite larger than the pion one), but still smaller than the β -beam rings. Since the neutrino beam

²²At present a low-energy alternative is being discussed as well [92,93].

comes from a single decay mode it has less beam backgrounds than in the Super-Beam case and a well defined kinematics. The energy and flavour spectra of a ν -factory beam is easily and accurately computed. Finally, conventional neutrino beams from π^- (or π^+) decays are dominantly composed by $\bar{\nu}_\mu$ (or ν_μ). On the contrary, a neutrino beam produced by decays of μ^- (or μ^+) consists of $\nu_\mu + \bar{\nu}_e$ (or $\bar{\nu}_\mu + \nu_e$). So, the main advantages of the NF are:

- It is a very intense neutrino source with low backgrounds.
- Precise knowledge on neutrino flux.
- Both muon (anti-)neutrinos and electron (anti-)neutrinos are available. The high energy NF version has enough energy to study oscillations into ν_τ . Many oscillation channels are in principle available.

NF disadvantages are:

- The determination of (θ_{13}, δ) is not free of ambiguities [94–97]. The degeneracy problem is more severe in a NF than in Super-Beams or β -Beams because matter effects can mimic CP violation. However one can take advantage of the matter effects, using two appropriate baselines, to solve this problem [94], measuring at the same time the sign of Δm_{31}^2 . Considering only one baseline but different oscillation channels can give similar effects [98].
- The previous point could lead to a more demanding NF setup from the economical and experimental point of view. In addition, the muon manipulation, acceleration and storage will require the development of novel machines in high energy physics accelerators with a consequent long timescale.

In the rest of the thesis, when we study the sensitivity of future neutrino oscillation experiments to different NP sources, we will always be focused on the NF option because of several reasons. The most evident one is our interest into the study of the $\nu_\mu \rightarrow \nu_\tau$ channel. We will show that it could be a very interesting tool in order to study new sources of CP violation associated to NP. On the other hand, one can take advantage of the impressive statistics that the NF could achieve and of the different studies available concerning all the NF details, not only on the physics side but also in the experimental one. The community has been organized conforming the *International Scoping Study for a future Neutrino Factory and Super-Beam facility* (ISS) [99], which prepared a complete review of the NF (and their competitors) status at 2007. The present continuation of that working group is the *International Design Study* (IDS) [99, 100].

Chapter 2

Minimal Unitarity Violation

In the previous chapter it was shown that non-zero neutrino masses could be considered as a signal of physics beyond the SM, and its smallness interpreted as the existence of New Physics (NP) at higher scales. Within this hypothesis, the new scale M associated to the NP, is likely to be much higher than the electroweak scale. When $M \gg M_Z$, the effects of NP at the high energy scale can be parametrized at low energies, without loss of generality, by an effective lagrangian including:

- Corrections to the parameters of the SM lagrangian.
- The addition to the SM lagrangian of a set of *non-renormalizable* -with mass dimension greater than four- effective operators, which are $SU(3) \times SU(2)_L \times U_Y(1)$ gauge invariant. Their coefficients are suppressed by inverse powers of the large energy scale M .

The relative intensity of the different higher-dimensional effective operators is model-dependent. The SM couplings are expected to be generically modified, thus, in any scenario involving NP at high energy. We concentrate on modifications to those couplings in the present chapter and the next one.

Among the SM couplings, the PMNS mixing matrix is introduced in connection with charged current interactions of leptons by Eq. (1.30). Its departure from the unit matrix is the origin of the leptonic mixing and putative CP violation effects in neutrino physics, which are essential building blocks of the flavour puzzle. In typical analysis of experimental data, the mixing matrix is assumed to be unitary.

The complete lagrangian including NP is necessarily unitary and the probability is conserved. However, unitarity violation of the leptonic mixing matrix¹ is one typical low-energy signal of models of NP related with the generation of the observed small neutrino masses, though, when data are analysed at low energies in the framework of

¹Along this work, we will talk generically about unitarity violation always referring to deviations from unitarity of the leptonic mixing matrix, not to the unitarity of the theory.

the SM gauge group, with three light species of quarks, leptons and neutrinos, plus mass terms for the latter. For instance, any theory in which the neutrino mass matrix turns out to be part of a larger matrix, which involves heavy fields, may generically result in an effective low-energy non-unitary mixing matrix for the light leptonic fields [101–104, 104–110]. A paradigmatic example is the type-I seesaw model (see Sec. 1.2.1). In it, light neutrino masses take natural (i.e. non-fine-tuned) values, in contrast to all other fermion masses except the top quark mass. Heavy sterile (right-handed) neutrinos, with masses far above the electroweak scale, are introduced at the new high energy scale. Although the non-unitary mixing induced at low energies in the canonical -type I- seesaw model is typically expected to be too small for detection, this is not necessarily true for variants of the seesaw mechanism [111], or other theories beyond the SM.

Notice that deviations from unitarity of the CKM matrix, the analogous matrix in the quark sector, are considered a good window for physics beyond the SM and extensively studied. Similarly to the case of B-factories and Super B-factories, that will provide precision measurements of the CKM matrix element to search for NP, we are about to enter an era of high precision neutrino physics. With on-going and forthcoming experiments, as well as the future facilities under discussion, future neutrino oscillation experiments will be aiming at a measurement of the last unknown leptonic mixing angle θ_{13} , the sign of Δm_{31}^2 , as well as of leptonic CP violation (see Sec. 1.4.2). It is pertinent to ask whether such precision can shed further light on unitarity. Departures from it would probe the NP behind.

In this chapter we thus relax the assumption of unitarity in the low-energy leptonic mixing matrix of weak interactions, and let data rather freely tell us up to what point the measured elements of the mixing matrix arrange themselves in a unitary pattern. This will allow to identify the less constrained windows in flavour space and thus the most sensitive ones, as regards NP.

We will not work in any concrete model of neutrino masses. Nevertheless, as only neutrino masses clearly signal NP -in contrast to masses for charged leptons or the rest of the fermions-, it is plausible that the NP behind sneaks through at low energies primarily through its effects on neutrino sector. That is, in this work we implicitly assume that the physics of fields other than neutrinos will be that of the SM. We can summarize then our approximations on a set-up that we will dub **Minimal Unitarity Violation (MUV)**, based on the following assumptions:

- Sources of non-unitarity are allowed in those terms in the SM lagrangian which involve neutrinos.
- Only three light neutrino species are considered.

Leptonic and semileptonic decays, together with neutrino oscillations, will be analysed in this minimal set-up. Supplementary non-unitary contributions to physical transitions can result from NP affecting other SM couplings, for fields other than neutrinos and/or higher-dimensional operators in the effective lagrangian. Generically,

deviations from unitarity at low energies are induced whenever heavy fermions are involved, but could affect not only to the neutrino couplings but also, for instance, to the charged lepton ones which would give stronger constraints on the NP parameters [18]. The results obtained in our minimal analysis can be considered at least as conservative bounds on models of NP which, in addition to unitarity deviations affecting to the neutrino couplings, can give other effects not contemplated in the MUV scheme.

This chapter is organized as follows: Sec. 2.1 defines the framework and introduces the non-unitary mixing matrix N which replaces the unitary PMNS matrix U . In Sec. 2.2, a formalism is developed for the study of neutrino oscillations in vacuum and matter, with non-unitary leptonic mixing. Secs. 2.3 and 2.4 deal with data re-analysed in the MUV scheme: data from neutrino oscillation experiments are considered in Sec. 2.3 and the mixing matrix resulting from their analysis is obtained, while the unitarity constraints resulting from W and Z -decay data, lepton universality tests and rare charged lepton decays are presented in Sec. 2.4. The final mixing matrix resulting from the combination of oscillation and weak decays data is presented in Sec. 2.5. In Sec. 2.6, an overview of the future experiments impact on the results obtained in the previous sections is presented. All the results shown in this chapter come from Ref. [112].

2.1 The effective lagrangian

A pertinent question is whether there exists a $SU(2)_L \times U_Y(1)$ invariant formulation of the MUV scheme described above, as it should be. Consider a generic effective lagrangian valid at energies less than a high scale M of NP, $M \gg M_Z$, resulting after integrating out the heavy fields present above such scale. The effective lagrangian has a power series expansion in $1/M$ of the form

$$\mathcal{L}^{eff} = \mathcal{L}_{SM} + \delta\mathcal{L}^{d=5} + \delta\mathcal{L}^{d=6} + \dots, \quad (2.1)$$

where \mathcal{L}_{SM} contains all $SU(3) \times SU(2)_L \times U_Y(1)$ invariant operators of dimension $d \leq 4$ and the gauge invariant operators of $d > 4$, constructed from the SM fields, account for the physics effects of the heavy fields at energies $< M$. After EWSB, the operators with $d > 4$ will give corrections to the couplings present in the SM lagrangian *and* also produce new exotic couplings.

Is there this $SU(2)_L \times U_Y(1)$ gauge invariant formulation of the lagrangian which gives rise, after EWSB, to deviations from unitarity of the leptonic mixing matrix at low energies? The answer is affirmative indeed. There exists a $d = 6$ gauge invariant operator which precisely results in corrections to the unitary leptonic mixing. It is the operator characteristic of the canonical seesaw model [17]², and also of some extra-

²In addition to the well-known and already mentioned $d = 5$ operator responsible for neutrino masses, $\delta\mathcal{L}^{d=5} = \frac{1}{2} c_{\alpha\beta}^{d=5} \left(\overline{L}_\alpha^c \tilde{\phi}^* \right) \left(\tilde{\phi}^\dagger L_\beta \right) + h.c.$, where $c_{\alpha\beta}^{d=5}$ is the coefficient matrix of $\mathcal{O}(1/M)$.

dimensional constructions [113, 114],

$$\delta\mathcal{L}^{d=6} = c_{\alpha\beta}^{d=6} \left(\bar{L}_\alpha \tilde{\phi} \right) i\rlap{-}/\partial \left(\tilde{\phi}^\dagger L_\beta \right), \quad (2.2)$$

where L denotes left-handed leptonic doublets³, $c^{d=6}$ is the -model dependent- coefficient matrix of $\mathcal{O}(1/M^2)$ and $\tilde{\phi}$ is related to the standard Higgs doublet ϕ by $\tilde{\phi} = i\tau_2\phi^*$. After the EWSB, this operator results in corrections to the neutrino kinetic term in the flavour basis. This is the key point to obtain deviations from unitarity as we will see immediately. The MUV scheme effective lagrangian in the flavour basis is given, thus, by:

$$\begin{aligned} \mathcal{L}^{eff} = & \frac{1}{2} (i\bar{\nu}_\alpha \rlap{-}/\partial k_{\alpha\beta} \nu_\beta - \bar{\nu}_\alpha^c m_{\alpha\beta} \nu_\beta + h.c.) - \frac{g}{2\sqrt{2}} (W_\mu^- \bar{l}_\alpha \gamma^\mu (1 - \gamma_5) \nu_\alpha + h.c.) \\ & - \frac{g}{2\cos\theta_W} (Z_\mu \bar{\nu}_\alpha \gamma^\mu (1 - \gamma_5) \nu_\alpha + h.c.) + \dots, \end{aligned} \quad (2.3)$$

In this basis, we have a general non-diagonal kinetic and neutrino mass terms ($k_{\alpha\beta}$ and $m_{\alpha\beta}$ are both non-diagonal matrices after the correction of the dimension 6 operator) while weak couplings remain diagonal. However, these kinetic and mass terms do not have the canonical form. Therefore, in order to have a well defined description of the neutrino kinematic properties, we need to transform the neutrino fields in such a way that canonical kinetic and mass terms are obtained. A neutrino mass term can always be diagonalized by a unitary transformation (or bi-unitary in the case of Dirac neutrinos), leading to a unitary contribution to the mixing matrix, as in the standard treatment. Kinetic terms must be both diagonalized *and normalized* in order to obtain canonical kinetic energies. These hypothetical different normalizations, induced in the kinetic energy of neutrino fields by the NP, is essential to obtain non-unitarity effects in neutrino mixing. Whenever at least two normalizations of neutrino fields differ, a general non-unitary weak mixing matrix N follows, connecting the quantum fields in the flavour basis with those in the mass basis,

$$\nu_\alpha = N_{\alpha i} \nu_i. \quad (2.4)$$

After the diagonalization through the above transformation we obtain the following lagrangian in the mass basis:

$$\begin{aligned} \mathcal{L}^{eff} = & \frac{1}{2} (\bar{\nu}_i \rlap{-}/\partial \nu_i - \bar{\nu}_i^c m_i \nu_i + h.c.) - \frac{g}{2\sqrt{2}} (W_\mu^- \bar{l}_\alpha \gamma_\mu (1 - \gamma_5) N_{\alpha i} \nu_i + h.c.) \\ & - \frac{g}{2\cos\theta_W} (Z_\mu \bar{\nu}_i \gamma^\mu (1 - \gamma_5) (N^\dagger N)_{ij} \nu_j + h.c.) + \dots, \end{aligned} \quad (2.5)$$

³As the factors in parenthesis in this equation are singlets of $SU(2)_L \times U_Y(1)$, $\rlap{-}/\partial$ is tantamount to $\rlap{-}/\partial$ in this operator.

where ν_i denotes four-component left-handed fields. Eq. (2.5) is the usual lagrangian for neutrinos in the mass basis, albeit with the unitary matrix U_{PMNS} in the charged current substituted by a general non-unitary matrix N . The neutral current coupling has been modified as well, in such a way that all the mixing appear in the neutrino couplings through a unique mixing matrix N . Notice that the lagrangian includes a Majorana mass term for neutrinos, for the sake of definiteness, although for our numerical analysis below it would make no difference to consider neutrinos of the Dirac type.

Aside the effective operator given in Eq. (2.2), other $SU(2)_L \times U_Y(1)$ invariant operators, may be written as well, resulting generically -after EWSB- in corrections to both the neutrino and charged leptons kinetic energy. That is exactly the case of the type-III seesaw model [18], where these corrections to both lagrangian kinetic terms give rise not only to corrections to the charged current and neutral current couplings which involve neutrinos, but also to the neutral current coupling of the charged leptons. There exist even $SU(2)_L \times U_Y(1)$ invariant operators contributing to the charged lepton kinetic energy and not to that of neutrinos, such as

$$\delta\mathcal{L}^{d=6} = c'_{\alpha\beta}{}^{d=6} (\bar{L}_\alpha\phi) i\cancel{D}(\phi^\dagger L_\beta), \quad (2.6)$$

with $c'^{d=6}$ being the coefficient matrix of order $\mathcal{O}(1/M^2)$. Theories with Yukawa couplings to heavy extra fermions -be it of Dirac or Majorana type- can easily give rise to such effective couplings at low energy. Such an operator leads -after EWSB- to a lagrangian with the same couplings to the W boson as in Eq. (2.5), albeit with corrections in the Z -charged lepton couplings instead of in the Z -neutrino ones. It means that all results obtained below from W exchange alone would also hold for the purpose of constraining such theories.

In summary, a generic model is expected to give rise after EWSB to modifications of the standard couplings, as well as new exotic ones. In the minimal scheme analysed in this work, MUV, only the former will be taken into account and more precisely only those couplings involving neutrinos as specified above. This simplification should provide a sensible estimation of the best windows for non-unitarity (after the publication of Refs. [112,115] this subject has been object of the interest of the community dedicated to the BSM searches in the leptonic sector, see for instance Refs. [116–118]). Since the MUV scheme is a model-independent approach, the prize we have to pay is that the bounds derived here have to be considered as conservative constraints. When a concrete model is studied the bounds can be stronger due to additional effects which do not only involve neutrino couplings but, for instance, also the charged leptons neutral current coupling (as in the type-III seesaw) or other SM couplings. Particularly, the type-I seesaw is the model which fits better to the MUV scheme. However, even in that case, once the low energy data are analysed in the specific framework of the type-I seesaw model the bounds derived slightly differ from the ones presented along this thesis.

Non-unitary mixing matrix

It is necessary to clarify the relation between mass and flavour eigenstates. When considering a unitary rotation from the flavour to the mass basis, the corresponding quantum states basis are both mutually orthonormal. This is no longer true when the rotation is performed through a non-unitary matrix N , as it is the case in the MUV scheme. As we have shown above, N connects the quantum fields in the mass basis with those in the flavour basis where the weak couplings are diagonal through the following relation:

$$\nu_\alpha = N_{\alpha i} \nu_i. \quad (2.7)$$

While the canonical kinetic and mass terms in Eq. (2.5) give rise to orthonormal mass eigenstates,

$$\langle \nu_i | \nu_j \rangle = \delta_{ij}, \quad (2.8)$$

consistency between quantum states and fields requires the identification [119]

$$|\nu_\alpha\rangle = \frac{1}{\sqrt{(NN^\dagger)_{\alpha\alpha}}} \sum_i N_{\alpha i}^* |\nu_i\rangle \equiv \sum_i \tilde{N}_{\alpha i}^* |\nu_i\rangle, \quad (2.9)$$

where, on the right-hand side, the normalization factor has been absorbed in the definition of \tilde{N} . It follows from Eq. (2.9) that flavour eigenstates are no more orthogonal⁴:

$$\langle \nu_\beta | \nu_\alpha \rangle = (\tilde{N}\tilde{N}^\dagger)_{\beta\alpha} \neq \delta_{\alpha\beta}, \quad (2.10)$$

which will induce relevant physical effects, as it will be shown later on.

Prior to any predictions for physical transitions, it has to be remarked that the physical constants of the lagrangian are extracted from the experimental data. Therefore, it is important to take into account that the lagrangian expression is no longer the one of the SM when extracting the physical parameters from experiments. In particular, the weak coupling in Eq. (2.5) differs from the SM expression. Accordingly, the Fermi constant measured from the muon decay data G_μ can not be identified anymore with the SM one $G_F = \sqrt{2}g^2/(8M_W^2)$, due to non-unitarity. The Fermi constant G_μ extracted from the decay $\mu \rightarrow \nu_\mu e \bar{\nu}_e$ is related to G_F by⁵

$$G_F = \frac{G_\mu}{\sqrt{(NN^\dagger)_{ee}(NN^\dagger)_{\mu\mu}}}. \quad (2.11)$$

The rest of the parameters of the lagrangian coincide with those in the standard treatment.

⁴Notice that these are effective low-energy flavour eigenstates. In the corresponding complete -high energy- hypothetical theory, it should be possible to define an orthonormal flavour basis.

⁵The Fermi constant can be measured through other processes as hadronic ones, but the muon decay is usually considered because it is the most precise option.

2.2 Neutrino oscillations without unitarity

Let us consider now the impact of the lagrangian in Eq. (2.5) on neutrino oscillations, both in vacuum and in matter.

2.2.1 Vacuum oscillations

Consider free neutrino propagation, described by the free Hamiltonian \hat{H}^{free} , resulting from the first two terms in the lagrangian, Eq. (2.5). The time evolution of mass eigenstates follows the usual pattern. Indeed,

$$i\frac{d}{dt}|\nu_i\rangle = \hat{H}^{free}|\nu_i\rangle \quad (2.12)$$

and because of the orthogonality of the mass basis,

$$\langle\nu_j|\hat{H}^{free}|\nu_i\rangle \equiv \delta_{ij} E_i, \quad (2.13)$$

where E_i are the eigenvalues. Using now the completeness relation in the mass basis, $\sum_j |\nu_j\rangle\langle\nu_j| = 1$ ⁶, Eq. (2.12) reads:

$$i\frac{d}{dt}|\nu_i\rangle = \sum_j |\nu_j\rangle\langle\nu_j|\hat{H}^{free}|\nu_i\rangle = E_i|\nu_i\rangle, \quad (2.14)$$

which is the usual time propagation for free states.

Consider now instead the free evolution in the flavour basis, which is *not* orthonormal and for which there is not the usual completeness relation, as $\sum_\alpha |\nu_\alpha\rangle\langle\nu_\alpha| \neq 1$. The time evolution is given by

$$i\frac{d}{dt}|\nu_\alpha\rangle = \hat{H}^{free}|\nu_\alpha\rangle, \quad (2.15)$$

which, using the orthogonality and completeness of the mass basis, results into

$$i\frac{d}{dt}|\nu_\alpha\rangle = \sum_j |\nu_j\rangle\langle\nu_j|\hat{H}^{free}|\nu_\alpha\rangle = \sum_\beta (\tilde{N}^* E (\tilde{N}^*)^{-1})_{\alpha\beta} |\nu_\beta\rangle, \quad (2.16)$$

where $E \equiv \text{diag}(E_1, E_2, E_3)$. This is to be compared with the N -dependence of the matrix elements between flavour eigenstates, given by

$$\langle\nu_\beta|\hat{H}^{free}|\nu_\alpha\rangle = (\tilde{N}^* E \tilde{N}^t)_{\alpha\beta}. \quad (2.17)$$

⁶In fact, this relation is only a consequence of the orthonormality of the mass basis Eq. (2.8). The flavour basis is also complete (we assume implicitly that $\det N \neq 0$) but not orthonormal, for this reason the relation does not hold for flavour states.

That is, the evolution in flavour space is driven by the combination $(\tilde{N}^* E (\tilde{N}^*)^{-1})$ and **not** by the product $(\tilde{N}^* E \tilde{N}^t)$ appearing in Eq. (2.17), in contrast to the customary expression in standard -unitary- treatments. Because of the non-unitarity of N both expressions are no more equivalent. Technically, this is a key point in the different results for the non-standard case, to be obtained below.

Notice, moreover, that the combination $(\tilde{N}^* E (\tilde{N}^*)^{-1})$ is not Hermitian, even if the free Hamiltonian itself is Hermitian. This in turn implies that the evolution of flavour bra states, $\langle \nu_\alpha |$, differs from the evolution of the flavour kets, but leading both to the same probability equation, as they should.

The analysis of free propagation in space is analogous to that for time evolution described above and we will not repeat it in detail (for a detailed analysis in the unitary case see Sec. 1.3.1). Flavour eigenstates, after a distance L , transform into

$$|\nu_\alpha(L)\rangle = \sum_{i\gamma} \tilde{N}_{\alpha i}^* e^{i P_i L} (\tilde{N}^*)_{i\gamma}^{-1} |\nu_\gamma\rangle, \quad (2.18)$$

where P_i are the momentum eigenvalues, $P_i = \sqrt{E_i^2 - m_i^2}$. The oscillation probability after travelling a distance L can now be obtained,

$$\begin{aligned} P_{\nu_\alpha \rightarrow \nu_\beta}(E, L) &\equiv |\langle \nu_\beta | \nu_\alpha(L) \rangle|^2 = \frac{|\sum_i N_{\alpha i}^* e^{i P_i L} N_{\beta i}|^2}{(NN^\dagger)_{\alpha\alpha} (NN^\dagger)_{\beta\beta}} = \\ &= \frac{1}{(NN^\dagger)_{\alpha\alpha} (NN^\dagger)_{\beta\beta}} \left[(NN^\dagger)_{\alpha\alpha} (NN^\dagger)_{\beta\beta} + \right. \\ &\quad + 2 \operatorname{Re} \{ N_{\alpha 1} N_{\alpha 2}^* N_{\beta 1}^* N_{\beta 2} \} \cos(\Delta_{21} L) - 2 \operatorname{Im} \{ N_{\alpha 1} N_{\alpha 2}^* N_{\beta 1}^* N_{\beta 2} \} \sin(\Delta_{21} L) \\ &\quad + 2 \operatorname{Re} \{ N_{\alpha 2} N_{\alpha 3}^* N_{\beta 2}^* N_{\beta 3} \} \cos(\Delta_{32} L) - 2 \operatorname{Im} \{ N_{\alpha 2} N_{\alpha 3}^* N_{\beta 2}^* N_{\beta 3} \} \sin(\Delta_{32} L) \\ &\quad \left. + 2 \operatorname{Re} \{ N_{\alpha 1} N_{\alpha 3}^* N_{\beta 1}^* N_{\beta 3} \} \cos(\Delta_{31} L) - 2 \operatorname{Im} \{ N_{\alpha 1} N_{\alpha 3}^* N_{\beta 1}^* N_{\beta 3} \} \sin(\Delta_{31} L) \right], \end{aligned} \quad (2.19)$$

where $\Delta_{ij} = \Delta m_{ij}^2 / 2E$, with $\Delta m_{ij}^2 = m_i^2 - m_j^2$, as usual. Written in this way, the expression is easily seen to reduce to the standard one if N was unitary, as it should.

The first very important consequence of Eq. (2.19) is that the non-unitarity of N is shown to generate a “zero-distance” effect [101], i.e. a flavour transition already at the source before oscillations can take place (directly a consequence of Eq. (2.10)). Indeed, for $L = 0$, it follows that

$$P_{\nu_\alpha \rightarrow \nu_\beta}(E, L = 0) = \frac{|(NN^\dagger)_{\beta\alpha}|^2}{(NN^\dagger)_{\beta\beta} (NN^\dagger)_{\alpha\alpha}} \neq 0, \quad (2.20)$$

an effect that can be tested in near detectors, thus setting strong limits on unitarity as we will see later. Nevertheless, due to non-unitarity, the probability as defined in Eq. (2.19) does not sum up to a total probability of 100%. This behaviour is not completely unexpected: as we are working at low energies within an effective theory,

some of the degrees of freedom of the complete theory behind can be integrated out. This loss of information at low energies with respect to the complete theory is reflected in the possible non-conservation of the total probability. To make contact with data, let us discuss the implications of our treatment for the production and detection cross-sections and, finally, for the number of events detected in a given experiment.

Production/detection cross-sections and widths

The non-unitarity of the mixing matrix N implies the following corrections, for processes computed at tree-level:

- Charged current (CC) cross-sections and fluxes involving only one neutrino flavour α are given by

$$\sigma_{\alpha}^{CC} = \sigma_{\alpha}^{CC(SM)} (NN^{\dagger})_{\alpha\alpha}, \quad \frac{d\Phi_{\alpha}^{CC}}{dE} = \frac{d\Phi_{\alpha}^{CC(SM)}}{dE} (NN^{\dagger})_{\alpha\alpha}, \quad (2.21)$$

where $\sigma_{\alpha}^{CC(SM)}$ and $\Phi_{\alpha}^{CC(SM)}$ are the SM cross-section and flux, respectively. The same correction factor affects decay widths involving one neutrino flavour.

- Charged current cross-sections involving two neutrino flavours, α, β , will be modified into

$$\sigma_{\alpha,\beta}^{CC} = \sigma_{\alpha,\beta}^{CC(SM)} (NN^{\dagger})_{\alpha\alpha} (NN^{\dagger})_{\beta\beta}, \quad (2.22)$$

with the same weight factor affecting widths or fluxes involving two neutrino flavours.

- Neutral current (NC) processes are weighted by a different combination. A decay width involving two neutrino mass eigenstates, ν_i, ν_j , is given by

$$\Gamma(Z \rightarrow \bar{\nu}_i \nu_j) = \Gamma^{SM}(Z \rightarrow \bar{\nu}_i \nu_i) |(N^{\dagger}N)_{ij}|^2. \quad (2.23)$$

Analogously, when “detecting” a neutrino ν_i through neutral current interactions, as in SNO [35, 120, 121], modified cross-sections will have to be considered,

$$\sigma_i^{NC} = \sum_j \sigma^{NC(SM)} |(N^{\dagger}N)_{ij}|^2, \quad (2.24)$$

where the sum over j is due to the fact that the final neutrino ν_j remains undetected.

Number of events

The number of events in a detector located at a distance L away from the source would be given, apart from backgrounds, by the convolution of the production flux, the

oscillation probability, the detection cross-section and the detector efficiency, integrated over energy. In short,

$$n_{events} \sim \int dE \frac{d\Phi_\alpha(E)}{dE} P_{\nu_\alpha \rightarrow \nu_\beta}(E, L) \sigma_\beta(E) \epsilon(E), \quad (2.25)$$

where $d\Phi_\alpha(E)/dE$ is the neutrino flux, $\sigma_\beta(E)$ is the detection cross section and $\epsilon(E)$ the detection efficiency. In the presence of MUV, all factors in Eq. (2.25) should be corrected, as discussed above. It is easy to see that there are cancellations between the different N dependent factors they exhibit.

For instance, for experiments in which both production and detection take place via charged currents, involving each one neutrino flavour, the denominator of $P_{\nu_\alpha \rightarrow \nu_\beta}$ -Eq. (2.19)- cancels the correction factors in the flux and cross-section, Eq. (2.21). This allows to express in this case the number of events simply as

$$n_{events} \sim \int dE \frac{d\Phi_\alpha^{CC(SM)}(E)}{dE} \hat{P}_{\nu_\alpha \rightarrow \nu_\beta}(L, E) \sigma_\beta^{CC(SM)}(E) \epsilon(E), \quad (2.26)$$

where $\hat{P}_{\nu_\alpha \rightarrow \nu_\beta}(L, E)$ is the probability in Eq. (3.9), removing the normalization factors in its denominator,

$$\hat{P}_{\nu_\alpha \rightarrow \nu_\beta}(L, E) \equiv \left| \sum_i N_{\alpha i}^* e^{i P_i L} N_{\beta i} \right|^2. \quad (2.27)$$

It turns out that, in practice, most experiments extract the probabilities from the measured number of events, parametrized -via Monte Carlo simulations- in terms of the SM fluxes and cross-sections, precisely as in Eq. (2.26). Within MUV, their analysis thus provides a direct estimation of $\hat{P}_{\nu_\alpha \rightarrow \nu_\beta}(L, E)$ in Eq. (2.27). This is the case for the very large number of experiments in which neutrinos are detected via charged current interactions and produced from decays of hadrons like π , K or β decays.

Obviously, there are exceptions. For instance, if the neutrino flux expected in the far detector of the previous example is not taken from a Monte Carlo simulation, but from a direct measurement in a near detector, the cancellation described in the previous paragraph would not be complete and extra N -dependent factors will have to be taken into account.

Besides, when the production mechanism is not hadronic, but leptonic, as from μ or even τ decays, the fluxes would need two corrections instead of one, since the production involves two insertions of N , as in Eq. (2.22). For instance, the neutrino fluxes produced at a Neutrino Factory (see Sec. 1.4) from μ decay should thus be corrected by the factor $(NN^\dagger)_{\mu\mu}(NN^\dagger)_{ee}$.

Finally, the analysis of detection through neutral current processes is modified as well. Since such processes are sensitive to the sum of all neutrino species, the number of events is given by

$$n_{events} \sim \int dE \frac{d\Phi_\alpha^{CC(SM)}(E)}{dE} \sum_i \hat{P}_{\nu_\alpha \rightarrow \nu_i}(L, E) \sigma_i^{NC}(E) \epsilon(E), \quad (2.28)$$

with $\sigma_i^{NC}(E)$ as in Eq. (2.24). For instance, for propagation in vacuum, we would have

$$\sum_i \hat{P}_{\nu_\alpha \nu_i}(L, E) \equiv \sum_i |N_{\alpha i}|^2. \quad (2.29)$$

2.2.2 Matter effects

In Sec. 1.3.2 it was shown that the effect of matter when neutrinos pass through it is the modification of the evolution and consequently of the oscillation probability. Let us see if the non-unitarity give rise to the same effects. Considering ordinary matter, the derivation of the Hamiltonian density (Eq. (1.61)) in the flavour basis is exactly the same as in Sec. 1.3.2 because the mixing matrix does not play any role on it (and therefore the non-unitarity either). Then, we consider the same usual Hamiltonian density

$$\mathcal{H}^{int} = A \bar{\nu}_e \gamma_0 P_L \nu_e - A_n \sum_\alpha \bar{\nu}_\alpha \gamma_0 P_L \nu_\alpha, \quad (2.30)$$

where A and A_n were presented in Sec. 1.3.2. As we have already seen, the first term corresponds to charged interactions, while the second term corresponds to neutral interactions. In the mass basis within MUV, Eq. (2.30) reads

$$\mathcal{H}^{int} = A \sum_{i,j} N_{ei}^* N_{ej} \bar{\nu}_i \gamma_0 P_L \nu_j - A_n \sum_{\alpha,i,j} N_{\alpha i}^* N_{\alpha j} \bar{\nu}_i \gamma_0 P_L \nu_j, \quad (2.31)$$

In order to know the time evolution of states passing through matter, consider the interaction Hamiltonian, $\hat{H}^{int} = \int d^3x \mathcal{H}^{int}$, corresponding to Eqs. (2.30) and (2.31). Its matrix elements in the mass basis read

$$H_{ij}^{int} \equiv \langle \nu_j | \hat{H}^{int} | \nu_i \rangle = A N_{ei} N_{ej}^* - A_n (N^\dagger N)_{ji}, \quad (2.32)$$

or, in matrix notation

$$H^{int} \equiv [N^\dagger \text{diag}(A - A_n, -A_n, -A_n) N]^t. \quad (2.33)$$

The evolution equation for mass eigenstates in matter is then given by

$$i \frac{d}{dt} |\nu_i\rangle = \sum_j [E + H^{int}]_{ij} |\nu_j\rangle, \quad (2.34)$$

where E is the energy matrix for free eigenstates, introduced in Eq. (2.16). In contrast, the evolution through matter of flavour eigenstates is given by

$$i \frac{d}{dt} |\nu_\alpha\rangle = \sum_\beta \left[\tilde{N}^* (E + H^{int}) (\tilde{N}^*)^{-1} \right]_{\alpha\beta} |\nu_\beta\rangle, \quad (2.35)$$

where again $(\tilde{N}^*)^{-1}$ cannot be traded by \tilde{N}^t -as it is usually done in the standard case- because N is not unitary.

It is easy, although cumbersome, to write now explicitly the equations above for the three family case. To illustrate the main new effects, it is enough to write here explicitly the effective flavour potential in the second term in Eq. (2.35), for the case of two families:

$$\begin{aligned} \tilde{N}^* H^{int} (\tilde{N}^*)^{-1} &= \tilde{N}^* N^t \begin{pmatrix} A - A_n & 0 \\ 0 & -A_n \end{pmatrix} N^* (\tilde{N}^*)^{-1} = \\ &= \begin{pmatrix} (A - A_n)(NN^\dagger)_{ee} & -A_n \sqrt{\frac{(NN^\dagger)_{\mu\mu}}{(NN^\dagger)_{ee}}} (NN^\dagger)_{\mu e} \\ (A - A_n) \sqrt{\frac{(NN^\dagger)_{ee}}{(NN^\dagger)_{\mu\mu}}} (NN^\dagger)_{e\mu} & -A_n (NN^\dagger)_{\mu\mu} \end{pmatrix}. \end{aligned} \quad (2.36)$$

Consequently, MUV results generically in exotic couplings in the evolution through matter. This effective potential is not diagonal, in contrast to the unitary case. Moreover, the neutral current contribution can not be rewritten as a global phase in the evolution equation and thus it contributes to the oscillation probabilities. The new effects are proportional to the amount of non-unitarity, as it should.

2.3 Matrix elements from neutrino oscillations

We will now use some relevant data on neutrino oscillations, to determine the elements of the mixing matrix, without assuming unitarity. In this work, we do not perform an exhaustive analysis of *all* existing oscillation data; our aim is rather to estimate what is the role played by the different experiments in constraining the matrix elements.

Most of the positive oscillation signals available nowadays correspond to disappearance experiments⁷. Since the disappearance oscillation probability in vacuum is given by

$$\begin{aligned} \hat{P}_{\nu_\alpha \rightarrow \nu_\alpha} &= |N_{\alpha 1}|^4 + |N_{\alpha 2}|^4 + |N_{\alpha 3}|^4 + 2|N_{\alpha 1}|^2 |N_{\alpha 2}|^2 \cos(\Delta_{21} L) \\ &+ 2|N_{\alpha 1}|^2 |N_{\alpha 3}|^2 \cos(\Delta_{31} L) + 2|N_{\alpha 2}|^2 |N_{\alpha 3}|^2 \cos(\Delta_{32} L), \end{aligned} \quad (2.37)$$

disappearance experiments may provide information on the moduli of elements, while phases will remain unknown, as in the unitary case. Furthermore, as no ν_τ disappearance experiment has been performed, this type of vacuum experiments will only constrain the elements of the e and the μ -rows, as Eq. (2.37) indicates. Nevertheless, the no-oscillation results from some appearance experiments will also provide useful non-unitarity constraints.

⁷Except for the LSND experiment [49, 50], which result has not been confirmed so far by any experiment, including MiniBooNe [122], and which we will not consider in this work.

Vacuum oscillations

The exact appearance and disappearance probabilities in vacuum, Eqs. (2.19) and (2.27), will be used in the numerical analysis. To illustrate the discussion, the amputated probabilities can be approximated as follows, though, for some experiments studied below, depending on the range of L/E :

- **$\Delta_{21}\mathbf{L} \simeq \mathbf{0}$.** Eq. (2.37) reduces then to -for instance for the case of $\bar{\nu}_e$ disappearance and ν_μ disappearance-

$$\begin{aligned} \hat{P}_{\bar{\nu}_e \rightarrow \bar{\nu}_e} &\simeq (|N_{e1}|^2 + |N_{e2}|^2)^2 + |N_{e3}|^4 \\ &+ 2(|N_{e1}|^2 + |N_{e2}|^2)|N_{e3}|^2 \cos(\Delta_{32}L), \end{aligned} \quad (2.38)$$

$$\begin{aligned} \hat{P}_{\nu_\mu \rightarrow \nu_\mu} &\simeq (|N_{\mu1}|^2 + |N_{\mu2}|^2)^2 + |N_{\mu3}|^4 \\ &+ 2(|N_{\mu1}|^2 + |N_{\mu2}|^2)|N_{\mu3}|^2 \cos(\Delta_{32}L), \end{aligned} \quad (2.39)$$

respectively. Relevant experiments in this class include CHOOZ (see Sec. 1.4), a reactor experiment sensitive to $\bar{\nu}_e$ disappearance, as well as the ν_μ disappearance atmospheric and accelerator experiments such as K2K [43, 44] or MINOS. Eqs. (2.38) and (2.39) indicate that this type of vacuum experiments cannot disentangle by themselves the element $|N_{\alpha1}|$ from $|N_{\alpha2}|$, as they appear in the combinations $|N_{e1}|^2 + |N_{e2}|^2$ and $|N_{\mu1}|^2 + |N_{\mu2}|^2$, respectively. In addition, the equations show as well the presence of a degeneracy between those combinations versus $|N_{e3}|$ and $|N_{\mu3}|$, respectively.

- **$\Delta_{21}\mathbf{L} \neq \mathbf{0}$ with $\Delta_{32}\mathbf{L} \gg \mathbf{1}$.** The latter -atmospheric- oscillation frequency is averaged resulting in -for instance for $\bar{\nu}_e$ disappearance-

$$\hat{P}_{\bar{\nu}_e \rightarrow \bar{\nu}_e} \simeq |N_{e1}|^4 + |N_{e2}|^4 + |N_{e3}|^4 + 2|N_{e1}|^2|N_{e2}|^2 \cos(\Delta_{21}L). \quad (2.40)$$

KamLAND is a reactor experiment with a longer baseline than CHOOZ and falling into this category. Notice that the dependence on $|N_{e1}|$ and $|N_{e2}|$ in Eq. (2.40) differs from that in Eq. (2.38), suggesting that the combination of both type of experiments may help to tell those elements apart, as it will be shown later on.

- **$\Delta_{21}\mathbf{L} \simeq \mathbf{0}$ and $\Delta_{32}\mathbf{L} \simeq \mathbf{0}$.** The appearance and disappearance probabilities correspond then to a simple formula (see Eq. (2.20)):

$$\hat{P}_{\nu_\alpha \rightarrow \nu_\beta} \simeq |(NN^\dagger)_{\beta\alpha}|^2. \quad (2.41)$$

KARMEN [123] and NOMAD [124] are appearance experiments in this class, well described by Eq. (2.41); the same holds for the data on ν_μ disappearance at the near detector in MINOS and on $\bar{\nu}_e$ disappearance at Bugey [125].

Oscillations in matter

A very important experiment in this class is SNO [35, 120, 121]. In the unitary treatment, the ν_e produced at the core of the sun are approximately eigenstates of the total Hamiltonian, since the interaction Hamiltonian dominates the evolution in this region of the sun. A ν_e in the center of the sun is approximately [126] the following combination of effective eigenstates in matter $|\tilde{\nu}_i\rangle$:

$$|\nu_e\rangle \simeq \sqrt{0.1}|\tilde{\nu}_1\rangle + \sqrt{0.9}|\tilde{\nu}_2\rangle, \quad (2.42)$$

within a 2% accuracy. The state then evolves adiabatically so that, when leaving the sun, the $|\tilde{\nu}_i\rangle$ states can be replaced by the vacuum eigenstates $|\nu_i\rangle$, leading to

$$\hat{P}_{\nu_e \rightarrow \nu_e} \simeq 0.1|N_{e1}|^2 + 0.9|N_{e2}|^2, \quad (2.43)$$

which allows a clean measurement of $|N_{e2}|^2$.

Within the MUV scheme, *a priori* the analysis varies. This was illustrated in Eq. (2.36) for two-family oscillations in matter, which exhibits exotic non-diagonal terms and where the neutral currents may play *a priori* a significant role. Nevertheless, we will see below that the absence of oscillation signals at near detectors constrain deviations from unitarity, for all (NN^\dagger) elements but $(NN^\dagger)_{\tau\tau}$, to be smaller than $\mathcal{O}(10^{-1})$. In fact, it will turn out that all bounds on (NN^\dagger) , including $(NN^\dagger)_{\tau\tau}$, are improved also from weak decays and the values of the off-diagonal elements constrained to be smaller than a few percent, as it will be shown in the next Section. In consequence, for the level of precision aimed at in this work, it is unnecessary to perform the complete MUV analysis of SNO data and Eq. (2.43) keeps being an appropriate approximation. This determination of $|N_{e2}|$ will be a major input in resolving the MUV degeneracy between $|N_{e1}|$ and $|N_{e2}|$.

In all numerical analysis below, the values of Δm_{21}^2 and Δm_{32}^2 , resulting from our fits in the MUV scheme, will not be shown: they coincide with those obtained in the unitary treatment, as expected from the fact that the oscillation frequencies are not modified in the MUV scheme, unlike the amplitudes.

2.3.1 Constraints on the e -row

In Fig. 2.1 (left) we present the 1, 2 and 3σ contours of a three-family fit to CHOOZ data, combined with the information on Δm_{32}^2 resulting from an analysis of K2K data [43], The dotted line represents the unitarity condition $(NN^\dagger)_{ee} = 1$.

Since CHOOZ data are compatible with the no-oscillation hypothesis, the fit shows allowed regions in which the first line in Eq. (2.38) is close to one, while the second -oscillatory- term vanishes. That is, either $|N_{e1}|^2 + |N_{e2}|^2 \simeq 1$ with $|N_{e3}|^2 \simeq 0$, or $|N_{e1}|^2 + |N_{e2}|^2 \simeq 0$ with $|N_{e3}|^2 \simeq 1$. The detection of the L/E dependence in KamLAND

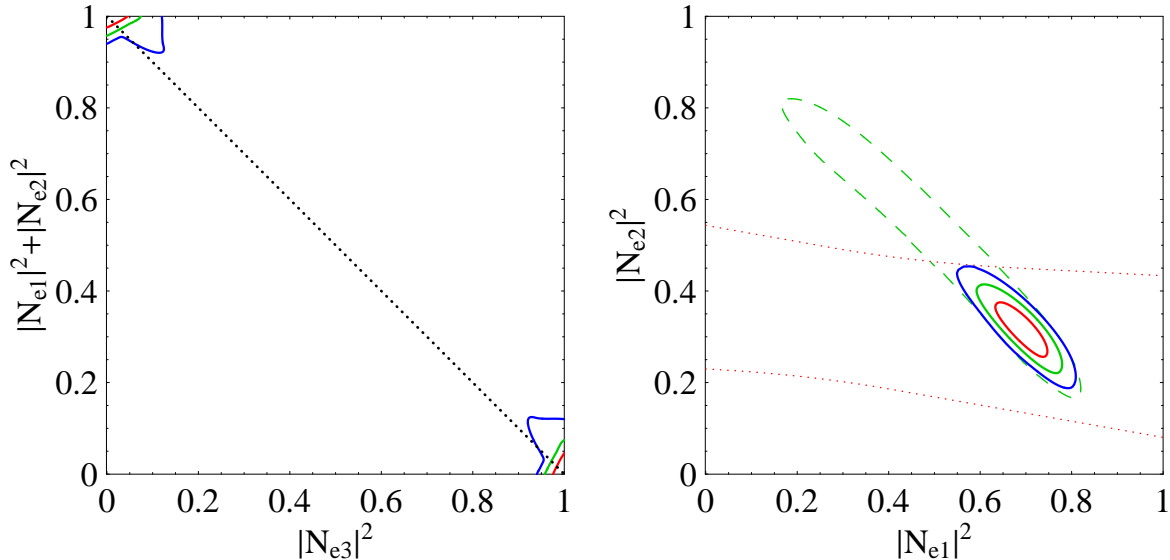


Figure 2.1: *Left: 1, 2 and 3 σ contours for CHOOZ and K2K data (solid lines) with unitarity condition (dotted line). Right: 3 σ contours for CHOOZ, K2K and KamLAND data (dashed line), SNO data (dotted line) and their combination at 1, 2 and 3 σ (solid lines).*

selects the first combination, though, see Eq. (2.40). The significant loss of sensitivity to $|N_{e3}|$ of the 3 σ contour with respect to the 1 and 2 σ ones can be understood from the fact that CHOOZ loses its sensitivity for $\Delta m_{32}^2 \simeq 0.001 eV^2$, as can be seen in Fig. 55 of Ref. [40]. Indeed K2K excludes such small values of Δm_{32}^2 at 1 and 2 σ , but not at 3 σ , where the loss of sensitivity occurs. Notice that the 3 σ contour intersects the unitarity condition at $|N_{e3}|^2 \simeq 0.05$, which agrees with the usual bounds for $|N_{e3}|^2$, obtained under the assumption of unitarity.

KamLAND also helps to disentangle $|N_{e1}|^2$ from $|N_{e2}|^2$, as illustrated in Fig. 2.1 (right), in which the 3 σ contour of a fit to KamLAND data is presented (dashed line), combined with those from CHOOZ and K2K. Since CHOOZ constrained $|N_{e1}|^2 + |N_{e2}|^2$ to be close to 1, only a narrow strip near the diagonal is allowed. The region is still large, though, due to the symmetry of Eq. (2.40) under the interchange of $|N_{e1}|^2$ with $|N_{e2}|^2$.

This final degeneracy can be lifted with information from SNO. The SNO data on the ratio of the charged-current over neutral-current fluxes results in the rather horizontal 3 σ strip (dotted line) in Fig. 2.1 (right). To determine this region, the ratio of charged-current over neutral-current fluxes [121] can be approximated by Eq. (2.43). A 5% variation has been allowed, to take into account the corrections stemming from Eqs. (2.28) and (2.36). Furthermore, we have verified that even a 10% variation in those coefficients would not change significantly the results of the fit.

The combined fit of CHOOZ, KamLAND, SNO and K2K data is depicted at 1, 2 and 3 σ by the solid contours in Fig. 2.1 (right). The Figure shows then that the combination of all this complementary information constrains all elements of the e -row

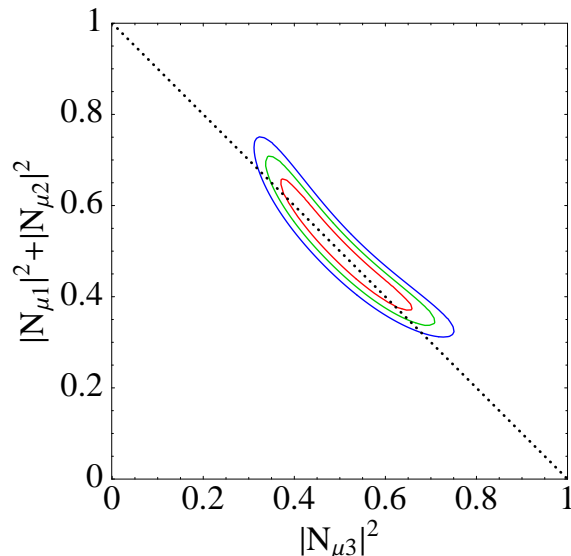


Figure 2.2: 1, 2 and 3 σ contours for K2K and SK data (solid line) with unitarity condition (dotted line).

with a precision only slightly inferior to that of the usual unitary analysis.

2.3.2 Constraints on the μ -row

In Fig. 2.2 we show the 1, 2 and 3 σ contours (solid lines) of a fit to K2K data, combined with an estimation for SK. The latter resulted from translating the measured value of $\sin^2(2\theta_{23})$ in Ref. [38] to matrix elements, using Eq. (2.39). The dotted line represents the unitarity condition, $(NN^\dagger)_{\mu\mu} = 1$. Without additional information at different L/E , $|N_{\mu 1}|^2$ and $|N_{\mu 2}|^2$ can not be disentangled and our knowledge of the μ -row is much worse than when imposing unitarity.

Putting together all the information developed above from the different oscillation experiments considered, the following allowed ranges are obtained -at 3 σ -, for the elements of the leptonic mixing matrix:

$$|N| = \begin{pmatrix} 0.75 - 0.89 & 0.45 - 0.66 & < 0.34 \\ [(|N_{\mu 1}|^2 + |N_{\mu 2}|^2)^{1/2} = 0.57 - 0.86] & 0.57 - 0.86 & \\ ? & ? & ? \end{pmatrix}. \quad (2.44)$$

We observe that, without the assumption of unitarity, the oscillation signals analysed can only determine half of the matrix elements. The elements of the first row have all been determined or constrained ($|N_{e2}|^2$ mainly by SNO, $|N_{e3}|^2$ mainly by CHOOZ and $|N_{e1}|^2$ by KamLAND combined with the others). In contrast, for the second row, atmospheric and accelerator experiments are unable to discriminate between $|N_{\mu 1}|^2$

and $|N_{\mu 2}|^2$. Finally, no direct information can be obtained on the τ -row in the absence of ν_τ oscillations signals.

2.3.3 Constraints on non-unitarity from near detectors

NOMAD [124], KARMEN [123], Bugey [125] and the near detector at MINOS provide constraints on the elements of NN^\dagger as it follows from Eq. (2.41). We obtain, at the 90%CL,

$$|NN^\dagger| \approx \begin{pmatrix} 1.00 \pm 0.04 & < 0.05 & < 0.09 \\ < 0.05 & 1.00 \pm 0.05 & < 0.013 \\ < 0.09 & < 0.013 & ? \end{pmatrix}. \quad (2.45)$$

With this information, $|N_{\mu 1}|$ and $|N_{\mu 2}|$ in Eq. (2.44) can now be disentangled. All in all, the mixing matrix resulting from analyzing oscillation data within the MUV scheme is given by

$$N = \begin{pmatrix} 0.75 - 0.89 & 0.45 - 0.66 & < 0.27 \\ 0.00 - 0.69 & 0.22 - 0.81 & 0.57 - 0.85 \\ ? & ? & ? \end{pmatrix}. \quad (2.46)$$

Notice that, even adding the constraints obtained at near detectors, not all matrix elements can be determined from oscillation data.

2.4 Constraints on non-unitarity from electroweak decays

Neutrino oscillations are evidence of a non-trivial leptonic mixing, allowing to determine the individual elements of the mixing matrix from its data, as done in the previous Section. In contrast, leptonic and semileptonic decay data are not appropriate for this task. This is because, contrary to the quark sector, where the different quark mass eigenstates can be tagged, neutrino eigenstates are not detected separately. The experimentally measured rates correspond then to sums over all possible mass eigenstates, resulting only in sums of *products* of matrix elements, unlike in the unitary case.

Then in the MUV scheme, leptonic and semileptonic decays may be sensitive to leptonic non-unitarity. This sensitivity is a manifestation of the non-unitarity in the leptonic sector equivalent to the “zero-distance” effect, encoded by the non-orthogonality of the flavour basis (Eq. (2.10)). The combinations $(NN^\dagger)_{\alpha\beta}$ can be extracted from them, as suggested by Eqs. (2.21)-(2.24). With that aim, W , Z , π and lepton decays are analysed in this chapter, in the MUV scheme. The results will further constrain the mixing matrix obtained from neutrino oscillation processes.

2.4.1 W decays

With a non-unitary leptonic mixing matrix N , the decay widths for W into charged leptons and neutrinos are given -as in Eq. (2.21)- by

$$\Gamma(W \rightarrow \ell_\alpha \nu_\alpha) = \sum_i \Gamma(W \rightarrow \ell_\alpha \nu_i) = \frac{G_F M_W^3}{6\sqrt{2}\pi} (NN^\dagger)_{\alpha\alpha}. \quad (2.47)$$

G_F has been related to the Fermi constant G_μ , measured from the decay $\mu \rightarrow \nu_\mu e \bar{\nu}_e$, by Eq. (2.11), allowing to extract now from Eq. (2.47) the following combinations:

$$\frac{(NN^\dagger)_{\alpha\alpha}}{\sqrt{(NN^\dagger)_{ee}(NN^\dagger)_{\mu\mu}}} = \frac{\Gamma(W \rightarrow \ell_\alpha \nu_\alpha) 6\sqrt{2}\pi}{G_\mu M_W^3} \equiv f_\alpha. \quad (2.48)$$

Using the results for the W decay widths and mass from Ref. [127], as well as $G_\mu = (1.16637 \pm 0.00001) \cdot 10^{-5}$, the parameters f_α are

$$\begin{aligned} f_e &= 1.000 \pm 0.024, \\ f_\mu &= 0.986 \pm 0.028, \\ f_\tau &= 1.002 \pm 0.032. \end{aligned} \quad (2.49)$$

2.4.2 Invisible Z decay

Further constraints stem from the invisible Z -decay width, which, for non-unitary leptonic mixing N , is given by (see Eq. (2.24))

$$\Gamma(Z \rightarrow \text{invisible}) = \sum_{i,j} \Gamma(Z \rightarrow \bar{\nu}_i \nu_j) = \frac{G_F M_Z^3}{12\sqrt{2}\pi} \sum_{i,j} |(N^\dagger N)_{ij}|^2. \quad (2.50)$$

Using Eq. (2.11), the equality $\sum_{i,j} |(N^\dagger N)_{ij}|^2 = \sum_{\alpha,\beta} |(NN^\dagger)_{\alpha\beta}|^2$ and the data provided in Ref. [127], the following constraint is obtained

$$\frac{\sum_{\alpha,\beta} |(NN^\dagger)_{\alpha\beta}|^2}{\sqrt{(NN^\dagger)_{ee}(NN^\dagger)_{\mu\mu}}} = \frac{12\sqrt{2}\pi \Gamma(Z \rightarrow \text{invisible})}{G_\mu M_Z^3} = 3.008 \pm 0.009. \quad (2.51)$$

2.4.3 Universality tests

In addition, ratios of lepton, W and π decays, used often in order to test universality [127–129], can be interpreted as tests of lepton mixing unitarity. They result in constraints for the diagonal elements of NN^\dagger , as suggested by Eqs. (2.21)-(2.24) and resumed in Table 2.1.

The processes investigated so far constrained the diagonal elements of the product NN^\dagger . Limit values for its off-diagonal elements can be obtained instead from rare decays of charged leptons, as we show next.

Constraints on	Process	Bound
$\frac{(NN^\dagger)_{\mu\mu}}{(NN^\dagger)_{ee}}$	$\frac{\Gamma(\tau \rightarrow \nu_\tau \mu \bar{\nu}_\mu)}{\Gamma(\tau \rightarrow \nu_\tau e \bar{\nu}_e)}$	0.9999 ± 0.0020
$\frac{(NN^\dagger)_{\mu\mu}}{(NN^\dagger)_{ee}}$	$\frac{\Gamma(\pi \rightarrow \mu \bar{\nu}_\mu)}{\Gamma(\pi \rightarrow e \bar{\nu}_e)}$	1.0017 ± 0.0015
$\frac{(NN^\dagger)_{\mu\mu}}{(NN^\dagger)_{ee}}$	$\frac{\Gamma(W \rightarrow \mu \bar{\nu}_\mu)}{\Gamma(W \rightarrow e \bar{\nu}_e)}$	0.997 ± 0.010
$\frac{(NN^\dagger)_{\tau\tau}}{(NN^\dagger)_{\mu\mu}}$	$\frac{\Gamma(\tau \rightarrow \nu_\tau e \bar{\nu}_e)}{\Gamma(\mu \rightarrow \nu_\mu e \bar{\nu}_e)}$	1.0004 ± 0.0023
$\frac{(NN^\dagger)_{\tau\tau}}{(NN^\dagger)_{\mu\mu}}$	$\frac{\Gamma(\tau \rightarrow \nu_\tau \pi)}{\Gamma(\pi \rightarrow \mu \bar{\nu}_\mu)}$	0.9999 ± 0.0036
$\frac{(NN^\dagger)_{\tau\tau}}{(NN^\dagger)_{ee}}$	$\frac{\Gamma(\tau \rightarrow \nu_\tau \mu \bar{\nu}_\mu)}{\Gamma(\mu \rightarrow \nu_\mu e \bar{\nu}_e)}$	1.0002 ± 0.0022
$\frac{(NN^\dagger)_{\tau\tau}}{(NN^\dagger)_{ee}}$	$\frac{\Gamma(W \rightarrow \tau \bar{\nu}_\tau)}{\Gamma(W \rightarrow e \bar{\nu}_e)}$	1.034 ± 0.014

Table 2.1: Constraints on $(NN^\dagger)_{\alpha\alpha}$ from a selection of processes.

2.4.4 Rare charged lepton decays

The leptonic process $l_\alpha \rightarrow l_\beta \gamma$ only occurs at one loop, as illustrated in Fig. 2.3. As the photon is on-shell, there are no divergent contributions to the diagram. The 1-loop branching ratio in the MUV scheme is given by the same expression [130–135] as in the unitary case, substituting U_{PMNS} by N ,

$$\frac{\Gamma(l_\alpha \rightarrow l_\beta \gamma)}{\Gamma(l_\alpha \rightarrow \nu_\alpha l_\beta \bar{\nu}_\beta)} = \frac{3\alpha}{32\pi} \frac{|\sum_k N_{\alpha k} N_{k\beta}^\dagger F(x_k)|^2}{(NN^\dagger)_{\alpha\alpha} (NN^\dagger)_{\beta\beta}}, \quad (2.52)$$

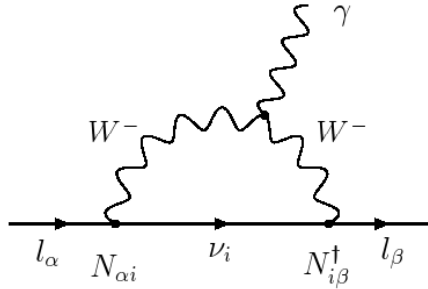


Figure 2.3: One-loop diagram contributing to rare lepton decays.

where $x_k \equiv m_k^2/M_W^2$ with m_k being the masses of the light neutrinos and

$$F(x) \equiv \frac{10 - 43x + 78x^2 - 49x^3 + 4x^4 + 18x^3 \ln x}{3(x-1)^4}. \quad (2.53)$$

Would N be unitary, the x -independent term would vanish exactly through the GIM mechanism [136], for $\alpha \neq \beta$. With N non-unitary and $(NN^\dagger)_{\alpha\beta} \neq \delta_{\alpha\beta}$, that term remains and can be the leading contribution to the branching ratio. With the -very accurate- approximation $F(x) \approx 10/3$, it follows that

$$\frac{\Gamma(\ell_\alpha \rightarrow \ell_\beta \gamma)}{\Gamma(\ell_\alpha \rightarrow \nu_\alpha \ell_\beta \bar{\nu}_\beta)} = \frac{100\alpha}{96\pi} \frac{|(NN^\dagger)_{\alpha\beta}|^2}{(NN^\dagger)_{\alpha\alpha}(NN^\dagger)_{\beta\beta}}, \quad (2.54)$$

leading to the constraint

$$\frac{|(NN^\dagger)_{\alpha\beta}|^2}{(NN^\dagger)_{\alpha\alpha}(NN^\dagger)_{\beta\beta}} = \frac{\Gamma(\ell_\alpha \rightarrow \ell_\beta \gamma)}{\Gamma(\ell_\alpha \rightarrow \nu_\alpha \ell_\beta \bar{\nu}_\beta)} \frac{96\pi}{100\alpha}. \quad (2.55)$$

Strong constraints can now be obtained for the off-diagonal elements of (NN^\dagger) , using the following experimental bounds [137–139]

$$Br(\tau \rightarrow \mu \gamma) < 6.8 \cdot 10^{-8}, \quad (2.56)$$

$$Br(\tau \rightarrow e \gamma) < 1.1 \cdot 10^{-7}, \quad (2.57)$$

$$Br(\mu \rightarrow e \gamma) < 1.2 \cdot 10^{-11}, \quad (2.58)$$

together with the experimental values $Br(\tau \rightarrow \nu_\tau \mu \bar{\nu}_\mu) = 0.1736 \pm 0.0006$, $Br(\tau \rightarrow \nu_\tau e \bar{\nu}_e) = 0.1784 \pm 0.0006$ and $Br(\mu \rightarrow \nu_\mu e \bar{\nu}_e) \approx 100\%$ [127].

The strong experimental bound on $\mu \rightarrow e \gamma$ results in⁸ $(NN^\dagger)_{e\mu(\mu e)} < 10^{-4}$, while the other off-diagonal elements are constrained to be less than a few percent.

Finally, other lepton-flavour violating decays like $\ell_i \rightarrow 3\ell$, as well as $\ell_i \rightarrow \ell_j$ conversion in nuclei, impose additional constraints close to those above. They may become increasingly relevant, depending on the experimental sensitivities attained in the future, as it will be discussed in Sec. 2.6.

2.4.5 Summary of constraints on non-unitarity from decays

All in all, a global fit to the constraints listed in this Section proves that the NN^\dagger elements agree with those expected in the unitary case, within a precision better than a few percent, at the 90% CL:

$$|NN^\dagger| \approx \begin{pmatrix} 1.002 \pm 0.005 & < 7.2 \cdot 10^{-5} & < 1.6 \cdot 10^{-2} \\ < 7.2 \cdot 10^{-5} & 1.003 \pm 0.005 & < 1.3 \cdot 10^{-2} \\ < 1.6 \cdot 10^{-2} & < 1.3 \cdot 10^{-2} & 1.003 \pm 0.005 \end{pmatrix}. \quad (2.59)$$

⁸This strong bound also rules out the possibility of explaining the LSND anomaly with the “zero-distance” effect, at least in our minimal scheme.

In contrast, there is no direct information from decays on the product $N^\dagger N$, except that resulting from the invisible decay width of the Z boson.

We can infer strong limits on the $N^\dagger N$ elements from those in Eq. (2.59). Parametrize the matrix N as $N \equiv H V$, where V is a unitary matrix and H Hermitian,

$$N N^\dagger = H^2 \equiv 1 + \varepsilon \quad (2.60)$$

with $\varepsilon = \varepsilon^\dagger$ and

$$N^\dagger N = V^\dagger H^2 V = 1 + V^\dagger \varepsilon V \equiv 1 + \varepsilon' . \quad (2.61)$$

ε (ε') parametrizes the allowed deviation of $N N^\dagger$ ($N^\dagger N$) from the unit matrix. It follows that

$$|\varepsilon'_{ij}|^2 \leq \sum_{ij} |\varepsilon'_{ij}|^2 = \sum_{\alpha\beta} |\varepsilon_{\alpha\beta}|^2, \quad (2.62)$$

where the unitarity of V has been used, resulting in the constraint

$$|\varepsilon'_{ij}| \leq \left(\sum_{\alpha\beta} |\varepsilon_{\alpha\beta}|^2 \right)^{1/2} = 0.032 . \quad (2.63)$$

$N^\dagger N$ is thus constrained as follows:

$$|N^\dagger N| \approx \begin{pmatrix} 1.00 \pm 0.032 & < 0.032 & < 0.032 \\ < 0.032 & 1.00 \pm 0.032 & < 0.032 \\ < 0.032 & < 0.032 & 1.00 \pm 0.032 \end{pmatrix} . \quad (2.64)$$

The results in Eqs. (2.59) and (2.64) prove that, within the MUV scheme, unitarity in the lepton sector is experimentally confirmed from data on weak decays with a precision better than 4%, and does *not* need to be imposed as an assumption, within that accuracy. This means as well that the leptonic unitarity triangles [140, 141] and normalization conditions -corresponding to the elements of $N N^\dagger$ and $N^\dagger N$ - are experimentally checked with a precision of a few % (or much higher, as for instance for the $\mu - e$ triangle).

2.5 The mixing matrix

The elements of the mixing matrix obtained from the analysis of neutrino oscillation experiments, Eq. (2.46), can now be combined with the unitarity constraints obtained from weak decays in Eqs. (2.59) and (2.64). The resulting mixing matrix in the MUV scheme is

$$|N| = \begin{pmatrix} 0.76 - 0.89 & 0.45 - 0.65 & < 0.20 \\ 0.19 - 0.54 & 0.42 - 0.73 & 0.57 - 0.82 \\ 0.13 - 0.56 & 0.36 - 0.75 & 0.54 - 0.82 \end{pmatrix} . \quad (2.65)$$

All the elements are now significantly constrained to be rather close to those stemming from the usual unitary analysis [63],

$$|U_{PMNS}| = \begin{pmatrix} 0.77 - 0.86 & 0.50 - 0.63 & < 0.22 \\ 0.22 - 0.56 & 0.44 - 0.73 & 0.57 - 0.80 \\ 0.21 - 0.55 & 0.40 - 0.71 & 0.59 - 0.82 \end{pmatrix}. \quad (2.66)$$

The constraints resulting for the N_{e1} and N_{e2} elements are somewhat looser than their partners in the unitary analysis. This is due to the large uncertainties allowed for the values of the coefficients in Eq. (2.42), together with the fact that, among all data available from solar experiments, we have only included in our analysis the SNO ratio of charged to neutral current events. Notice also that the elements of the τ -row are significantly less bounded than in the unitary analysis, their values being inferred only indirectly. There are also small discrepancies in the μ -row which come from the fact that, in this work, the MINOS data have been not analysed. Finally, in the standard analysis the bound on the third element of the e-row (basically θ_{13}) is slightly softer. This is because, taking into account very recent oscillation data, it appears some tension in the parameter space which point to a θ_{13} value different from zero (see Sec. 1.4).

2.6 Future experiments

Matrix elements

In order to measure independently $|N_{\mu 1}|^2$ and $|N_{\mu 2}|^2$ without relying on indirect decay information, a ν_μ disappearance experiment sensitive to Δm_{21}^2 (with the oscillations driven by Δm_{32}^2 averaged out), as the one proposed in Ref. [141], would be needed, as suggested by Eq. (2.40) replacing e by μ . This experiment is quite challenging, requiring an intense ν_μ low-energy beam ($\simeq 500$ MeV) and a very long baseline ($\simeq 2000$ km).

Future facilities under discussion (see Sec. 1.4) include Super-Beams, β -Beams and Neutrino Factories. The latter would be energetic enough for the $\nu_e \rightarrow \nu_\tau$ and $\nu_\mu \rightarrow \nu_\tau$ oscillation channels to be accessible [94, 142]. The τ -row could thus be tested directly and without relying on indirect decay information.

So far the phases of the matrix elements remain completely unknown. A very important task to do in the future is thus measuring these CP-phases. Notice that the just mentioned future facilities are designed to search for CP violation in appearance channels. Unlike vacuum disappearance experiments, measurements at these facilities will be sensitive to the phases of the matrix⁹. In the next chapter we will focus on this possibility, studying the CP violation oscillation effects in the MUV scheme context.

⁹Notice that, as we will see in the next chapter, long baseline experiments can give us some information about the phases through the ν_μ -disappearance channel thanks to the matter effects. However a clear CP-violating signal could only be accessible through the appearance channels.

$(NN^\dagger)_{\mu e}$

As regards to unitarity bounds, the constraints on non-unitarity from decays are also likely to improve. If no positive signal is found for $\mu \rightarrow e\gamma$, the bound on its branching ratio is expected to reach $2 \cdot 10^{-14}$ in the near future [143], which can be translated into a unitarity constraint $(NN^\dagger)_{\mu e} < 2.9 \cdot 10^{-6}$. At a Neutrino Factory, the branching ratio for $\mu \rightarrow e\gamma$ could be further constrained to $< 10^{-15}$ [144, 145], which would result in $(NN^\dagger)_{\mu e} < 6.4 \cdot 10^{-7}$, at the 90%CL.

Important improvements are also expected regarding the bounds for μ to e conversion in nuclei. This process is more suppressed than $\mu \rightarrow e\gamma$, though, due to the extra electromagnetic coupling. In a Neutrino Factory, sensitivities down to 10^{-18} could be achieved [144, 145] which, translated to $(NN^\dagger)_{\mu e} \simeq 3.2 \cdot 10^{-7}$, are only a factor two stronger than the bound expected from $\mu \rightarrow e\gamma$. Similar ultimate sensitivities are being discussed as regards the PRISM/PRIME project [146, 147].

$(NN^\dagger)_{e\tau}$ and $(NN^\dagger)_{\mu\tau}$

On the other hand, the bounds on rare τ decays are not likely to improve much without a dedicated facility, since Babar and Belle are now limited by the background and an increase in statistics would not significantly improve the relevant measurements [148].

In contrast, the possibility of detecting ν_τ at a near detector of a Neutrino Factory would allow to improve the bounds on $(NN^\dagger)_{e\tau}$ and $(NN^\dagger)_{\mu\tau}$. We have considered an OPERA-like detector, located at a 100m baseline from a Neutrino Factory beam¹⁰, with a total mass of 4 kton and the efficiencies and backgrounds considered in Ref. [149]. Assuming a conservative 5% systematic error, the present bounds could be improved to $(NN^\dagger)_{e\tau} < 2.9 \cdot 10^{-3}$ and $(NN^\dagger)_{\mu\tau} < 2.6 \cdot 10^{-3}$, at the 90%CL.

¹⁰This is only an example of the potential of detecting ν_τ near the Neutrino Factory beam. A detailed study of whether the performance of an OPERA-like detector can be extrapolated to the neutrino luminosities so close to the source would be required, though.

Chapter 3

CP-violation from non-unitarity leptonic mixing

In Chapt. 2 the so-called MUV (minimal unitarity violation) scheme was developed and the *absolute* values of the elements of the matrix N were determined, using data from neutrino oscillation experiments and weak decays. It turned out that non-unitary contributions, if present, are constrained at the percent level. As for the *phases*, a non-unitary mixing 3×3 matrix has three phases in excess over those in the unitary case. No information on the size of the phases of the mixing matrix is available, neither on the standard “unitary” phases nor on the new non-unitary ones, as present oscillation data correspond mainly to disappearance experiments.

It is the purpose of this chapter to explore the future sensitivity to the NP parameters, in case the leptonic mixing matrix turns out to be non-unitary. All oscillation channels will be analysed studying specially the sensitivity to the new CP-phases associated to the non-unitarity. In particular, it will be shown that CP-asymmetries in the $\nu_\mu \rightarrow \nu_\tau$ channel are an excellent probe of such new physics. Notice that CP-odd effects in that channel are strongly suppressed in the standard unitary case (the standard $\nu_\mu \rightarrow \nu_\tau$ oscillations are dominated by a large CP-even component) in which the golden channel for CP violation is $\nu_e \rightarrow \nu_\mu$. On the experimental side, our quest has led us to consider several future facilities. Because of the interest of tau detection, measurements at a Neutrino Factory (see Sec. 1.4) will be considered in detail and favored over Super-Beams [150] and β -Beams [82], even the highest energy ones. We have found that a Neutrino Factory would be excellent for probing some unitarity-violating parameters.

Some *a priori* different avenues for new physics explored in the literature are the “Non-Standard neutrino Interactions” (NSI) [151–153]. These are usually implemented through the addition of effective four-fermion operators to the SM lagrangian. These operators can affect the production and detection processes or modify the matter effects in the propagation. We will clarify the relationship between our framework and those proposals. The channels we will explore and the sensitivities we will predict will be

shown to generically apply to them as well.

In Section 3.1 we introduce a convenient parametrization for the mixing matrix N , traducing and updating the bounds obtained in the previous chapter to the new parameters. Section 3.2 contains the main qualitative argument about the direct observability of CP-violating effects related to non-unitarity. Sect. 3.3 explores the sensitivity to CP-odd effects induced in the $\nu_\mu \rightarrow \nu_\tau$ and the $\nu_e \rightarrow \nu_\mu$ channels considering a special Neutrino Factory set-up with a detector located at 130km from the source. In Sect. 3.4 we analyse the potential of a more realistic Neutrino Factory set up (the IDS one [99, 100]) for determining or constraining the parameters of the non-unitary leptonic mixing matrix, paying special attention to the CP-phases. The comparison with the results in “Non-Standard neutrino Interactions”-scenarios is performed in Sect. 3.5. Finally, App. A introduce a formalism to derive oscillation probabilities in matter with constant density, in the MUV scheme. Most of the results shown in this chapter come from Refs. [115] and [154].

3.1 Parametrization of N

Let us parametrize the general non-unitary matrix N , which relates flavour and mass fields

$$\nu_\alpha = N_{\alpha i} \nu_i, \quad (3.1)$$

as the product of an hermitian and a unitary matrix, defined by

$$N \equiv (1 + \eta)U, \quad (3.2)$$

with $\eta^\dagger = \eta$. As one can see in the above equation the hermitian matrix η parametrizes the deviations from unitarity of the mixing matrix. The present bounds derived in the previous chapter (see Sect. 2.4.5) for the modulus of the elements of NN^\dagger from universality tests, rare lepton decays and the invisible width of the Z , also apply to the elements of η , since $NN^\dagger = (1 + \eta)^2 \approx 1 + 2\eta$ and it follows that

$$|\eta| = \begin{pmatrix} |\eta_{ee}| < 5.5 \cdot 10^{-3} & |\eta_{e\mu}| < 3.5 \cdot 10^{-5} & |\eta_{e\tau}| < 8.0 \cdot 10^{-3} \\ |\eta_{\mu e}| < 3.5 \cdot 10^{-5} & |\eta_{\mu\mu}| < 5.0 \cdot 10^{-3} & |\eta_{\mu\tau}| < 5.1 \cdot 10^{-3} \\ |\eta_{\tau e}| < 8.0 \cdot 10^{-3} & |\eta_{\tau\mu}| < 5.1 \cdot 10^{-3} & |\eta_{\tau\tau}| < 5.0 \cdot 10^{-3} \end{pmatrix}, \quad (3.3)$$

at the 90% confidence level. The bound on $\eta_{\mu\tau}$ has been updated with the latest experimental bound on $\tau \rightarrow \mu\gamma$ [155].

On the other hand, these bounds have been derived without taking into account the quark sector experimental results. However, the unitarity constraints in the first row of the CKM matrix is experimentally tested to very high precision. So, comparing leptonic and hadronic processes can give us interesting constraints, which have not been take into account in the previous chapter. V_{ud} is measured through β decays, V_{us} through kaon decays, while V_{cb} has an experimental value smaller than the precision of

the just mentioned matrix elements being, thus, negligible. Both processes depend on G_F , which is usually extracted through the μ decay in which case it is called G_μ (see Eq. (2.11)). Thus, if we assume that the CKM matrix is unitary, these experimental bounds on the CKM matrix elements provide excellent constraints in $\eta_{\mu\mu}$ [156]. This constraint plays the role of the Z decay in the previous chapter, being stronger than the latter. In combination with the rest of the constraints, the following updated bounds are obtained:

$$|\eta| = \begin{pmatrix} |\eta_{ee}| < 2.0 \cdot 10^{-3} & |\eta_{e\mu}| < 3.5 \cdot 10^{-5} & |\eta_{e\tau}| < 8.0 \cdot 10^{-3} \\ |\eta_{\mu e}| < 3.5 \cdot 10^{-5} & |\eta_{\mu\mu}| < 8.0 \cdot 10^{-4} & |\eta_{\mu\tau}| < 5.1 \cdot 10^{-3} \\ |\eta_{\tau e}| < 8.0 \cdot 10^{-3} & |\eta_{\tau\mu}| < 5.1 \cdot 10^{-3} & |\eta_{\tau\tau}| < 2.7 \cdot 10^{-3} \end{pmatrix}. \quad (3.4)$$

We have to remind again that we are performing a model-independent approach, and thus the constraints above are softer than the ones which can be obtained within a concrete model which generates non-unitarity. To illustrate this, let us consider the type-I seesaw model, the one which fits better to the MUV scheme since only affects to the neutrino couplings at low energies. In that case η , which basically would be the coefficient of the dimension 6 operator responsible of generating non-unitarity, takes the form: $\eta \propto Y^\dagger \frac{1}{M^\dagger} \frac{1}{M} Y$ [18]. Therefore, in the type-I seesaw η is, by construction, a positive-definite matrix. As a result stronger constraints in some of the non-diagonal elements can be inferred from the diagonal ones [156]: $|\eta_{e\mu}| < 6.0 \cdot 10^{-5}$, $|\eta_{e\tau}| < 1.6 \cdot 10^{-3}$, $|\eta_{\mu\tau}| < 1.1 \cdot 10^{-3}$. Notice that the bound on $|\eta_{e\mu}|$ is slightly softer than in Eq. (3.4) because the contribution of diagrams mediated by the heavy fields in the $\mu \rightarrow e\gamma$ have been considered, something which is not taken into account in the MUV scheme. The bounds on the diagonal elements of η remain exactly the same as in Eq. (3.4). In any case, since we do not attach ourselves to any model, we will consider the bounds inferred directly from the experiments (Eq. (3.4)) in the rest of this chapter.

3.2 New CP-asymmetries

Eq. (3.4) shows that the matrix N is constrained to be unitary, within accuracy better than 10^{-2} . The unitary matrix U in Eq. (3.2) can thus be identified with the usual unitary mixing matrix $U = U_{PMNS}$, within the same accuracy. The flavour eigenstates can then be conveniently expressed as¹

$$|\nu_\alpha \rangle = \frac{(1 + \eta^*)_{\alpha\beta} U_{\beta i}^*}{[1 + 2\eta_{\alpha\alpha} + (\eta^2)_{\alpha\alpha}]^{1/2}} |\nu_i \rangle \equiv \frac{(1 + \eta^*)_{\alpha\beta}}{[1 + 2\eta_{\alpha\alpha} + (\eta^2)_{\alpha\alpha}]^{1/2}} |\nu_\beta^{SM} \rangle. \quad (3.5)$$

¹As neutrino masses are forbidden in the SM, the handy superscript SM is an abuse of language, that we allow ourselves to describe the flavour eigenstates of the standard unitary analysis.

It follows that the neutrino oscillation amplitude, at first order in η , is given simply by

$$\langle \nu_\beta | \nu_\alpha(L) \rangle = A_{\alpha\beta}^{SM}(L) (1 - \eta_{\alpha\alpha} - \eta_{\beta\beta}) + \sum_\gamma (\eta_{\alpha\gamma}^* A_{\gamma\beta}^{SM}(L) + \eta_{\beta\gamma} A_{\alpha\gamma}^{SM}(L)), \quad (3.6)$$

with

$$A_{\alpha\beta}^{SM}(L) \equiv \langle \nu_\beta^{SM} | \nu_\alpha^{SM}(L) \rangle \quad (3.7)$$

being the usual oscillation amplitude of the unitary analysis.

New unequivocal CP violation signals arising from the new phases in η , require to contemplate appearance channels, $\alpha \neq \beta$. The best sensitivities to such phases will be achieved in a regime where the first term in Eq. (3.6) is suppressed. This happens at short enough baselines, where the standard appearance amplitudes become vanishingly small, while the disappearance ones are still $A_{\alpha\alpha}^{SM}(L) \simeq 1$. Precisely, to take advantage of these properties in Sec. 3.3 we will consider a $\mathcal{O}(100)$ km baseline using a Neutrino Factory beam. The total amplitude is then well approximated by

$$\langle \nu_\beta | \nu_\alpha(L) \rangle = A_{\alpha\beta}^{SM}(L) + 2\eta_{\alpha\beta}^* + \mathcal{O}(\eta A), \quad (3.8)$$

where $\mathcal{O}(\eta A)$ only includes appearance amplitudes and η components with flavour indices other than $\alpha\beta$. This is an interesting property as it implies that, at short enough baselines, each oscillation probability in a given flavour channel, $P_{\alpha\beta}$, is most sensitive to the corresponding $\eta_{\alpha\beta}$. The other elements of the η matrix can be safely disregarded in the analysis of Sec. 3.3, without implying to assume zero values for them. That is, their effect is generically subdominant, a fact that will be numerically checked for the main contributions, as explained later on. This also means that the subleading corrections from the cross-sections and fluxes discussed in Chap. 2, which induce also $\mathcal{O}(\eta A)$ corrections, do not need to be taken into account.

For instance, in a two family scenario and within the above-described approximation, the oscillation probability would read:

$$P_{\alpha\beta} = \sin^2(2\theta) \sin^2\left(\frac{\Delta L}{2}\right) - 4|\eta_{\alpha\beta}| \sin \delta_{\alpha\beta} \sin(2\theta) \sin\left(\frac{\Delta L}{2}\right) + 4|\eta_{\alpha\beta}|^2, \quad (3.9)$$

where $\Delta = \Delta m^2/2E$ and $\eta_{\alpha\beta} = |\eta_{\alpha\beta}| e^{-i\delta_{\alpha\beta}}$. The first term in Eq. (3.9) is the usual oscillation probability when the mixing matrix is unitary. The third term is the zero-distance effect stemming from the non-orthogonality of the flavour eigenstates. Finally, the second term is the CP-violating interference between the other two. Notice that the latter is linearly sensitive to both phases and moduli, a fact which will be at the origin of the improvement in the sensitivity to the moduli, for non-trivial values of the phases $\delta_{\alpha\beta}$ in Sec. 3.3, as compared to analysis of near detectors (see Sec. 2.6). In this same two-family approximation, the CP-asymmetry can be written as

$$\mathcal{A}_{\alpha\beta}^{CP} = \frac{P_{\alpha\beta} - P_{\bar{\alpha}\bar{\beta}}}{P_{\alpha\beta} + P_{\bar{\alpha}\bar{\beta}}} \sim \frac{-4|\eta_{\alpha\beta}| \sin \delta_{\alpha\beta}}{\sin(2\theta) \sin\left(\frac{\Delta L}{2}\right)}, \quad (3.10)$$

where, for illustration, it is implicitly assumed that we work in a regime in which the term quadratic in η in Eq. (3.9) is negligible with respect to the first term, that is, with respect to the standard contributions.

In the section below we consider a short enough baseline Neutrino Factory setup where Eq. (3.8) and the properties described above apply. Within that setup, we will analyse the new sources of CP violation in the $\nu_e \rightarrow \nu_\tau$ and the $\nu_\mu \rightarrow \nu_\tau$ appearance channels, since present constraints in $\eta_{e\mu}$ are too strong to allow a signal in the $\nu_e \rightarrow \nu_\mu$ channel (see Eq. (3.4)). When numerically computing a given $P_{\alpha\beta}$, the only approximation performed will be to neglect all η elements but that corresponding to the channel under consideration, $\eta_{\alpha\beta}$. They should be indeed subdominant, as illustrated by Eq. (3.8). Furthermore, we have checked this approximation as follows. The numerical fits have been performed in two ways. First, setting to zero all the elements of η except $\eta_{\alpha\beta}$. Next, allowing the other off-diagonal elements of η to vary (except for $\eta_{e\mu}$, which is extremely well constrained). The results are indistinguishable within the accuracy explored. The effect of the diagonal elements is expected to be even smaller since they cannot induce CP asymmetries.

On the other hand, future facilities as the Neutrino Factory are being designed to optimize their performance to look for the still unknown parameters of the standard unitary treatment, including the Dirac CP-phase. None of these future experimental proposals under study contemplate a τ -detector located at $\mathcal{O}(100)$ km from the source. For this reason, in Sec. 3.4 we will analyse the future sensitivity to the MUV parameters in a more feasible Neutrino Factory setup, the IDS proposal, scanning the complete MUV parameter space and paying special attention to the CP-phases.

Finally, the parametrization of N in Eq. (3.2) is on purpose very similar to that used to study non-standard neutrino interactions from four-fermion operators, widely explored in the neutrino literature. Some CP-odd effects have also been considered in these scenarios [157]. We leave to Section 3.5 the task of clarifying the similarities and differences with our framework, their equivalence in certain regimes and the range of application of our numerical bounds to those constructions.

3.3 Sensitivity to the new CP-odd phases. A tuned Neutrino Factory set-up.

As suggested by Eqs. (3.9) and (3.10), the best sensitivities to CP violation will be achieved at short baselines and high energies, where the standard term is suppressed by $\sin^2(\frac{\Delta L}{2})$. In this section, we will therefore study a Neutrino Factory beam resulting from the decay of 50 GeV muons, to be detected at a 130 km baseline, which matches for example the CERN-Frejus distance. For these values, $\sin(\frac{\Delta_{31}L}{2}) \simeq 1.7 \cdot 10^{-2}$ and $\sin(\frac{\Delta_{21}L}{2}) \simeq 6 \cdot 10^{-4}$, where $\Delta_{jk} \equiv (m_j^2 - m_k^2)/2E$. All terms in the oscillation probability Eq. (3.9) can then be of similar order for the channels $\nu_\mu \rightarrow \nu_\tau$ and $\nu_e \rightarrow \nu_\tau$, if the corresponding $\eta_{\alpha\beta}$ values are close to their experimental limits in Eq. (3.4). In what

follows, we will assume $2 \cdot 10^{20}$ useful decays per year and five years running with each polarity.

The appearance of ν_τ s will be contemplated assuming a 5 kton Opera-like detector. The efficiencies and backgrounds for the measurement of $\nu_e \rightarrow \nu_\tau$ transitions at a Neutrino Factory have been taken from Ref. [149]. A similarly detailed analysis for the $\nu_\mu \rightarrow \nu_\tau$ channel is still lacking in the literature. In fact, $\nu_\mu \rightarrow \nu_\tau$ oscillations are one of the main backgrounds in the detection of $\nu_e \rightarrow \nu_\tau$ transitions. In any case, magnetizing the detector it may be possible to study not only the τ into μ decay mode, but all the rest of the τ decay modes gaining a factor of 5 in sensitivity which, on the other side, will mean larger backgrounds. Since in the $\nu_\mu \rightarrow \nu_\tau$ channel the expected signal-to-background ratio is quite larger than in the $\nu_e \rightarrow \nu_\tau$ one, we decide to consider a magnetized version of the detector when analysing the first one. We have thus considered efficiencies and backgrounds a factor 5 larger² when analysing the $\nu_\mu \rightarrow \nu_\tau$ channel than those used for the $\nu_e \rightarrow \nu_\tau$ channel. On the other hand, it has to be remarked that the magnetization of the detector would limitate its size around 5 kt at most.

In the numerical analysis, the complete oscillation probabilities in matter have been used (albeit with the simplifications on η previously described). It is interesting, though, to understand qualitatively and in detail the role of matter effects and, whenever relevant, the dependence on small neutrino parameters, such as $\Delta_{21}L$ and $\sin 2\theta_{13}$. For this purpose, we will consider below an expansion of the oscillation probabilities at higher order than that implied by Eq. (3.9). Taking into account that $\Delta_{31}L \sim AL \sim 10^{-2}$, where $A = \sqrt{2}G_F n_e$, with G_F being the Fermi constant and n_e the electron density in the Earth crust, $\Delta_{21}L \sim 10^{-3.5}$, $\sin 2\theta_{13} \lesssim 10^{-0.5}$, $|\eta_{\alpha\beta}| \lesssim 10^{-2}$ and $|\eta_{e\mu}| < 3.6 \cdot 10^{-5}$, it is consistent to expand to second order in the following parameters:

$$\sin^2 2\theta_{13}, \Delta_{21}L, (\Delta_{31}L)^2, (AL)^2, \eta_{\alpha\beta}, \quad (3.11)$$

with $\eta_{e\mu}$ set to zero, since it is already strongly constrained (see Eq. (3.4)) and its contributions are always suppressed by extra small parameters.

3.3.1 The $\nu_\mu \rightarrow \nu_\tau$ channel

The expression for $P_{\mu\tau}$ expanded to the order just described can be found in Appendix A. For this set-up matter effects are subleading. On the other hand, this probability is not suppressed by small standard parameters such as $\sin \theta_{13}$ or Δ_{21} . The two family approximation in Eq. (3.9) is thus very accurate to understand qualitatively the results and reads

$$P_{\mu\tau} = \sin^2(2\theta_{23}) \sin^2\left(\frac{\Delta_{31}L}{2}\right) - 2|\eta_{\mu\tau}| \sin \delta_{\mu\tau} \sin(2\theta_{23}) \sin(\Delta_{31}L) + 4|\eta_{\mu\tau}|^2. \quad (3.12)$$

²Notice that this is an estimation, a detailed studied about the behaviour of this detector is still lacking in the literature.

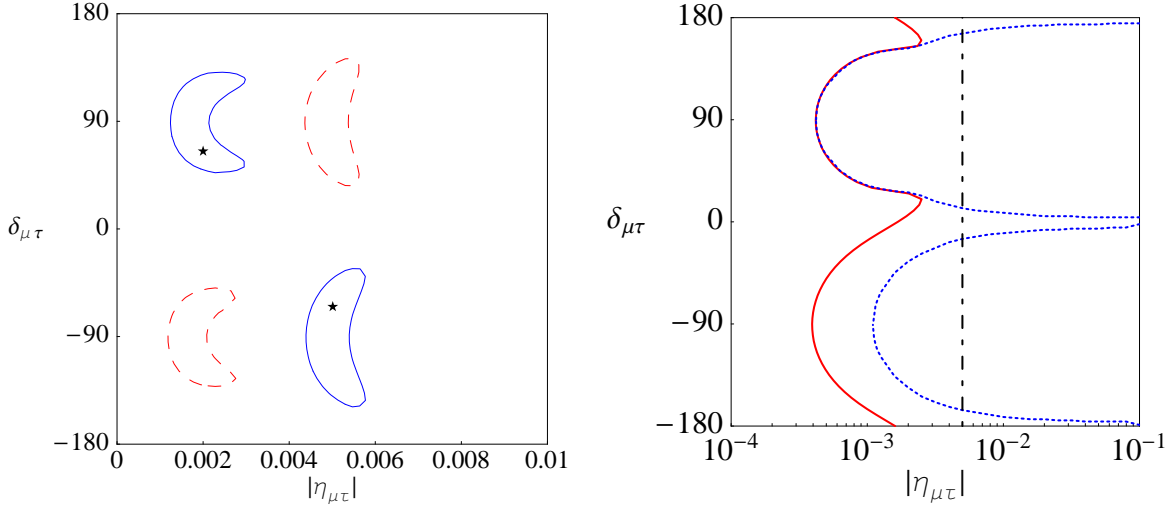


Figure 3.1: *Left: 3σ contours for two input values of $|\eta_{\mu\tau}|$ and $\delta_{\mu\tau}$ represented by the stars. Right: the solid line represents the 3σ sensitivity to $|\eta_{\mu\tau}|$ as a function of $\delta_{\mu\tau}$, the dotted line the 3σ sensitivity to $\delta_{\mu\tau}$ and the dotted-dashed line represents the present bound from $\tau \rightarrow \mu\gamma$.*

This equation indicates that the CP-odd interference term is only suppressed linearly in $|\eta_{\mu\tau}|$. This can indeed be observed in the result of the complete numerical computation, Fig. 3.1, which shows the sensitivities to $|\eta_{\mu\tau}|$ and $\delta_{\mu\tau}$ obtained. The left panel represents two fits to two different input values of $|\eta_{\mu\tau}|$ and $\delta_{\mu\tau}$ (depicted by stars). The dashed lines correspond to fits done assuming the *wrong* hierarchy, that is the opposite sign for Δ_{31} to that with which the number of events were generated. As expected from Eq. (3.12), a change of sign for the mass difference can be traded by a change of sign for $\delta_{\mu\tau}$. Nevertheless, this does not spoil the potential for the discovery of CP violation, since a non-trivial value for $|\delta_{\mu\tau}|$ is enough to indicate CP violation. Furthermore, the sinusoidal dependence implies as well a degeneracy between $\delta_{\mu\tau} \rightarrow 180^\circ - \delta_{\mu\tau}$, as reflected in the figure.

The right panel in Fig. 3.1 depicts the 3σ sensitivities to $|\eta_{\mu\tau}|$ (solid line) and $\delta_{\mu\tau}$ (dotted line), while the present bound from $\tau \rightarrow \mu\gamma$ is also shown (dashed line). The poorest sensitivity to $|\eta_{\mu\tau}|$, around 10^{-3} , is found in the vicinity of $\delta_{\mu\tau} = 0$ and $\delta_{\mu\tau} = 180^\circ$, where the CP-odd interference term vanishes and the bound is placed through the subleading $|\eta_{\mu\tau}|^2$ term. The latter is also present at zero distance and its effects were already considered in Chap. 2, obtaining a bound of similar magnitude. The sensitivity to $|\eta_{\mu\tau}|$ peaks around $|\eta_{\mu\tau}| \simeq 4 \cdot 10^{-4}$ for $\delta_{\mu\tau} \simeq \pm 90^\circ$, where $\sin \delta_{\mu\tau}$ is maximum. That is, for non-trivial values of $\delta_{\mu\tau}$ not only CP violation could be discovered, but values of $|\eta_{\mu\tau}|$ an order of magnitude smaller could be probed.

3.3.2 The $\nu_e \rightarrow \nu_\tau$ channel

Contrary to $P_{\mu\tau}$, all terms in $P_{e\tau}$, standard and new ones, are suppressed by at least one of the two small standard parameters $\sin \theta_{13}$ and Δ_{21} . The oscillation probability, expanded to second order in the parameters in Eq. (3.11), reads

$$\begin{aligned}
P_{e\tau} &= c_{23}^2 \sin^2 2\theta_{13} \left(\frac{\Delta_{31}L}{2}\right)^2 + s_{23}^2 \sin^2 2\theta_{12} \left(\frac{\Delta_{21}L}{2}\right)^2 \\
&- c_{13} \sin 2\theta_{12} \sin 2\theta_{23} \sin 2\theta_{13} \cos \delta \left(\frac{\Delta_{21}L}{2}\right) \left(\frac{\Delta_{31}L}{2}\right) \\
&- 2|\eta_{e\tau}|c_{23} \sin 2\theta_{13} \sin(\delta + \delta_{e\tau})(\Delta_{31}L) \\
&+ 2|\eta_{e\tau}|s_{23}c_{13} \sin 2\theta_{12} \sin \delta_{e\tau} \sin(\Delta_{21}L) \\
&+ 4|\eta_{e\tau}|^2,
\end{aligned} \tag{3.13}$$

where s_{ij} , c_{ij} stand for $\cos \theta_{ij}$, $\sin \theta_{ij}$, respectively.

The first three terms in Eq. (3.13) are the usual unitary contributions, suppressed quadratically in $\sin \theta_{13}$ and Δ_{21} . The next two are interference terms between the unitary oscillation contribution and the non-unitarity parameter $\eta_{e\tau}$, and are CP-odd and suppressed³ by $|\eta_{e\tau}|$ and either $\sin \theta_{13}$ or Δ_{21} . The last term is the zero distance effect only proportional to $|\eta_{e\tau}|^2$. Notice that Eq. (3.13) would also be valid for the $P_{e\mu}$ oscillation probability replacing $s_{23} \rightarrow -c_{23}$, $c_{23} \rightarrow s_{23}$ and $\eta_{e\tau} \rightarrow \eta_{e\mu}$. Although in the numerical analysis we have used the full oscillation probability in matter, the approximation in which Eq. (3.13) has been obtained shows no sensitivity to matter effects.

Fig. 3.2 shows the sensitivities to $|\eta_{e\tau}|$ and $\delta_{e\tau}$ with this setup. The left panel depicts a fit to the input value represented by the star: the dependence on $\delta_{e\tau}$ is seen to be very mild and no measurement of this quantity can be performed. This is easily understood from Eq. (3.13), for $|\eta_{e\tau}| > 10^{-3}$: the last term, proportional to $|\eta_{e\tau}|^2$, dominates over the CP-violating ones and no information on $\delta_{e\tau}$ can be extracted. In consequence, in the right panel we find 3σ sensitivities to $|\eta_{e\tau}|$ around 10^{-3} , but no sensitivity to $\delta_{e\tau}$. The sensitivity to $|\eta_{e\tau}|$ from the $|\eta_{e\tau}|^2$ term is also present at zero distance and already studied in Chap. 2, where a similar bound was obtained. We have checked that increasing the statistics by a factor 100, values of $|\eta_{e\tau}|$ an order of magnitude smaller would be accessible and the CP-violating terms would start to dominate, providing sensitivity to $\delta_{e\tau}$.

³This dependence was previously observed for $\nu_e \rightarrow \nu_\mu$ transitions in a related context in Ref. [157].

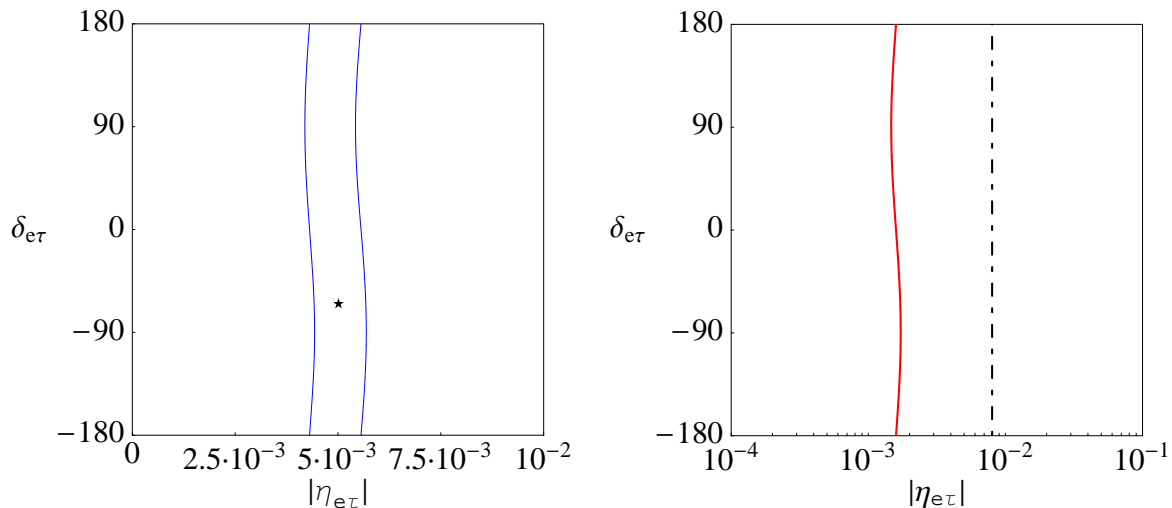


Figure 3.2: *Left: 3σ contour for an input value of $|\eta_{e\tau}|$ and $\delta_{e\tau}$ represented by the star; the $|\eta_{e\tau}|^2$ term dominates and there is no sensitivity to the CP-violating phase. Right: 3σ sensitivity to $|\eta_{e\tau}|$ as a function of $\delta_{e\tau}$, the dashed line represents the present bound from $\tau \rightarrow e\gamma$.*

3.4 IDS Neutrino Factory sensitivity to non-unitary leptonic mixing

In the previous section we have analysed a very particular Neutrino Factory set-up, with a ν_τ detector located at $L = 130$ km, tuned to maximize the new CP violation effects. However, future neutrino oscillation experiments, as a Neutrino Factory, are being designed to achieve ultimate performance for standard physics. We will now discuss the sensitivity to the different parameters of the MUV scheme in a more realistic Neutrino Factory setup, the one proposed in the International Design Study (IDS) [99, 100], which consists of ν_e and ν_μ beams from $5 \cdot 10^{20}$ muon decays per year per baseline. We consider a setting where the experiment is assumed to run for five years in each polarity. The parent muons are assumed to have an energy of 25 GeV. The beams are detected at two far sites, the first located at 4000 km with a 50 kton Magnetised Iron Neutrino Detector (MIND) [158] and a 10 kton Emulsion Cloud Chamber (ECC) for τ detection [142, 149], and the second located close to the magic baseline [94, 159] at 7500 km with an iron detector identical to the one at 4000 km.

A clean signal of a non-unitary mixing is the presence of “zero-distance effects” stemming from the non-orthogonality of the flavour states (see Eq. (2.20)). As we have commented before, if the flavour basis is not orthogonal, a neutrino of flavour α can be detected with flavour β without the need of flavour conversion in the propagation. This translates to a baseline-independent term in the oscillation probabilities, which is best probed at short distances, since the flux is larger and it cannot be hidden by the

standard oscillations. For short baselines, this term is ($\alpha \neq \beta$)

$$P_{\alpha\beta}(L = 0) = 4|\eta_{\alpha\beta}|^2 + \mathcal{O}(\eta^3). \quad (3.14)$$

The oscillation probabilities for longer baselines up to second order in the small parameters are derived in App. A. Near detectors are thus excellent for probing the zero-distance effect, in particular τ detectors are of importance, since the present bounds on $\eta_{e\mu}$ and $\eta_{\mu\mu}$ are rather strong. We will therefore study the impact of near τ detectors of different sizes located at 1 km from the beam source. In particular, we will present all the results for near detector sizes of 100 ton, 1 kton, and 10 kton, as well as the results without any near τ detector. Notice that 10 kton is the detector mass discussed for the ECC detector located at 4000 km. However, we have seen no improvement adding such a detector at that baseline while the gain in sensitivity that a near detector capable of τ detection can provide is significant, as we will discuss below. Therefore, we have also considered the largest mass to show what could be achieved with the planned 10 kton detector located at 1 km instead of 4000 km. To simulate the near detector, we use the point-source and far-distance approximations. These assumptions are reasonable, although somewhat optimistic in the high-energy region, as can be seen in Fig. 12 of Ref. [160]. However, the loss of flux at higher energies, which corresponds to the on-axis neutrinos, may be recovered by using rather elongated geometries of the near detector. These are precisely the kind of geometries that are being discussed for a magnetized version of the ECC (MECC). Such a detector would be limited in size by the above mentioned geometrical considerations and is not likely to be larger than 4 kton. On the other hand, as we have commented in the previous section, all the decay channels of the τ could be studied in the magnetized version, which would translate into an increase of the efficiency and backgrounds by a factor 5 with respect to the ECC search for τ decays into μ considered here. In anycase, we will consider the no-magnetized version of the ECC to be consistent with the IDS proposal. The impact of near μ detectors is still essentially to normalise the neutrino flux and cross-sections, since the bounds on $\eta_{\mu\mu}$ and $\eta_{e\mu}$ from the unitarity of the CKM matrix and $\mu \rightarrow e\gamma$ are particularly strong [112, 156].

In our simulations, we will study the “golden” $\nu_e \rightarrow \nu_\mu$ and ν_μ disappearance channels in the MIND detectors and the “silver” [142, 149] $\nu_e \rightarrow \nu_\tau$ and the $\nu_\mu \rightarrow \nu_\tau$ channels at the ECC detectors, both near and far. For the detector efficiencies and backgrounds, we follow the study in Ref. [158] of the MIND detector exposed to the Neutrino Factory beam. The efficiencies and backgrounds for the silver channel with an ECC detector are carefully discussed in Ref. [149] and we follow the results of that reference. Lacking an analogous study for the $\nu_\mu \rightarrow \nu_\tau$ channel, we assume the same efficiencies and backgrounds as those for the silver channel described in Ref. [149].

In the previous section we have scanned the relevant MUV parameters corresponding to each channel, having checked numerically that the impact of the rest of the parameters is irrelevant. In this section we go one step beyond: for our numerical simulations, we scan the complete MUV parameter space, adding nine unitarity-violating parameters to the six standard neutrino oscillation parameters. The scan is performed

using the MonteCUBES software [161, 162], which allows to perform Markov Chain Monte Carlo (MCMC) simulations with GLoBES [163, 164]. For the implementation of the unitarity deviations in the neutrino oscillation probabilities, we use the NonUnitarity Engine (NUE) distributed along with the MonteCUBES package. Using the MCMC technique allows the study of possible parameter correlations in the full parameter space without restricting the search to varying only a small subset of the parameters⁴. It is also important to note that, unlike in the standard usage of the GLoBES software, the use of MCMC techniques is based on Bayesian rather than frequentist parameter estimation and, as such, the result depends on the adopted priors. As priors, we will consider the current bounds on both the standard and the unitarity violating parameters, except for parameters to which the Neutrino Factory has superior sensitivity, for which we use flat priors.

Before discussing the more detailed studies, let us comment on some of the general results from the simulations. First of all, one of the most remarkable features is that the results do not contain significant correlations between any of the unitarity-violating parameters, nor are the unitarity-violating parameters significantly correlated with the standard neutrino oscillation parameters. The only exception are some mild correlations between θ_{13} , δ and the modulus and phase of $\eta_{e\tau}$ in the absence of near τ detectors which, however, do not lead to new degeneracies between these parameters or spoil the determination of θ_{13} and δ at the Neutrino Factory. Furthermore, the addition of a near τ detector of only 100 ton is enough to almost completely erase these correlations. This implies that the Neutrino Factory setup considered here has enough sensitivity to distinguish the effects induced by unitarity violation from changes in the standard parameters. Second, the sensitivities of the Neutrino Factory to the diagonal parameters of the η matrix, as well as to $\eta_{\mu e}$, do not improve with respect to the bounds derived from electroweak decays, which are too stringent to allow for observable effects at the Neutrino Factory. Notice that none of the oscillation probabilities studied here depend on η_{ee} , as shown in App. B.

We will thus concentrate on the sensitivities to $\eta_{\mu\tau}$ and $\eta_{e\tau}$ in the next subsections, even though the other unitarity-violating parameters and standard oscillation parameters are allowed to vary in the simulations. In all our simulations we assume [63, 166] $\theta_{12} = 33^\circ$, $\theta_{23} = 45^\circ$, $\Delta m_{21}^2 = 8 \cdot 10^{-5} \text{ eV}^2$ and $\Delta m_{31}^2 = 2.6 \cdot 10^{-3} \text{ eV}^2$. We also assumed 4 % priors on θ_{12} and Δm_{21}^2 at 1σ , flat priors were used for the rest of the standard oscillation parameters. For the unitarity-violating parameters, we consider Gaussian priors given by the ranges mentioned in Eq. 3.4.

⁴This is due to the fact that the number of evaluations required by Monte Carlo techniques increases at most polynomially with the number of parameters, while a scan based on grids in the parameter space would require to evaluate the event rates and likelihoods at a number of points that grows exponentially. For all of our figures, we have used simulations with four MCMC chains containing 2×10^6 samples each. In addition, we have checked that the chains have reached proper convergence, in all cases better than $R - 1 = 10^{-2}$ [165]

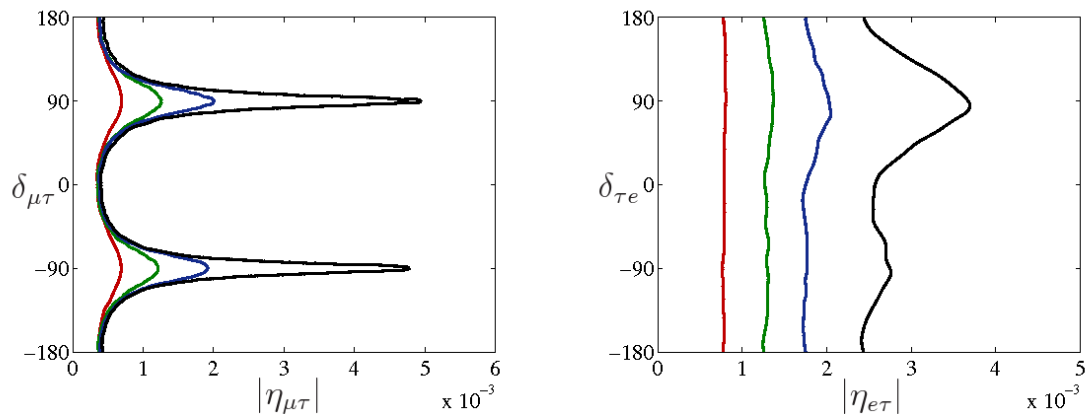


Figure 3.3: The 90 % confidence level sensitivity of the IDS Neutrino Factory to the unitarity-violating parameters $\eta_{\mu\tau}$ (left) and $\eta_{e\tau}$ (right). The different curves correspond to different sizes of the near τ detector, from left to right, 10 kton, 1 kton, 100 ton, no near detector.

3.4.1 Sensitivity to $\eta_{\mu\tau}$

In the left panel of Fig. 3.3, we show the sensitivity to the $\eta_{\mu\tau}$ parameter for the four different sizes considered for the near ECC. The input values for all the non-unitarity parameters and θ_{13} were set to zero to derive these curves. We have checked that the results do not depend strongly on this assumption. The most remarkable feature of this figure is the extreme sensitivity to the real part of $\eta_{\mu\tau}$ which is present already without any near detector. This sensitivity mainly originates from the matter effect on the disappearance channel, where the leading non-unitarity correction to the “amputated” oscillation probability⁵ is given by

$$\hat{P}_{\mu\mu} = P_{\mu\mu}^{\text{SM}} - 2 \text{Re}(\eta_{\mu\tau})AL \sin(\Delta_{31}L) + \mathcal{O}(\eta_{\mu\mu}), \quad (3.15)$$

where again $A = \sqrt{2}G_F n_e$, the terms we have omitted can be found in App. B. Notice that the $\nu_\mu \rightarrow \nu_\tau$ channel also depends linearly on $\eta_{\mu\tau}$ and that the dependence is CP-violating. On the other hand, the mass and efficiency of the ECC detector are much smaller compared to those of the MIND detectors for the ν_μ disappearance channel and therefore the sensitivity is dominated by the latter. As can be seen in the figure, a near τ detector will determine the modulus of $\eta_{\mu\tau}$ through the zero-distance effect. This would translate into a vertical band in the left panel of Fig. 3.3 and thus the increase of the mass of the near detector improves the measurement of the imaginary part. However, given the linear dependence due to the matter effects on propagation, the bound on the real part from the disappearance channel remains stronger. We can also see that the bound on the modulus does not require a very large near detector, the bound on the imaginary part is essentially only improved by approximately 30 % in moving from a 1 kton to a 10 kton ECC detector.

⁵The probability expression after removing the normalization factors (see Eq. (2.27)).

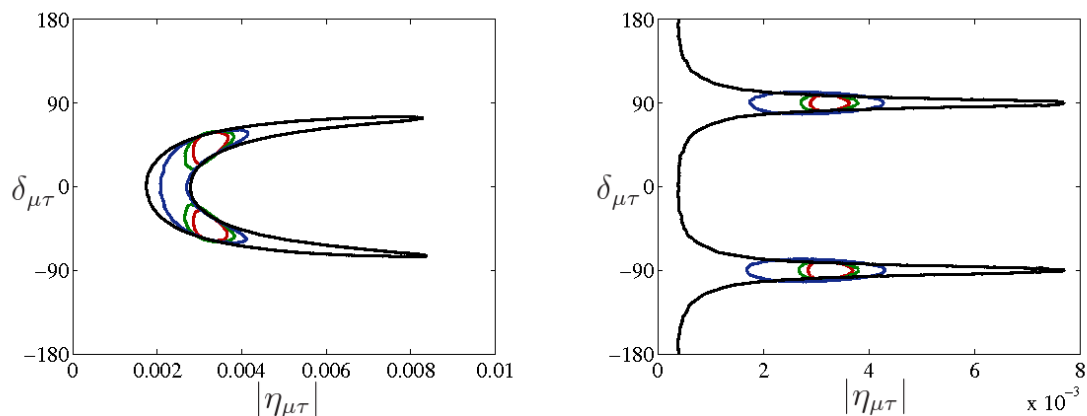


Figure 3.4: The sensitivity of the IDS Neutrino Factory to the unitarity violating parameter $\eta_{\mu\tau}$, assuming that it takes the value $\eta_{\mu\tau} = 3.2 \cdot 10^{-3} \exp(-i\pi/4)$ (left) and $\eta_{\mu\tau} = i 3.2 \cdot 10^{-3}$ (right). The different curves correspond to different sizes of the near τ detector, from inner to outer curves, 10 kton, 1 kton, 100 ton, no near detector.

Another important question is how well the Neutrino Factory would be able to measure the unitarity-violating parameters if they are non-zero. For this reason, in Fig. 3.4, we show the sensitivity to $\eta_{\mu\tau}$ assuming that $|\eta_{\mu\tau}| = 3.2 \cdot 10^{-3}$ as well as $\delta_{\mu\tau} = -45^\circ$ (left panel) and 90° (right panel), respectively, which is disfavoured at only 1σ by current bounds. Thus, this gives a flavour of the best possible situation for actually discovering unitarity violation and a new source of CP violation. Again, we can see that the sensitivity without the near detector is only to the real part of $\eta_{\mu\tau}$. In this setting, there is a degeneracy extending essentially as $|\eta_{\mu\tau}| \propto 1/\cos(\delta_{\mu\tau})$, along which the real part of $\eta_{\mu\tau}$ is constant and the imaginary part is changing. For the case with purely imaginary $\eta_{\mu\tau}$ in the right panel of Fig. 3.4, it is also no surprise that the results without the near detector are compatible with $\eta_{\mu\tau} = 0$. The introduction of near detectors results in an effective measurement of $|\eta_{\mu\tau}|$, *i.e.*, a vertical band in the plot, which intersects the far detector measurement giving rise to two degenerate solutions, one for positive and one for negative imaginary part. Again, the actual size of the near detector is not crucial and no significant gain is seen beyond 1 kton.

These figures also show the strong complementarity between the near and far detectors when it comes to measuring the phase of the unitarity-violating parameter, and thus also a non-standard source of CP violation. Neither the near nor the far detectors alone can establish a CP-violating phase by themselves. However, combining the two results excludes CP-conservation at 90 % confidence level.

Note that the slight widening of the allowed region when including the near detector results from the use of Bayesian statistics. Since the near detectors discard a large range of allowed values for $\delta_{\mu\tau}$ when $|\eta_{\mu\tau}|$ is close to zero, a slightly larger region in $\delta_{\mu\tau}$ close to the correct absolute value of $\eta_{\mu\tau}$ is needed in order to include 90 % of the probability distribution.

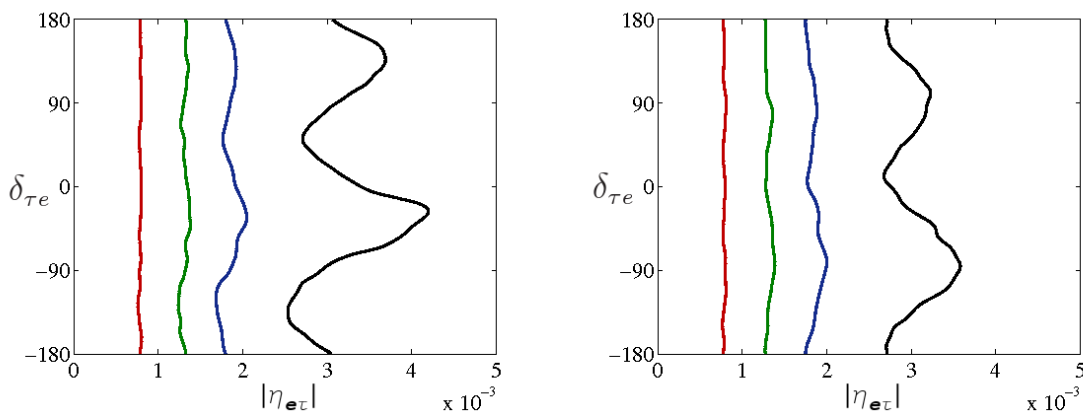


Figure 3.5: The 90 % confidence level sensitivity of the IDS Neutrino Factory to the unitarity-violating parameter $\eta_{e\tau}$ with $\theta_{13} = 5^\circ$ as well as $\delta = \pi/4$ (left) and $\delta = 0$ (right). The different curves correspond to different sizes of the near τ detector, from left to right, 10 kton, 1 kton, 100 ton, no near detector.

3.4.2 Sensitivity to $\eta_{e\tau}$

The right panel of Fig. 3.3 shows the sensitivity to the unitarity violation parameter $\eta_{e\tau}$ when the input values for θ_{13} and all the unitarity-violating parameters are set to zero. Analogously to the sensitivity to $\eta_{\mu\tau}$, the setup with only the far detectors is more sensitive to the real part of the parameter than to the imaginary one, although the difference is not as pronounced as for $\eta_{\mu\tau}$. Furthermore, as can be seen in the oscillation probabilities in App. B, the probabilities that depend on $\eta_{e\tau}$ are only the golden, silver and the $\nu_\mu \rightarrow \nu_\tau$ channels, where the dependence is quadratic rather than linear, which translates into a weaker bound. Thus, the inclusion of the near τ detector has a major impact also on the bound which is placed on the real part of $\eta_{e\tau}$. Indeed, for a 1 kton near τ detector, the sensitivity is essentially flat as a function of $\delta_{e\tau}$ and is dominated by the near detector. Again, the larger mass and efficiency of the MIND detector compared to the ECC translates into the golden rather than the silver or the $\nu_\mu \rightarrow \nu_\tau$ channels dominating the sensitivity to $\eta_{e\tau}$ from the far detectors alone. However, unlike the ν_μ disappearance channel, the golden channel is strongly dependent on the unknown parameters θ_{13} and δ and the input values assumed for them will influence the expected sensitivity to $\eta_{e\tau}$. Indeed, the $\nu_e \rightarrow \nu_\mu$ probability in

presence of non-unitarity is modified to:

$$\begin{aligned}
\hat{P}_{e\mu} = & P_{e\mu}^{\text{SM}} + |\eta_{e\tau}|^2 \sin^2 \left(\frac{\Delta_{31}L}{2} \right) \\
& + \text{Im} \left\{ \eta_{e\tau} \left[\frac{1}{2} \frac{\Delta_{21}}{A} \sin(2\theta_{12}) + \frac{\Delta_{31}s_{13}e^{i\delta}}{A - \Delta_{31}} \right] \right\} \sin \left(\frac{AL}{2} \right) \sin \left(\frac{\Delta_{31}L}{2} \right) \sin \left(\frac{\Delta_{31} - A}{2}L \right) \\
& + \text{Re} \left\{ \eta_{e\tau} \left[\frac{1}{\sqrt{2}} \frac{\Delta_{21}}{A} \sin(2\theta_{12}) \sin \left(\frac{AL}{2} \right) \cos \left(\frac{\Delta_{31} - A}{2}L \right) \right. \right. \\
& \quad \left. \left. - \frac{2\sqrt{2}\Delta_{31}s_{13}e^{i\delta}}{A - \Delta_{31}} \cos \left(\frac{AL}{2} \right) \sin \left(\frac{\Delta_{31} - A}{2}L \right) \right] \right\} \sin \left(\frac{\Delta_{31}L}{2} \right) \\
& + \mathcal{O}(\eta^3).
\end{aligned} \tag{3.16}$$

It is then clear that the relative importance of the real and imaginary parts of $\eta_{e\tau}$ in this probability strongly depends on the actual values of θ_{13} and δ . As an example of this dependence, in Fig. 3.5, we again show the sensitivity to $\eta_{e\tau}$, but for input values of $\theta_{13} = 5^\circ$, $\delta = \pi/4$ (left panel) and $\delta = 0$ (right panel).

Notice that while for $\delta = \pi/4$ the far MIND detectors are more sensitive to the imaginary part of $\eta_{e\tau}$ the situation is reversed for $\delta = 0$. However, the addition of the near τ detector for the silver channel dominates the bound and the curves incorporating the near detectors forecast the same sensitivity regardless of the true values of θ_{13} and δ .

In Fig. 3.6, we show the analogue of Fig. 3.4 for $\eta_{e\tau}$. In this case, we assume $|\eta_{e\tau}| = 5.0 \cdot 10^{-3}$ and $\delta_{\tau e} = 45^\circ$ and -90° , which again corresponds to the 1σ disfavoured region. For this example, CP violation would not be discovered for the $\delta_{\tau e} = -5^\circ$ case (left panel) at the 90 % CL, but it would be constrained roughly around its true value already by the far detectors. In addition, the inclusion of a near τ detector would again constrain the modulus and therefore be complementary to the far detector result. For the $\delta_{\tau e} = -90^\circ$ case (right panel), the complementarity of the near and far detectors is able to exclude CP-conservation at the 90 % CL.

3.5 MUV vs NSI

An interesting question, from the phenomenological point of view, is how the results presented in this chapter for the MUV scheme can apply to the more general framework of the so-called Non-Standard neutrino Interactions (NSI), widely studied in the neutrino physics literature.

The NSI are a phenomenological way to parametrize all the possible effects that NP can give in neutrino oscillation experiments. The idea is simple: adding to the SM lagrangian the effective four fermion operators which can lead to some effect in neutrino oscillations. Depending on the structure of the operators considered, they can affect to neutrino production or detection processes [153] or modify matter effects

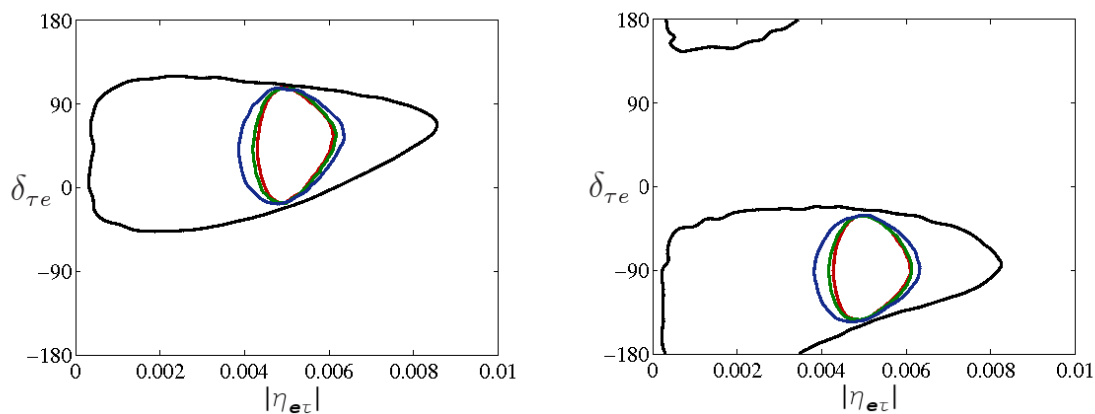


Figure 3.6: The sensitivity of the IDS Neutrino Factory to the unitarity-violating parameter $\eta_{e\tau}$, assuming that it takes the value $\eta_{e\tau} = 5.0 \cdot 10^{-3} \exp(-i\pi/4)$ (left) and $\eta_{e\tau} = i 5.0 \cdot 10^{-3}$ (right). The different curves correspond to different sizes of the near τ detector, from inner to outer curves, 10 kton, 1 kton, 100 ton, no near detector.

in propagation [151, 152]. The goal of the NSI analysis is to study, in a completely model-independent way, how the NP can affect to neutrino oscillations. It consists, thus, in a totally phenomenological approach. In a concrete model there would be some relationships among the coefficients of these operators and, even more, it can appear other operators affecting not only to the neutrino sector. In such a way that the NP coming from a model would be probably much more constrained than the NSI. As a result of this completely model-independent approach, the constraints in the NSI parameters are very mild (generically order 10^{-1} or even order one). For a recent review on the model-independent constraints on NSI see Ref. [167].

In order to clarify the impact of each operator, let us first write the effective SM lagrangian after integrating out the W field ⁶. In the flavour basis, it reads

$$-\mathcal{L}^{CC} = \frac{4G_F}{\sqrt{2}} \left[\sum_{\alpha\beta} (\bar{\nu}_\alpha^{SM} \gamma_\mu P_L l_\alpha) (\bar{d}_\beta \gamma_\mu P_L u_\beta) + (\bar{\nu}_\alpha^{SM} \gamma_\mu P_L l_\alpha) (\bar{l}_\beta \gamma_\mu P_L \nu_\beta^{SM}) + h.c. \right]. \quad (3.17)$$

The first term in Eq. (3.17) contributes to hadronic detection and production processes such as $\nu_\alpha d \rightarrow l_\alpha^- u$. The second term describes leptonic production and detection processes involving two neutrinos, such as muon decay at the Neutrino Factory, $\mu^+ \rightarrow e^+ \nu_e \bar{\nu}_\mu$, as well as matter effects for $\alpha = \beta = e$.

Non-standard neutrino interactions are introduced through analogous effective operators that can be non-diagonal in flavour. In Ref. [157], the following four-fermion

⁶For simplicity, we do not show the neutral current interactions nor the terms coming from CC interactions which would involve only quarks, since they are not relevant for this discussion.

operators were introduced:

$$\begin{aligned}\delta\mathcal{L}^P &= \frac{-4}{\sqrt{2}} \sum_{\alpha \neq e} G_{e\alpha}^P (\bar{\mu}\gamma_\mu P_L \nu_\mu^{SM}) (\bar{\nu}_\alpha^{SM} \gamma_\mu P_L e) + h.c., \\ \delta\mathcal{L}^D &= \frac{-4}{\sqrt{2}} \sum_{\beta \neq \mu} G_{\mu\beta}^D (\bar{\nu}_\beta^{SM} \gamma_\mu P_L \mu) (\bar{d}\gamma_\mu P_L u) + h.c.,\end{aligned}\quad (3.18)$$

which affect the production ($\delta\mathcal{L}^P$) and detection ($\delta\mathcal{L}^D$) processes at a Neutrino Factory, but do not correct matter effects. Adding these operators to the effective lagrangian of Eq. (3.17), the relevant terms in the interaction lagrangian are modified as follows:

$$\begin{aligned}-\mathcal{L}^{int} &= \frac{4G_F}{\sqrt{2}} \sum_\alpha \left[\left(\delta_{\alpha\mu} + \frac{G_{\mu\alpha}^D}{G_F} \right) (\bar{\nu}_\alpha^{SM} \gamma_\mu P_L \mu) (\bar{d}\gamma_\mu P_L u) + h.c. \right. \\ &\quad \left. + \left(\delta_{\alpha e} + \frac{G_{e\alpha}^P}{G_F} \right) (\bar{\nu}_\alpha^{SM} \gamma_\mu P_L e) (\bar{\mu}\gamma_\mu P_L \nu_\mu^{SM}) + h.c. \right].\end{aligned}\quad (3.19)$$

Defining now $\nu_\alpha^{SM} \equiv U_{\alpha i} \nu_i$, with U being the PMNS matrix, the effective production and detection states are given by:

$$\begin{aligned}|\nu_e^p\rangle &= (1 + \epsilon^{*p})_{e\beta} |\nu_\beta^{SM}\rangle = (1 + \epsilon^{*p})_{e\beta} U_{\beta i}^* |\nu_i\rangle \\ |\nu_\mu^d\rangle &= (1 + \epsilon^{*d})_{\mu\beta} |\nu_\beta^{SM}\rangle = (1 + \epsilon^{*d})_{\mu\beta} U_{\beta i}^* |\nu_i\rangle,\end{aligned}\quad (3.20)$$

where $\epsilon_{\alpha\beta}^{p(d)} = \frac{G_{\alpha\beta}^{P(D)}}{G_F}$, up to normalization factors.

These expressions are very similar to our parametrization of the effects of a non-unitary mixing matrix, Eq. (3.5). In fact, the latter can also be encoded in terms of effective four-fermion operators, after integrating out the W and Z bosons. The difference is that, in the case of a non-unitary mixing matrix, the coefficients of the different effective operators induced by it and contributing to production, detection and matter effects are not independent but related. For instance, it follows from Eq. (3.2) that $\eta_{\alpha\beta} = \eta_{\beta\alpha}^*$. If the relation $\epsilon_{\alpha\beta}^p = \epsilon_{\beta\alpha}^{d*}$ between NSI parameters in production and detection holds, a constraint usually not required when introducing non-standard interactions, the oscillation physics induced by NSI is equivalent in vacuum to that stemming from non-unitarity in the MUV scheme. Furthermore, even if no such relations among $\epsilon_{\alpha\beta}^p$ and $\epsilon_{\alpha\beta}^d$ are assumed, the order of magnitude of the bounds obtained in Sec. 3.3 should apply as well to non-standard interactions, barring fine-tuned cancellations. The new CP signals analysed in that section are also probes of the phases of non-standard interactions.

Finally, in Chap. 2 it was shown that matter effects are also modified in a very definite way in the presence of a non-unitarity mixing matrix. These new matter effects are not independent from the production/detection effects, contrary to the customary assumption in studies of NSI. Nevertheless, in the case studied in Sec. 3.3, as we have studied a setup such that matter effects - standard and new ones - are negligible, the

bounds derived there can be applied directly to the case of NSI. On the other hand, in the setup considered in Sec. 3.4 the matter effects are not at all negligible. Actually, the most interesting results for this setup come from the new matter effects that appear linearly in the $\nu_\mu - \nu_\tau$ sector (see Eq. 3.15). In order to understand to what extent these results could apply to the NSI case, let us very briefly study the case of the NSI affecting to propagation in matter (see for example Ref. [168]). These NSI effects come from the following four fermion effective operators:

$$\delta\mathcal{L}^{matter} = -2\sqrt{2}G_F \sum_{f,P} \epsilon_{\alpha\beta}^{fP} (\bar{\nu}_\alpha \gamma^\mu P_L \nu_\beta) (\bar{f} \gamma_\mu P f) , \quad (3.21)$$

where G_F is the Fermi constant, f stands for the index running over fermion species in the earth, $f = e, u, d$, and P stands for a projection operator which is either $P_L \equiv \frac{1}{2}(1 - \gamma_5)$ or $P_R \equiv \frac{1}{2}(1 + \gamma_5)$, and $\alpha, \beta = e, \mu, \tau$. The effect of these operators appear in the neutrino evolution equation modifying the effective potential in matter (see Eq. (1.63)), which in the ‘‘SM’’ flavour basis would read⁷:

$$A^{NSI} = A \begin{pmatrix} 1 + \epsilon_{ee}^m & \epsilon_{e\mu}^m & \epsilon_{e\tau}^m \\ \epsilon_{e\mu}^{m*} & \epsilon_{\mu\mu}^m & \epsilon_{\mu\tau}^m \\ \epsilon_{e\tau}^{m*} & \epsilon_{\mu\tau}^{m*} & \epsilon_{\tau\tau}^m \end{pmatrix} , \quad (3.22)$$

The corresponding effective potential, in the same basis, for the MUV scheme can be written as:

$$A^{MUV} = A \begin{pmatrix} 1 + \eta_{ee} & 0 & 0 \\ 0 & -\eta_{\mu\mu} & -\eta_{\mu\tau} \\ 0 & -\eta_{\mu\tau}^* & -\eta_{\tau\tau} \end{pmatrix} + \mathcal{O}(\eta^2) , \quad (3.23)$$

at first order in η , which has to be compared with Eq. (3.22). Then, we can conclude that the bounds on $\eta_{\mu\tau}$ obtained in Sec. 3.4 without considering near detectors, should apply as well to the NSI parameter $\epsilon_{\mu\tau}$ when only NSI affecting propagation are considered. Remember that the sensitivity to $\eta_{\mu\tau}$ in the IDS setup comes mainly from the matter effect on the disappearance channel, where the leading non-unitarity correction to the oscillation probability is given by the linear term presented in Eq. (3.15). This leading term is also the dominant one in the NSI case as it should be [169]. Notice that in case of the MUV scheme, near ν_τ -detector measurement is complementary to the disappearance sensitivity. This near detector is sensitive to the modulus giving some sensitivity to the imaginary part of $\eta_{\mu\tau}$ as a result of the combination with the disappearance channel measurements. However, this do not apply to the NSI case unless NSI effects in production/detection, with $\epsilon_{\mu\tau}^p = \epsilon_{\tau\mu}^{d*} = \epsilon_{\mu\tau}$, would be considered in the analysis as well.

⁷Notice that for completeness we have added the standard contribution to the effective potential.

Chapter 4

Sterile Neutrinos, a low energy source of three flavour unitarity violation

As we have already discussed in Sec. 1.4, in order to determine precisely the remaining parameters in the standard approach (assuming three light neutrinos and unitarity), $\text{sign}(\Delta m_{31}^2)$, θ_{13} and δ , long baseline experiments with intense neutrino beams have been proposed (see Sec. 1.4 for a brief discussion about the future neutrino oscillation facilities and Ref. [99] for a complete review). These precision measurements would allow us to look for deviation from the standard three flavour oscillations scenario, as we have shown for the MUV scheme case (see Chap. 3). Some of these new scenarios also break unitarity of the PMNS matrix, as the NSI which affect the neutrino production and detection processes (see Sec. 3.5) or the presence of light sterile neutrinos [27]. In this chapter we will focus on the latter.

Basically, the sterile neutrinos are nothing but fermionic singlets under the SM gauge group. The origin of neutrino masses could involve the presence of sterile neutrinos not only at high energies, like in the well known seesaw model (see Sec. 1.2.1), but also in the low-energy spectrum. If any of these sterile neutrinos is really in the low-energy spectrum, it could affect strongly to the oscillation physics. That is precisely what LSND seemed to indicate [48–50].

Four-neutrino mass schemes have attracted much attention since the announcement by the LSND group on evidence for neutrino oscillations $\bar{\nu}_\mu \rightarrow \bar{\nu}_e$ with a mass squared difference $\Delta m^2 \sim O(1) \text{ eV}^2$. Because the mass squared difference suggested by the LSND result is much larger than those for the solar and atmospheric neutrino oscillations, in order to explain all these data in terms of neutrino oscillations, it is necessary to introduce *at least* a fourth light neutrino state. From the LEP data [170,171], which indicate that the number of weakly interacting light neutrinos is three, the fourth state has to be a sterile neutrino. For this reason, the LSND signal could be considered as an evidence for the existence of a sterile neutrino. Recently the MiniBooNE ex-

periment [122] gave a negative result for neutrino oscillations with the mass squared difference $\Delta m^2 \sim O(1) \text{ eV}^2$ which was suggested by the LSND data, and it has become difficult for four-neutrino models to explain the LSND data. The so-called (3+2)-scheme with two sterile neutrinos has also been proposed [172] to account for LSND, but also in this case, tension with the disappearance experiments remains, as long as we take into account the LSND data. Adding a third sterile neutrino does not seem to help [173], and in general global analysis seem to indicate that sterile neutrinos alone are not enough to account for all the data in terms of neutrino oscillations. Models with sterile neutrinos and exotic physics have been therefore proposed [174–178].

While the efforts to account for all the data including the LSND in terms of neutrino oscillations have been unsuccessful, sterile neutrino scenarios which satisfy all the experimental constraints *except* LSND are still possible. Even if the inclusion of light sterile neutrinos is not needed to explain the present experimental data, it is certainly worth investigating scenarios where sterile neutrinos do appear and constrain their parameter space. Many theories of NP such as, for instance, in extra-dimensions models [179] or in the NMSSM [180–189] have in their low-energy spectrum fermionic singlets, therefore studying sterile neutrino models from a phenomenological point of view results still interesting.

In Ref. [190] the (3+1)-scheme without imposing the LSND constraint was studied in the context of the CNGS experiments [191], finding that if the OPERA detector is exposed to the nominal CNGS beam intensity, a null result can improve a bit the present bound on θ_{13} , but not those on the active-sterile mixing angles, θ_{14} , θ_{24} and θ_{34} .

In this chapter, we have extended the analysis in Ref. [190] to the case of a Neutrino Factory experiment (see Sec. 1.4 and, for a detailed description of the setup considered in this chapter, Sec. B.2). The main reason to consider this future oscillation experiment among all the proposed long baseline ones is again because a Neutrino Factory with multi-GeV muons results a powerful facility to look for τ 's signals, if detectors dedicated to τ -detection are provided. This point is of particular relevance for NP searches in neutrino oscillations, since the $\nu_\mu \rightarrow \nu_\tau$ oscillations could provide one promising signal of non-standard physics in oscillations, specially concerning possible new CP-violating signals associated to NP: it is the case in the MUV scheme and NSI (see Sec. 3.3, Sec. 3.5 and Refs. [115, 117, 192, 193]) and for sterile neutrinos as it will be shown along this chapter of the thesis.

We have first of all extended the analytic computation of the oscillation probabilities for the (3 + 1)-model at long baseline experiments in matter using the formalism by Kimura-Takamura-Yokomakura (KTY) [194, 195]. Approximated formulæ in powers of θ_{13} , of the deviations from maximality of θ_{23} ($\delta\theta_{23}$) and of the active-sterile mixing angles, θ_{i4} , have been obtained. On the basis of this analysis, we have found that the greatest sensitivity to the active-sterile mixing angles is achieved using the $\nu_\mu \rightarrow \nu_\mu$ and $\nu_\mu \rightarrow \nu_\tau$ channels (as it was noticed, for example, in Refs. [196, 197] and refs. therein). To take full advantage of these signals, detectors capable of both ν_μ and ν_τ identification are needed. In our numerical analysis we have, thus, assumed a detector of the Hybrid-

MIND type [158]: a 50 kton magnetized iron calorimeter next to a 4 kton Emulsion Cloud Chamber with magnetized iron plates (MECC). As it was already mentioned in the previous chapter, this detector has a greater efficiency to $\nu_\mu \rightarrow \nu_\tau$ than the standard OPERA-type ECC, with lead plates acting as target.

Four signals have been considered: the “standard” Neutrino Factory channels, the golden channel $\nu_e \rightarrow \nu_\mu$ and the silver channel $\nu_e \rightarrow \nu_\tau$; the ν_μ disappearance channel; and the novel signal $\nu_\mu \rightarrow \nu_\tau$. We have found that, as expected, the Golden channel has a similar great θ_{13} sensitivity to the one obtained in the three family analysis. So the Golden channel is still the best one to look for θ_{13} even in the presence of sterile neutrinos. We have also found that the Golden channel and the Silver one are sensitive only to an special combination of the active-sterile new mixing angles. On the other hand, thanks to the $\nu_\mu - \nu_\tau$ sector we could improve a lot the constraints on θ_{14} and θ_{24} with the set-up considered here. Finally, we show that the $\nu_\mu \rightarrow \nu_\tau$ channel has high-sensitivity to new CP-violating signals associated to the sterile neutrino physics, as found from the theoretical analysis of oscillation probabilities and confirmed with the numerical simulations.

An analysis such as this is not completely new: first studies of sterile neutrinos at a Neutrino Factory were presented at the first NuFact workshop in Lyon in 1999 [198,199] in the framework of the so-called (2+2)-schemes and subsequently extended to the case of (3+1)-schemes in Ref. [196]. The possibility to use the Neutrino Factory detectors, optimized to look for three-family oscillations, to disentangle three- from four-neutrino signals was considered in Ref. [197,200]. Recently, in Ref. [201] a four-family neutrino analysis in the spirit of Ref. [190] has been performed. The main differences between this work and Ref. [201] are (i) that careful numerical analysis are carried out here by taking into account backgrounds, efficiencies and systematic errors specific to the considered signals and setup, and (ii) that the four channels $\nu_\mu \rightarrow \nu_\tau$, $\nu_\mu \rightarrow \nu_\mu$, $\nu_e \rightarrow \nu_\mu$, $\nu_e \rightarrow \nu_\tau$ at the Neutrino Factory are considered and their contributions are clarified in the present chapter of the thesis.

This chapter is organized as follows. In Sec. 4.1 the main features of four-neutrino schemes and the present bounds on the mixing angles in these scenarios are briefly summarized. Furthermore we compute approximated oscillation probabilities in matter in the atmospheric regime using the KTY formalism [194,195] (details of our computations are given in Sec. B.5 of the corresponding Appendix). In Sec. 4.2 we present our results for the sensitivities and the analysis of the CP-violating signals, using various channels at the Neutrino Factory. Complementarily, in App. B we have also studied the region of the four-family parameter space for which a four-neutrino signal cannot be confused with the three-family model. Furthermore, in App. B we also remind the details of the considered Neutrino Factory setup and investigate the dependence of the different channel sensitivities on the systematic errors. All the results presented in this chapter come from Ref. [202].

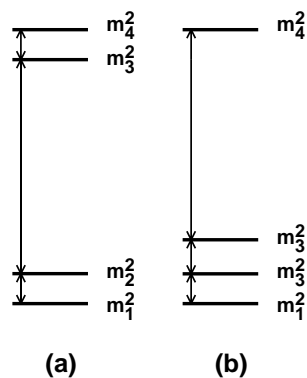


Figure 4.1: The two classes of four-neutrino mass spectra, (a): (2+2) and (b): (3+1).

4.1 Four neutrino schemes

Four-neutrino schemes consist of one extra sterile state in addition to the three weakly interacting ones. Depending on whether one or two mass eigenstate(s) are separated from the others by the largest mass-squared gap¹, the schemes are called (3+1)- and (2+2)-schemes, as is shown in Fig. 4.1. In the (3+1) schemes, there is a group of three close-by neutrino masses that is separated from the fourth one by the larger gap. In (2+2) schemes, there are two pairs of close masses separated by the large gap. These two classes lead to very different phenomenological consequences.

4.1.1 (2+2)-schemes

A characteristic feature of (2+2) schemes is that the extra sterile state cannot simultaneously decouple from *both* solar and atmospheric oscillations. The fraction of sterile neutrino contributions to solar and atmospheric oscillations is given by $\eta_s \equiv |U_{s1}|^2 + |U_{s2}|^2$ and $1 - \eta_s \equiv |U_{s3}|^2 + |U_{s4}|^2$, respectively, where the mass squared differences Δm_{21}^2 and $|\Delta m_{43}^2|$ are assumed to be those of the solar and atmospheric oscillations. The experimental results show that mixing among active neutrinos give dominant contributions to both the solar and atmospheric oscillations (see, e.g., Ref. [166]). In particular, in Fig. 19 of Ref. [166] we can see that at the 99% level $\eta_s \leq 0.25$ and $1 - \eta_s \leq 0.25$, which contradicts the unitarity condition $\sum_{j=1}^4 |U_{sj}|^2 = 1$. In fact the (2+2)-schemes are excluded at 5.1σ CL [166]. This conclusion is independent of whether we take the LSND data into consideration or not and we will not consider (2+2)-schemes in the rest of this paper.

¹The only assumption for the largest mass-squared difference is that oscillations caused by this mass-squared difference are averaged. So the results hold for any value of $\Delta m_{\text{sBL}}^2 \gtrsim 0.1 \text{ eV}^2$. Interesting models with “sterile” neutrino with masses $m \sim O(1) \text{ KeV}$ can be found, for example, in Ref. [203].

4.1.2 (3+1)-schemes with the LSND constraint

On the other hand, (3+1)-schemes are not affected by the tension between the solar and atmospheric constraints on sterile neutrino oscillations, because as long as the mixing of sterile neutrino is small, then phenomenology of solar and atmospheric oscillations is approximately the same as that of the three flavour framework. The (3+1) schemes start having a problem only when one tries to account for LSND and all other negative results of the short baseline experiments. To explain the LSND data while satisfying the constraints from other disappearance experiments, the oscillation probabilities of the appearance and disappearance channels have to satisfy the following relation [204,205]:

$$\sin^2 2\theta_{\text{LSND}}(\Delta m^2) \lesssim \frac{1}{4} \sin^2 2\theta_{\text{Bugey}}(\Delta m^2) \cdot \sin^2 2\theta_{\text{CDHSW}}(\Delta m^2) \quad (4.1)$$

where $\theta_{\text{LSND}}(\Delta m^2)$, $\theta_{\text{CDHSW}}(\Delta m^2)$, $\theta_{\text{Bugey}}(\Delta m^2)$ are the value of the effective two-flavour mixing angle as a function of the mass squared difference Δm^2 in the allowed region for LSND ($\bar{\nu}_\mu \rightarrow \bar{\nu}_e$), the CDHSW experiment [206] ($\nu_\mu \rightarrow \nu_\mu$), and the Bugey experiment [125] ($\bar{\nu}_e \rightarrow \bar{\nu}_e$), respectively. The reason that the (3+1)-scheme to explain LSND is disfavored is basically because Eq. (4.1) is not satisfied for any value of Δm^2 . A (3+2)-scheme with two sterile neutrino has also been proposed [172] to account for LSND, and it may be possible to reconcile the LSND and MiniBooNE data by introducing a CP phase [173,207]. Also in this case, however, tension with CDHSW [206] and Bugey [125] remains, as in the case of the (3+1)-scheme.

4.1.3 (3+1)-schemes without the LSND constraint

If we give up our effort to account for the LSND data, on the other hand, we no longer have the constraint (4.1). In this case we have only the upper bound on the extra mixing angles and this scenario satisfies all the experimental constraints (except that of LSND). Throughout the work presented in this chapter, therefore, we will consider a (3+1)-scheme without taking the LSND data into account while satisfying all the negative constraints, as it was done in Ref. [190].

It has been discussed that the mixing angles of four neutrino schemes may be constrained by big-bang nucleosynthesis (see Refs. [204,208] and references therein), and if such arguments are applied, then the mixing angles of sterile neutrinos would have to be very small. However, it is known that in some model [209] neutrino oscillations themselves create large lepton asymmetries which prevent sterile neutrinos from being in thermal equilibrium, so it is not so clear whether the arguments in Refs. [204,208] hold. At present, therefore, it is fair to say that there is not yet general consensus on this issue (see Ref. [210] and references therein). In this paper we will not impose cosmological constraints on our scheme.

Within the 3 + 1-scheme the mixing matrix U can be conveniently parametrized in terms of six independent rotation angles θ_{ij} and three (if neutrinos are Dirac fermions) or six (if neutrinos are Majorana fermions) phases δ_i . In oscillation experiments, only

the so-called ‘‘Dirac phases’’ can be measured, since the ‘‘Majorana phases’’ appear only as an overall phase of the oscillation amplitude and disappear in the oscillation probability (see Sec. 1.3.1). The Majorana or Dirac nature of neutrinos can thus be tested only in $\Delta L = 2$ transitions such as neutrino-less double β -decay (see Sec. 1.4.1) or lepton number violating decays [170]. In the following analysis, with no loss in generality, we will restrict ourselves to the case of 4 Dirac-type neutrinos only.

A generic rotation in a four-dimensional space can be obtained by performing six different rotations along the Euler axes. Since the ordering of the rotation matrices R_{ij} (where ij refers to the plane in which the rotation takes place) is arbitrary, plenty of different parametrizations of the mixing matrix U are allowed. In this paper we are interested in the so-called ‘‘atmospheric regime’’, with oscillations driven by the atmospheric mass difference, $\Delta_{\text{atm}} = \Delta m_{\text{atm}}^2 L/2E \sim O(1)$. We will then make use of the following parametrization, adopted in Ref. [173]:

$$U = R_{34}(\theta_{34}, 0) R_{24}(\theta_{24}, 0) R_{23}(\theta_{23}, \delta_3) R_{14}(\theta_{14}, 0) R_{13}(\theta_{13}, \delta_2) R_{12}(\theta_{12}, \delta_1). \quad (4.2)$$

In Eq. (4.2), $R_{ij}(\theta_{ij}, \delta_l)$ are the complex rotation matrices in the ij -plane defined as:

$$[R_{ij}(\theta_{ij}, \delta_l)]_{pq} = \begin{cases} \cos \theta_{ij} & p = q = i, j \\ 1 & p = q \neq i, j \\ \sin \theta_{ij} e^{-i\delta_l} & p = i; q = j \\ -\sin \theta_{ij} e^{i\delta_l} & p = j; q = i \\ 0 & \text{otherwise.} \end{cases} \quad (4.3)$$

It is convenient to put phases in R_{12} (so that it automatically drops in the limit $\Delta_{\text{sol}} = \Delta m_{\text{sol}}^2 L/2E \rightarrow 0$) and R_{13} (so that it reduces to the ‘‘standard’’ three-family Dirac phase when sterile neutrinos are decoupled). The third phase can be put anywhere; we will place it in R_{23} . Note that in the one-mass dominance regime [211] (i.e. for $\Delta_{\text{atm}}, \Delta_{\text{sol}} \rightarrow 0$) all the phases automatically disappear from the oscillation probabilities.

The mixing matrix elements in the parametrization (4.2) are given in the Appendix B.1.

This parametrization has been used in Ref. [190] to put bounds on the active-sterile mixing angles θ_{i4} using existing data (including MiniBooNE but neglecting LSND). These bounds can be summarized as follows:

1. Bounds from ν_e disappearance reactor experiments

Reactor experiments such as Bugey and CHOOZ can put stringent bounds on θ_{13} and θ_{14} in this parametrization: $\theta_{13} \leq 13^\circ$ and $\theta_{14} \leq 10^\circ$ at 99% CL, for any value of $\Delta m_{\text{SBL}}^2 > 0.1 \text{ eV}^2$, with some correlation between the two (in particular the four-family CHOOZ bound on θ_{13} is slightly modulated by θ_{14}).

2. Bounds from ν_μ disappearance experiments

A “negative” result in a ν_μ disappearance experiment at “atmospheric” L/E (such as K2K or MINOS), in which ν_μ oscillations can be very well fitted in terms of three-family oscillations, puts a stringent bound on the mixing angle θ_{24} . The bound from such experiments found in Ref. [190] is: $\theta_{24} \leq 14^\circ$ at 99% CL, for $\Delta m_{\text{SBL}}^2 \geq 0.1 \text{ eV}^2$.

3. Bounds on θ_{34}

Neither ν_e nor ν_μ disappearance probabilities in vacuum depend strongly on θ_{34} (as it can be seen in Ref. [190]). An upper bound on θ_{34} , however, can be drawn as the result of indirect searches for $\nu_\mu \rightarrow \nu_s$ conversion in atmospheric neutrino experiments, that take advantage of the different interaction with matter of active and sterile neutrinos. Present bounds on θ_{34} arise, thus, from a measurement of spectral distortion. On the other hand, bounds on θ_{13}, θ_{14} and θ_{24} are mainly drawn by a flux normalization measurement. As a consequence, the bound on θ_{34} that we can draw by non-observation of $\nu_\mu \rightarrow \nu_s$ oscillation in atmospheric experiments is less stringent than those we have shown before. For this reason, θ_{34} can be somewhat larger than θ_{13}, θ_{14} and θ_{24} : $\theta_{34} \leq 32^\circ$ at 99% CL.

These bounds are depicted in Fig. 2 of Ref. [190], where 90%, 95%, 99% and 3σ CL contours in the $(\theta_{13} - \theta_{14})$ - and $(\theta_{24} - \theta_{34})$ -planes are shown for $\Delta_{\text{sol}} \rightarrow 0$ and $\Delta m_{\text{atm}}^2 = 2.4 \times 10^{-3} \text{ eV}^2$ and $\theta_{23} = 45^\circ$.

4.1.4 Oscillation probabilities at the Neutrino Factory in the (3+1)-scheme

To understand the details of the different channels with the greatest sensitivity to the four-family neutrino schemes, it is useful to obtain simple analytical expressions for the different channels in matter. Hereafter, we will assume a constant Earth density along the neutrino path, computed using the PREM [212]. Notice that, in the framework of Neutrino Factory experiments simulations, the impact of non-constant matter density has been thoroughly studied, showing that for the baselines and the muon energy considered in this paper the details of the density profile crossed by neutrinos does not modify the results.²

To derive the oscillation probabilities, we adopt again the KTY formalism [194, 195] this time applied to the sterile neutrino case (the details are given in the Appendix, Sec. B.5). Furthermore, to get simplified forms of the formulæ, it is convenient to obtain the probabilities expanding with respect to the following small parameters:

$$\epsilon \equiv \theta_{34} \sim \sqrt{\theta_{13}} \sim \sqrt{\theta_{14}} \sim \sqrt{\theta_{24}} \sim \sqrt{\delta\theta_{23}} \lesssim 4 \times 10^{-1},$$

with $\delta\theta_{23} = \theta_{23} - \pi/4$.

²This is totally different, for example, in the case of β -Beams with Li/B decaying ions. In those setups, a resonance is crossed for $O(5 \text{ GeV})$ neutrinos for $L = O(10000) \text{ km}$ baselines [86].

The relevant oscillation probabilities in matter, expanded to third order in ϵ , are given by

$$P_{ee} \sim 1 + O(\epsilon^4), \quad (4.4)$$

$$P_{e\mu} \sim P_{e\tau} \sim P_{es} \sim O(\epsilon^4), \quad (4.5)$$

$$P_{\mu\mu} = 1 - \sin^2 \frac{\Delta_{31}L}{2} - 2(A_n L) s_{24} s_{34} \cos \delta_3 \sin \Delta_{31}L + O(\epsilon^4), \quad (4.6)$$

$$P_{\mu\tau} = (1 - s_{34}^2) \sin^2 \frac{\Delta_{31}L}{2} + \{s_{24} s_{34} \sin \delta_3 + 2(A_n L) s_{24} s_{34} \cos \delta_3\} \sin \Delta_{31}L + O(\epsilon^4), \quad (4.7)$$

$$P_{\mu s} = s_{34}^2 \sin^2 \frac{\Delta_{31}L}{2} - s_{24} s_{34} \sin \delta_3 \sin \Delta_{31}L + O(\epsilon^4), \quad (4.8)$$

where as always along this thesis $\Delta_{31} = \Delta m_{31}^2/2E$, and we take the convention that the central value of $|\Delta m_{31}^2|$ is Δm_{atm}^2 , which is determined by the two flavour analysis of the atmospheric neutrino data. The matter density parameter A_n is $A_n = \sqrt{2}G_F n_n/2$. Notice that at $O(\epsilon^3)$ the expansion parameter $\delta\theta_{23}$ is not present in the oscillation probabilities (it only arises at the next order in ϵ). Take into account that this is a very rough approximation, but useful to understand the physics behind as we will see.

From Eqs. (4.4)-(4.8), it can be easily verified that unitarity of the PMNS matrix is satisfied to this order in ϵ . As it can be seen, moreover, the ν_e decouples within this approximation. We can thus conclude that the ‘‘classic’’ Neutrino Factory channels, such as the ‘‘golden channel’’ $\nu_e \rightarrow \nu_\mu$ and the ‘‘silver channel’’ $\nu_e \rightarrow \nu_\tau$, are of limited interest to study sterile neutrinos, as we will see later in the numerical analysis.³ Leading sensitivity to θ_{34} is provided by the first term in $P_{\mu\tau}$, Eq. (4.7), that is proportional to $(1 - s_{34}^2)$. Sensitivity to θ_{24} is best achieved using the $\nu_\mu \rightarrow \nu_\mu$ oscillations, though the relevant term appears at $O(\epsilon^4)$, as it will be shown in Sec. 4.2.3. In Eqs. (4.6)-(4.7) we can also see that combined sensitivity to θ_{24} and θ_{34} is achievable through the $O(\epsilon^3)$ matter-dependent $s_{24}s_{34} \cos \delta_3$ term in $P_{\mu\mu}, P_{\mu\tau}$. The bounds on these two angles are those that can be improved the most by the Neutrino Factory experiments. We can thus safely say that the ν_μ disappearance channel and the $\nu_\mu \rightarrow \nu_\tau$ appearance channel are the most relevant signals to look for sterile neutrinos. This will be confirmed by the numerical analysis later.

Notice that θ_{34} is considerably less constrained than the rest of the new angles (which are as constrained as θ_{13}). Therefore, the $\nu_\mu \rightarrow \nu_\tau$ channel would have at the theoretical level the strongest sensitivity to sterile neutrino parameter space: $P_{\mu\tau}$ is the only one (with the exception of $P_{\mu s}$, that cannot be directly measured) that is of $O(\epsilon^2)$ in the expansion parameters. Moreover, $\nu_\mu \rightarrow \nu_\tau$ can also look for CP-violating signals in four-family scenarios through the $O(\epsilon^3)$ matter-independent $s_{24}s_{34} \sin \delta_3$ term, something out of the reach of the ν_μ disappearance channel (that can only measure δ_3 through CP-conserving signals).

³This has been known since long. See for example Refs. [190, 196, 197].

As it is well known, τ -detection experiments are extremely difficult at the experimental level. If the experimental problems could be overcome, $\nu_\mu \rightarrow \nu_\tau$ would be an important channel to study sterile neutrinos as well as other kinds of NP, such as unitarity violations coming from heavy fermions (see Sec. 3.3 and [117]), or the non-standard interactions (see Sec. 3.5 and [192, 193]). In particular, if CP violation occurs due to these NP, then the $\nu_\mu \rightarrow \nu_\tau$ channel is quite powerful in measuring the new CP-violating phases. For this reason, it has been named in Ref. [202] as “*the discovery channel*”.

4.2 Sensitivity to (3+1) sterile neutrinos at the Neutrino Factory

We have considered two experimental set-ups. First, to take advantage of the ν_τ detection, a 50 GeV Neutrino Factory which has 2×10^{20} useful muon decays per year aimed at two detectors of the Hybrid-MIND type located at $L = 3000$ km and $L = 7500$ km from the source, with both polarities running for 4 years each. These Hybrid-MIND detectors are made of a 4 kton magnetized Emulsion Cloud Chamber (MECC) sector to detect taus, next to a 50 kton magnetized iron calorimeter (MIND) to detect muons. The reason to consider such a high energy set-up is because from the ν_τ detection point of view going to higher energies clearly makes a difference (see Fig. B.1 of App. B). As a consistency check, we have also studied the case of a 20 GeV Neutrino Factory which has 5×10^{20} useful muon decays per year aimed at the same two detectors of the Hybrid-MIND located at $L = 4000$ km and $L = 7500$ km, again with both polarities running for 4 years each. The latter option is a scenario inspired in the International Scoping Study for a future Neutrino Factory and Super-Beam facility (ISS)⁴. The relevant backgrounds, efficiencies and systematic errors have been taken into account. All the details can be found in the Appendix B.2. We should remark again that future oscillation facilities as the Neutrino Factory are designed in order to measure the standard unknown parameters, mainly: θ_{13} , $sign(\Delta m_{31}^2)$, and the Dirac CP-phase δ . Therefore, these new long baseline facilities are focused on the measurement of standard oscillation physics and not on NP. For instance, near detectors at a Neutrino Factory with multi-GeV muons could perform better than the $\mathcal{O}(10^3)$ km ones to study sterile neutrino oscillations. This is because the new mass difference associated to the extra sterile neutrino, $\Delta m_{4i}^2 \gtrsim 0.1 eV^2$, is much larger than the atmospheric and solar ones (which for very short baselines produce negligible effects in the oscillation). However, we limitate our study to a Neutrino Factory set-up without near detectors, leaving for future works the possibility of considering them in this context. In any case, the impressive statistics of the Neutrino Factory and the opportunity of studying $\nu_\mu \rightarrow \nu_\tau$ oscillations can provide very interesting sensitivities to the 3 + 1 sterile neutrino parameters, as we will show below.

⁴The ISS is a previous step with respect to the already mentioned IDS study, for this reason the Neutrino Factory setup suggested by the ISS working group is actually more open than the IDS one

In this section we study the physics reach of the 50 GeV Neutrino Factory setup, discussed in App. B.2, to (3+1)-model sterile neutrinos, comparing the results with the case of the ISS inspired setup. We will make use of all possible oscillation channels available at this setup, namely the golden channel $\nu_e \rightarrow \nu_\mu$ and the disappearance channel $\nu_\mu \rightarrow \nu_\mu$ using the MIND section of the detector; the silver channel $\nu_e \rightarrow \nu_\tau$ and the “discovery channel” $\nu_\mu \rightarrow \nu_\tau$ using the MECC section of the detector.

In the numerical analysis (see App. B.3 for details) along this chapter, unless otherwise stated, the following parameters in common between three- and four-family models have been kept fixed to their central values: $\theta_{12} = 34^\circ$ and $\Delta m_{21}^2 = 7.9 \times 10^{-5} \text{ eV}^2$ ⁵. The following two parameters specific to the four-family model have been also kept fixed: $\Delta m_{41}^2 = 1 \text{ eV}^2$ and $\delta_1 = 0$. In any case, since our set-up is mainly sensitive to the “*atmospheric regimen*” the biggest mass differences Δm_{4i}^2 are in very good approximation averaged out, therefore our results actually hold for any value of $\Delta m_{41}^2 \gtrsim 0.1 \text{ eV}^2$. For the same reason fixing the solar parameters, θ_{12} and Δm_{21}^2 , have no significant impact on the results. δ_1 has been kept fixed to zero for simplicity. To take into account the information from present oscillation experiments, priors have been introduced (see App. B.3 for details) for the atmospheric parameters, θ_{23} and Δm_{31}^2 , as well as for the following small angles: θ_{13} , θ_{14} , θ_{24} and θ_{34} . The input values assumed for the atmospheric parameters are: $\theta_{23} = 45^\circ$ and $\Delta m_{31}^2 = 2.4 \times 10^{-3} \text{ eV}^2$. Finally, matter effects have been included considering a constant matter density $\rho = 3.4 \text{ g/cm}^3$ for the shortest baseline and $\rho = 4.3 \text{ g/cm}^3$ for the longest one, computed averaging over the density profile in the PREM [212] along the neutrino path. We have checked that marginalization over a 10% matter density uncertainty does not modify our results.

4.2.1 Sensitivity to $(\theta_{13}, \theta_{14})$

In this section first we discuss sensitivity to $(\theta_{13}, \theta_{14})$ at the Neutrino Factory. As we will see below, sensitivity to θ_{14} turns out to be poor. So we will consider sensitivity to other combinations of the mixing matrix elements in Sec. 4.2.2.

Sensitivity to $(\theta_{13}, \theta_{14})$

In the numerical analysis of this subsection, we have chosen the following relevant set of parameters to marginalize over: $\theta_{24} \in [0, 12^\circ]$, $\theta_{34} \in [0, 35^\circ]$ and $\delta_2, \delta_3 \in [0, 360^\circ]$.

It is useful to show here the analytic expressions for the golden and silver channels oscillation probabilities in vacuum. For both channels it is mandatory to go beyond the $O(\epsilon^3)$ of the expansion in power of small parameters that was shown in Eqs. (4.4-4.8). At high orders in powers of ϵ , it is no longer possible to neglect terms proportional to the solar mass difference. In particular, for the short baseline $L = 3000 \text{ km}$ (the only case in which vacuum formulæ give some insight on the numerical results), the parameter $\Delta_{21}L$

⁵We will not introduce any label to distinguish these parameters between three- and four-family models.

ranges from $O(\epsilon^3)$ to $O(\epsilon^4)$, depending on the neutrino energy. We will thus show the oscillation probabilities $P_{e\mu}$ and $P_{e\tau}$ to order ϵ^8 in powers of $\sqrt{\theta_{13}}$, $\sqrt{\theta_{14}}$, $\sqrt{\theta_{24}}$, $\sqrt{\delta\theta_{23}}$, θ_{34} and $(\Delta_{21}L)^{1/4}$. For completeness, we have also computed the oscillation probability $P_{e\bar{s}}$ and P_{ee} to the same order in ϵ ($P_{e\bar{s}}$ can be found in the App. B.5), checking unitarity of the mixing matrix. Oscillation probabilities in matter at this order in ϵ are difficult to obtain and they will not be presented here.

The golden channel oscillation probability expanded to order ϵ^8 in vacuum is:

$$\begin{aligned}
P_{e\mu} = & 2\theta_{14}^2\theta_{24}^2 + 2\{\theta_{13}^2(1 + 2\delta\theta_{23} - \theta_{13}^2 - \theta_{14}^2 - \theta_{24}^2)\} \sin^2 \frac{\Delta_{31}L}{2} \\
& + 2\sqrt{2}\theta_{13}\theta_{14}\theta_{24}(1 + \delta\theta_{23}) \sin\left(\delta_2 - \delta_3 + \frac{\Delta_{31}L}{2}\right) \sin \frac{\Delta_{31}L}{2} \\
& + \sin 2\theta_{12}\theta_{13}(\Delta_{21}L) \cos\left(\delta_1 - \delta_2 + \delta_3 - \frac{\Delta_{31}L}{2}\right) \sin \frac{\Delta_{31}L}{2} \\
& + \frac{1}{\sqrt{2}} \sin 2\theta_{12}\theta_{14}\theta_{24}(\Delta_{21}L) \sin \delta_1 - s_{12}^2\theta_{13}^2(\Delta_{21}L) \sin \Delta_{31}L + \frac{1}{2} \sin^2 2\theta_{12}(\Delta_{21}L)^2,
\end{aligned} \tag{4.9}$$

whereas the silver channel oscillation probability at the same order is:

$$\begin{aligned}
P_{e\tau} = & 2\theta_{14}^2\theta_{34}^2 \\
& + 2\{\theta_{13}^2(1 - 2\delta\theta_{23} - \theta_{13}^2 - \theta_{14}^2 - \theta_{34}^2 + 2\delta\theta_{23}\theta_{34}^2) - \theta_{13}^2\theta_{24}\theta_{34} \cos \delta_3\} \sin^2 \frac{\Delta_{31}L}{2} \\
& - 2\sqrt{2}\theta_{13}\theta_{14}\theta_{24}\theta_{34}^2 \sin\left(\delta_2 - \delta_3 + \frac{\Delta_{31}L}{2}\right) \sin \frac{\Delta_{31}L}{2} \\
& + 2\sqrt{2}\theta_{13}\theta_{14}\theta_{34} \left(1 - \delta\theta_{23} - \frac{\theta_{34}^2}{2}\right) \sin\left(\delta_2 + \frac{\Delta_{31}L}{2}\right) \sin \frac{\Delta_{31}L}{2} \\
& - \sin 2\theta_{12}\theta_{13}(1 - \theta_{34}^2)(\Delta_{21}L) \cos\left(\delta_1 - \delta_2 + \delta_3 - \frac{\Delta_{31}L}{2}\right) \sin \frac{\Delta_{31}L}{2} \\
& - \frac{1}{\sqrt{2}} \sin 2\theta_{12}\theta_{14}\theta_{34}(\Delta_{21}L) \sin(\delta_1 + \delta_3) - s_{12}^2\theta_{13}^2(\Delta_{21}L) \sin \Delta_{31}L + \frac{1}{2} \sin^2 2\theta_{12}(\Delta_{21}L)^2.
\end{aligned} \tag{4.10}$$

Notice that the golden and silver channel expressions have leading terms proportional to θ_{13}^2 , i.e. they are $O(\epsilon^4)$ (as it was anticipated in Sec. 4.1.4). This is the same order at which leading terms arise in the three-family model. We expect, thus, a similar sensitivity to θ_{13} in both three- and four-model analysis at the Neutrino Factory using these channels. On the other hand, we expect poor sensitivity to θ_{14} using these channels. First of all, dependence on θ_{14} in the golden and silver channel arise only at higher orders in ϵ (at $O(\epsilon^6)$ for the golden channel and at $O(\epsilon^5)$ for the silver channel, respectively). Secondly, all the terms proportional to θ_{14} in the above probabilities appear in combination with either θ_{34} or θ_{24} , so when we evaluate the value of $\Delta\chi^2$ by marginalizing over θ_{34} and θ_{24} , both of which have tendency to be small because

of the priors, these two probability can become almost independent of θ_{14} . For this reason, we expect poor sensitivity to θ_{14} using these channels. Nevertheless we discuss the sensitivities to both θ_{13} and θ_{14} because the sensitivity to θ_{13} can have nontrivial dependence on the true value of θ_{14} in the four neutrino case, as we will see below.

Eventually, the ν_e disappearance probability is:

$$\begin{aligned}
P_{ee} = & 1 - 2\theta_{14}^2(1 - \theta_{14}^2) - 4\theta_{13}^2(1 - \theta_{13}^2 - 2\theta_{14}^2)\sin^2\frac{\Delta_{31}L}{2} \\
& + 2s_{12}^2\theta_{13}^2(\Delta_{21}L)\sin\Delta_{31}L - \sin^2 2\theta_{12}(\Delta_{21}L)^2
\end{aligned} \tag{4.11}$$

Notice that this channel has leading $O(\epsilon^4)$ dependence on both θ_{13} and θ_{14} . For this reason the most stringent bound on this angle has been obtained by reactor experiments, as we have shown in Sec. 4.1.3. A detector with an extremely good electron identification efficiency is needed to perform this task, however, something beyond the reach of the MIND or MECC detectors. We are, thus, not considering this channel in the present work.

Figs. 4.2 and 4.3 present the sensitivity to (3+1)-sterile neutrinos in the $(\theta_{13}^{(4\text{fam})}, \theta_{14})$ -plane at 90% CL at the 50 GeV Neutrino Factory setup for several representative choices of δ_2 and δ_3 . In particular, δ_3 has been fixed to $\delta_3 = 0$ and 90° in Fig. 4.2 and Fig. 4.3, respectively. In both cases, the phase δ_2 (that reduces to the three-family CP-violating phase δ in the limit $\theta_{i4} \rightarrow 0$) has been fixed to $\delta_2 = 0, 90^\circ, 180^\circ$ and 270° . Results for the two baselines are shown both separately and summed: blue lines stand for the shortest baseline data; red lines stand for the longest baseline data; green lines stand for the sum of the two baselines. Solid lines stand for golden channel data, only, whereas dashed lines stand for the sum of golden and silver channels data. Eventually, the horizontal dashed grey line represents the present bound on θ_{14} that takes into account the four-family analysis of the atmospheric and reactor data.

First of all, notice that the golden and silver channel data show a very limited sensitivity to θ_{14} when marginalizing over θ_{24} and θ_{34} , as it was expected by inspection of the oscillation probabilities $P_{e\mu}$ and $P_{e\tau}$, Eqs. (4.9,4.10).

Secondly, when we focus on the golden channel results (solid lines), we notice a rather different behavior at the short and long baseline. At the short baseline, the sensitivity to $\theta_{13}^{(4\text{fam})}$ is significantly phase-dependent: the maximal sensitivity to $\theta_{13}^{(4\text{fam})}$ ranges from $\sin^2 2\theta_{13}^{(4\text{fam})} = 1.5 \times 10^{-5}$ for $\delta_2 = \delta_3 = 0$ to 6×10^{-3} for $\delta_2 = \delta_3 = 90^\circ$, with a strong dependence on the θ_{14} value. This is a consequence of cancellations between the term proportional to $\theta_{13}(\Delta_{21}L)$ in the third line of Eq. (4.9), that in three-family represents the interference between solar and atmospheric oscillations, and the term proportional to $\theta_{13}\theta_{14}\theta_{24}$ in the second line of the same equation.

The behavior is extremely different when we consider the golden channel at the long baseline. The location of the far detector corresponds to the three-family ‘‘magic baseline’’ [159], where the three-family dependence on the CP-violating phase δ vanishes. Notice that this happens as a consequence of the vanishing of the term in the third line of Eq. (4.9) when computed in the Earth matter. This is, indeed, the only term

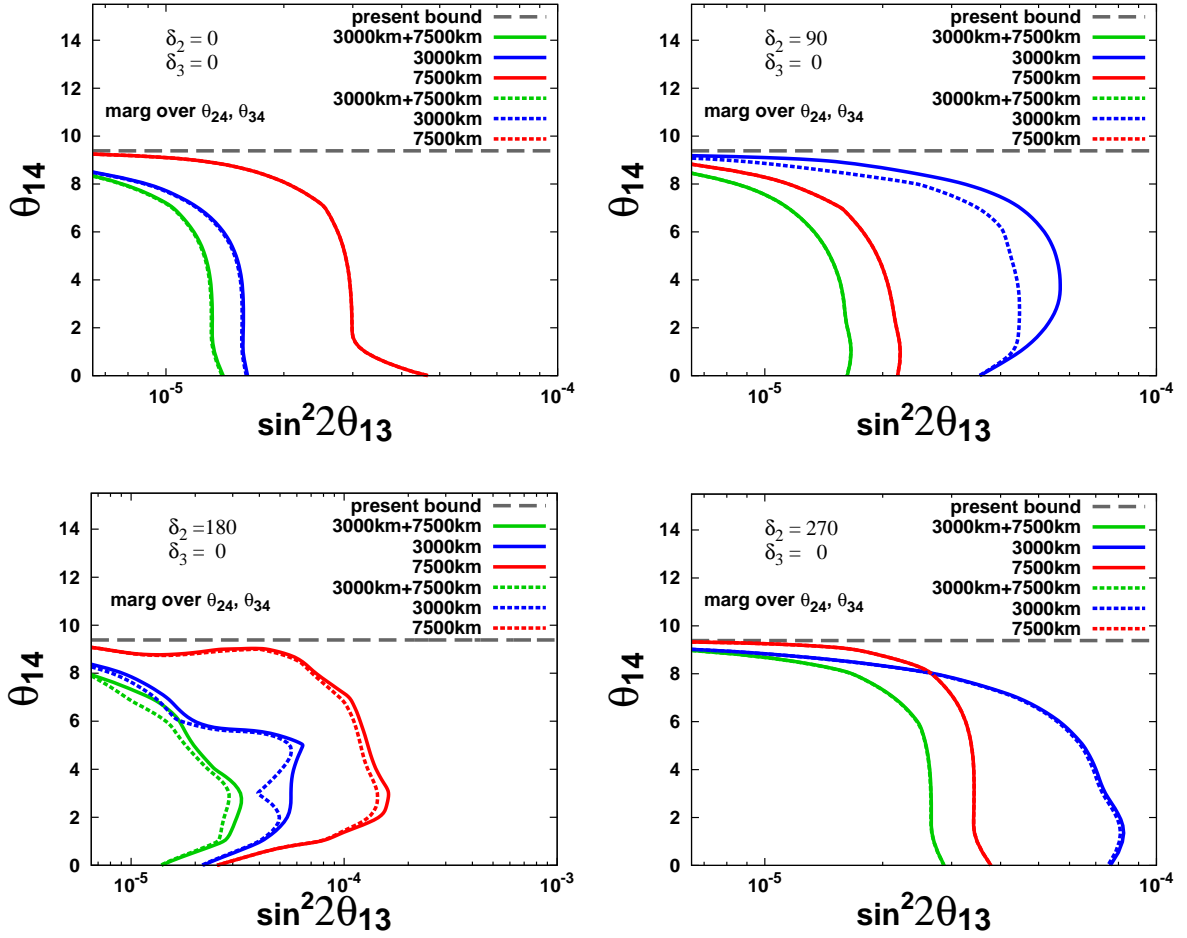


Figure 4.2: Sensitivity limit at 90% CL in the $(\sin^2 2\theta_{13}, \theta_{14})$ plane for $\delta_3 = 0$ and different values of δ_2 . The solid lines refer to the golden channel results, only. Dashed lines stand for the sum of golden and silver channel results. The colors are: blue for $L = 3000$ km; red for $L = 7500$ km; green for the combination of the two baselines; the horizontal dashed grey line represents the present bound on θ_{14} . The four panels represent our results for: $\delta_2 = 0$ (top left); $\delta_2 = 90^\circ$ (top right); $\delta_2 = 180^\circ$; (bottom left); $\delta_2 = 270^\circ$ (bottom right).

through which a δ -dependence enters into the three-family golden channel oscillation probability. The four-family term in the second line of Eq. (4.9), disappears for vanishing θ_{i4} , while the third term reduces to the three-family one when δ_1 and δ_3 vanish as well. Therefore, no cancellations between different terms occur at this baseline and sensitivity to $\theta_{13}^{(4\text{fam})}$ depends much less than for the short baseline on the values of δ_2, δ_3 and θ_{14} . This is precisely what we can see in all panels of Fig. 4.2 and 4.3.

A similar effect can be observed when we add the silver channel data to the golden channel ones at the short baseline. In this case, the term in the third line of Eq. (4.9) cancels with the term in the fifth line of Eq. (4.10) at the leading order, leaving an $O(\epsilon^8)$ term suppressed by $\theta_{13}\theta_{34}^2(\Delta_{21}L)$. Also in this case, we see indeed in all panels

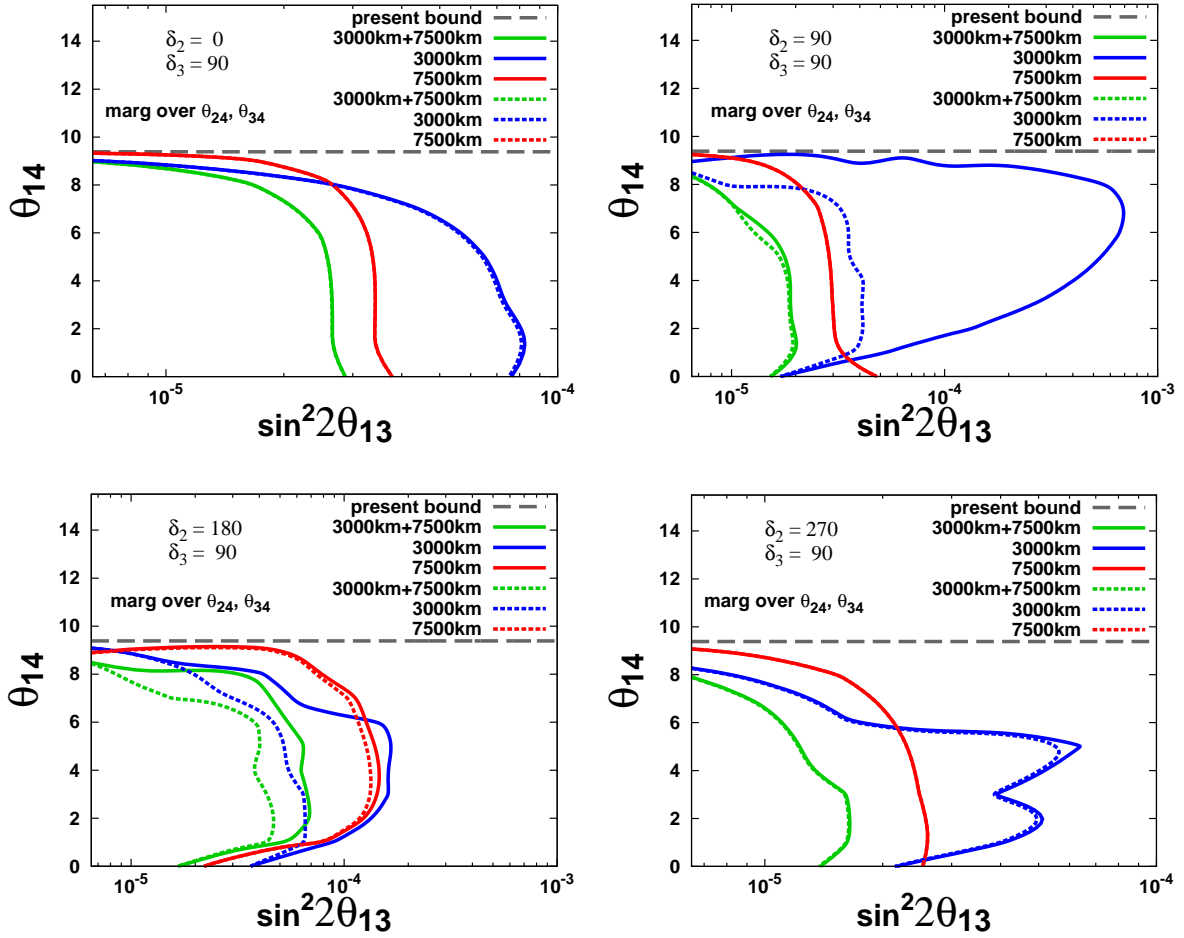


Figure 4.3: Sensitivity limit at 90% CL in the $(\sin^2 2\theta_{13}, \theta_{14})$ plane for $\delta_3 = 90^\circ$ and different values of δ_2 . The solid lines refer to the golden channel results, only. Dashed lines stand for the sum of golden and silver channel results. The colors are: blue for $L = 3000$ km; red for $L = 7500$ km; green for the combination of the two baselines; the horizontal dashed grey line represents the present bound on θ_{14} . The four panels represent our results for: $\delta_2 = 0$ (top left); $\delta_2 = 90^\circ$ (top right); $\delta_2 = 180^\circ$; (bottom left); $\delta_2 = 270^\circ$ (bottom right).

of both figures that a reduced dependence of the sensitivity to $\theta_{13}^{(4\text{fam})}$ from δ_2, δ_3 and θ_{14} is achieved. Particularly striking is the case of $\delta_2 = \delta_3 = 90^\circ$, Fig. 4.3 (top right), where we can see that the sensitivity to $\theta_{13}^{(4\text{fam})}$ goes from $\sin^2 2\theta_{13}^{(4\text{fam})} = 6 \times 10^{-3}$ for the golden channel alone to $\sin^2 2\theta_{13}^{(4\text{fam})} = 3 \times 10^{-5}$ for the combination of golden and silver channels. On the other hand, the silver channel statistics at $L = 7500$ km from the source is extremely poor (see Tab. B.1). For this reason we have no impact whatsoever of this channel on the $\theta_{13}^{(4\text{fam})}$ sensitivity at the long baseline.

The performance of the detectors located at the two baselines differ significantly depending on the specific choices of δ_2 and δ_3 . For most of the choices of (δ_2, δ_3) , the longest baseline outperforms the shortest one, with the only exceptions of $\delta_2 =$

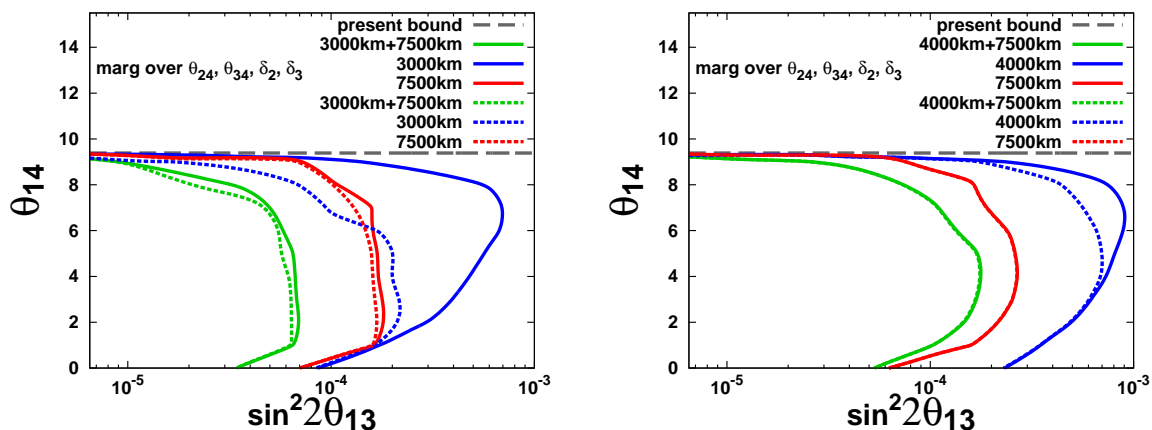


Figure 4.4: Sensitivity limit at 90% CL in the $(\sin^2 2\theta_{13}, \theta_{14})$ plane, marginalizing over $\theta_{24}, \theta_{34}, \delta_2$ and δ_3 . The solid lines refer to the golden channel results, only. Dashed lines stand for the sum of golden and silver channel results. The colors are: blue for the shortest baseline; red for longest baseline; green for the combination of the two baselines; the horizontal dashed grey line represents the present bound on θ_{14} . Left panel: 50 GeV Neutrino Factory; Right panel: 20 GeV Neutrino Factory.

$0, 180^\circ; \delta_3 = 0$ (Fig. 4.2, left panels) and $\delta_2 = 180^\circ; \delta_3 = 90^\circ$ (Fig. 4.3, bottom left panel).

The combination of the two channels and the two baselines at the 50 GeV Neutrino Factory has a rather good sensitivity to $\theta_{13}^{(4\text{fam})}$: in the absence of a signal, we can exclude values of $\theta_{13}^{(4\text{fam})}$ larger than $\sin^2 2\theta_{13}^{(4\text{fam})} \leq 4 \times 10^{-5}$ for any of the choices of (δ_2, δ_3) shown. The sensitivity to the active-sterile mixing angle θ_{14} , on the other hand, is $\theta_{14} \leq 9^\circ$ when marginalizing over θ_{24} and θ_{34} .

We eventually compare the results obtained using the 50 GeV Neutrino Factory setup, Fig. 4.4(left), with those that can be achieved using the 20 GeV Neutrino Factory ISS-inspired setup, Fig. 4.4(right). As before, solid lines stand for golden channel data, only, whereas dashed lines stand for the combination of golden and silver channel data. Blue lines stand for the shortest baseline (3000 km or 4000 km); red lines for the longest baseline (7500 km in both setups); green lines for the combination of the two; eventually, the grey dashed line represents the present bound on θ_{14} . In addition to θ_{24} and θ_{34} , we have marginalized over the CP-violating phases δ_2 and δ_3 , with $\delta_2, \delta_3 \in [0, 360^\circ]$. The rest of the parameters have been kept fixed to the values given above.

First of all notice that for both setups the $\theta_{13}^{(4\text{fam})}$ -sensitivity that can be reached using golden channel data, only, is much poorer at the short baseline than at the long baseline. We have found $\theta_{13}^{(4\text{fam})} \leq 6 \times 10^{-4} (9 \times 10^{-4})$ for any value of θ_{14} at the short baseline for the 50 GeV (20 GeV) setup, to be compared with $\theta_{13}^{(4\text{fam})} \leq 2 \times 10^{-4} (3 \times 10^{-4})$ at the long baseline for the 50 GeV (20 GeV) setup. The second relevant point is that,

if only the shortest baseline is considered, the silver channel significantly improves the $\theta_{13}^{(4\text{fam})}$ -sensitivity for the 50 GeV setup, but only marginally for the 20 GeV one. We can see that the $\theta_{13}^{(4\text{fam})}$ -sensitivity at the short baseline using the combination of golden and silver channels becomes $\theta_{13}^{(4\text{fam})} \leq 2 \times 10^{-4} (6 \times 10^{-4})$ for the 50 GeV (20 GeV) setup. When considering the long baseline we can see, however, that the impact of the silver channel becomes marginal.

The $\theta_{13}^{(4\text{fam})}$ -sensitivity that can be reached using the combination of the two baselines is: $\theta_{13}^{(4\text{fam})} \leq 6 \times 10^{-5} (1.5 \times 10^{-4})$ for any value of θ_{14} at the 50 GeV (20 GeV) setup. The inclusion of the silver channel data does not modify significantly these results.

Our conclusion is that the higher energy setup has a much greater ultimate sensitivity to $\theta_{13}^{(4\text{fam})}$ than the ISS-inspired 20 GeV one, thanks mainly to the higher statistics of the first. On the other hand, both setups are not able to improve the present bounds on θ_{14} when marginalizing over θ_{24}, θ_{34} . The silver channel can significantly improve the $\theta_{13}^{(4\text{fam})}$ -sensitivity when only one baseline is considered at the 50 GeV setup. However, it has a negligible impact when the combination of the golden channel data at the two baselines is considered.

Eventually, we have studied the impact of the correlated systematic errors α_s, β_s in Eq. (B.5) on our results. For both the 50 GeV and 20 GeV setups, we have found that the results shown in Fig. 4.4 do not change for $\alpha_s = \beta_s = 0$. Golden and silver channels are indeed dominated by statistical errors.

4.2.2 Sensitivity to $U_{e4}U_{\mu4}$ and $U_{e4}U_{\tau4}$

Since sensitivity to θ_{14} at the Neutrino Factory is poor, it is worth investigating whether the Neutrino Factory has sensitivity to other combinations of the mixing matrix elements. From the form of the appearance oscillation probability in vacuum

$$P(\nu_\alpha \rightarrow \nu_\beta) = 4\text{Re} [U_{\alpha3}U_{\beta3}^*(U_{\alpha3}^*U_{\beta3} + U_{\alpha4}^*U_{\beta4})] \sin^2 \left(\frac{\Delta m_{31}^2 L}{4E} \right) + \dots,$$

we can expect that the golden and silver channels have some sensitivity to $U_{e4}U_{\mu4}$ and $U_{e4}U_{\tau4}$. In the present parametrization (4.2) of the mixing matrix, we have $U_{e4}U_{\mu4} = s_{14}c_{14}s_{24} = s_{14}s_{24} + O(\epsilon^6)$ and $U_{e4}U_{\tau4} = s_{14}c_{14}c_{24}s_{34} = s_{14}s_{34} + O(\epsilon^5)$, where we have used the fact that θ_{14} and θ_{24} are small. In the analysis of sensitivity to $U_{e4}U_{\mu4}$ ($U_{e4}U_{\tau4}$), instead of using θ_{14} and θ_{24} (θ_{14} and θ_{34}) as the independent variables, it is convenient to take $s_{14}s_{24}$ and s_{14}/s_{24} ($s_{14}s_{34}$ and s_{14}/s_{34}) as the independent ones, respectively. Taking this basis we have performed analysis on sensitivity to $U_{e4}U_{\mu4}$ and $U_{e4}U_{\tau4}$. The results are shown in Fig. 4.5 and they indicate that the combination of the golden and silver channels has good sensitivity to these variables. To see how much improvement we have, we take the square root of $U_{e4}U_{\mu4}$ or $U_{e4}U_{\tau4}$, so that these factors correspond roughly to sine of some angle. Then the upper bound for $\sqrt{U_{e4}U_{\mu4}}$ by the 50 GeV (20 GeV) Neutrino Factory is $\sqrt{5 \times 10^{-4}}$ ($\sqrt{1 \times 10^{-3}}$), which is about 15% (20%) of the

current bound, $\sqrt{U_{e4}U_{\mu4}} \leq \sqrt{0.02}$. Similarly, the upper bound for $\sqrt{U_{e4}U_{\tau4}}$ by both 50 GeV and 20 GeV Neutrino Factory is $\sqrt{2} \times 10^{-3}$, which is about 20% of the current bound, $\sqrt{U_{e4}U_{\tau4}} \leq 0.06$.

For both $U_{e4}U_{\mu4}$ and $U_{e4}U_{\tau4}$ plots, we see that both the golden and silver channels play a role in giving the constraints. As it is expected from statistics, the result by the 50 GeV Neutrino Factory is better for $U_{e4}U_{\mu4}$, but the sensitivity to $U_{e4}U_{\tau4}$ is almost the same for the two setups (notice that the scale on the vertical axis for the left and right panels are different). For the 20 GeV case, the data at 7500 km perform very well and the combined data of 4000 km and 7500 km give a result almost comparable to that of 50 GeV.

It is interesting to note that the golden channel also plays a role in improving sensitivity to $U_{e4}U_{\tau4} \propto s_{34}$. We have obtained a lengthy analytic formula for the golden channel in matter with some approximation, i.e., to quartic order in ϵ while keeping all orders in θ_{34} and we have found that dependence on θ_{34} appears through the form of $O(\epsilon^4) \times s_{34}^2 A_e / \Delta E_{31}$. This explains why the golden channel has some sensitivity to $U_{e4}U_{\tau4}$ through the matter effect at the longer baseline, once we choose a suitable set of the independent parameters to vary.

4.2.3 Sensitivity to $(\theta_{24}, \theta_{34})$

We have chosen the following input values for θ_{13} and δ (δ is the three-family CP-phase): $\theta_{13} = 5.7^\circ$; $\delta_2 = \delta = 0$. Notice that, to be conservative, in this section we assume a true value for θ_{13} different from zero. On the other hand we consider $\theta_{14} = 0$ as the central value of the active-sterile mixing angle which we are going to marginalize over.

The sensitivity to (3+1)-sterile neutrinos at the 90% CL in the $(\theta_{24}, \theta_{34})$ -plane for the 50 GeV Neutrino Factory setup is shown in Figs. 4.6 and 4.7. In these figures, we have studied how the marginalization over θ_{23} , Δm_{31}^2 and δ_3 modify our results by varying them in the ranges $\theta_{23} \in [40^\circ, 50^\circ]$, $\Delta m_{31}^2 \in [2.0, 2.8] \times 10^{-3} \text{eV}^2$ and $\delta_3 \in [0, 360^\circ]$. We have also checked the impact of the marginalization over all the other parameters (otherwise fixed to their central values given at the beginning of the section), by studying them one by one in combination with θ_{23} , Δm_{31}^2 and δ_3 . The considered marginalization ranges are: $\theta_{12} \in [30^\circ, 36^\circ]$; $\theta_{13} \in [0, 10^\circ]$; $\theta_{14} \in [0, 10^\circ]$; $\Delta m_{21}^2 \in [7.0, 8.3] \times 10^{-5} \text{eV}^2$; $\delta_1 \in [0, 360^\circ]$ and $\delta_2 \in [0, 360^\circ]$. We have found that none of these parameters modify significantly our results, contrary to the case of θ_{23} , Δm_{31}^2 and δ_3 . Eventually, we have checked that changing the sign of Δm_{31}^2 does not modify our results, either.⁶

First of all, in Fig. 4.6 we show the sensitivity limit at 90% CL to θ_{24} and θ_{34} , for fixed $\delta_3 = 0$, whilst marginalizing over θ_{23} and Δm_{31}^2 in the range just mentioned in the above paragraph. Notice that the considered allowed range for θ_{23} is a bit smaller

⁶Notice that we are not sensitive to the sign of the largest mass difference, Δm_{41}^2 .

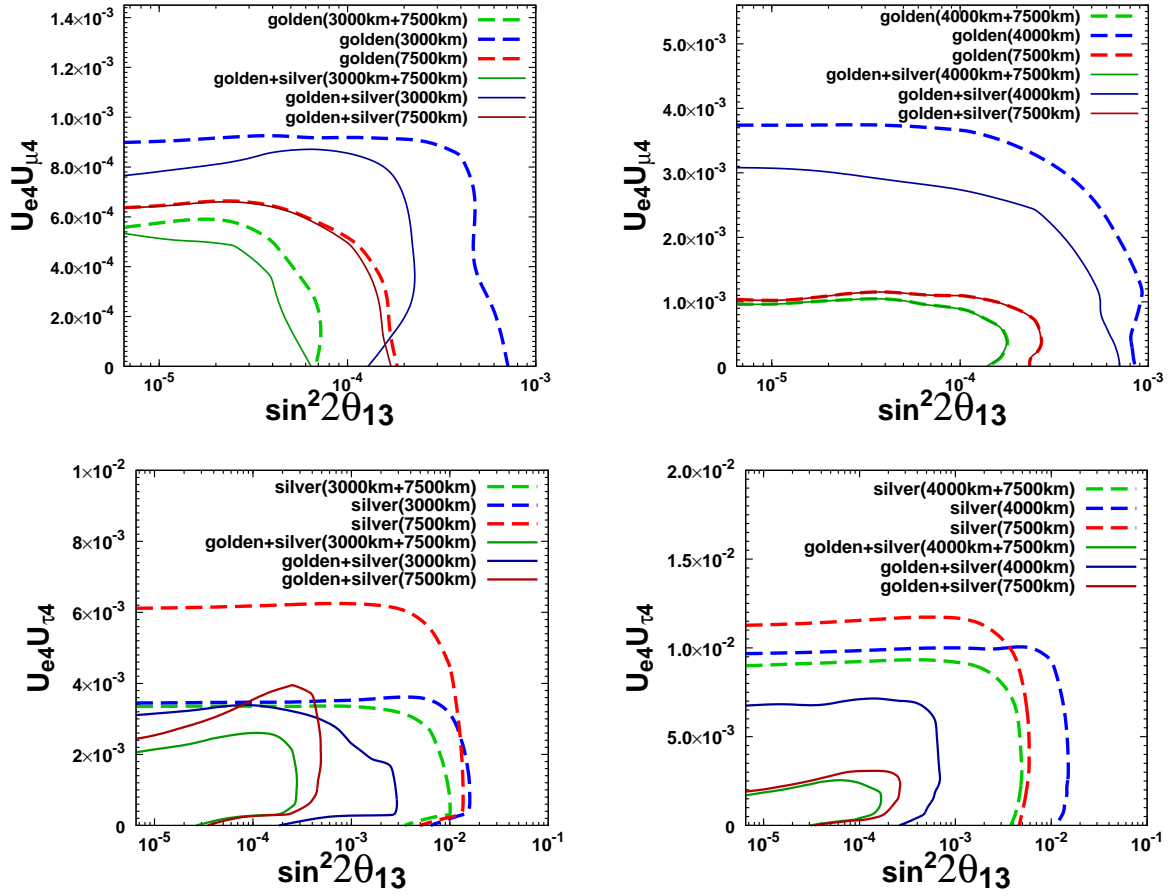


Figure 4.5: Sensitivity limit at 90% CL to $U_{e4}U_{\mu4}$ and $U_{e4}U_{\tau4}$. $\Delta\chi^2$ is evaluated for a fixed set of values of $(\sin^2 2\theta_{13}, U_{e4}U_{\mu4})$ (upper panels) or a fixed set of values of $(\sin^2 2\theta_{13}, U_{e4}U_{\tau4})$ (lower panels), marginalizing over $s_{14}/s_{24}, \theta_{34}, \delta_2$ and δ_3 (upper panels), or over $s_{14}/s_{34}, \theta_{24}, \delta_2$ and δ_3 (lower panels). Left panels: 50 GeV Neutrino Factory; Right panels: 20 GeV Neutrino Factory. The current bound on $U_{e4}U_{\mu4}$ ($U_{e4}U_{\tau4}$) is 0.02 (0.06).

than its present allowed range from the three-family global analysis. The Neutrino Factory, however, has an enormous potential for improving the measurement of the three-family atmospheric parameters through the ν_μ disappearance channel as it was shown, for example, in Ref. [213]. It is, therefore, absolutely reasonable to vary θ_{23} over a reduced range. In the two plots, red lines stand for the $\nu_\mu \rightarrow \nu_\mu$ disappearance channel data; blue lines stand for the $\nu_\mu \rightarrow \nu_\tau$ discovery channel data; green lines stand for the combination of both; the dashed grey line represents the present bound on θ_{24} and θ_{34} .

We discuss first the left panel of Fig. 4.6, that refers to the results at the shortest baseline, $L = 3000$ km. Notice that the disappearance channel has the strongest sensitivity to θ_{24} , that can be excluded above $\theta_{24} \sim 8^\circ$ for any value of θ_{34} . On the other

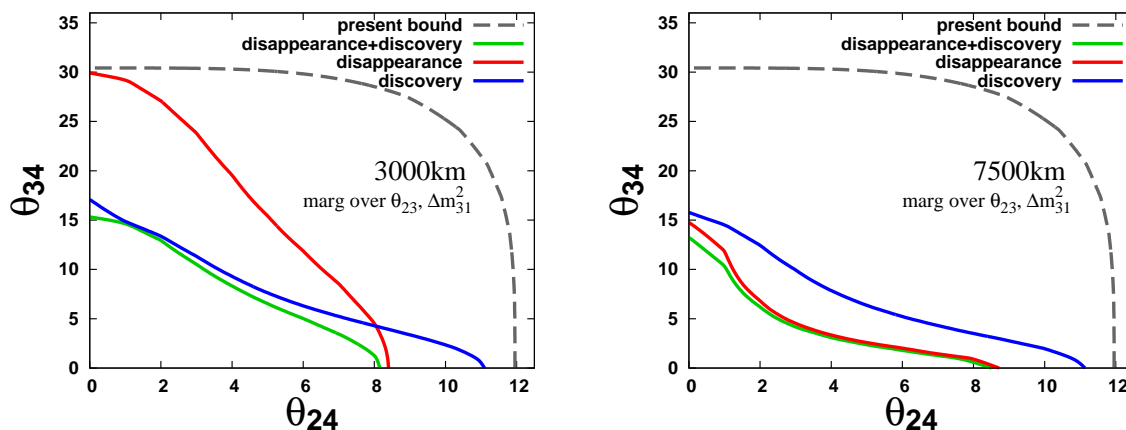


Figure 4.6: Sensitivity limit at 90% CL to θ_{24} and θ_{34} , for fixed $\delta_3 = 0$, whilst marginalizing over θ_{23} in the range $\theta_{23} \in [40^\circ, 50^\circ]$ and Δm_{31}^2 in the range $\Delta m_{31}^2 \in [2.0, 2.8] \times 10^{-3} \text{ eV}^2$. Red lines stand for the disappearance channel $\nu_\mu \rightarrow \nu_\mu$; blue lines stand for the discovery channel $\nu_\mu \rightarrow \nu_\tau$; green lines stand for the combination of both; the dashed grey line represents the present bound on θ_{24} and θ_{34} . Left: $L = 3000 \text{ km}$ baseline, Right: $L = 7500 \text{ km}$ baseline.

hand, the $\nu_\mu \rightarrow \nu_\tau$ channel gives the ultimate sensitivity to θ_{34} for vanishing θ_{24} , $\theta_{34} \leq 15^\circ$. In both channels, we can see a strong correlation between θ_{24} and θ_{34} , with a bound on θ_{34} that is strongly dependent on the specific value of θ_{24} considered. This behavior can be understood by looking at Eqs. (4.6,4.7) in Sec. 4.1. The strong correlation between the two mixing angles is induced by the subleading $O(\epsilon^3)$ terms, proportional to $(A_n L) s_{24} s_{34} \cos \delta_3$ (since we are considering $\delta_3 = 0$ the term proportional to $\sin \delta_3$ in $P_{\mu\tau}$ vanishes). The $(\theta_{24}, \theta_{34})$ -correlation in the ν_μ disappearance channel is softer than in the $\nu_\mu \rightarrow \nu_\tau$ one: a consequence of the different statistical significance of this term in appearance and disappearance channels. Eventually, the combination of the two channels gives a very good sensitivity to both mixing angles.

A similar combined sensitivity is achieved at the longest baseline, $L = 7500 \text{ km}$, whose results are shown in the right panel of Fig. 4.6. We can see comparing the blue lines on both panels that the $\nu_\mu \rightarrow \nu_\tau$ channel sensitivity to $(\theta_{24}, \theta_{34})$ is substantially the same when changing baseline (the expected number of events for this channel at the two baselines is very similar, see Tab. B.1). On the other hand, the ν_μ disappearance channel data (the red line) has a much stronger sensitivity than at the short baseline: a consequence of the increased significance of the subleading term with respect to the dominant one in the disappearance channel due to larger matter effects at 7500 km.

The sensitivity of the disappearance channel to θ_{34} arises at a higher order in the expansion that we have presented in Eqs. (4.6,4.7). If we introduce terms to fourth order in ϵ (under the assumption $\theta_{13} = \theta_{14} = 0$, and taking into account the deviations

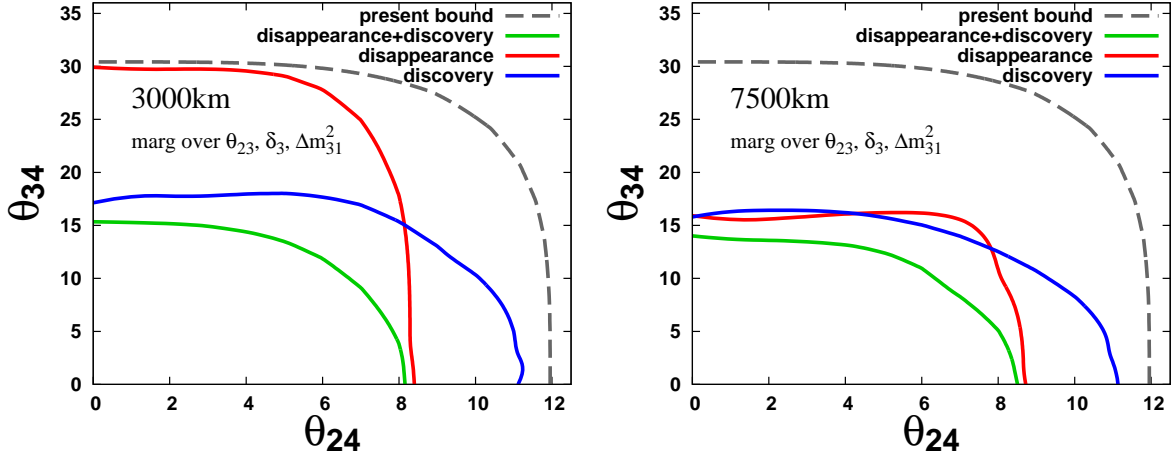


Figure 4.7: Sensitivity limit at 90% CL to θ_{24} and θ_{34} , marginalizing over $\theta_{23} \in [40^\circ, 50^\circ]$, the CP-violating phase $\delta_3 \in [0, 360^\circ]$ and $\Delta m_{31}^2 \in [2.0, 2.8] \times 10^{-3} \text{eV}^2$. Red lines stand for the disappearance channel $\nu_\mu \rightarrow \nu_\mu$; blue lines stand for the discovery channel $\nu_\mu \rightarrow \nu_\tau$; green lines stand for the combination of both; the grey dashed line represents the present bound on θ_{24} and θ_{34} . Left: $L = 3000$ km baseline, Right: $L = 7500$ km baseline.

from maximality of θ_{23}), we get:

$$P_{\mu\mu} = 1 - 2\theta_{24}^2 - \left[1 - 4(\delta\theta_{23})^2 - 2\theta_{24}^2 + \theta_{34}^2 \frac{A_n}{\Delta_{31}} \left(4\delta\theta_{23} - \theta_{34}^2 \frac{A_n}{\Delta_{31}} \right) \right] \sin^2 \frac{\Delta_{31}L}{2} - (A_n L) \left\{ 2\theta_{24}\theta_{34} \cos \delta_3 - \frac{\theta_{34}^2}{2} \left(4\delta\theta_{23} - \theta_{34}^2 \frac{A_n}{2\Delta_{31}} \right) \right\} \sin \Delta_{31}L + O(\epsilon^5), \quad (4.12)$$

$$P_{\mu\tau} = \left\{ 1 - 4(\delta\theta_{23})^2 - \theta_{24}^2 - \theta_{34}^2 \left[1 - \frac{\theta_{34}^2}{3} - \frac{A_n}{\Delta_{31}} \left(4\delta\theta_{23} - \theta_{34}^2 \frac{A_n}{\Delta_{31}} \right) \right] \right\} \sin^2 \frac{\Delta_{31}L}{2} + \left\{ \theta_{24}\theta_{34} \sin \delta_3 + (A_n L) \left[2\theta_{24}\theta_{34} \cos \delta_3 - \frac{\theta_{34}^2}{2} \left(4\delta\theta_{23} - \theta_{34}^2 \frac{A_n}{2\Delta_{31}} \right) \right] \right\} \sin \Delta_{31}L + O(\epsilon^5), \quad (4.13)$$

$$P_{\mu s} = 2\theta_{24}^2 + \left[\theta_{34}^2 \left(1 - \frac{\theta_{34}^2}{3} \right) - \theta_{24}^2 \right] \sin^2 \frac{\Delta_{31}L}{2} - \theta_{24}\theta_{34} \sin \delta_3 \sin \Delta_{31}L + O(\epsilon^5). \quad (4.14)$$

Most of the θ_{34} -dependent terms in Eq. (4.12) are proportional to the matter parameter $(A_n L)$. This means that the impact of these terms will be more important at the longest baseline, than at the shortest one (as we have seen in Fig. 4.6). On the other hand, the θ_{24} -sensitivity arises from the θ_{24}^2 term at $O(\epsilon^4)$ in Eq. (4.12).

These behaviors are strongly modified if we marginalize over the CP-violating phase δ_3 , as it can be seen in Fig. 4.7, where we present the sensitivity limit at 90% CL to θ_{24}

and θ_{34} , whilst marginalizing over θ_{23} , Δm_{31}^2 and δ_3 . As before, red lines stand for the $\nu_\mu \rightarrow \nu_\mu$ disappearance channel data; blue lines stand for the $\nu_\mu \rightarrow \nu_\tau$ discovery channel data; green lines stand for the combination of both; the grey dashed line represents the present bound on θ_{24} and θ_{34} .

Notice that the correlation between θ_{24} and θ_{34} in the ν_μ disappearance data (red lines) has vanished. This is a straightforward consequence of the marginalization over δ_3 , that removes the term proportional to $(A_n L) s_{24} s_{34} \cos \delta_3$ in Eq. (4.6), responsible for that correlation. We have found that the sensitivity on the two active-sterile mixing angles θ_{24} and θ_{34} is now represented by vertical and horizontal lines (similar to the results in Fig. 4.4). A similar effect is found for the $\nu_\mu \rightarrow \nu_\tau$ appearance channel data (blue lines), though softer. We can see that, at both baselines (but more significantly at the longest one) some remnants of the $(\theta_{24}, \theta_{34})$ -correlation can still be observed for this channel. Comparing the results of the two channels, we have found again that at the short baseline the $\nu_\mu \rightarrow \nu_\mu$ data give the best sensitivity to θ_{24} , whereas the $\nu_\mu \rightarrow \nu_\tau$ data give the best sensitivity to θ_{34} . At the long baseline, $\nu_\mu \rightarrow \nu_\mu$ is as good as $\nu_\mu \rightarrow \nu_\tau$ in the θ_{34} -sensitivity.

We, eventually, compare the 90% CL $(\theta_{24}, \theta_{34})$ -sensitivity that can be obtained using the combination of the two channels and of the two baselines at the 50 GeV Neutrino Factory setup, Fig. 4.8(left), with the one that can be achieved using the 20 GeV Neutrino Factory ISS-inspired setup, Fig. 4.8(right). As before, red lines stand for ν_μ disappearance channel data; blue lines for the $\nu_\mu \rightarrow \nu_\tau$ discovery channel data; green lines for the combination of both channels; the grey dashed line represents the present bound on θ_{24} and θ_{34} . Data for the two baselines are always summed. In these plots, we have marginalized over the whole set of relevant parameters: θ_{23} , Δm_{31}^2 and δ_3 . The rest of the parameters have been kept fixed to the values given previously.⁷

First of all, we can see by comparing red lines (the disappearance channel data) between Fig. 4.8(left) and Fig. 4.8(right) that the ultimate sensitivities to θ_{24} and θ_{34} at the two setups are very similar: the upper bounds $\theta_{24} \leq 7.5^\circ (8^\circ)$ and $\theta_{34} \leq 12^\circ (14^\circ)$ can be inferred from the data for the 50 GeV (20 GeV) setup. When we eventually combine the results for the disappearance and the discovery channels, however, we find that the 50 GeV Neutrino Factory outperforms the 20 GeV ISS-inspired one, as it can be seen comparing the green lines in Fig. 4.8. This can be easily explained pointing out that the discovery channel data (blue lines) are able to exclude a significantly larger region of the parameter space when going to higher energy, a straightforward consequence of the higher statistics due to the higher neutrino energy and, consequently, the higher $\nu_\tau N$ cross-section.

In Fig. 4.8 we have also studied the impact of the correlated systematic errors α_s, β_s (see Sec. (B.3.1)) on our results. Dashed blue, red and green lines represent the 90% CL sensitivities to $(\theta_{24}, \theta_{34})$ when the correlated systematic errors α_s, β_s are not included and only the uncorrelated bin-to-bin systematic errors f_j (see Sec. B.3.1) are taken

⁷We have checked that the effect of the marginalization on the rest of the parameters do not affect the results.

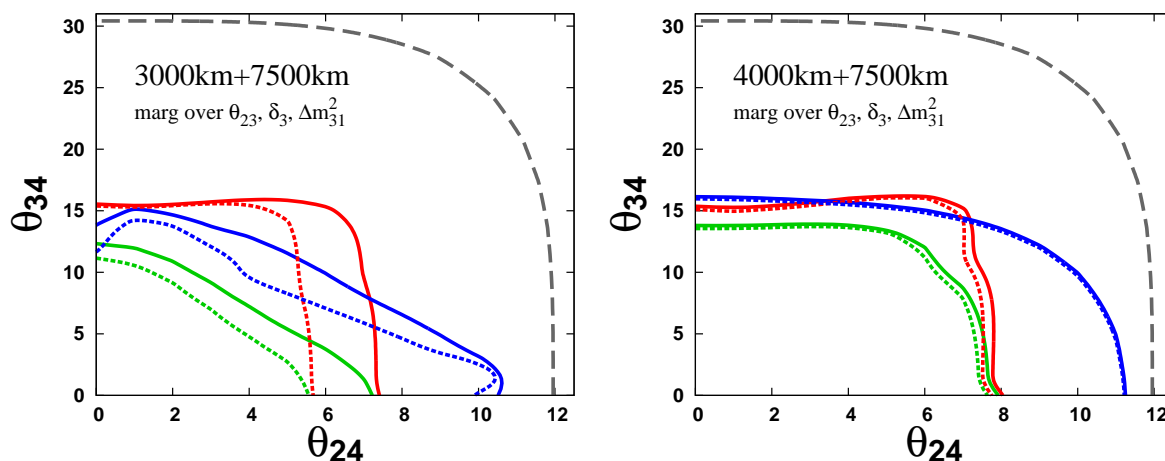


Figure 4.8: Sensitivity limit at 90% CL to θ_{24} and θ_{34} , marginalizing over $\theta_{23} \in [40^\circ, 50^\circ]$, the CP-violating phase $\delta_3 \in [0, 360^\circ]$ and $\Delta m_{31}^2 \in [2.0, 2.8] \times 10^{-3} \text{eV}^2$, for the combination of the two baselines. Dashed lines stand for the results without the correlated systematic errors. Red lines stand for the disappearance channel $\nu_\mu \rightarrow \nu_\mu$; blue lines stand for the discovery channel $\nu_\mu \rightarrow \nu_\tau$; green lines stand for the combination of both. Left panel: 50 GeV Neutrino Factory; Right panel: 20 GeV Neutrino Factory.

into account, considering $f_j = 5\%$ for the ν_μ disappearance channel and $f_j = 10\%$ for the discovery channel, irrespectively of the energy bin, of the baseline and of the stored muon polarity)

Comparing dashed and solid lines at the 20 GeV Neutrino Factory (right panel), we can see that the inclusion of the correlated systematic errors has a negligible impact when analysing the data at this setup. On the other hand, when studying the data for both channels at the 50 GeV setup, we can see that the inclusion of these errors modify our results. In particular, the sensitivity to θ_{24} through the ν_μ disappearance channel goes from $\theta_{24} \leq 6^\circ$ when only f_j is considered to $\theta_{24} \leq 7.5^\circ$ when α_s, β_s are also taken into account.

Our final conclusion is the following: using the 20 GeV ISS-inspired Neutrino Factory, we get two roughly independent limits on the two angles θ_{24} and θ_{34} : $\theta_{24} \leq 8^\circ$ for any value of θ_{34} and $\theta_{34} \leq 14^\circ$ for any value of θ_{24} at the 90 % CL. Slightly stronger ultimate limits are obtained at the 50 GeV Neutrino Factory: $\theta_{24} \leq 7.5^\circ$ for vanishing θ_{34} and $\theta_{34} \leq 12^\circ$ for vanishing θ_{24} . The significantly large discovery channel statistics at the 50 GeV Neutrino Factory with respect to the 20 GeV one, however, strongly increase the sensitivity of this setup to the combination of θ_{24} and θ_{34} , such that a roughly diagonal line in the $(\theta_{24}, \theta_{34})$ plane connecting $(\theta_{24}, 0)$ and $(0, \theta_{34})$ can be drawn.

4.2.4 CP-violating sterile neutrino signals

In Secs. 4.2.1, 4.2.2 and 4.2.3 we have considered the case of a null result for sterile neutrino searches at the Neutrino Factory after 4 years running for both muon polarities, showing exclusion plots both in the $(\theta_{13}^{(4\text{fam})}, \theta_{14})$ - and in the $(\theta_{24}, \theta_{34})$ -planes. However, due to the impressive statistics achievable at the Neutrino Factory, it could well be possible that a positive signal is found (if sterile neutrinos with $O(1\text{eV}^2)$ mass difference with respect to active ones do exist). For this reason we will present in this section a first analysis of the precision achievable in our setup in the simultaneous measurement of mixing angles and CP-violating phases⁸. We first focus on θ_{24}, θ_{34} and on the CP-violating phase δ_3 . Notice that each of the three possible CP-violating signals in a four-family model is related to a different Jarlskog invariant, proportional to a different combination of the mixing angles. The Jarlskog invariant that depends on $\sin \delta_3$ is, in our parametrization, proportional to the combination $\sin 2\theta_{23}s_{24}s_{34} \sin \delta_3$, as it can be seen in Eqs. (4.12,4.13). A measurement of δ_3 is thus possible only if both θ_{24} and θ_{34} are simultaneously non-vanishing. We will thus show 99% CL contours in the (θ_{34}, δ_3) -plane for particular input pairs $(\bar{\theta}_{34}, \bar{\delta}_3)$ for fixed non-vanishing values of θ_{24} .

The measurement of (θ_{34}, δ_3) is achieved combining data from the ν_μ disappearance channel and the $\nu_\mu \rightarrow \nu_\tau$ discovery channel. This analysis, of course, does not pretend to be as exhaustive as those that have been presented in the framework of the three-family model. In particular, we will not address within a comprehensive approach the problem of degeneracies in four-family models. Notice that this problem, extremely severe in the three-family oscillation studies at the Neutrino Factory (see, for example, Refs. [94, 97] and [98]), is expected to be even more complicated in a four-neutrino model. In the particular case of the δ_3 -dependent CP-violating signal, that can be extracted using the $\nu_\mu \rightarrow \nu_\mu$ and $\nu_\mu \rightarrow \nu_\tau$ channels, we do expect to observe at least degeneracies due to the (θ_{34}, δ_3) -correlation (the so-called ‘‘intrinsic degeneracies’’, [94]); those dependent on the wrong reconstruction of the sign of the atmospheric mass difference⁹ Δm_{31}^2 (known as ‘‘sign degeneracies’’, [96]); and, eventually, those dependent on a wrong reconstruction of the ‘‘atmospheric’’ mixing angle θ_{23} octant (known as ‘‘octant degeneracies’’, [214]).

Notice that we have also studied the simultaneous measurement of θ_{24}, θ_{34} and δ_3 using the combination of the $\nu_\mu \rightarrow \nu_\mu$ and $\nu_\mu \rightarrow \nu_\tau$ channels, finding that sensitivity to δ_3 is lost for values of the product $s_{24}s_{34}$ smaller than $(s_{24}s_{34})_{\min} \sim 0.01$. The results that we show have been obtained for choices of the input parameters $(\bar{\theta}_{24}, \bar{\theta}_{34})$ such that $s_{24}s_{34} \geq (s_{24}s_{34})_{\min}$.

We show in Fig. 4.9 the 2 d.o.f.’s 99 %CL contours for the simultaneous measurement of θ_{34} and δ_3 using the combined data from the disappearance and the discovery channels for two representative input values of θ_{24} : $\bar{\theta}_{24} = 3^\circ$ (left panels) and $\bar{\theta}_{24} = 5^\circ$

⁸In addition, in App. B.6 we show the region of the parameter space for which it is possible to distinguish the (3+1)-model from three-family oscillations

⁹At long baselines we are not sensitive to the sign of the SBL mass difference Δm_{41}^2 .

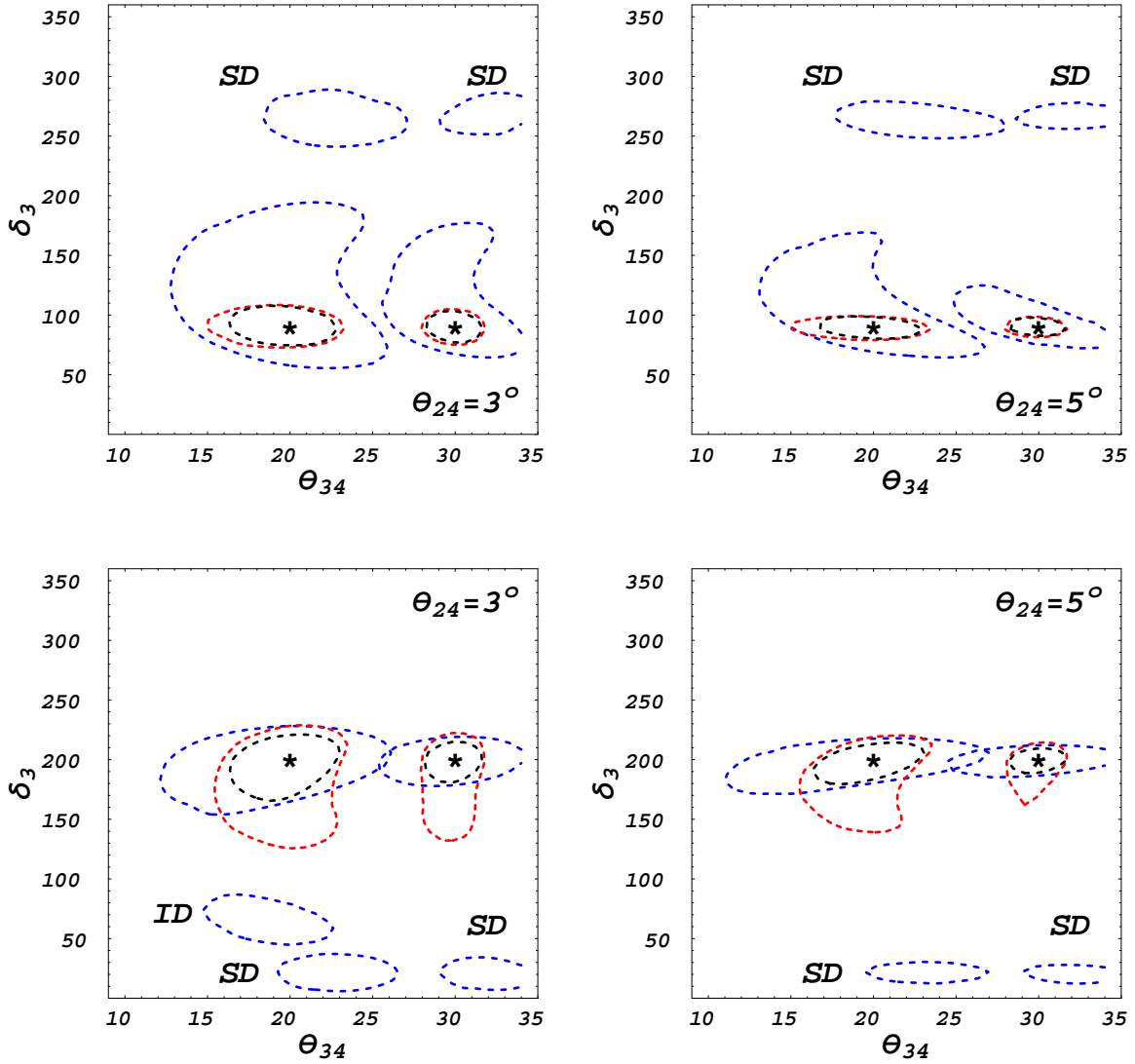


Figure 4.9: 99% CL contours for the simultaneous measurement of θ_{34} and δ_3 using the combined data from the ν_μ disappearance and the $\nu_\mu \rightarrow \nu_\tau$ discovery channels. Two different values of θ_{24} have been considered: $\theta_{24} = 3^\circ$ (left panels); $\theta_{24} = 5^\circ$ (right panels). The input pairs of $(\bar{\theta}_{34}, \bar{\delta}_3)$, marked by a star in the plots, are: $\bar{\theta}_{34} = 20^\circ, 30^\circ; \bar{\delta}_3 = 90^\circ$ (upper panels) and 200° (lower panels). In the plots, “ID” stands for “Intrinsic Degeneracy”; “SD” stands for “Sign Degeneracy”. Blue dashed lines represent the $L = 3000$ km baseline data; red dashed lines the $L = 7500$ km baseline data; black dashed lines stand for the combination of both baselines.

(right panels). Blue dashed lines stand for the $L = 3000$ km baseline; red dashed lines stand for the $L = 7500$ km baseline; black dashed lines stand for the combination of both baselines.

In the numerical analysis, to be conservative we consider a non vanishing value for θ_{13} as in the previous subsection: $\theta_{13} = 5.7^\circ$. For simplicity, we do not marginalize over any parameter along this subsection. Particularly the atmospheric angle has been fixed to $\theta_{23} = 45^\circ$. We do not expect any ‘‘octant degeneracies’’, thus. The input values that we have studied to illustrate the discovery potential of our setup are: $\bar{\theta}_{34} = 20^\circ, 30^\circ$; $\bar{\delta}_3 = 90^\circ$ (upper panels) and $\bar{\delta}_3 = 200^\circ$ (lower panels).

First of all, we can see that the combination of the two channels at the shortest baseline (blue lines) is not enough to solve the sign degeneracies (labeled with ‘‘SD’’ in the plot), that can be observed for all of the choices of the three input parameters $(\bar{\theta}_{24}, \bar{\theta}_{34}, \bar{\delta}_3)$. The sign clones are located at the point $(\theta_{34}^{\text{SD}}, \delta_3^{\text{SD}})$, where $\theta_{34}^{\text{SD}} \sim \bar{\theta}_{34}$ and δ_3^{SD} satisfies the relation $\sin \bar{\delta}_3 \sin \Delta_{31} L = -\sin \delta_3^{\text{SD}} \sin \Delta_{31} L$, with $\delta_3^{\text{SD}} \sim -90^\circ$ for $\bar{\delta}_3 = 90^\circ$ and $\delta_3^{\text{SD}} \sim 20^\circ$ for $\bar{\delta}_3 = 200^\circ$. The intrinsic degeneracy is also found for one specific choice of the input parameter $(\bar{\theta}_{24} = 3^\circ, \bar{\theta}_{34} = 20^\circ, \bar{\delta}_3 = 200^\circ)$. On the other hand, no intrinsic or sign degeneracy are found at the longest baseline (red lines). When combining the two baselines we see that the degeneracies are solved and that a very good precision on the simultaneous measurement of θ_{34} and δ_3 is achieved for all the choices of the input parameters that we have considered. In particular, the error in δ_3 at the 99% CL is of the order of a few tens of degrees. At the same time, the mixing angle θ_{34} can be measured for these particular inputs with a precision of a few degrees.

We summarize our results for the simultaneous measurement of θ_{34} and δ_3 in Fig. 4.10, where the 99% CL ‘‘ δ_3 -discovery potential’’ in the (θ_{34}, δ_3) -plane for different values of $\bar{\theta}_{24}$ is shown.¹⁰ We define the ‘‘ δ_3 -discovery potential’’ as the region in the $(\sin^2 2\theta_{34}, \delta_3)$ -plane for which a given (non-zero) value of the CP-violating phase δ_3 can be distinguished at the 99% CL (for 2 d.o.f.’s) from the CP-conserving case, i.e., $\delta_3 = 0, \pi$. Note that we have also taken into account the effects of the sign degeneracy in this analysis.

In the left panel, only data from the $\nu_\mu \rightarrow \nu_\mu$ disappearance channel are shown. In the right panel, we have combined data from the ν_μ disappearance channel with those from the $\nu_\mu \rightarrow \nu_\tau$ appearance channel. Upper panels refer to $\bar{\theta}_{24} = 3^\circ$; lower panels to $\bar{\theta}_{24} = 5^\circ$. Blue dashed lines stand for the $L = 3000$ km baseline; red dashed lines stand for the $L = 7500$ km baseline; eventually, black dashed lines stand for the combination of the two baselines.

We can see from Fig. 4.10(left) that, using ν_μ disappearance channel only, we are able to measure a non-vanishing δ_3 for values of θ_{34} above $\sin^2 2\theta_{34} \geq 0.4$ ($\theta_{34} \geq 18^\circ$). The CP-coverage¹¹ is $\sim 50\%$, with a very smooth dependence on θ_{34} , being a bit larger for larger $\bar{\theta}_{24}$.

The situation is completely different when the $\nu_\mu \rightarrow \nu_\tau$ discovery channel data are

¹⁰Notice that, as we stressed at the beginning of this section, sensitivity to δ_3 is lost when the product $s_{24}s_{34}$ is smaller than $(s_{24}s_{34})_{\text{min}} \sim 0.01$.

¹¹The CP-coverage is the fraction of the δ_3 -parameter space for which we are able to exclude $\delta_3 = 0, \pi$ at the 99% CL for a given value of θ_{34} .

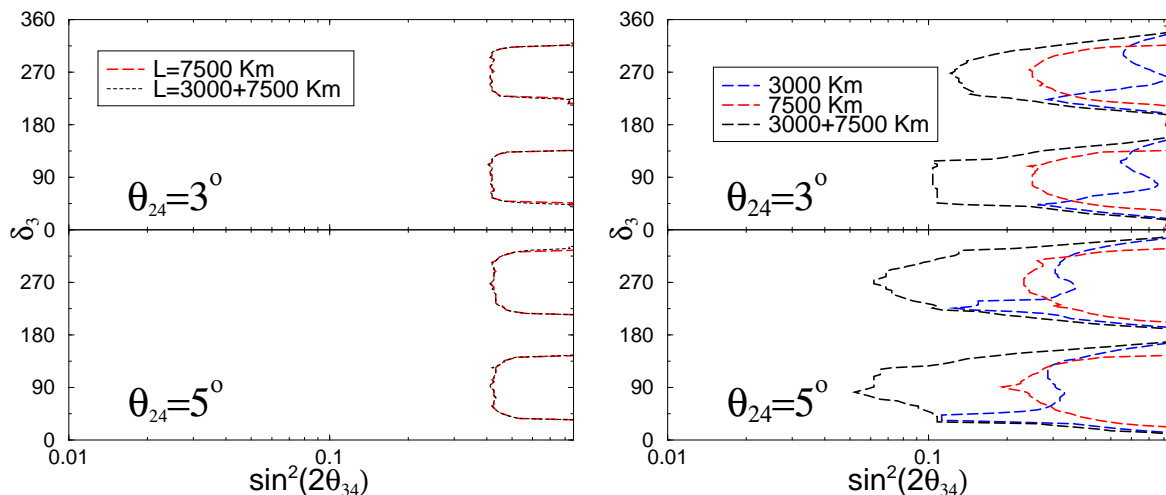


Figure 4.10: The 99 % CL “ δ_3 -discovery potential” in the (θ_{34}, δ_3) -plane. Left: only $\nu_\mu \rightarrow \nu_\mu$ disappearance channel data; Right: combination of $\nu_\mu \rightarrow \nu_\mu$ disappearance and $\nu_\mu \rightarrow \nu_\tau$ appearance channels data. Upper panels have been obtained for $\bar{\theta}_{24} = 3^\circ$; lower panels for $\bar{\theta}_{24} = 5^\circ$. Blue dashed lines stand for $L = 3000$ km baseline data; red dashed lines stand for $L = 7500$ km baseline data; black dashed lines stand for the combination of the two baselines.

added to the ν_μ disappearance ones, Fig. 4.10(right). First of all, we see that the $L = 3000$ km detector is no longer useless to measure δ_3 : spikes of δ_3 -sensitivity for particular values of δ_3 can be observed, in some cases outperforming the far detector results. However, it is in the combination of the two baselines where we can see that a dramatic improvement in the δ_3 -discovery potential is achievable. When the $\nu_\mu \rightarrow \nu_\tau$ data are included, a non-vanishing δ_3 can be measured for values of θ_{34} as small as $\sin^2 2\theta_{34} = 0.06$ ($\theta_{34} = 7^\circ$) for $\bar{\theta}_{24} = 5^\circ$ and $\sin^2 2\theta_{34} = 0.10$ ($\theta_{34} = 9^\circ$) for $\bar{\theta}_{24} = 3^\circ$. For $\sin^2 2\theta_{34} \geq 0.4$ ($\theta_{34} \geq 20^\circ$), roughly 80% (60%) of CP-coverage is achieved for $\bar{\theta}_{24} = 5^\circ$ (3°). The striking improvement in the δ_3 -discovery potential is a consequence of the synergy of the two channels and of the two baselines, whose combination is able to solve most of the correlations that otherwise strongly limits the potential of the ν_μ disappearance channel.

For completeness, we also present in Fig. 4.11 results for the sensitivity of the golden and silver channels to the phase δ_2 , that reduces to the three-family CP-violating phase δ in the limit $\theta_{i4} \rightarrow 0$. A comment is in order: as it can be seen from Eq. (4.9), using the parametrization in Eq. (4.2), the golden channel oscillation probability in vacuum depends on the combination $(\delta_2 - \delta_3)$ up to the eighth-order in ϵ . This means that, in the (3+1)-model, a CP-conserving result in the golden channel may be found for non-vanishing values of δ_2 and δ_3 if $\delta_1 = 0$; $(\delta_2 - \delta_3) = 0, \pi$. This degeneracy could be broken only by adding new information, such as that obtained using the silver channel, see Eq. (4.10), ν_μ disappearance or $\nu_\mu \rightarrow \nu_\tau$ appearance data. Golden channel data at the $L = 3000$ km baseline may not be able, thus, to detect a non-vanishing CP-violating signal even when both δ_2, δ_3 are different from $0, \pi$.

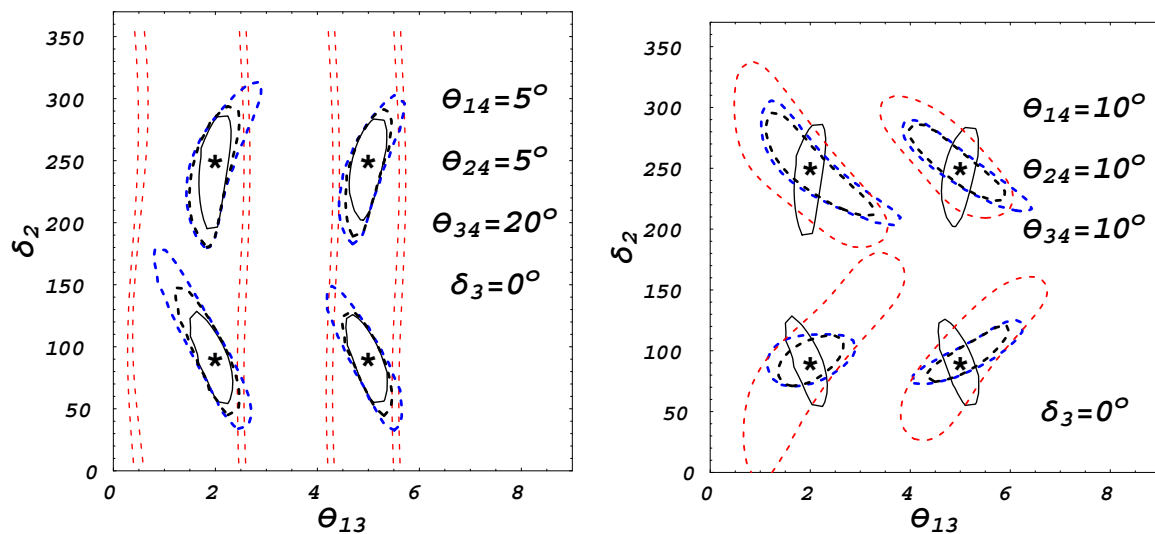


Figure 4.11: 99% CL contours for the simultaneous measurement of θ_{13} and δ_2 using the combined data from the $\nu_e \rightarrow \nu_\mu$ and the $\nu_e \rightarrow \nu_\tau$ golden and silver channels. Two different choices of the active-sterile mixing angles have been considered: $\theta_{14} = \theta_{24} = 5^\circ; \theta_{34} = 20^\circ$ (left panel); $\theta_{14} = \theta_{24} = \theta_{34} = 10^\circ$ (right panel). The input pairs (θ_{13}, δ_2) , marked by a star in the plots, are: $\bar{\theta}_{13} = 2^\circ, 5^\circ; \bar{\delta}_2 = 90^\circ, 250^\circ$. Golden and silver channels data are always summed. Four-family results are shown for the two baselines separately and summed: blue dashed lines stand for the $L = 3000$ km baseline data; red dashed lines stand for the $L = 7500$ km baseline data; black dashed lines stand for the combination of all data. Eventually, black solid lines stand for the three-family results for the combination of the baselines.

Results have been obtained for $\bar{\theta}_{13}^{(4\text{fam})} = 2^\circ, 5^\circ$ and $\bar{\delta}_2 = 90^\circ, 250^\circ$. For simplicity, we show results for $\delta_1 = \delta_3 = 0$ in these plots (remember that the measured phase should be interpreted as $\delta = (\delta_2 - \delta_3)$ for $\delta_1 = 0$). Eventually, the three active-sterile mixing angles are: $\theta_{14} = \theta_{24} = 5^\circ; \theta_{34} = 20^\circ$ in Fig. 4.11(left); and $\theta_{14} = \theta_{24} = \theta_{34} = 10^\circ$ in Fig. 4.11(right). In the plots, golden and silver channels data are always summed. Four-family results are shown for the two baselines separately and summed: blue dashed lines stand for the $L = 3000$ km baseline data; red dashed lines stand for the $L = 7500$ km baseline data; black dashed lines stand for the combination of all data. For comparison, black solid lines stand for the three-family results for the combination of the baselines.

We can see from the plots in Fig. 4.11 (left) that, when the active-sterile mixing angles θ_{14} and θ_{24} are “small”, the four-family results are extremely similar to those obtained by a fit in the three-family model.¹² The 99% CL contours in the four-family model are slightly larger than the three-family ones. The shape of contours in the $(\theta_{13}^{(4\text{fam})}, \delta_2)$ -plane is identical for the four- and three-family. This means that the

¹²Results do not depend significantly on θ_{34} : as it can be seen in Eqs. (4.9) and (4.10), this angle only enters in the silver channel oscillation probability, statistically less relevant than the golden channel data.

correlation between the two parameters is not modified by contributions proportional to θ_{14}, θ_{24} with respect to three-family expressions.

In Fig. 4.11 (right) we see that, when θ_{14} and θ_{24} assume values near their upper bound, the results for the four-family contours can significantly differ from the three-family ones. In particular, the four-family contours in the $(\theta_{13}^{(4\text{fam})}, \delta_2)$ -plane are orthogonal to the three-family ones. This is easily understood by looking at the approximated expressions for the oscillation probabilities of the golden and silver channels expanded to order ϵ^8 in Sec. 4.2.1. As we can see, the two terms with a δ_2 -dependence in the second and third lines of Eq. (4.9) are proportional to $s_{13}s_{14}s_{24} \sin(\delta_2 + \Delta_{31}L/2)$ and to $s_{13}(\Delta_{21}L) \cos(\delta_2 + \Delta_{31}L/2)$, respectively. When the first term becomes as large as the solar-suppressed one, the two terms give a destructive interference. Eventually, if the first term becomes larger than the second, the $(\theta_{13}^{(4\text{fam})}, \delta_2)$ -correlation changes, becoming orthogonal to the three-family-like one, as it can be seen in the figure. Notice that, when θ_{14} and θ_{24} assume values near their upper bound, there is a little sensitivity to the CP-phases at the longer baseline. Since this baseline corresponds to the magic baseline, we can conclude that this is an effect characteristic to the four neutrino scheme.

Summary and conclusions

The flavour mixing matrix present in leptonic weak currents may be generically non-unitary, as a result of new physics whenever extra fermions mix with the SM neutrinos or charged leptons. In this thesis we have analysed, from a phenomenological point of view, two possible sources of unitarity violation of the leptonic mixing matrix PMNS due to: (1) the effective operators which mainly arise whenever heavy fermions which mix with the SM leptons are integrated out and (2) the inclusion of additional light neutral fermions under the SM gauge group (ie, sterile neutrinos). Both options, as it was explained, induce a non-unitary three-family mixing matrix.

The first avenue we have explored is the one coming from high energies. Without attaching ourselves to any particular model, we have studied a minimal scheme of unitarity violation -MUV-, considering only three light neutrino species and assuming that all the new effects appear in the neutrino couplings. Clarifying the formalism for studying neutrino oscillations in this scheme, we have looked into interesting new effects. Considering a non-unitary mixing matrix results in the “zero-distance” flavour-changing transitions, very interesting in order to constrain leptonic unitarity. It is also remarkable that neutrino propagation in matter exhibits exotic couplings and an active role of the neutral current couplings, unlike in the standard unitary analysis.

We have used relevant data from neutrino oscillation experiments to determine, within the MUV scheme, the elements of the mixing matrix: about half of its elements remain unconstrained at this level. Data from weak decays cannot determine the values of the elements of the mixing matrix. They provide very stringent tests of unitarity, though, which turn out to be satisfied at the level of a few percent. The combination of data from weak decays and neutrino oscillation experiments results, within the MUV scheme, in a set of absolute values for the elements of the mixing matrix, which is very close to that from the unitary analysis. However, thanks to the analysis from present data we have been able to clarify which are the best avenues to look for deviations from unitarity. After the publication of Refs. [112, 115] this subject has been object of the interest of the community dedicated to the BSM searches in the leptonic sector.

Future facilities could establish the first signs of non-unitarity (or new physics in general). As a starting point, we have discussed the potential of some of them to improve unitarity constraints and determine all matrix elements without assuming unitarity. While the unitarity bounds expected from traditional $\mu \rightarrow e\gamma$ experiments will remain very powerful, experiments at a Neutrino Factory can also set stringent

unitarity constraints, allowing a direct determination of the elements in the τ row of the mixing matrix and furthermore being sensitive to the phases of the matrix elements. Precisely, a non-unitary matrix has not only more moduli than a unitary one, but also supplementary phases which may lead to new signals of CP violation. In particular, an asymmetry between the strength of $\nu_\mu \rightarrow \nu_\tau$ oscillations versus that for $\bar{\nu}_\mu \rightarrow \bar{\nu}_\tau$ has been shown to be a beautiful and excellent probe of new physics, when measured at short-baselines ~ 100 km using a Neutrino Factory beam of energy $\mathcal{O}(50\text{GeV})$.

However, future oscillation experiments such as the Neutrino Factory are being designed and optimised to look for standard neutrino physics. In this sense, the Neutrino Factory setup proposed here with a τ -detector at ~ 100 km is very demanding, since this detector would be not very useful for standard physics. Therefore, we have studied as well the sensitivity of a more feasible Neutrino Factory setup optimized to study the standard physics, the IDS one, to MUV. Our results imply that this Neutrino Factory set-up will be excellent for probing some of the unitarity-violating parameters. In particular, a sensitivity of $\mathcal{O}(10^{-4})$ to the real part of the unitarity-violating parameter $\eta_{\mu\tau}$ is found. On the other hand, we find that a near τ detector with a mass as small as 100 ton would dominate the sensitivity to $\eta_{e\tau}$, as well as that to the imaginary part of $\eta_{\mu\tau}$, through the measurement of the zero-distance effect, providing sensitivities down to $\mathcal{O}(10^{-3})$. Both sensitivities are an order of magnitude better than the present experimental bounds.

Furthermore, we find no degeneracies neither among the different unitarity-violating parameters, nor between the unitarity-violating parameters and the small standard neutrino oscillation parameters, such as θ_{13} . This means that the sensitivities to the standard oscillation parameters are robust even in presence of unitarity violation.

Regarding the prospects of an actual detection of unitarity violation, and especially CP violation stemming from non-unitary mixing, we find that the near and far detectors play a very complementary role. In the case of $\eta_{\mu\tau}$, the far detectors are only sensitive to the real part of the unitarity-violating parameter while the near detector can measure its modulus, neither is sensitive to unitarity-violating CP violation by themselves. However, it can be effectively probed by considering the combination of the two. An important warning is pertinent here: this kind of complementarity could lead us to see a new indirect signal of CP violation. However, since it would be tested through CP-conserving channels this would not constitute an unequivocal signal of CP violation. For that purpose it is necessary going to appearance channels as the $\nu_\mu \rightarrow \nu_\tau$ one.

Finally, we have studied the potential of a similar Neutrino Factory to search for signature of the (3+1)-scheme, where the largest mass squared difference Δm_{SBL}^2 can be any value larger than 0.1 eV^2 , as long as oscillations driven by Δm_{SBL}^2 are averaged for the range of the energy and the baseline at the Neutrino Factory considered. The two setups considered in this case are inspired by the ISS Physics Report. The main difference between them is the energy beam with muon energies of: $E_\mu = 50 \text{ GeV}$ and $E_\mu = 20 \text{ GeV}$ respectively. We have looked at the sensitivity to θ_{13} and θ_{14} analysing the golden and silver channels. We find that while no useful constraints on θ_{14} are

obtained, strong sensitivity to $\sin^2 2\theta_{13}$ is found as in the standard three-flavour unitary framework. Combining the disappearance and $\nu_\mu \rightarrow \nu_\tau$ channels, we have found that both the 50 GeV (20 GeV) Neutrino Factories can constrain θ_{34} and θ_{24} significantly, down to 12° (14°) and 7.5° (8°), respectively. This result has to be compared with the present bounds: around 30° and 12° respectively. On the other hand, in case we have a positive signal of the sterile neutrino mixing, we have found that we could measure again a new CP phase, in this case associated to the sterile neutrino physics, by combining the disappearance and $\nu_\mu \rightarrow \nu_\tau$ channels. The CP-violating phase δ_3 can be measured at 99% CL for values of $\sin^2 2\theta_{34} \geq 0.06$ (notice that, using only the disappearance channel, δ_3 can be measured at 99% CL for $\sin^2 2\theta_{34} \geq 0.4$, only).

We would like to stress that, while the $\nu_\mu \rightarrow \nu_\tau$ channel at a Neutrino Factory is not really useful for the measurements of the three-flavour standard oscillation parameters, it is a very important channel to search for new physics beyond the standard scenario. Mainly, when we focus on searches for new CP violation sources associated to NP, as those coming from non-unitarity, NSI or the sterile neutrino framework studied in this thesis. For this reason, in Ref. [202] it has been nicknamed as the "discovery channel". The $\nu_\mu \rightarrow \nu_\tau$ discovery channel at a Neutrino Factory deserves, thus, further studies.

As a concluding remark, we have shown that a signal of deviation from unitarity of the PMNS matrix would be a clear evidence of new physics, generically related to neutrino masses. Moreover, these deviations include as well new signals of CP violation. Even if the effects are expected to be extremely small in the simplest models of neutrino masses, this is not necessarily true for some variants of the seesaw mechanism [111], or other theories beyond the SM. Therefore, studying possible sources of NP beyond the SM through the measurement of unitarity violation of the PMNS matrix can be as important as the corresponding studies carried out at Φ and B-factories to look for NP in the framework of hadronic mixing. We should remark that experimental neutrino physics is a field in rapid expansion. In the near future new oscillation experiments: super-beams, β -beams or a high energy Neutrino Factory, can enlighten the origin of neutrino masses. Thanks to the high precision of these future experiments, we could well be able to discover new physics beyond the SM in a clean leptonic framework, complementary to the promising LHC searches.

Resultados y conclusiones

La matriz de mezcla presente en las corrientes leptónicas débiles podría no ser unitaria como resultado de nueva física, genéricamente asociada a la mezcla de nuevos fermiones con los neutrinos o leptones cargados del Modelo Estándar (ME). En la presente tesis hemos analizado, desde un punto de vista fenomenológico, dos posibles fuentes de violación de la unitariedad de la matriz de mezcla leptónica PMNS: (1) básicamente debidas a operadores efectivos que surgen cuando fermiones pesados que se mezclan con los leptones del ME son integrados “out” y (2) a incluir fermiones ligeros, neutros bajo el grupo gauge del ME (i.e, neutrinos estériles). Ambas opciones, como ya ha sido explicado, inducen la aparición de una matriz de mezcla no unitaria para tres familias.

La primera fuente que hemos explorado es la correspondiente a altas energías. Sin restringirnos a un modelo particular, hemos estudiado un esquema minimal de violación de unitariedad -MUV-, considerando sólo tres neutrinos ligeros y asumiendo que los nuevos efectos aparecen sólo en los acoplos que incluyen neutrinos. Aclarando el formalismo de cara al estudio de las oscilaciones de neutrinos dentro de este esquema, hemos examinado interesantes nuevos efectos. Considerar una matriz de mezcla no unitaria da lugar a transiciones de “flavour” a “distancia-cero”, algo que resulta muy interesante a la hora de acotar la no unitariedad. De igual modo, cabe resaltar que en la propagación de neutrinos en materia aparecen acoplos nuevos y un papel no despreciable de los asociados a las corrientes neutras, al contrario que en el análisis unitario estándar.

Hemos analizado, dentro del MUV, datos provenientes de experimentos de oscilaciones de neutrinos para determinar los elementos de la matriz de mezcla: a partir de estos datos, sólo pueden ser determinados la mitad de los elementos de matriz. Los datos procedentes de desintegraciones débiles no son sensibles a los elementos de matriz de forma individual, sin embargo, permiten realizar un preciso test de unitariedad, ésta se cumple al nivel del tanto por ciento. La combinación de datos procedentes de experimentos de oscilaciones de neutrinos y desintegraciones débiles, dentro del MUV, se traduce en una serie de valores para los módulos de los elementos de la matriz de mezcla, que resultan muy próximos a los obtenidos en el análisis unitario. Sin embargo, el análisis de los datos actuales nos ha permitido aclarar cuáles son las mejores ventanas en la búsqueda de desviaciones de unitariedad. Después de la publicación de Refs. [112,115] este tema está atrayendo la atención de parte de la comunidad dedicada a la búsqueda de física más allá del ME en el sector leptónico.

Experimentos futuros podrían dar lugar a las primeras señales de no unitariedad (o nueva física en general). Como punto de partida, hemos discutido el potencial de algunos de ellos a la hora de mejorar las cotas sobre no unitariedad o determinar todos los elementos de matriz sin asumir unitariedad. Mientras que las cotas provenientes de los experimentos tradicionales de $\mu \rightarrow e\gamma$ seguirán siendo una potente herramienta, experimentos en una “Neutrino Factory” podrían dar lugar también a fuertes cotas de unitariedad, permitir la medida directa de los elementos de matriz en la fila de los taus y, más aún, ser sensibles a las fases de los elementos de matriz. Precisamente, una matriz de mezcla no unitaria no sólo tiene más módulos que una unitaria, sino también fases adicionales que podrían dar lugar a nuevas señales de violación de CP. En particular, hemos mostrado como la asimetría CP entre los canales $\nu_\mu \rightarrow \nu_\tau$ y $\bar{\nu}_\mu \rightarrow \bar{\nu}_\tau$ supone un excelente test de esta nueva física, utilizando una “Neutrino Factory” de $\mathcal{O}(50\text{GeV})$ con un detector de taus localizado a una distancia corta detector-fuente ~ 100 km.

Sin embargo, los futuros experimentos de oscilaciones como la “Neutrino Factory” están siendo diseñados y optimizados con el objetivo de estudiar la física de neutrinos estándar. En este sentido, la “Neutrino Factory” propuesta aquí con un detector a ~ 100 km no es totalmente realista, ya que dicho detector no sería muy útil para la física estándar. Por esta razón, también hemos estudiado la sensibilidad al MUV de una versión de “Neutrino Factory” optimizada de cara a la física estándar, inspirada en la IDS. En nuestro análisis encontramos que esta propuesta sería muy útil para acotar los nuevos parámetros asociados a la no unitariedad en el futuro. En particular, encontramos una sensibilidad orden $\mathcal{O}(10^{-4})$ a la parte real de $\eta_{\mu\tau}$ (recordemos que η parametriza las desviaciones de unitariedad). Por otro lado, encontramos que un detector cercano de taus con una masa tan pequeña como 100 ton dominaría la sensibilidad a $\eta_{e\tau}$, así como a la parte imaginaria de $\eta_{\mu\tau}$, a través de la medida del efecto distancia cero, proporcionando sensibilidades de hasta $\mathcal{O}(10^{-3})$. Notar que las cotas mencionadas serían un orden de magnitud mayores que las cotas experimentales actuales.

Además, no encontramos degeneraciones ni entre los diferentes parámetros asociados a la no unitariedad, ni entre estos parámetros y los parámetros estándar del análisis unitario como θ_{13} . Esto se traduce en que la medida de los parámetros estándar no se vería afectada por la presencia de no unitariedad.

En cuanto a las perspectivas de una medida de violación de unitariedad, especialmente de violación de CP procedente de la mezcla no unitaria, encontramos que detectores lejanos y cercanos jugarían un papel altamente complementario. En el caso de $\eta_{\mu\tau}$, los detectores lejanos son básicamente sólo sensibles a la parte real de este parámetro mientras que un near detector podría medir su módulo, pero no es sensible a las fases de CP por sí mismo. Sin embargo, la combinación de ambos sí es sensible a la fase tanto si conserva CP como si no. Ahora bien, aunque este tipo de complementaridad podría permitirnos obtener una medida indirecta de violación de CP, es importante tener en cuenta que no constituiría una señal inequívoca de violación de CP dado que sería obtenida a través de canales que conservan CP. Para tal propósito

es necesario acudir a canales de aparición como $\nu_\mu \rightarrow \nu_\tau$.

Finalmente, hemos estudiado el potencial que tendría una versión similar de una “Neutrino Factory” en la búsqueda de una señal asociada al modelo $3 + 1$ de neutrinos estériles, donde la diferencia de masas más grande Δm_{SBL}^2 podría tomar cualquier valor mayor de 0.1 eV^2 , dado que las oscilaciones debidas a dicha diferencia de masa estarían promediadas para el rango de energías y distancias detector-fuente consideradas. Las dos propuestas estudiadas en este caso están inspiradas en el “ISS Physics Report”. La principal diferencia entre ambas es la energía del haz de neutrinos: $E_\mu = 50 \text{ GeV}$ y $E_\mu = 20 \text{ GeV}$ respectivamente. En primer lugar, hemos estudiado la sensibilidad a θ_{13} y θ_{14} analizando los canales de oscilación “golden” y “silver”. Encontramos que, mientras la sensibilidad a θ_{14} no es mejor que la cota actual, se obtiene una fuerte sensibilidad a θ_{13} al igual que en el análisis estándar en tres familias. Combinando los canales $\nu_\mu \rightarrow \nu_\mu$ y $\nu_\mu \rightarrow \nu_\tau$, obtenemos que ambas propuestas, $E_\mu = 50 \text{ GeV}$ y ($E_\mu = 20 \text{ GeV}$), podrían llegar a acotar θ_{34} y θ_{24} de manera significativa: hasta 12° (14°) y 7.5° (8°) respectivamente. Resultado que debe ser comparado con las cotas actuales: alrededor de 30° y 12° respectivamente. Por otro lado, analizamos también la posibilidad de encontrar una señal positiva de la existencia de neutrinos estériles. Encontramos de nuevo que las nuevas fases de violación de CP, esta vez asociadas a neutrinos estériles, podrían llegar a ser medidas combinando la información procedente de los canales $\nu_\mu \rightarrow \nu_\mu$ y $\nu_\mu \rightarrow \nu_\tau$. La nueva fase de violación de CP δ_3 podría medirse al 99% CL para valores de $\sin^2 2\theta_{34} \geq 0.06$ (recordemos que analizando solo el canal $\nu_\mu \rightarrow \nu_\mu$, δ_3 podría medirse al 99% CL sólo para $\sin^2 2\theta_{34} \geq 0.4$).

Nos gustaría resaltar que, mientras que el canal $\nu_\mu \rightarrow \nu_\tau$ en una “Neutrino Factory” no es muy útil de cara a las medidas de los parametros asociados al análisis estándar (en 3 familias y asumiendo unitariedad), resulta ser un canal muy importante de cara a estudiar nueva física. Principalmente, en lo que se refiere a la búsqueda de nuevas señales de violación de CP asociadas a ella, como aquellas procedentes del MUV, las “Non Standard Interactions” o de la existencia de neutrinos estériles ligeros, como hemos mostrado a lo largo de la tesis. Esta es la razón de que en Ref. [202] el mencionado canal de oscilación haya sido apodado como “discovery channel”. El canal $\nu_\mu \rightarrow \nu_\tau$ merece por tanto ser estudiado con mayor profundidad en el futuro.

Como comentario final, a lo largo de esta tesis hemos mostrado que una señal de desviación de unitariedad de la matriz de mezcla PMNS, que a su vez puede incluir nuevas señales de violación de CP, supondría una clara evidencia de nueva física principalmente relacionada con las masas de los neutrinos. Estos efectos se espera que sean extremadamente pequeños en los modelos más típicos de masas de neutrinos, sin embargo esto no es necesariamente cierto para ciertas versiones del “seesaw” [111] o en otras teorías de física más allá del ME. Por tanto, estudiar posibles fuentes de nueva física a través de la medida de violación de unitariedad de la matriz de mezcla leptónica, puede ser tan relevante como los correspondientes estudios realizados en Φ y “B-factories”, en los que se busca nueva física en el marco de la mezcla hadrónica. En el futuro próximo, nuevos experimentos de oscilaciones como “super-beams”, “ β -beams” o una “Neutrino Factory” de altas energías, podrían iluminar el origen de la

masa de los neutrinos. A la luz de la alta precisión de estos futuros experimentos, el descubrimiento de nueva física más allá del EM en un marco leptónico limpio parece realmente factible, complementariamente a la más que prometedora búsqueda de nueva física en LHC.

Agradecimientos

Bueno, llegó el difícil momento de los agradecimientos. Afortunadamente, en el momento en que estoy escribiendo esto, no tengo mucho tiempo para pensar en ello. Así, las posibilidades de que me ponga extremadamente tierno se reducen considerablemente.

Lo cierto es que, aunque por supuesto hay mucha gente a la que agradecer estos últimos años (en todos los sentidos), quiero hacerlo especialmente a mis *compis* del departamento y del IFT. Son muchas las cosas que hemos vivido juntos, tanto en el plano personal como en el científico, y ellos son realmente los que más han servido de apoyo en esto de la tesis (y aspectos adyacentes). Vosotros sabéis quienes sois, pero habrá que hacer una lista (eso sí, en orden alfabético como en los papers). En primer lugar a los que a fecha de hoy comparten penurias relacionadas con la tesis: Adolfo, Alfonso e Irene. A los que ya están por ahí danzando de posdocs o similar: Antón, Carlitos, Florian, Josemi y Meggi. A alguno que se pasó al lado oscuro como Fernando. A mis *compis* de despacho: Bea, Jose, Luis y Paola. También a esos desertores que son Carol, Edu y Elías. A los últimos fichajes: Giovanni, María, Miguelito y Nuri. A esas generaciones intermedias con Dani, Javi, Luisfer y Paula como principales exponentes. A la vieja guardia que nos cedió el testigo: Alberto, Ernesto, Javi, Jose, Nico, Sergio, Tomás, etc. Y unos que no son compañeros de *curro* pero como si lo fueran: Amalio, Carmelo, Mario y Vital (a excepción de Mario, juntos formamos un elenco de nombres sin duda incomparable).

Mis agradecimientos van también dirigidos a mi familia. Sobre todo a mis padres y a mis hermanos Roberto y Natalia. Mención especial merece mi abuelo, que aunque creo que nunca se ha llegado a creer del todo que esto sea un trabajo, sé que está muy orgulloso de que su nieto ande por ahí “investigando”. A mis tíos Alfonso y Mari Carmen que sé que también están orgullosos. Y bueno, a Arantxa, que no es de la familia pero que al menos durante 2/3 de la tesis (y algún tiempito más antes) es como si lo hubiera sido. Finalmente sería injusto no ser también agradecido con Nemo, compañero fiel de fatigas estos últimos años.

Por supuesto, quiero agradecer profundamente a mis jefes, Belén y Andrea, todo lo que han hecho por mi durante estos años. Si nos ponemos un poco técnicos ellos deberían, sin duda, estar en primer lugar. Evidentemente, ellos son los que me han iniciado en esto de la ciencia y no con malos consejos precisamente. Gracias también a todos aquellos con los que he trabajado y discutido sobre Física que también son,

claramente, parte de esto. En este contexto, como no, también se agradece el apoyo de mis hermanos académicos: Enrique (el mayor) y María Pilar (la pequeña).

Finalmente, por completitud, un agradecimiento muy especial a mis amigos del barrio (de la *Pili*) y de Portonovo (ciudad sin ley): ¡también va por vosotros chavales!

Appendix A

Oscillation probabilities in presence of unitarity violation

In this Appendix, a convenient formalism is introduced to derive oscillation probabilities $P_{\alpha\beta}$ in matter with constant density, in the MUV scheme. As a detailed example, the results are then applied first to the $\nu_\mu \rightarrow \nu_\tau$ channel at the short distance setup defined in Sec.3.3. Afterwards we apply the same formalism in order to calculate the relevant oscillation probabilities in the general case, independently of the baseline.

Several years ago Kimura, Takamura and Yokomakura derived a nice compact formula [194,195] for the neutrino oscillation probability in matter with constant density¹. They showed that the quantity $\tilde{U}_{\alpha j}^* \tilde{U}_{\beta j}$ in matter can be expressed as a linear combination of the quantity $U_{\alpha j}^* U_{\beta j}$ in vacuum, where $U_{\alpha j}$ and $\tilde{U}_{\alpha j}$ stand for the matrix element of the PMNS matrix in vacuum and in matter, respectively. A simple derivation of their formula and its generalization are given in Ref. [215]. Here it is shown that the framework in Ref. [215] can be applied also to the MUV case.

Time evolution of the neutrino mass eigenstate $\Psi_m \equiv (|\nu_1\rangle, |\nu_2\rangle, |\nu_3\rangle)^T$ in matter with constant density in the MUV framework is given by

$$i \frac{d\Psi_m}{dt} = (\mathcal{E} + N^T \mathcal{A} N^*) \Psi_m, \quad (\text{A.1})$$

where $\mathcal{E} \equiv \text{diag}(E_1, E_2, E_3)$ is the energy matrix in the mass basis in vacuum, the non-unitary matrix N relates the flavour fields to the mass fields (cf. Eq. (2.4)) and

$$\mathcal{A} \equiv \sqrt{2} G_F \text{diag}(n_e - n_n/2, -n_n/2, -n_n/2), \quad (\text{A.2})$$

n_e and n_n are the electron and neutron density respectively. Assuming that the electron and neutron number densities are equal² (*i.e.*, $n_e = n_n$), \mathcal{A} can be expressed as

¹Another proof of the KTY formalism was given in Ref. [140,215]

²This is a very good approximation in the case of neutrino oscillations in the Earth.

$$\mathcal{A} \equiv \text{diag}(A/2, -A/2, -A/2), \quad (\text{A.3})$$

with $A = \sqrt{2}G_F n_e$. Diagonalizing the hermitian matrix $\mathcal{E} + N^T \mathcal{A} N^*$ with a unitary matrix W

$$\mathcal{E} + N^T \mathcal{A} N^* = W \tilde{\mathcal{E}} W^\dagger, \quad (\text{A.4})$$

where $\tilde{\mathcal{E}} \equiv \text{diag}(\tilde{E}_1, \tilde{E}_2, \tilde{E}_3)$ is the energy matrix in matter in the MUV scheme, the mass eigenstate at distance L can be solved as

$$\Psi_m(L) = W \exp(-i\tilde{\mathcal{E}}L) W^\dagger \Psi_m(0). \quad (\text{A.5})$$

We define the modified amplitude $\hat{A}(\nu_\alpha \rightarrow \nu_\beta) \equiv A(\nu_\alpha \rightarrow \nu_\beta) (NN^\dagger)_{\alpha\alpha}^{1/2} (NN^\dagger)_{\beta\beta}^{1/2}$,

$$\hat{A}(\nu_\alpha \rightarrow \nu_\beta) = [N^* W \exp(-i\tilde{\mathcal{E}}L) W^\dagger N^T]_{\alpha\beta},$$

and the modified probability $\hat{P}(\nu_\alpha \rightarrow \nu_\beta) \equiv |\hat{A}(\nu_\alpha \rightarrow \nu_\beta)|^2$ is given by

$$\begin{aligned} \hat{P}(\nu_\alpha \rightarrow \nu_\beta) &= |(N^* N^T)_{\alpha\beta}|^2 - 4 \sum_{j < k} \text{Re}(\tilde{X}_j^{\alpha\beta} \tilde{X}_k^{\alpha\beta*}) \sin^2(\Delta \tilde{E}_{jk} L / 2) \\ &\quad + 2 \sum_{j < k} \text{Im}(\tilde{X}_j^{\alpha\beta} \tilde{X}_k^{\alpha\beta*}) \sin(\Delta \tilde{E}_{jk} L), \end{aligned} \quad (\text{A.6})$$

where $\Delta \tilde{E}_{jk} \equiv \tilde{E}_j - \tilde{E}_k$ and $\tilde{X}_j^{\alpha\beta} \equiv (N^* W)_{\alpha j} (N W^*)_{\beta j}$ ($j = 1, 2, 3$). As in the case of the standard neutrino scenario [194, 215], $\tilde{X}_j^{\alpha\beta}$ can be expressed in terms of the quantity $X_j^{\alpha\beta} \equiv U_{\alpha j}^* U_{\beta j}$ in vacuum and \tilde{E}_j . To show it, let us first note the following relations:

$$\begin{aligned} \sum_j (\tilde{E}_j)^m \tilde{X}_j^{\alpha\beta} &= \sum_j (N^* W)_{\alpha j} (\tilde{E}_j)^m (N W^*)_{\beta j} = [N^* (\mathcal{E} + N^T \mathcal{A} N^*)^m N^T]_{\alpha\beta} \equiv Y_{m+1}^{\alpha\beta} \\ &\quad \text{for } m = 0, 1, 2. \end{aligned} \quad (\text{A.7})$$

Secondly we rewrite Eqs. (A.7) as

$$\sum_{m=1}^3 V_{jm} \tilde{X}_m^{\alpha\beta} = Y_j^{\alpha\beta} \quad \text{for } j = 1, 2, 3, \quad (\text{A.8})$$

where $V_{jm} \equiv (\tilde{E}_m)^{j-1}$ are the elements of the van der Monde matrix V . The simultaneous equation (A.8) can be easily solved by inverting V :

$$\tilde{X}_j^{\alpha\beta} = \sum_{m=1}^3 (V^{-1})_{jm} Y_m^{\alpha\beta} = \sum_{m=1}^3 (V^{-1})_{jm} [N^* (\mathcal{E} + N^T \mathcal{A} N^*)^{m-1} N^T]_{\alpha\beta}, \quad (\text{A.9})$$

where

$$V^{-1} = \begin{pmatrix} (1/\Delta \tilde{E}_{21} \Delta \tilde{E}_{31})(\tilde{E}_2 \tilde{E}_3, & -(\tilde{E}_2 + \tilde{E}_3), & 1) \\ (1/\Delta \tilde{E}_{21} \Delta \tilde{E}_{32})(\tilde{E}_3 \tilde{E}_1, & -(\tilde{E}_3 + \tilde{E}_1), & 1) \\ (1/\Delta \tilde{E}_{31} \Delta \tilde{E}_{32})(\tilde{E}_1 \tilde{E}_2, & -(\tilde{E}_1 + \tilde{E}_2), & 1) \end{pmatrix} \quad (\text{A.10})$$

Taking into account Eq. (A.6), Eq. (A.9) and Eq. (A.10), it is easy to realise that, once the effective eigenvalues in matter are known, it is straightforward to obtain the expressions for the neutrino oscillation probabilities. However, in order to obtain reasonably simple expressions, it is necessary to expand them in small parameters as we do in the following subsections.

A.1 Short baseline limit

In the present section we focus on the short distance case, i.e., the case where $|\Delta E_{jk}L| \ll 1$, $|\Delta \tilde{E}_{jk}L| \ll 1$, $|AL| \ll 1$. It turns out that terms of order $(\Delta \tilde{E}_{jk}L)^3$ or higher are negligible at short distance and we expand the sine functions in the probability (A.6) to quadratic order in the argument $\Delta \tilde{E}_{jk}L$:

$$\sin^2(\Delta \tilde{E}_{jk}L/2) \simeq (\Delta \tilde{E}_{jk}L/2)^2, \quad \sin(\Delta \tilde{E}_{jk}L) \simeq \Delta \tilde{E}_{jk}L$$

Plugging Eq. (A.9) in the probability (A.6) and using the form of V^{-1} in Eq. (A.10), we can show that the first terms take the following simple forms:

$$\begin{aligned} \sum_{j < k} \text{Re}(\tilde{X}_j^{\alpha\beta} \tilde{X}_k^{\alpha\beta*}) (\Delta \tilde{E}_{jk}L/2)^2 &= (L/2)^2 [\text{Re}(Y_1^{\alpha\beta} Y_3^{\alpha\beta*}) - |Y_2^{\alpha\beta}|^2], \\ \sum_{j < k} \text{Im}(\tilde{X}_j^{\alpha\beta} \tilde{X}_k^{\alpha\beta*}) \Delta \tilde{E}_{jk}L &= -L \text{Im}(Y_1^{\alpha\beta} Y_2^{\alpha\beta*}) \end{aligned}$$

Hence we obtain the probability at short distance

$$\hat{P}(\nu_\alpha \rightarrow \nu_\beta) \simeq |(NN^\dagger)_{\alpha\beta}|^2 - L^2 [\text{Re}(Y_1^{\alpha\beta} Y_3^{\alpha\beta*}) - |Y_2^{\alpha\beta}|^2] - 2L \text{Im}(Y_1^{\alpha\beta} Y_2^{\alpha\beta*}). \quad (\text{A.11})$$

We are interested in the MUV scheme with small values of η , where η was defined in Eq. (3.2), so we evaluate $Y_j^{\alpha\beta}$ only to first order in η :

$$\begin{aligned} Y_1^{\alpha\beta} &\simeq \delta_{\alpha\beta} + 2\eta_{\alpha\beta}, \\ Y_2^{\alpha\beta} &\simeq \sum_{j=2}^3 \Delta_{j1} X_j^{\alpha\beta} + \sum_{\gamma} \sum_{j=2}^3 \Delta_{j1} (X^{\alpha\gamma} \eta_{\gamma\beta} + X^{\gamma\beta} \eta_{\alpha\gamma}) + \mathcal{A}_{\alpha\beta} + 2\eta_{\alpha\beta} (\mathcal{A}_{\alpha\alpha} + \mathcal{A}_{\beta\beta}), \\ Y_3^{\alpha\beta}|_{\eta \rightarrow 0} &= \sum_{j=2}^3 (\Delta_{j1})^2 X_j^{\alpha\beta} + \sum_{j=2}^3 \Delta_{j1} X_j^{\alpha\beta} (\mathcal{A}_{\alpha\alpha} + \mathcal{A}_{\beta\beta}) + (\mathcal{A}_{\alpha\beta})^2, \end{aligned} \quad (\text{A.12})$$

where we have used the energy matrix $\mathcal{E} - E_1 \mathbf{1} + N^T \mathcal{A} N^*$ instead of (A.4) for ease of calculation, since the shift $(-E_1 \mathbf{1})$ only changes the phase of the amplitude $\hat{A}(\nu_\alpha \rightarrow \nu_\beta)$. $Y_3^{\alpha\beta}$ was evaluated only in the limit $\eta_{\alpha\beta} \rightarrow 0$, as it always appears together with $Y_1^{\alpha\beta}$, which is first order in $\eta_{\alpha\beta}$.

It is straightforward to obtain the components $Y_j^{\mu\tau}$ for $j = 1, 2, 3$ from Eqs. (A.12). Keeping only terms to second order in $\sin^2 \theta_{13}$, $\Delta_{21}L$, $(\Delta_{31}L)^2$, $(AL)^2$ and first in $\eta_{\alpha\beta}$, and setting $\eta_{e\mu} = 0$, we get the probability $P_{\mu\tau} = \hat{P}(\nu_\mu \rightarrow \nu_\tau)/(NN^\dagger)_{\mu\mu}(NN^\dagger)_{\tau\tau}$:

$$\begin{aligned}
P_{\mu\tau} &= \sin^2 2\theta_{23}(\Delta_{31}L/2)^2 - 2|\eta_{\mu\tau}| \sin \delta_{\mu\tau} \sin 2\theta_{23}(\Delta_{31}L) + 4|\eta_{\mu\tau}|^2 \\
&- (1/2)c_{12}^2 \sin^2 2\theta_{23}(\Delta_{31}L)(\Delta_{21}L) - |\eta_{\mu\tau}| \sin 2\theta_{23} \cos \delta_{\mu\tau}(AL)(\Delta_{31}L) \\
&+ (1/4)c_{12}^4 \sin^2 2\theta_{23}(\Delta_{21}L)^2 + 2|\eta_{\mu\tau}|c_{12}^2 \sin \delta_{\mu\tau} \sin 2\theta_{23}(\Delta_{21}L) \\
&- (1/4)s_{13} \sin 4\theta_{23} \sin 2\theta_{12} \cos \delta(\Delta_{31}L)(\Delta_{21}L).
\end{aligned} \tag{A.13}$$

Notice that matter effects in this channel are clearly subdominant. All terms but those in the first line of Eq. (A.13) are numerically smaller than 10^{-4} for the setup considered in Sec. 3.3 and have thus negligible practical effects.

For the $e \rightarrow \tau$ channel the same formalism has been used to obtain the expanded probability, presented in Eq. (3.13).

A.2 More on oscillation probabilities in presence of unitarity violation

In this section, we derive the probabilities $P_{\alpha\beta}$ in matter without any assumption about the size of the baseline. Again, since the constraint on $\eta_{e\mu}$ is strong enough to safely neglect $\eta_{e\mu}$ in the oscillation probabilities, we will assume $\eta_{e\mu} = 0$ below. However, it has been considered in the numerical analysis presented in Sec. 3.4.

The parameters that appear linearly in the normalisation factors are η_{ee} , $\eta_{\mu\mu}$, and $\eta_{\tau\tau}$, which are already better constrained by other considerations than the sensitivities we find for a Neutrino Factory. Thus, the determination of the fluxes and cross-sections by the near detectors only suffer from a minor additional theoretical uncertainty. We will present the oscillation probabilities $\hat{P}(\nu_\alpha \rightarrow \nu_\beta) = \hat{P}_{\alpha\beta}$ without taking the normalisation factors into account. Notice that this will not be at all relevant for the golden and silver channels, since the probabilities are already order η^2 before taking the normalization factors into account. Thus, the corrections would be at most $\mathcal{O}(\eta^3)$.

As we have said above, in order to obtain reasonably simple expressions, it is necessary to expand them in small parameters. Here, we present the oscillation probabilities to second order in the parameters listed in Tab. A.1.

To second order in η (η_{sm} and $\eta_{\alpha\beta}$), we can find the eigenvalues by using perturbation theory. We find that

SM expansion parameters (η_{sm})	MUV expansion parameters
$\theta_{13}, \Delta m_{21}^2/\Delta m_{31}^2, \delta\theta_{23} = \theta_{23} - \pi/4$	$\eta_{\alpha\beta}$

Table A.1: *The small expansion parameters used in our neutrino oscillation probabilities. We will refer to the set of SM expansion parameters as η_{sm} . The full set of expansion parameters will be referred to as η , while only the set of MUV expansion parameters will be denoted by $\eta_{\alpha\beta}$.*

$$\begin{aligned}
\tilde{E}_1 &= A \left[1 + \frac{\Delta_{21}}{A} s_{12}^2 + \left(\frac{\Delta_{21}}{2A} \right)^2 \sin^2(2\theta_{12}) + \frac{\Delta_{31} s_{13}^2}{A - \Delta_{31}} + \eta_{ee} + \frac{\eta_{ee}^2}{2} - \frac{|\eta_{e\tau}|^2}{2} \right] + \mathcal{O}(\eta^3), \\
\tilde{E}_2 &= A \left\{ \frac{\Delta_{21}}{A} c_{12}^2 - \left(\frac{\Delta_{21}}{2A} \right)^2 \sin^2(2\theta_{12}) + \text{Re}(\eta_{\mu\tau}) \left[1 + \frac{1}{2}(\eta_{\mu\mu} + \eta_{\tau\tau}) \right] - \frac{1}{2}(\eta_{\mu\mu} + \eta_{\tau\tau}) \right. \\
&\quad \left. - \frac{1}{4}(\eta_{\mu\mu}^2 + \eta_{\tau\tau}^2) - \frac{|\eta_{\mu\tau}|^2}{2} + \frac{|\eta_{e\tau}|^2}{4} - \delta\theta_{23} \left[\eta_{\tau\tau} - \eta_{\mu\mu} + \frac{1}{2}(\eta_{\tau\tau}^2 - \eta_{\mu\mu}^2) - |\eta_{e\tau}|^2/2 \right] \right. \\
&\quad \left. - \frac{A}{\Delta_{31}} \text{Re}(\eta_{\mu\tau})^2 - \frac{A}{4\Delta_{31}} (\eta_{\tau\tau} - \eta_{\mu\mu})^2 \right\} + \mathcal{O}(\eta^3), \\
\tilde{E}_3 &= A \left\{ \frac{\Delta_{31}}{A} - \frac{\Delta_{31} s_{13}^2}{A - \Delta_{31}} - \text{Re}(\eta_{\mu\tau}) \left[1 + \frac{1}{2}(\eta_{\mu\mu} + \eta_{\tau\tau}) \right] + \delta\theta_{23}(\eta_{\tau\tau} - \eta_{\mu\mu}) \right. \\
&\quad \left. - \frac{1}{2}(\eta_{\mu\mu} + \eta_{\tau\tau}) - \frac{1}{4}(\eta_{\tau\tau}^2 + \eta_{\mu\mu}^2) - \frac{|\eta_{\mu\tau}|^2}{2} + \frac{|\eta_{e\tau}|^2}{4} \right\} + \mathcal{O}(\eta^3). \tag{A.14}
\end{aligned}$$

Notice that, for $\eta_{\alpha\beta} \rightarrow 0$, we recover the SM results as expected. These results allow us to obtain V^{-1} at second order. Thus, we only need to compute $Y_j^{\alpha\beta}$ at the same order, the computation is straightforward but tedious (see Eq. (A.9)). For brevity, we do not present the results for V^{-1} and $Y_j^{\alpha\beta}$ here. However, we would like to comment that, for the golden and silver channels, it is enough to compute these quantities to first order, since $\tilde{X}_j^{\alpha\beta}$ is already of first order in η . This is not true in the case of the ν_μ - ν_τ sector, where $\tilde{X}_2^{\mu\mu}|_{\eta=0} = \tilde{X}_3^{\mu\mu}|_{\eta=0} = -\tilde{X}_2^{\tau\mu}|_{\eta=0} = \tilde{X}_3^{\tau\mu}|_{\eta=0} = 1/2$. The advantage of this sector, from the point of view of discovering new physics, is that the effects of the new physics can appear in the probability at first order as an interference term between the SM and the new physics without additional suppression by η . For this reason, we keep only the interference between the $\mathcal{O}(\eta_{\alpha\beta})$ terms and the $\mathcal{O}(\eta_{sm})$ ones at second order³ in that sector.

In the end, we obtain the following expanded oscillation probabilities at the orders

³It could also be justified to neglect the $\mathcal{O}\left(\eta_{\alpha\beta} \frac{\Delta m_{21}^2}{\Delta m_{31}^2}\right)$ terms, since the maximal allowed value of $\frac{\Delta m_{21}^2}{\Delta m_{31}^2}$ is at least one order of magnitude smaller than the maximal allowed values of s_{13} and $\delta\theta_{23}$. However, we keep also these terms for completeness.

mentioned above:

$$\begin{aligned}
\hat{P}_{\mu\mu} &= P_{\mu\mu}^{\text{SM}} + 4\eta_{\mu\mu} + 4\eta_{\mu\mu}^2 \\
&+ 4 \left\{ -\eta_{\mu\mu} + 2 \operatorname{Re}(\eta_{\mu\tau})\delta\theta_{23} - 2\delta\theta_{23}(\eta_{\mu\mu} - \eta_{\tau\tau})\frac{A}{\Delta_{31}} \right\} \sin^2 \left(\frac{\Delta_{31}L}{2} \right) \\
&- [2 \operatorname{Re}(\eta_{\mu\tau}) - \delta\theta_{23}(\eta_{\mu\mu} - \eta_{\tau\tau})] AL \sin(\Delta_{31}L) + \mathcal{O}(\eta_{\alpha\beta}^2), \tag{A.15}
\end{aligned}$$

$$\begin{aligned}
\hat{P}_{\mu\tau} &= P_{\mu\tau}^{\text{SM}} + 4|\eta_{\mu\tau}|^2 \\
&+ \left[2 \operatorname{Re}(\eta_{\mu\mu} + \eta_{\tau\tau}) + 8\delta\theta_{23}(\eta_{\mu\mu} - \eta_{\tau\tau})\frac{A}{\Delta_{31}} \right] \sin^2 \left(\frac{\Delta_{31}L}{2} \right) \\
&+ [-2 \operatorname{Im}(\eta_{\mu\tau}) - \delta\theta_{23}(\eta_{\mu\mu} - \eta_{\tau\tau})AL] \sin(\Delta_{31}L) \\
&- \sqrt{2} \operatorname{Im} \left\{ \eta_{e\tau} \left[\frac{\Delta_{21}}{A} \sin(2\theta_{12}) + \frac{2\Delta_{31}s_{13}e^{i\delta}}{A - \Delta_{31}} \right] \right\} \sin \left(\frac{AL}{2} \right) \sin \left(\frac{\Delta_{31}L}{2} \right) \sin \left(\frac{\Delta_{31} - A}{2}L \right) \\
&+ \sqrt{2} \operatorname{Re} \left\{ \eta_{e\tau} \left[\frac{\Delta_{21}}{A} \sin(2\theta_{12}) \sin \left(\frac{AL}{2} \right) \cos \left(\frac{\Delta_{31} - A}{2}L \right) \right. \right. \\
&\quad \left. \left. - \frac{2\Delta_{31}s_{13}e^{i\delta}}{A - \Delta_{31}} \cos \left(\frac{AL}{2} \right) \sin \left(\frac{\Delta_{31} - A}{2}L \right) \right] \right\} \sin \left(\frac{\Delta_{31}L}{2} \right) \\
&+ \mathcal{O}(\eta_{\alpha\beta}^2), \tag{A.16}
\end{aligned}$$

$$\begin{aligned}
\hat{P}_{e\mu} &= P_{e\mu}^{\text{SM}} + |\eta_{e\tau}|^2 \sin^2 \left(\frac{\Delta_{31}L}{2} \right) \\
&+ \operatorname{Im} \left\{ \eta_{e\tau} \left[\frac{1}{2} \frac{\Delta_{21}}{A} \sin(2\theta_{12}) + \frac{\Delta_{31}s_{13}e^{i\delta}}{A - \Delta_{31}} \right] \right\} \sin \left(\frac{AL}{2} \right) \sin \left(\frac{\Delta_{31}L}{2} \right) \sin \left(\frac{\Delta_{31} - A}{2}L \right) \\
&+ \operatorname{Re} \left\{ \eta_{e\tau} \left[\frac{1}{\sqrt{2}} \frac{\Delta_{21}}{A} \sin(2\theta_{12}) \sin \left(\frac{AL}{2} \right) \cos \left(\frac{\Delta_{31} - A}{2}L \right) \right. \right. \\
&\quad \left. \left. - \frac{2\sqrt{2}\Delta_{31}s_{13}e^{i\delta}}{A - \Delta_{31}} \cos \left(\frac{AL}{2} \right) \sin \left(\frac{\Delta_{31} - A}{2}L \right) \right] \right\} \sin \left(\frac{\Delta_{31}L}{2} \right) \\
&+ \mathcal{O}(\eta^3), \tag{A.17}
\end{aligned}$$

$$\begin{aligned}
\hat{P}_{e\tau} &= P_{e\tau}^{\text{SM}} + 4|\eta_{e\tau}|^2 - 2 \left[|\eta_{e\tau}|^2 - \frac{\sqrt{2}\Delta_{31}s_{13}}{A - \Delta_{31}} \text{Re}(\eta_{e\tau}e^{i\delta}) \right] \sin^2 \left(\frac{\Delta_{31} - A}{2} L \right) \\
&\quad - 2 \left[|\eta_{e\tau}|^2 - \frac{1}{\sqrt{2}} \frac{\Delta_{21}}{A} \sin(2\theta_{12}) \text{Re}(\eta_{e\tau}) \right] \sin^2 \left(\frac{AL}{2} \right) \\
&\quad - \text{Im} \left\{ \eta_{e\tau}^* \left[\frac{1}{\sqrt{2}} \frac{\Delta_{21}}{A} \sin(2\theta_{12}) \sin(AL) - \frac{\sqrt{2}\Delta_{31}s_{13}e^{-i\delta}}{A - \Delta_{31}} \sin(\{\Delta_{31} - A\}L) \right] \right\} \\
&\quad - 2\sqrt{2} \text{Re} \left\{ \eta_{e\tau} \left[\frac{1}{2} \frac{\Delta_{21}}{A} \sin(2\theta_{12}) - \frac{\Delta_{31}s_{13}e^{i\delta}}{A - \Delta_{31}} \right] \right\} \sin \left(\frac{AL}{2} \right) \cos \left(\frac{\Delta_{31}L}{2} \right) \sin \left(\frac{\Delta_{31} - A}{2} L \right) \\
&\quad + \text{Im} \left\{ \eta_{e\tau} \left[\sqrt{2} \frac{\Delta_{21}}{A} \sin(2\theta_{12}) \sin \left(\frac{AL}{2} \right) \cos \left(\frac{\Delta_{31} - A}{2} L \right) \right. \right. \\
&\quad \quad \left. \left. + \frac{2\sqrt{2}\Delta_{31}s_{13}e^{i\delta}}{A - \Delta_{31}} \cos \left(\frac{AL}{2} \right) \sin \left(\frac{\Delta_{31} - A}{2} L \right) \right] \right\} \cos \left(\frac{\Delta_{31}L}{2} \right) \\
&\quad + \mathcal{O}(\eta^3) . \tag{A.18}
\end{aligned}$$

Notice that we do not neglect the zero-distance effect in the ν_μ - ν_τ sector. Although this is not within the order of the expansion, we keep it as it plays an important role in the analysis of the neutrino flavour transitions at near detectors.

Appendix B

Sterile Neutrinos

B.1 The mixing matrix elements $U_{\alpha j}$

The mixing matrix elements in the parametrization (4.2) are given by the following:

$$\begin{cases} U_{e1} = c_{12}c_{13}c_{14} \\ U_{e2} = c_{13}c_{14}s_{12}e^{-i\delta_1} \\ U_{e3} = c_{14}s_{13}e^{-i\delta_2} \\ U_{e4} = s_{14} \end{cases} \quad (\text{B.1})$$

$$\begin{cases} U_{\mu 1} = -c_{23}c_{24}s_{12}e^{i\delta_1} - c_{12} [c_{24}s_{13}s_{23}e^{i(\delta_2-\delta_3)} + c_{13}s_{14}s_{24}] \\ U_{\mu 2} = c_{12}c_{23}c_{24} - s_{12}e^{-i\delta_1} [c_{24}s_{13}s_{23}e^{i(\delta_2-\delta_3)} + c_{13}s_{14}s_{24}] \\ U_{\mu 3} = c_{13}c_{24}s_{23}e^{-i\delta_3} - s_{13}s_{14}s_{24}e^{-i\delta_2} \\ U_{\mu 4} = c_{14}s_{24} \end{cases} \quad (\text{B.2})$$

$$\begin{cases} U_{\tau 1} = s_{12}e^{i\delta_1} [c_{34}s_{23}e^{i\delta_3} + c_{23}s_{24}s_{34}] \\ \quad - c_{12} \{ c_{13}c_{24}s_{14}s_{34} + s_{13}e^{i\delta_2} [c_{23}c_{34} - s_{23}s_{24}s_{34}e^{-i\delta_3}] \} \\ U_{\tau 2} = -c_{12} [c_{34}s_{23}e^{i\delta_3} + c_{23}s_{24}s_{34}] \\ \quad - s_{12}e^{-i\delta_1} \{ c_{13}c_{24}s_{14}s_{34} + s_{13}e^{i\delta_2} [c_{23}c_{34} - s_{23}s_{24}s_{34}e^{-i\delta_3}] \} \\ U_{\tau 3} = -c_{24}s_{13}s_{14}s_{34}e^{-i\delta_2} + c_{13} [c_{23}c_{34} - s_{23}s_{24}s_{34}e^{-i\delta_3}] \\ U_{\tau 4} = c_{14}c_{24}s_{34} \end{cases} \quad (\text{B.3})$$

$$\begin{cases} U_{s1} = s_{12}e^{i\delta_1} [c_{23}c_{34}s_{24} - s_{23}s_{34}e^{i\delta_3}] \\ \quad - c_{12} \{ c_{13}c_{24}c_{34}s_{14} - s_{13}e^{i\delta_2} [c_{34}s_{23}s_{24}e^{-i\delta_3} + c_{23}s_{34}] \} \\ U_{s2} = -c_{12} [c_{23}c_{34}s_{24} - s_{23}s_{34}e^{i\delta_3}] \\ \quad - s_{12}e^{-i\delta_1} \{ c_{13}c_{24}c_{34}s_{14} - s_{13}e^{i\delta_2} [c_{34}s_{23}s_{24}e^{-i\delta_3} + c_{23}s_{34}] \} \\ U_{s3} = -c_{24}c_{34}s_{13}s_{14}e^{-i\delta_2} - c_{13} [c_{34}s_{23}s_{24}e^{-i\delta_3} + c_{23}s_{34}] \\ U_{s4} = c_{14}c_{24}c_{34} \end{cases} \quad (\text{B.4})$$

where $c_{ij} = \cos \theta_{ij}$ and $s_{ij} = \sin \theta_{ij}$.

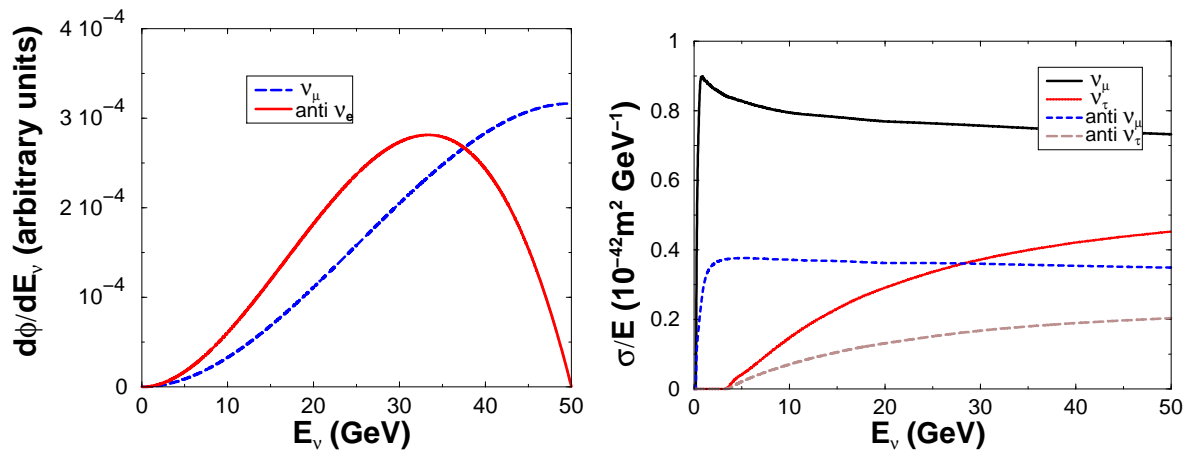


Figure B.1: *Left: 50 GeV Neutrino Factory fluxes at $L = 3000$ km; Right: the $\nu_\mu N$ and $\nu_\tau N$ cross-sections on iron [225, 226].*

B.2 The Neutrino Factory and the Hybrid-MIND detector

In a Neutrino Factory [90,91] muons are first produced with a multi-MW proton source, accelerated up to energies of several GeV's, and finally injected into a storage ring with long straight sections aiming to one or more detectors. The muon decays $\mu^+ \rightarrow e^+ \nu_e \bar{\nu}_\mu$ and $\mu^- \rightarrow e^- \bar{\nu}_e \nu_\mu$ provide a very well known two-flavour neutrino flux [216] with energies in the range $E_\nu \in [0, E_\mu]$. Neutrino Factory designs have been proposed in Europe [217, 218], the US [219–222], and Japan [223]. The dedicated *International Scoping Study for a future Neutrino Factory and Super-Beam facility* [99] showed that, provided sufficient resources, an accelerator complex capable of providing about 10^{21} muon decays of a given polarity per year can be built.

The Neutrino Factory setup that we propose for sterile neutrinos searches and that we examine in detail in the rest of the appendix and Chap. 4 is defined as follows: muons of both polarities are accelerated up to $E_\mu = 50$ GeV and injected into one storage ring with a geometry that allows to aim at two far detectors, the first located at 3000 km and the second at 7500 km from the source. An alternative option, considered in the final ISS Accelerator Report [224], is to inject the muon beam into different storage rings, each of them aimed to a single far detector. The number of useful muon decays per year aimed at each detector has been fixed to 2×10^{20} . This number is rather conservative since, in the final ISS Physics Report [99], with a similar storage ring(s) geometry, 5×10^{20} useful muon decays per year aimed at each detector are considered (i.e., 10^{21} total useful muon decays per year). Four years of data taking for each muon polarity are envisaged.

The Neutrino Factory fluxes (for μ^- accumulated in the storage ring) at $L = 3000$ km as a function of the neutrino energy for $E_\mu = 50$ GeV are shown in Fig. B.1(left).

Two detectors of different technologies have been considered to detect the ν_μ and ν_τ signals. The first one is a magnetized iron calorimeter [227], that was proposed with a slightly different design in Ref. [228] to measure the “golden” $\nu_e \rightarrow \nu_\mu$ wrong-sign muons signal. The second detector is a Magnetized Emulsion Cloud Chamber (MECC) [158], an evolution of the ECC modeled after OPERA that was first considered for Neutrino Factory studies in Refs. [142, 149] to look for the “silver channel” $\nu_e \rightarrow \nu_\tau$.

The $\nu_\mu N$ and $\nu_\tau N$ cross-sections on iron as a function of the neutrino energy for both neutrinos and anti-neutrinos are shown in Fig. B.1(right).

Notice that the adopted setup, similar to those proposed in the first Neutrino Factory studies (see, for example, Refs. [79, 94]), slightly differs from the setup that was suggested in the final ISS Physics Report. The latter consists in stored muons with energies in the range $E_\mu \in [20, 30]$ GeV, aiming to two detectors located at $L = 4000$ km and $L = 7500$ km from the source. The longest baseline corresponds to the so-called “magic baseline” [159], where three-family CP-violating effects vanish. We have chosen the same baseline for the far detector in our setup, although in the (3+1)-neutrino model not all of the CP-violating phases dependence decouple at this distance (as it can be seen from Eqs. (4.6,4.7) and in Sec. 4.2). The shortest baseline was optimized in the ISS Physics Report to look for CP-violating three-family signals, finding that a detector with a baseline of $L = 4000$ km performed slightly better than at $L = 3000$ km. This optimization, however, is no longer valid when looking for the (3+1)-neutrino model signals. We decided, therefore, to adopt the $L = 3000$ km baseline used in previous studies, for which possible sites have already been explored.¹ Eventually, we use a stored muon energy that is larger than the optimal value adopted in the ISS Physics Report. It is indeed well known from previous studies (see, for example, Ref. [229] for an optimization of the muon energy to look for NSI signals at the Neutrino Factory) that to look for new physics the higher the muon energy the better. An evident motivation for this is that the $\nu_\mu \rightarrow \nu_\tau$ channel is very important to look for new physics in neutrino oscillations, and high neutrino energies are required to circumvent the extremely low $\nu_\tau N$ cross-section in the tens of GeV energy range (see Fig. B.1, right).

To show that the 50 GeV Neutrino Factory setup proposed above is more suited to look for sterile neutrino signals, we have compared our results with an ISS-inspired Neutrino Factory, defined as follows: muons of both polarities are accelerated up to $E_\mu = 20$ GeV and injected into storage ring(s) with a geometry that allows to aim at two far detectors, the first located at 4000 km and the second at 7500 km from the source. The number of useful muon decays per year aimed at each detector has been fixed in this case to 5×10^{20} , following the final ISS Physics Report [99]. Four years of data taking for each muon polarity are envisaged. When studying the performance of the ISS-inspired 20 GeV setup, we consider the same detectors as in the case of the 50 GeV Neutrino Factory.

¹For example, the island of La Palma in the Canary Islands, the island of Longyearbyen in Norway or the Oulu mine in Pyhösalmi in Finland are possible options for the location of a detector at approximately 3000 km from the source for a CERN-based Neutrino Factory.

B.2.1 The MIND detector: $\nu_e \rightarrow \nu_\mu$ and $\nu_\mu \rightarrow \nu_\mu$

The baseline detector, a 50 kton magnetized iron calorimeter of the MINOS type, was originally optimized to reduce the background to the wrong-sign muon signal for $\nu_e \rightarrow \nu_\mu$ oscillations (represented dominantly by right-sign muons with a wrong charge assignment and charmed meson decays) to the 10^{-6} level. To achieve this extremely ambitious signal-to-background ratio, tight kinematical cuts were applied. Such cuts, although strongly reducing the background, have the disadvantage of an important suppression of the signal below 10 GeV, an energy region that, on the other hand, has been shown to be extremely important. A non-negligible signal below and above the first oscillation peak (that, for $L \sim 3000$ km, lies precisely in this energy range) is crucial to solve many of the parametric degeneracies [94, 96, 97, 214] that bother the three-family (θ_{13}, δ) -measurement. To reduce such problems, a modification of the original detector proposal called MIND (Magnetized Iron Neutrino Detector) was presented in Ref. [227].

Studies of the four-family $\nu_e \rightarrow \nu_\mu$ oscillation (still the best channel to measure θ_{13}) are not different from those performed in the framework of the three-family model. In particular, no new sources of background are expected. Quite the contrary, those backgrounds induced by wrongly reconstructed $\bar{\nu}_\mu$ are expected to decrease for large values of θ_{34} , due to the increased oscillation into sterile neutrinos, see Eq. (4.8). When looking at $\nu_e \rightarrow \nu_\mu$ oscillations, we will therefore take advantage of the wrong-sign muon identification efficiency presented in the ISS Detector Report [158]: $\epsilon_{e\mu} = 0.7$ above 10 GeV, with the efficiency increasing linearly from $\epsilon_{e\mu} = 0.1$ at 1 GeV.

The MIND detector can also be used to look for $\nu_\mu \rightarrow \nu_\mu$ disappearance (one of the channels of interest to study sterile neutrino models), providing a very good measurement of the atmospheric parameters θ_{23} and Δm_{atm}^2 and giving some handle to solve the ‘‘octant degeneracy’’ (see, e.g., Ref. [213, 230]). For the right-sign muon sample there is no need to accurately tell the charge of the muon, since the background induced by misidentified wrong-signs muons is negligible with respect to the signal, [231]. We can safely use for this signal the muon identification efficiency of the MINOS experiment [232]: $\epsilon_{\mu\mu} = 0.9$ above 1 GeV. Notice that at the MIND detector it is not possible to single out τ 's decaying to muons. We cannot thus use MIND to study the leading $\nu_\mu \rightarrow \nu_\tau$ oscillation and the ‘‘silver’’ $\nu_e \rightarrow \nu_\tau$ channel.

We have considered as background for the ν_μ disappearance channel 10^{-5} of all neutral current events, *all* wrong-sign muon events and the right-sign muons coming from $\nu_\mu \rightarrow \nu_\tau$ oscillation with τ decaying into muons. The inclusion of this background has no effect on our results for this channel, that are remarkably systematic-dominated.

Different treatments of the energy response of the detector can be found. For example, in Ref. [79] a constant energy resolution $\Delta E_\nu = 0.2E_\mu$ was considered, by grouping events in five bins of energy width $\Delta E_\nu = 10$ GeV. On the other hand, in Ref. [233] a finer binning was adopted, with a more refined treatment of the energy resolution: 43 bins of variable ΔE_ν were considered in the energy range $E_\nu \in [1\text{GeV}, E_\mu]$, folding the

event distribution with a Gaussian resolution kernel of variable width, $\sigma_E = 0.15 \times E_\nu$. In this paper we have followed the first approach, grouping events into 10 constant energy resolution bins with $\Delta E_\nu = 0.1 E_\mu$, leaving possible improvements of the detector simulation following Ref. [233] (if needed) for future works.

Throughout our numerical simulations we have assumed 2% and 5% for the bin-to-bin uncorrelated systematic errors on the golden channel and on the ν_μ disappearance signal. We have also assumed 1% and 5% for normalization and energy spectrum distortion as the correlated systematic errors for all the channels.² The dependence of the sensitivities on the systematic errors will be discussed in section B.4.

Notice that a different proposal for a magnetized iron calorimeter that can be used for a Neutrino Factory experiment has been advanced in Ref. [234].

B.2.2 The MECC detector: $\nu_e \rightarrow \nu_\tau$ and $\nu_\mu \rightarrow \nu_\tau$

Two technologies were considered in the literature to study neutrino oscillations into τ 's: Liquid Argon detectors [230, 235] and Emulsion Cloud Chamber techniques. In both cases, the $\nu_e, \nu_\mu \rightarrow \nu_\tau$ signal can be tagged looking for right-sign muons in coincidence with a τ decay vertex, to distinguish them from ν_μ disappearance muons. Therefore, a detector with muon charge identification and vertex reconstruction is needed.

A dedicated analysis to use an ECC modeled after OPERA at the Neutrino Factory to look for the ‘‘silver channel’’ $\nu_e \rightarrow \nu_\tau$ [142] has been published in Ref. [149]. In that reference, a 5 kton ECC was considered, with a detailed study of the main sources of background.

The result of that analysis was that τ 's can be identified with a very low background, at the price of a very low efficiency, $O(5\%)$. One of the main motivation of such low efficiency was that only the $\tau \rightarrow \mu$ decay channel was used, i.e. only 17% of the total amount of produced τ 's. In the OPERA detector used at the CNGS and in the analysis of Ref. [149], the τ charge identification is achieved using two large spectrometers located at the end of two thick active sections, with bricks made of repeated layers of lead (acting as the target for $\nu_\tau N$ interactions) and emulsions. In the Magnetized ECC (MECC) proposal [158] the lead plates are replaced by iron plates, again interleaved with emulsions layers. The ECC can be, thus, directly magnetized through the iron plates. Emulsion spectrometers (currently in their test phase, [236]) are located at the end of the ECC section. Eventually, the MECC is placed in front of the MIND detector, to form the so-called Hybrid-MIND setup. The efficiency of this detector to τ 's is much higher than in the case of the standard ECC, since τ decay into electrons

²In principle, some of the correlated systematic errors could be common among the different channels (such as the detector volume uncertainty) or different baselines (such as the cross section uncertainty), but for simplicity we assume here that all the correlated systematic errors are independent among the different channels or different baselines. The results presented in Chap. 4 may be, therefore, somewhat conservative.

and into hadrons can be used in addition to $\tau \rightarrow \mu$ decays. The expected efficiency is, thus, approximately five times larger than in the case of the ECC (see, for example, Refs. [158, 237] and refs. therein).

The MECC bricks are bigger than the corresponding ECC ones, due to the replacement of the lead target with iron. The huge volume to be magnetized put, thus, a tight limit on the maximum foreseeable detector mass.

We will therefore consider throughout the paper a 4 kton MECC [238] located in front of the 50 kton MIND, and use this detector to study both the silver channel $\nu_e \rightarrow \nu_\tau$ and the novel “discovery channel” $\nu_\mu \rightarrow \nu_\tau$.

For the silver channel signal, we will use an energy dependent efficiency $\epsilon_{e\tau}$ taken from Ref. [149], multiplying it by a factor five to take into account that all τ 's decay channel can be used at the MECC. A detailed study of the efficiency to the $\nu_\mu \rightarrow \nu_\tau$ channel at the MECC, on the other hand, is lacking. We will therefore assume a constant efficiency $\epsilon_{\mu\tau} = 0.65$ above 5 GeV, increasing by a factor five the efficiency considered in Ref. [190]. This assumption must be checked in further studies of the MECC-type detectors exposed to a Neutrino Factory beam.

The backgrounds for the silver and the discovery channels should be also correspondingly increased at the MECC with respect to the ECC ones. At the ECC, the expected signal-to-background ratio (after some kinematical cuts) for $\nu_\mu \rightarrow \nu_\tau$ (using the $\tau \rightarrow \mu$ decay channel, only) is 50:1 or larger [190], the dominant source of background for the process $\nu_\mu \rightarrow \nu_\tau \rightarrow \tau^- \rightarrow \mu^-$ being represented by non-oscillated muons that produce charmed mesons eventually decaying into μ^- either through NC or CC in which the muon is not observed. No detailed study of the expected background for the $\nu_e \rightarrow \nu_\tau$ or the $\nu_\mu \rightarrow \nu_\tau$ signals at the MECC exposed to a Neutrino Factory beam has been performed yet, though. We have thus decided to make the assumption that, using MECC, all τ decay channels should be affected by similar backgrounds. We have therefore consistently multiplied the backgrounds for $\nu_e \rightarrow \nu_\tau$ and $\nu_\mu \rightarrow \nu_\tau$ computed in Refs. [149, 190] by a factor five. This is possibly a conservative assumption³, since the MECC is expected to have a signal-to-background ratio for this signal slightly better than the ECC [239]. We consider, however, this to be the only reasonable choice that we can take at this preliminary stage of four-family neutrino detailed study at the Neutrino Factory (not to be compared with the order-of-magnitude estimations made in previous works).

Also in this case, we have grouped events into 10 bins with $\Delta E_\nu = 5$ GeV constant energy resolution. We have assumed 10% for the bin-to-bin uncorrelated systematic errors, 1% and 5% for normalization and energy spectrum distortion as the correlated systematic errors throughout the numerical simulations for both the $\nu_e \rightarrow \nu_\tau$ and the

³Notice that, for the silver channel, at least the background induced by right-sign τ 's with wrong charge assignment should be depleted in a four-family neutrino scenario with respect to the standard three-family one. This particular background is strongly affected by active-sterile mixing angles, since, in the allowed region of the parameter space, $\nu_\mu \rightarrow \nu_\tau$ oscillations are significantly depleted with respect to the standard three-neutrino ones.

$(\theta_{13}; \theta_{14}; \theta_{24}; \theta_{34})$	$N_{\tau^-}^{CNGS}$	$N_{\tau^-}^{3000}$	$N_{\tau^+}^{3000}$	$N_{\tau^-}^{7500}$	$N_{\tau^+}^{7500}$
$(5^\circ; 5^\circ; 5^\circ; 20^\circ)$	8.9	559	10	544	2
$(5^\circ; 10^\circ; 5^\circ; 20^\circ)$		557	29	544	5
$(5^\circ; 5^\circ; 10^\circ; 20^\circ)$	8.3	474	11	529	2
$(5^\circ; 5^\circ; 10^\circ; 30^\circ)$	10.5	384	18	454	3
$(5^\circ; 10^\circ; 5^\circ; 30^\circ)$		424	59	441	11
$(5^\circ; 5^\circ; 10^\circ; 30^\circ)$	10.5	384	18	454	3
$(10^\circ; 5^\circ; 5^\circ; 20^\circ)$	8.5	522	22	512	2
$(10^\circ; 10^\circ; 5^\circ; 20^\circ)$		517	42	510	6
$(10^\circ; 5^\circ; 10^\circ; 20^\circ)$	7.9	443	22	498	2
$(10^\circ; 5^\circ; 5^\circ; 30^\circ)$	6.5	397	30	413	4
$(10^\circ; 10^\circ; 5^\circ; 30^\circ)$		389	74	412	11
$(10^\circ; 5^\circ; 10^\circ; 30^\circ)$	10.3	361	30	428	4
3 families, $\theta_{13} = 5^\circ$	15.1	797	3	666	0
3 families, $\theta_{13} = 10^\circ$	14.4	755	12	632	1

Table B.1: Event rates for the $\nu_\mu \rightarrow \nu_\tau$ and $\bar{\nu}_e \rightarrow \bar{\nu}_\tau$ channels for 1 kton MECC detector, exposed to a 2×10^{20} ($\nu_\mu, \bar{\nu}_e$) flux for one year, for different values of θ_{14}, θ_{24} and θ_{34} in the (3+1) scheme. The other unknown angle, θ_{13} has been fixed to: $\theta_{13} = 5^\circ, 10^\circ$. The CP-violating phases are: $\delta_1 = \delta_2 = 0; \delta_3 = 90^\circ$. As a reference, rates at the 1.8 kton OPERA detector (exposed to the nominal CNGS beam intensity) and the expected event rates for 1 kton MECC detector in the case of the three-family model (i.e., for $\theta_{i4} = 0$ and maximal CP-violating phase δ) are also shown. In all cases, perfect efficiency is assumed.

$\nu_\mu \rightarrow \nu_\tau$ signals. Once again, the results in Chap. 4 may be slightly conservative because we may be overcounting the systematic errors.

In Tab. B.1 we show the expected number of τ^- from $\nu_\mu \rightarrow \nu_\tau$ and τ^+ from $\bar{\nu}_e \rightarrow \bar{\nu}_\tau$ for a 1 kton MECC detector with perfect efficiency, exposed to a 2×10^{20} ($\nu_\mu, \bar{\nu}_e$) flux for one year, for different values of $\theta_{13}, \theta_{14}, \theta_{24}$ and θ_{34} . The other parameters are: $\theta_{12} = 34^\circ; \theta_{23} = 45^\circ; \Delta m_{\text{sol}}^2 = 7.9 \times 10^{-5} \text{ eV}^2; \Delta m_{\text{atm}}^2 = 2.4 \times 10^{-3} \text{ eV}^2$ and $\Delta m_{\text{SBL}}^2 = 1 \text{ eV}^2$ (all mass differences are taken to be positive). Eventually, phases have been fixed to: $\delta_1 = \delta_2 = 0; \delta_3 = 90^\circ$. For comparison, the rates at the CNGS (for the nominal CNGS flux, of 4.5×10^{19} pot/year, an active lead target mass of 1.8 kton and 5 years of data taking) and the expected number of events in the three-family model for a 1 kton MECC detector with perfect efficiency are also shown. We can see that the number of expected τ^- events at the 1 kton MECC is $O(500)$ at both baselines, with some dependence on the different mixing angles. The fact that at both baselines we expect a similar number of events is a consequence of the convolution of the $\nu_\mu \rightarrow \nu_\tau$ oscillation probability with the $\nu_\tau N$ cross-section and the ν_μ neutrino flux: at the shortest baseline, the probability is maximal below 10 GeV; at the longest baseline, the maximum is located in the 30 GeV bin. The higher cross-section for this energy bin compensates for the decrease in the ν_μ neutrino flux, thus giving a similar number of τ 's in the detector.

B.3 Simulation details

B.3.1 Section 4.2.1

The sensitivity is defined as follows: we first compute the expected number of events for $\nu_e \rightarrow \nu_\mu$ and $\nu_e \rightarrow \nu_\tau$ oscillations for the input values $\theta_{13}^{(4\text{fam})} = 0$, and $\theta_{14} = \theta_{24} = \theta_{34} = 0$, where $\theta_{jk}^{(4\text{fam})}$ ($(j, k) = (1, 2), (1, 3), (2, 3)$) and $\theta_{j4} \equiv \theta_{j4}^{(4\text{fam})}$ stand for the mixing angles in the four-family scheme denoted by (4fam).⁴ This number, that is identical in the three- and four-family models, is labeled as N^0 . We then compute the expected number of events in the $(\theta_{13}^{(4\text{fam})}, \theta_{14})$ -plane for the same oscillation channels in the four-family model. The $\Delta\chi^2$, computed with respect to the ‘‘true’’ value N^0 , is eventually evaluated. The contour for which the 2 d.o.f.’s $\Delta\chi^2$ is $\Delta\chi^2 = 4.61$ defines, then, the region of the parameter space of the (3+1)-sterile neutrino model that is non-compatible at 90% CL with the input data corresponding to vanishing $(\theta_{13}^{(4\text{fam})}, \theta_{14})$ (to the right of the contour line) and the region that it is still allowed (to the left of the line) at this CL.

The minimum of the χ^2 is computed as follows:

$$\Delta\chi^2 = \min_{\text{marg par}} \left[\sum_{\text{pol.}, (\text{chan.}), (L)} \min_{\alpha's, \beta's} \left\{ \sum_j \frac{1}{\sigma_j^2} ((1 + \alpha_s + x_j \beta_s) N_j(4\text{fam}) + (1 + \alpha_b + x_j \beta_b) B_j(4\text{fam}) - N_j^0 - B_j^0)^2 + \left(\frac{\alpha_s}{\sigma_{\alpha_s}} \right)^2 + \left(\frac{\alpha_b}{\sigma_{\alpha_b}} \right)^2 + \left(\frac{\beta_s}{\sigma_{\beta_s}} \right)^2 + \left(\frac{\beta_b}{\sigma_{\beta_b}} \right)^2 \right\} + \Delta\chi_{\text{atm+re}}^2(4\text{fam}) \right], \quad (\text{B.5})$$

where we have introduced the prior that comes from the four-family analysis of the atmospheric and reactor data:⁵

$$\Delta\chi_{\text{atm+re}}^2(4\text{fam}) = \frac{(s_{23}^{2(4\text{fam})} - 0.50)^2}{\sigma^2(s_{23}^2)} + \frac{(|\Delta m_{31}^{2(4\text{fam})}| - 2.4 \times 10^{-3} \text{eV}^2)^2}{\sigma^2(|\Delta m_{32}^{2(4\text{fam})}|)} + \frac{(s_{13}^{2(4\text{fam})} - 0.01)^2}{\sigma^2(s_{13}^2)} + \frac{(s_{14}^2)^2}{\sigma^2(s_{14}^2)} + \frac{(s_{24}^2)^2}{\sigma^2(s_{24}^2)} + \frac{(s_{34}^2)^2}{\sigma^2(s_{34}^2)}. \quad (\text{B.6})$$

where $|\Delta m_{31}^{2(4\text{fam})}|$ stands for the atmospheric mass squared difference in the four-family scheme, and the errors of the oscillation parameters in the four-flavour scheme in Eq.

⁴Using the four-family expressions for the oscillation probabilities in vacuum shown in Ref. [190], it can be seen that, for vanishing θ_{14} and θ_{24} , the four-family mixing angle $\theta_{13}^{(4\text{fam})}$ maps into the three-family one, $\theta_{13}^{(3\text{fam})}$. On the other hand, for non-vanishing θ_{14} , the four-family parameter is expected to be slightly smaller than the three-family one.

⁵Since $\Delta\chi^2$ depend little on the solar neutrino oscillation parameters, we will not vary the solar oscillation parameters throughout this work, so we omit the terms on the solar parameters here.

(B.6) are deduced from Refs. [61] and [190] as follows:

$$\begin{aligned}\sigma(s_{23}^2) &= 0.07, & \sigma(|\Delta m_{31}^2|) &= 0.12 \times 10^{-3} \text{eV}^2, & \sigma(s_{13}^2) &= 0.016, \\ \sigma(s_{14}^2) &= 0.013, & \sigma(s_{24}^2) &= 0.02, & \sigma(s_{34}^2) &= 0.12.\end{aligned}\tag{B.7}$$

In the minimization procedure in Eq. (B.5), “marg par” stands for the oscillation parameters to be marginalized over (that can be different for different plots), and α_s , α_b , β_s and β_b are the variables for the correlated systematic errors, which stand for the uncertainties in the overall normalization and in the linear distortion in the spectral shape in the magnitude of signal (s) or background (b) [240], where we have defined $x_j \equiv E_j/(E_{\max} - E_{\min})$ for neutrino energy E_j for the j -th bin. Following Ref. [240], we assume the correlated systematic errors $\sigma_{\alpha_s} = \sigma_{\alpha_b} = 0.01$ for the normalization and $\sigma_{\beta_s} = \sigma_{\beta_b} = 0.05$ for the spectrum distortion. In the analysis of the case with single baseline length, we have minimized the χ^2 for each baseline separately, i.e., no sum is performed over L , and in the analysis combining the two baselines, we have minimized the sum of χ^2 for each baseline. Similarly, in the analysis of a single channel, no sum is performed over the channels (“chan.”), while in the analysis combining the different channels we have summed over the different channels, i.e., golden and silver in this Section. In all cases we sum up χ^2 for the two possible stored muon polarities (“pol.”). The index j runs over 10 energy bins. B_j is the background correspondent to the j -th bin (B_j^0 stands for the expected background in the four-family model for vanishing $\theta_{13}^{(4\text{fam})}$ and θ_{14} in the j -th bin). Within this procedure, for any minimization that we perform the best-fit for the variables on which we marginalize over can be different. However, when we project onto the two-dimensional $(\theta_{13}^{(4\text{fam})}, \theta_{14})$ -plane (or onto the $(\theta_{24}, \theta_{34})$ -plane in Sec. 4.2.3) this information is lost.

The variance is defined as:

$$\sigma_j^2 = N_j^0 + B_j^0 + [f_j N_j^0]^2 + [f_j B_j^0]^2,\tag{B.8}$$

where f_j is the uncorrelated bin-to-bin systematic error in the j -th bin: 2% for the golden channel and 10% for the silver channel, irrespectively of the energy bin, of the baseline and of the stored muon polarity. Notice that we can use the Gaussian expression for the χ^2 throughout our numerical simulation, with the possible exception of the silver channel data at the longest baseline, for which a Poissonian expression could be more appropriate due to the extremely low statistics (as it can be seen from Tab. B.1). However, as it is shown in the discussion on the results of Sec. 4.2.1, the impact of the silver channel at that baseline is negligible.

B.3.2 Section 4.2.2

The sensitivity is defined as in the previous section with straightforward replacements.

B.3.3 Section 4.2.3

The sensitivity is defined again as in B.3.1: we first compute the expected number of events for $\nu_\mu \rightarrow \nu_\mu$ and $\nu_\mu \rightarrow \nu_\tau$ oscillations for the input values $\theta_{13}^{(4\text{fam})} = 0$ and $\theta_{14} = \theta_{24} = \theta_{34} = 0$, N^0 ; we then compute the expected number of events in the $(\theta_{24}, \theta_{34})$ -plane for the same oscillation channels in the four-family model. The $\Delta\chi^2$, computed as in Eq. (B.5) with respect to the “true” value N^0 , is eventually evaluated.

Contrary to the case of the golden and silver channels, however, the number of expected background events is much smaller than the signal for both the disappearance and discovery channels. The effect of α_b and β_b is, thus, negligible. Hence, we will not perform minimization with respect to α_b and β_b for these channels and put these parameters to zero in this case. As in the case of the golden and silver channels, the variance is defined by Eq. (B.8), where N_j^0 in this case are the number of events of the disappearance or discovery channels, and the uncorrelated bin-to-bin systematic error f_j is 5% for the ν_μ disappearance channel and 10% for the discovery channel, irrespectively of the energy bin, of the baseline and of the stored muon polarity.

B.3.4 Section 4.2.4

The contours in the (θ_{34}, δ_3) -plane have been obtained as follows: we have first computed the expected number of events for $\nu_\mu \rightarrow \nu_\mu$ and $\nu_\mu \rightarrow \nu_\tau$ oscillations in the four-family model for particular choices of the relevant parameters, $\theta_{24} = \bar{\theta}_{24}$, $\theta_{34} = \bar{\theta}_{34}$ and $\delta_3 = \bar{\delta}_3$. We have then computed the expected number of events in the (θ_{34}, δ_3) -plane for the same oscillation channels in the four-family model, varying $\theta_{34} \in [0, 35^\circ]$ and $\delta_3 \in [0, 360^\circ]$. The $\Delta\chi^2$ is then computed as follows:

$$\Delta\chi^2 = \left(\sum_j [N_j(\bar{\theta}_{24}, \theta_{34}, \delta_3) - N_j(\bar{\theta}_{24}, \bar{\theta}_{34}, \bar{\delta}_3)]^2 / \sigma_j^2 \right) \quad (\text{B.9})$$

where the minimum of the χ^2 is, trivially, obtained for $\theta_{34} = \bar{\theta}_{34}$; $\delta_3 = \bar{\delta}_3$. Again, j runs over the different signals: the ν_μ disappearance and the $\nu_\mu \rightarrow \nu_\tau$ discovery channels data, divided into 10 energy bins, for the two baselines and the two possible stored muons polarities. The variance σ_j is defined by Eq. (B.8), with $f_j = 5\%$ for the ν_μ disappearance channel and 10% for the $\nu_\mu \rightarrow \nu_\tau$ discovery channel. No correlated systematic errors have been considered in the plots of this section. The region in the (θ_{34}, δ_3) -plane compatible with the input values $(\bar{\theta}_{34}, \bar{\delta}_3)$ at the 2 d.o.f.’s 99% CL is eventually defined by drawing the contour line corresponding to $\Delta\chi^2 = 9.21$.

The contours in the $(\theta_{13}^{(4\text{fam})}, \delta_2)$ -plane have been obtained as follows: we have first computed the expected number of events for $\nu_e \rightarrow \nu_\mu$ and $\nu_e \rightarrow \nu_\tau$ oscillations in the four-family model for particular choices of the relevant parameters, $\theta_{13}^{(4\text{fam})} = \bar{\theta}_{13}^{(4\text{fam})}$ and $\delta_2 = \bar{\delta}_2$. We have then computed the expected number of events in the $(\theta_{13}^{(4\text{fam})}, \delta_2)$ -plane for the same oscillation channels in the four-family model, varying $\theta_{13}^{(4\text{fam})} \in [0, 10^\circ]$ and

$\delta_2 \in [0, 360^\circ]$. The $\Delta\chi^2$ is then computed as follows:

$$\Delta\chi^2 = \left(\sum_j \left[N_j(\theta_{13}^{(4\text{fam})}, \delta_2) - N_j(\bar{\theta}_{13}^{(4\text{fam})}, \bar{\delta}_2) \right]^2 / \sigma_j^2 \right) \quad (\text{B.10})$$

where the minimum of the χ^2 is, trivially, obtained for $\theta_{13}^{(4\text{fam})} = \bar{\theta}_{13}^{(4\text{fam})}$; $\delta_2 = \bar{\delta}_2$. As before, j runs over the different signals: the $\nu_e \rightarrow \nu_\mu$ and the $\nu_e \rightarrow \nu_\tau$ data, divided into 10 energy bins, for the two baselines and the two possible stored muons polarities. The variance σ_j is defined by Eq. (B.8), with $f_j = 2\%$ for the golden channel and 10% for the silver channel. No correlated systematic errors have been considered in the plots of this section. The region in the $(\theta_{13}^{(4\text{fam})}, \delta_2)$ -plane compatible with the input values $(\bar{\theta}_{13}^{(4\text{fam})}, \bar{\delta}_2)$ at the 2 d.o.f.'s 99% CL is eventually defined by drawing the contour line corresponding to $\Delta\chi^2 = 9.21$.

B.4 Dependence of sensitivity on the systematic errors

In this section of the appendix we have investigated the dependence of the performance of the four channels on the systematic errors.

As for the golden and silver channels, for which statistical errors are dominant, we have found from numerical calculations that the sensitivities of these two channels to $\theta_{13}^{(4\text{fam})}$ and θ_{14} depend only to some extent on σ_α (the correlated systematic error on the overall normalization), and they depend very little on f_j (the bin-to-bin uncorrelated error) and σ_β (the correlated systematic error in the linear distortion of the spectral shape).

The dependence of the discovery and disappearance channels on f_j , σ_α and σ_β (and on the MECC volume, in the case of the former) is shown in Fig. B.2. The upper panels present the discovery channel $(\theta_{24}, \theta_{34})$ -sensitivity, where we consider $f_j \equiv f_{\mu\tau} = 0.10, 0.03$, $\sigma_\alpha = 0.100, 0.050, 0.025, 0.010$, and the MECC mass either 4 or 8 kton. The lower panels present the disappearance channel $(\theta_{24}, \theta_{34})$ -sensitivity, assuming $f_j \equiv f_{\mu\mu} = 0.05, 0.02$ and $\sigma_\alpha = 0.100, 0.050, 0.025, 0.010$. We have checked numerically that the impact of the systematic error σ_β in the linear distortion of the spectral shape is small and it will not be discussed here. For both channels we have considered the 50 GeV setup performance (left panels) and the 20 GeV setup one (right panels). From Fig. B.2(upper panels), we see that $f_{\mu\tau}$ is the most important factor to improve the performance of the discovery channel for both the 50 GeV and 20 GeV neutrino factories. On the other hand, an increase of the MECC mass from 4 to 8 kton improves only marginally the discovery channel sensitivity. In Fig. B.2(lower panels), we see that a reduction of both $f_{\mu\mu}$ and σ_α should be pursued to increase the disappearance channel sensitivity. One important conclusion from Fig. B.2 is that an improvement of $f_{\mu\tau}$ below 10% is mandatory in order to take full advantage of the

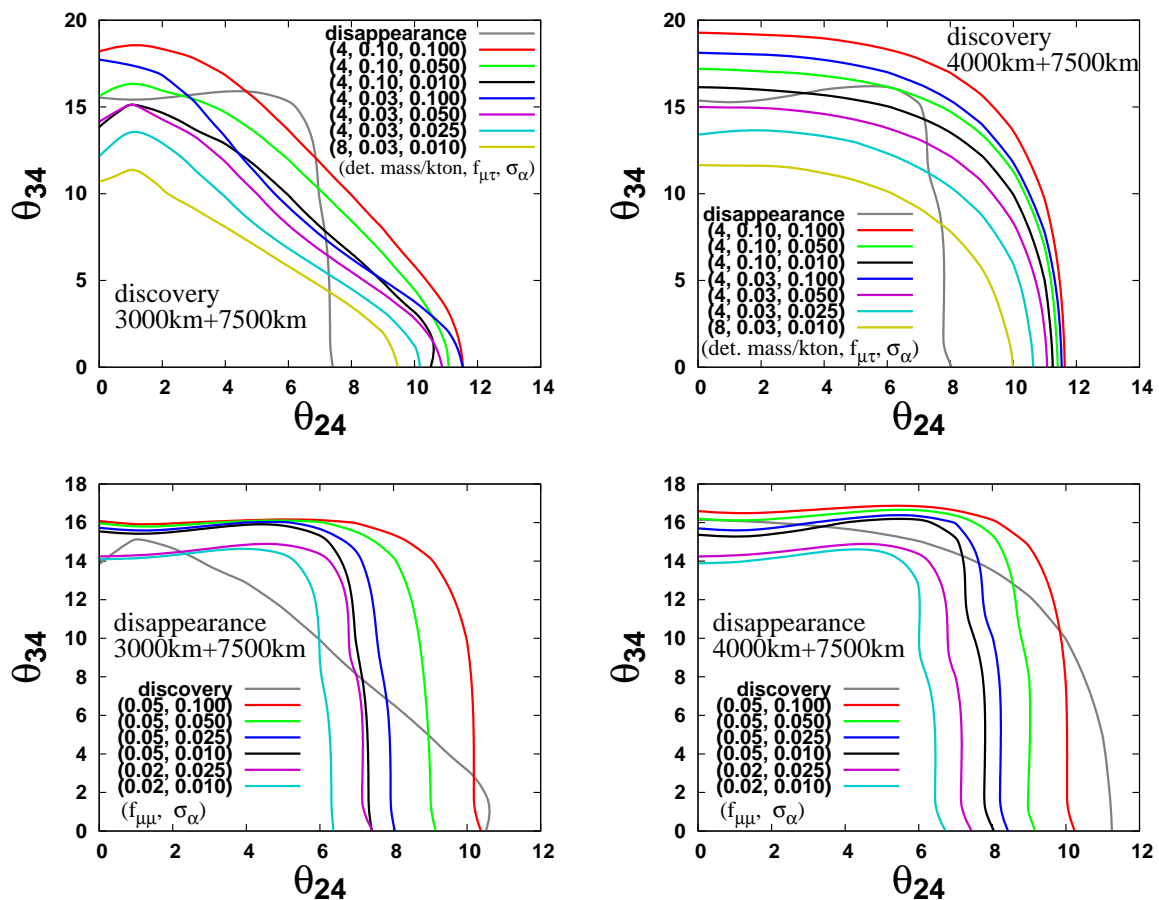


Figure B.2: The 90%CL sensitivity to $(\theta_{24}, \theta_{34})$ using the $\nu_\mu \rightarrow \nu_\tau$ (the upper panels) and $\nu_\mu \rightarrow \nu_\mu$ (the lower panels) channels for different values of the uncorrelated bin-to-bin systematic error $f_j \equiv f_{\mu\tau} = 0.1, 0.03$ and $f_j \equiv f_{\mu\mu} = 0.05, 0.02$, of the correlated systematic error on the overall normalization $\sigma_{\alpha_s} = 0.1, 0.05, 0.025, 0.01$ and of the MECC mass ($= 4, 8$ kton in the case of $\nu_\mu \rightarrow \nu_\tau$). Left panels: at the 50 GeV setup; Right panels: at the 20 GeV ISS-inspired setup. In all the figures black lines stand for the excluded region for the reference values used in the calculations in other sections. The grey lines stand for the excluded region using the disappearance (discovery) channel with $f_{\mu\mu} = 0.05$, $\sigma_{\alpha_s} = 0.01$ (with 4 kton, $f_{\mu\tau} = 0.1$, $\sigma_{\alpha_s} = 0.01$).

discovery channel at the Neutrino Factory, particularly for the 20 GeV setup. This error represents indeed our incomplete knowledge of the MECC detector. To improve our analysis on the discovery channel in the future, we need detailed information on the correlated and uncorrelated systematic errors, such as the uncertainties of the detection efficiency which depend only on the nature of MECC or depend on the characteristics of the individual detectors located at each of the two baselines. Although there has been no study on these systematic errors so far, they are expected to be better understood after the first years of data taking of the OPERA experiment (that started operation

in 2008).

B.5 Oscillation probabilities by the KTY formalism

To derive the expressions for the oscillation probabilities in matter, we use again the KTY formalism⁶. The evolution equation of flavour eigenstates⁷ is:

$$i \frac{d}{dt} |\nu_\alpha\rangle = \mathcal{H}_{\alpha\beta} |\nu_\beta\rangle \equiv [U\mathcal{E}U^\dagger + \mathcal{A}]_{\alpha\beta} |\nu_\beta\rangle,$$

where

$$\begin{aligned} \mathcal{E} &= \text{diag}\left(0, \frac{\Delta m_{21}^2}{2E}, \frac{\Delta m_{31}^2}{2E}, \frac{\Delta m_{41}^2}{2E}\right) \equiv \text{diag}(0, \Delta_{21}, \Delta_{31}, \Delta_{41}), \\ \mathcal{A} &= \sqrt{2} G_F \text{diag}(n_e, 0, 0, n_n/2) \equiv \text{diag}(A_e, 0, 0, A_n), \end{aligned} \quad (\text{B.11})$$

$\Delta_{ij} = \Delta m_{ij}^2/2E$, and n_e and n_n are respectively the electron and neutron densities. In Eq. (B.11), we have subtracted from \mathcal{H} the term $E_1 \mathbf{1} = \sqrt{E^2 + m_1^2} \mathbf{1}$, which contributes only to the phase of the oscillation amplitude and therefore does not affect the probability. In the KTY formalism, the oscillation probabilities in matter assume the following form:

$$P_{\alpha\beta} = \delta_{\alpha\beta} - 4 \sum_{i<j} \text{Re}(\tilde{X}_i^{\alpha\beta} \tilde{X}_j^{\alpha\beta*}) \sin^2\left(\frac{\Delta \tilde{E}_{ij} L}{2}\right) + 2 \sum_{i<j} \text{Im}(\tilde{X}_i^{\alpha\beta} \tilde{X}_j^{\alpha\beta*}) \sin(\Delta \tilde{E}_{ij} L), \quad (\text{B.12})$$

where $\Delta \tilde{E}_{ji} \equiv \tilde{E}_j - \tilde{E}_i$ and $\tilde{X}_j^{\alpha\beta} \equiv \tilde{U}_{\alpha j} \tilde{U}_{\beta j}^*$ ($j = 1, 2, 3, 4$). \tilde{E}_i and $\tilde{U}_{\alpha i}$ are the \mathcal{H} eigenvalues and the effective mixing matrix in matter, respectively, defined through

$$\mathcal{H} = \tilde{U} \text{diag}(\tilde{E}_j) \tilde{U}^\dagger.$$

The $\tilde{X}_j^{\alpha\beta}$ matrices can be expressed as follows:

$$\tilde{X}_j^{\alpha\beta} \equiv \sum_l (V^{-1})_{jl} [\mathcal{H}^{l-1}]_{\alpha\beta} = \sum_l (V^{-1})_{jl} [(U\mathcal{E}U^\dagger + \mathcal{A})^{l-1}]_{\alpha\beta}, \quad (\text{B.13})$$

where V is the Vandermonde matrix:

$$V = \begin{pmatrix} 1 & 1 & 1 & 1 \\ \tilde{E}_1 & \tilde{E}_2 & \tilde{E}_3 & \tilde{E}_4 \\ \tilde{E}_1^2 & \tilde{E}_2^2 & \tilde{E}_3^2 & \tilde{E}_4^2 \\ \tilde{E}_1^3 & \tilde{E}_2^3 & \tilde{E}_3^3 & \tilde{E}_4^3 \end{pmatrix},$$

⁶The KTY formalism was extended to four neutrino schemes in Ref. [241].

⁷Greek (Latin) indices label the flavour (mass) basis: $\alpha = e, \mu, \tau, s$ ($i = 1, 2, 3, 4$).

whose determinant is $\prod_{i<j} \Delta \tilde{E}_{ji}$. The inverse of V can then be easily obtained as long as we know the eigenvalues \tilde{E}_j of the effective Hamiltonian in matter \mathcal{H} , expressed in terms of A_e , A_n and the vacuum parameters:

$$V^{-1} = \begin{pmatrix} \frac{1}{\Delta \tilde{E}_{21} \Delta \tilde{E}_{31} \Delta \tilde{E}_{41}} (\tilde{E}_2 \tilde{E}_3 \tilde{E}_4, & -(\tilde{E}_2 \tilde{E}_3 + \tilde{E}_3 \tilde{E}_4 + \tilde{E}_4 \tilde{E}_2), & \tilde{E}_2 + \tilde{E}_3 + \tilde{E}_4, & -1) \\ \frac{-1}{\Delta \tilde{E}_{21} \Delta \tilde{E}_{32} \Delta \tilde{E}_{42}} (\tilde{E}_3 \tilde{E}_4 \tilde{E}_1, & -(\tilde{E}_3 \tilde{E}_4 + \tilde{E}_4 \tilde{E}_1 + \tilde{E}_1 \tilde{E}_3), & \tilde{E}_3 + \tilde{E}_4 + \tilde{E}_1, & -1) \\ \frac{1}{\Delta \tilde{E}_{31} \Delta \tilde{E}_{32} \Delta \tilde{E}_{43}} (\tilde{E}_4 \tilde{E}_1 \tilde{E}_2, & -(\tilde{E}_4 \tilde{E}_1 + \tilde{E}_1 \tilde{E}_2 + \tilde{E}_2 \tilde{E}_4), & \tilde{E}_4 + \tilde{E}_1 + \tilde{E}_2, & -1) \\ \frac{-1}{\Delta \tilde{E}_{41} \Delta \tilde{E}_{42} \Delta \tilde{E}_{43}} (\tilde{E}_1 \tilde{E}_2 \tilde{E}_3, & -(\tilde{E}_1 \tilde{E}_2 + \tilde{E}_2 \tilde{E}_3 + \tilde{E}_3 \tilde{E}_1), & \tilde{E}_1 + \tilde{E}_2 + \tilde{E}_3, & -1) \end{pmatrix}. \quad (\text{B.14})$$

Within the KTY formalism, thus, we only need to compute the eigenvalues of \mathcal{H} to derive the oscillation probabilities in matter.

A possible drawback of this approach is that the physical understanding of the oscillation probabilities (i.e. the dependence on the vacuum mixing matrix parameters) is encoded in the explicit expressions for the \tilde{X} coefficients. To make contact with the parameters to be measured in a manageable way, we thus need to introduce some approximations in the computation of the eigenvalues \tilde{E}_i and of the corresponding matrices $\tilde{X}_i^{\alpha\beta}$. Now, considering the present constraints from Ref. [190] in the standard and sterile small parameters, we see that θ_{13}, θ_{14} and θ_{24} cannot be much larger than 10° while the third active-sterile mixing angle, θ_{34} , can be as large as $\theta_{34} \sim 35^\circ$. Notice also that the present constraint on the θ_{23} deviation from the maximal mixing, $\delta\theta_{23} \equiv \theta_{23} - \pi/4$, is of the same order as those on θ_{13}, θ_{14} and θ_{24} . On the other hand, the solar and atmospheric mass differences, $\Delta m_{\text{sol}}^2, \Delta m_{\text{atm}}^2$, are much smaller than Δm_{SBL}^2 . In what follows, therefore, we expand all the quantities in power of a small parameter ϵ , and keep terms of cubic order in ϵ , where the small parameter is defined by

$$\begin{aligned} \epsilon &\equiv \theta_{34} \sim \sqrt{\theta_{13}} \sim \sqrt{\theta_{14}} \sim \sqrt{\theta_{24}} \sim \sqrt{\delta\theta_{23}} \lesssim 4 \times 10^{-1}, \\ \eta_2 &\equiv \Delta m_{21}^2 / \Delta m_{41}^2 \lesssim 10^{-4}, \\ \eta_3 &\equiv \Delta m_{31}^2 / \Delta m_{41}^2 \lesssim 10^{-3}, \\ \eta_{e(n)} &\equiv A_{e(n)} / \Delta E_{41} \lesssim 10^{-3}. \end{aligned}$$

Notice that, to third order in ϵ , in the expansion in the probabilities we have neglected all terms proportional to $\eta_{e,n,2,3}$. Although this can be a rather rough approximation, as we have seen in Chap. 4, it is very useful in order to understand the different physics potential of the various oscillation channels. Thus we have the following probabilities

to third order in ϵ :

$$\begin{aligned}
P_{ee} &\sim 1 + O(\epsilon^4), \\
P_{e\mu} &\sim P_{e\tau} \sim P_{es} \sim O(\epsilon^4), \\
P_{\mu\mu} &= 1 - \sin^2 \frac{\Delta_{31}L}{2} - 2(A_n L) s_{24} s_{34} \cos \delta_3 \sin \Delta_{31}L + O(\epsilon^4), \\
P_{\mu\tau} &= (1 - s_{34}^2) \sin^2 \frac{\Delta_{31}L}{2} + \{s_{24} s_{34} \sin \delta_3 + 2(A_n L) s_{24} s_{34} \cos \delta_3\} \sin \Delta_{31}L \\
&\quad + O(\epsilon^4), \\
P_{\mu s} &= s_{34}^2 \sin^2 \frac{\Delta_{31}L}{2} - s_{24} s_{34} \sin \delta_3 \sin \Delta_{31}L + O(\epsilon^4).
\end{aligned}$$

In Sec. 4.2.1 we had to go beyond $O(\epsilon^3)$ in order to explain our numerical results using the golden and silver channels. To this purpose, in the text we have shown the approximated expressions for $P_{e\mu}$ and $P_{e\tau}$ to order ϵ^8 in vacuum. To check unitarity of the four-family PMNS matrix at this order in ϵ , it is useful to show here the P_{es} oscillation probability, also:

$$\begin{aligned}
P_{es} &= 2\theta_{14}^2(1 - \theta_{14}^2 - \theta_{24}^2 - \theta_{34}^2) \\
&\quad + 2\left\{\theta_{13}^2(-2\theta_{14}^2 + \theta_{24}^2 + \theta_{34}^2 - 2\delta\theta_{23}\theta_{34}^2) + \theta_{13}^2\theta_{24}\theta_{34} \cos \delta_3\right\} \sin^2 \frac{\Delta_{31}L}{2} \\
&\quad - 2\sqrt{2}\theta_{13}\theta_{14}\theta_{24}(1 + \delta\theta_{23} - \theta_{34}^2) \sin\left(\delta_2 - \delta_3 + \frac{\Delta_{31}L}{2}\right) \sin \frac{\Delta_{31}L}{2} \\
&\quad - 2\sqrt{2}\theta_{13}\theta_{14}\theta_{34}\left(1 - \delta\theta_{23} - \frac{\theta_{34}^2}{2}\right) \sin\left(\delta_2 + \frac{\Delta_{31}L}{2}\right) \sin \frac{\Delta_{31}L}{2} \\
&\quad - \sin 2\theta_{12}\theta_{13}\theta_{34}^2(\Delta_{21}L) \cos\left(\delta_1 - \delta_2 + \delta_3 - \frac{\Delta_{31}L}{2}\right) \sin \frac{\Delta_{31}L}{2} \\
&\quad + \frac{1}{\sqrt{2}} \sin 2\theta_{12}\theta_{14}\theta_{34}(\Delta_{21}L) \sin(\delta_1 + \delta_3) - \frac{1}{\sqrt{2}} \sin 2\theta_{12}\theta_{14}\theta_{24}(\Delta_{21}L) \sin \delta_1.
\end{aligned}$$

As a final analytical contribution, we have calculated approximate probabilities associated to the channels under study, $P_{\mu\mu}$ and $P_{\mu\tau}$ (together with $P_{\mu s}$), to fourth order in ϵ but neglecting θ_{13} and θ_{14} :

$$\begin{aligned}
P_{\mu\mu} &= 1 - 2\theta_{24}^2 - \left[1 - 4(\delta\theta_{23})^2 - 2\theta_{24}^2 + \theta_{34}^2 \frac{A_n}{\Delta_{31}} \left(4\delta\theta_{23} - \theta_{34}^2 \frac{A_n}{\Delta_{31}}\right)\right] \sin^2 \frac{\Delta_{31}L}{2} \\
&\quad - (A_n L) \left\{2\theta_{24}\theta_{34} \cos \delta_3 - \frac{\theta_{34}^2}{2} \left(4\delta\theta_{23} - \theta_{34}^2 \frac{A_n}{2\Delta_{31}}\right)\right\} \sin \Delta_{31}L + O(\epsilon^5), \\
P_{\mu\tau} &= \left\{1 - 4(\delta\theta_{23})^2 - \theta_{24}^2 - \theta_{34}^2 \left[1 - \frac{\theta_{34}^2}{3} - \frac{A_n}{\Delta_{31}} \left(4\delta\theta_{23} - \theta_{34}^2 \frac{A_n}{\Delta_{31}}\right)\right]\right\} \sin^2 \frac{\Delta_{31}L}{2} \\
&\quad + \left\{\theta_{24}\theta_{34} \sin \delta_3 + (A_n L) \left[2\theta_{24}\theta_{34} \cos \delta_3 - \frac{\theta_{34}^2}{2} \left(4\delta\theta_{23} - \theta_{34}^2 \frac{A_n}{2\Delta_{31}}\right)\right]\right\} \sin \Delta_{31}L \\
&\quad + O(\epsilon^5),
\end{aligned}$$

$$\begin{aligned}
P_{\mu s} &= 2\theta_{24}^2 + \left[\theta_{34}^2 \left(1 - \frac{\theta_{34}^2}{3} \right) - \theta_{24}^2 \right] \sin^2 \frac{\Delta_{31}L}{2} - \theta_{24}\theta_{34} \sin \delta_3 \sin \Delta_{31}L \\
&+ O(\epsilon^5).
\end{aligned}$$

B.6 Discrimination of the four neutrino schemes

In the sections 4.2.1 and 4.2.3 we have discussed the sensitivity to θ_{13} , θ_{14} , θ_{24} , θ_{34} by looking at statistical significance of deviation of a four-flavour scheme from that with a certain set of reference values of the oscillation parameters. Here we will discuss whether the Neutrino Factory setup can distinguish our four-neutrino scheme from the three-flavour scenario.

We introduce the “sterile neutrino discovery potential”, defined as follows:

$$\begin{aligned}
\Delta\chi^2(4\text{fam}) = \min_{\text{marg par}} & \left[\sum_{\text{pol.},(\text{chan.}),L} \min_{\alpha'_s, \beta'_s} \left\{ \sum_j \frac{1}{\sigma_j^2} \left((1 + \alpha_s + x_j\beta_s)N_j(3\text{fam}) \right. \right. \right. \\
& + (1 + \alpha_b + x_j\beta_b)B_j(3\text{fam}) - N_j(4\text{fam}) - B_j(4\text{fam}) \left. \left. \right)^2 \right. \\
& \left. \left. + \left(\frac{\alpha_s}{\sigma_{\alpha s}} \right)^2 + \left(\frac{\alpha_b}{\sigma_{\alpha b}} \right)^2 + \left(\frac{\beta_s}{\sigma_{\beta s}} \right)^2 + \left(\frac{\beta_b}{\sigma_{\beta b}} \right)^2 \right\} + \Delta\chi_{\text{atm+re}}^2(4\text{fam}) \right],
\end{aligned} \tag{B.15}$$

where $\Delta\chi_{\text{atm+re}}^2(4\text{fam})$, defined in Eq. (B.6), is the prior from the four-flavour oscillation analysis of the atmospheric and reactor data, and the errors of the oscillation parameters in the prior $\Delta\chi_{\text{atm+re}}^2(4\text{fam})$ are given by Eq. (B.7).

A remark is in order. The definition of the $\Delta\chi^2$ in the present case, although looking similar, is slightly different from that used in the previous sections. In Secs. 4.2.1 and 4.2.3 we assumed that the minimum of the χ^2 corresponds to the “true” values of the four-family model, and therefore $\chi_{\text{min},4\text{fam}}^2 = 0$. The $\Delta\chi^2$ is then computed in the same model in which data are generated, and CL contours define the region of parameter space compatible at a given CL with the “true” values. In this Section we also assume that data are generated in the four-family model, but we try to fit them in the three-family model. The minimum of the χ^2 in the four-family model is located at the “true” values of the parameters and $\chi_{\text{min},4\text{fam}}^2 = 0$. On the other hand, when we try to fit the four-family-generated data in the three-family model we will in general find $\chi_{\text{min},3\text{fam}}^2 \neq 0$, since a “wrong” model is used to fit the data, except for the special case defined by $\theta_{j4} = 0$ ($j = 1, 2, 3$), $\theta_{ij}^{(4\text{fam})} = \theta_{ij}|_{\text{bestfit}}$ ($(i, j) = (1, 2), (1, 3), (2, 3)$), $\Delta m_{j1}^2(4\text{fam}) = \Delta m_{j1}^2|_{\text{bestfit}}$ ($j = 2, 3$), where the two models coincide and $\Delta\chi^2 = 0$. In the rest of the four-flavour parameter space, the $\Delta\chi^2$ defined in Eq. (B.15) corresponds to $\chi_{\text{min},3\text{fam}}^2 - \chi_{\text{min},4\text{fam}}^2$. CL contours define, then, regions in the four-family parameter space for which a three-family fit to the data is worse than a four-family fit to the data of a quantity $\Delta\chi^2$. For example, a point with $\Delta\chi^2 = 4.61$ is a point that is

fitted by the four-family model much better than by the three-family model. We will define points outside this contour as points for which the hypothesis that data can be fitted in the three-family model is “excluded at 90% CL”. Under these premises, we can use Eq. (B.15) to determine regions in which we are able to distinguish four- from three-family models in the four-flavour parameter space in the same manner as in the previous subsections.

In sections 4.2.1 and 4.2.3, we liked to obtain the most conservative excluded region, i.e., the common excluded region in the $(\theta_{24}, \theta_{34})$ plane irrespective of the values of $\theta_{13}^{(4\text{fam})}$ and θ_{14} , or the common excluded region in the $(\theta_{13}^{(4\text{fam})}, \theta_{14})$ plane irrespective of the values of θ_{24} and θ_{34} . In this case we will try to be more optimistic: to compare the results with those in the sections 4.2.1 and 4.2.3 we present the excluded region projected either in the $(\theta_{13}^{(4\text{fam})}, \theta_{14})$ plane, or in $(\theta_{24}, \theta_{34})$ plane for different input values of $(\theta_{24}, \theta_{34})$ and $(\theta_{13}^{(4\text{fam})}, \theta_{14})$ respectively. To obtain these projected excluded regions, in principle to be conservative we would have to marginalize $\Delta\chi^2$ not only with respect to all the three-family parameters but also with respect to the four-family ones, such as $\theta_{12}^{(4\text{fam})}, \theta_{23}^{(4\text{fam})}, \Delta m_{21}^2{}^{(4\text{fam})}, |\Delta m_{31}^2{}^{(4\text{fam})}|, \delta_1, \delta_2, \delta_3$, as well as $(\theta_{24}, \theta_{34})$ in the former case and $(\theta_{13}^{(4\text{fam})}, \theta_{14})$ in the latter. In marginalizing over the four-family parameters, however, we do not have to vary all the parameters for a couple of reasons. First of all, since the excluded region is expected to depend little on the solar neutrino oscillation parameters in the four-flavour scheme, we can fix the solar parameters $\theta_{12}^{(4\text{fam})}, \Delta m_{21}^2{}^{(4\text{fam})}, \delta_1$. Secondly, because of the prior $\Delta\chi_{\text{atm+re}}^2(4\text{fam})$, in practice we can fix the following parameters to the best fit values: $s_{23}^2{}^{(4\text{fam})} \simeq 0.5, |\Delta m_{31}^2{}^{(4\text{fam})}| \simeq 2.4 \times 10^{-3} \text{eV}^2$. While, as we have said before, we do not marginalize over $(\theta_{24}, \theta_{34})$ in the case of the $(\theta_{13}^{(4\text{fam})}, \theta_{14})$ plane and $(\theta_{13}^{(4\text{fam})}, \theta_{14})$ in the case of the $(\theta_{24}, \theta_{34})$ plane, but we consider several different input values for them. We do not marginalize over the just mentioned parameters to understand better which values of the key four family parameters⁸ could allow us to disentangle between three and four families. Thus, the only non-trivial four-family parameters to be marginalized over are δ_2 and δ_3 in the case of the $(\theta_{13}^{(4\text{fam})}, \theta_{14})$ plane, and δ_3 in the case of the $(\theta_{24}, \theta_{34})$ plane.

The results obtained are presented in Fig. B.3, where the dashed black line stands for the region which is excluded by the prior, i.e., by the present data of the atmospheric and reactor experiments. Upper panels show the “sterile neutrinos discovery potential” of golden and silver channels; lower panels the “discovery potential” of ν_μ disappearance and $\nu_\mu \rightarrow \nu_\tau$ appearance channel. On the left, we show results obtained for the 50 GeV Neutrino Factory; on the right, using the 20 GeV ISS-inspired setup. We can see in Fig. B.3 (upper panels) that if $\theta_{24} = \theta_{34} = 0$, then the golden and silver channels cannot discriminate between the three- and four-family models for both setups within the presently allowed region. If θ_{24} and/or θ_{34} would be non-vanishing, then we see in Fig. B.3 (upper panels) that the combination of golden and silver channels would be able to differentiate between three and four families. For example, for $\theta_{34} \sim 10^\circ$,

⁸Again, $(\theta_{24}, \theta_{34})$ in the case of the $(\theta_{13}^{(4\text{fam})}, \theta_{14})$ plane and $(\theta_{13}^{(4\text{fam})}, \theta_{14})$ in the case of the $(\theta_{24}, \theta_{34})$ plane

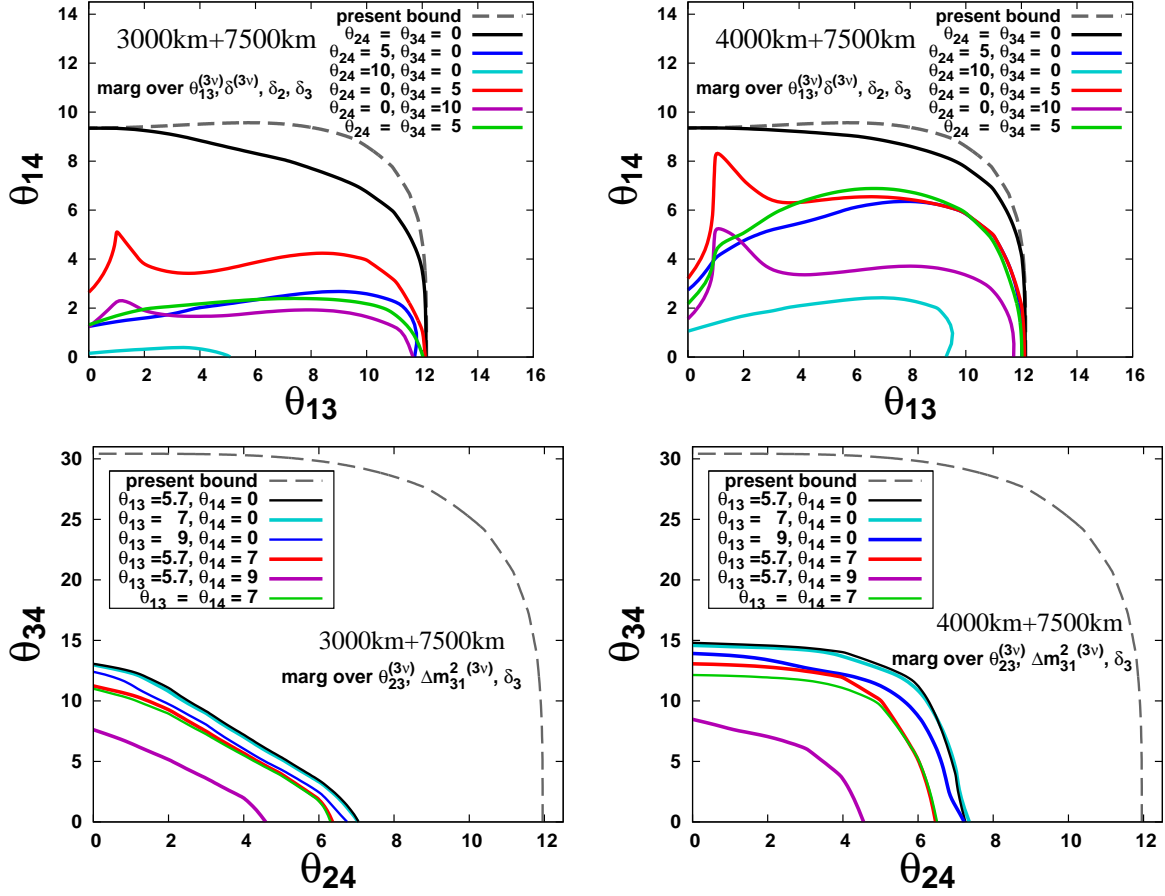


Figure B.3: *Left-upper panel:* The right upper part of each line is the region projected onto the $(\theta_{13}, \theta_{14})$ plane, in which the hypothesis of the three flavour scheme is excluded at 90% CL at the 50 GeV Neutrino Factory. It is obtained by marginalizing over $\theta_{13}^{(3\text{fam})}$ and $\delta^{(3\text{fam})}$ as well as δ_2 and δ_3 . The grey dashed lines stand for the excluded region obtained only from the prior $\Delta\chi_{\text{atm+re}}^2(4\text{fam})$ where terms other than $(s_{13}^{2(4\text{fam})} - 0.01)^2/\sigma^2(s_{13}^2) + (s_{14}^2)^2/\sigma^2(s_{14}^2)$ are assumed to be zero in Eq. (B.6). The excluded regions for nonvanishing θ_{24} or θ_{34} , which are always larger than the case for $\theta_{24} = \theta_{34} = 0$, are also depicted for information. *Left-lower panel:* Excluded region at 90% CL projected onto the $(\theta_{24}, \theta_{34})$ plane. It is obtained by marginalizing over $\theta_{23}^{(3\text{fam})}$, $|\Delta m_{31}^2(3\text{fam})|$ as well as δ_3 . The grey dashed lines stand for the excluded region obtained only from the prior $\Delta\chi_{\text{atm+re}}^2(4\text{fam})$ where terms other than $(s_{24}^2)^2/\sigma^2(s_{24}^2) + (s_{34}^2)^2/\sigma^2(s_{34}^2)$ are assumed to be zero in Eq. (B.6). *Right-upper(lower) panel:* The same figure as the left-upper(lower) panel for the 20 GeV ISS-inspired setup.

the 50 GeV (20 GeV) setup can distinguish the (3+1)-neutrino model from standard three-family oscillations for θ_{14} as small as $\theta_{14} \sim 2^\circ(4^\circ)$. This is because of the same reason that the Neutrino Factory has good sensitivity to $U_{e4}U_{\mu 4}$ and $U_{e4}U_{\tau 4}$, as was discussed in sect. 4.2.2.

In Fig. B.3 (lower panels) we can see that, irrespectively of the input value of $\theta_{13}^{(4\text{fam})}$

and θ_{14} , the combination of the ν_μ disappearance and the $\nu_\mu \rightarrow \nu_\tau$ discovery channels permits discrimination between the four- and three-neutrino oscillation models in a significant region of the presently allowed parameter space. For non-vanishing values of $\theta_{13}^{(4\text{fam})}$ and θ_{14} the region in which discrimination is possible increases.

We conclude that combination of the four channels would be very effective to tell the difference between the four- and three-flavour schemes in a significant region of the presently allowed parameter space. However notice that silver and golden channels (responsible of the sensitivity to $(\theta_{13}^{(4\text{fam})}, \theta_{14})$) are less effective than the $\nu_\mu - \nu_\tau$ sector (sensitive to $(\theta_{24}, \theta_{34})$).

Bibliography

- [1] Steven Weinberg. The Quantum Theory of Fields. *Cambridge University Press*, 1995, 1996, 2003.
- [2] Michael Aizenman. Proof of the Triviality of ϕ^4 Field Theory and Some Mean-Field Features of Ising Models for $d \leq 4$. *Phys. Rev. Lett.*, 47:886–886, 1981.
- [3] J. Frohlich. On the Triviality of ϕ^4 in D-Dimensions Theories and the Approach to the Critical Point in $D \geq 4$. *Nucl. Phys.*, B200:281–296, 1982.
- [4] Alan D. Sokal. AN ALTERNATE CONSTRUCTIVE APPROACH TO THE ϕ^4 in three- dimensions QUANTUM FIELD THEORY, AND A POSSIBLE DESTRUCTIVE APPROACH TO ϕ^4 in four-dimensions. *Annales Poincare Phys. Theor.*, 37A:317–398, 1982.
- [5] Steven Weinberg. Implications of Dynamical Symmetry Breaking: An Addendum. *Phys. Rev.*, D19:1277–1280, 1979.
- [6] Eldad Gildener and Steven Weinberg. Symmetry Breaking and Scalar Bosons. *Phys. Rev.*, D13:3333, 1976.
- [7] Peter Minkowski. $\mu \rightarrow e\gamma$ at a Rate of One Out of 1-Billion Muon Decays? *Phys. Lett.*, B67:421, 1977.
- [8] P. Ramond M. Gell-Mann and R. Slansky. In *Supergravity*, edited by P. van Nieuwenhuizen and D. Freedman, (North-Holland, 1979), p. 315.
- [9] Tsutomu Yanagida. Horizontal gauge symmetry and masses of neutrinos. In Proceedings of the Workshop on the Baryon Number of the Universe and Unified Theories, Tsukuba, Japan, 13-14 Feb 1979.
- [10] Rabindra N. Mohapatra and Goran Senjanović. Neutrino mass and spontaneous parity nonconservation. *Phys. Rev. Lett.*, 44(14):912–915, Apr 1980.
- [11] M. Fukugita and T. Yanagida. Baryogenesis Without Grand Unification. *Phys. Lett.*, B174:45, 1986.
- [12] Claude Amsler et al. Review of particle physics. *Phys. Lett.*, B667:1, 2008.

- [13] Steven Weinberg. Baryon and Lepton Nonconserving Processes. *Phys. Rev. Lett.*, 43:1566–1570, 1979.
- [14] H. Georgi and S. L. Glashow. Unity of All Elementary Particle Forces. *Phys. Rev. Lett.*, 32:438–441, 1974.
- [15] H. Georgi, Helen R. Quinn, and Steven Weinberg. Hierarchy of Interactions in Unified Gauge Theories. *Phys. Rev. Lett.*, 33:451–454, 1974.
- [16] (ed.) Gerard 't Hooft et al. Recent Developments in Gauge Theories. Proceedings, Nato Advanced Study Institute, Cargese, France, August 26 - September 8, 1979. New York, Usa: Plenum (1980) 438 P. (Nato Advanced Study Institutes Series: Series B, Physics, 59).
- [17] A. Broncano, M. B. Gavela, and Elizabeth Ellen Jenkins. The effective Lagrangian for the seesaw model of neutrino mass and leptogenesis. *Phys. Lett.*, B552:177–184, 2003.
- [18] A. Abada, C. Biggio, F. Bonnet, M. B. Gavela, and T. Hambye. Low energy effects of neutrino masses. *JHEP*, 12:061, 2007.
- [19] M. Magg and C. Wetterich. NEUTRINO MASS PROBLEM AND GAUGE HIERARCHY. *Phys. Lett.*, B94:61, 1980.
- [20] J. Schechter and J. W. F. Valle. Neutrino Masses in $SU(2) \times U(1)$ Theories. *Phys. Rev.*, D22:2227, 1980.
- [21] C. Wetterich. Neutrino Masses and the Scale of B-L Violation. *Nucl. Phys.*, B187:343, 1981.
- [22] George Lazarides, Q. Shafi, and C. Wetterich. Proton Lifetime and Fermion Masses in an $SO(10)$ Model. *Nucl. Phys.*, B181:287, 1981.
- [23] Rabindra N. Mohapatra and Goran Senjanovic. Neutrino Masses and Mixings in Gauge Models with Spontaneous Parity Violation. *Phys. Rev.*, D23:165, 1981.
- [24] Robert Foot, H. Lew, X. G. He, and Girish C. Joshi. SEESAW NEUTRINO MASSES INDUCED BY A TRIPLET OF LEPTONS. *Z. Phys.*, C44:441, 1989.
- [25] Francesco Vissani. Do experiments suggest a hierarchy problem? *Phys. Rev.*, D57:7027–7030, 1998.
- [26] J. A. Casas, J. R. Espinosa, and I. Hidalgo. Implications for new physics from fine-tuning arguments. I: Application to SUSY and seesaw cases. *JHEP*, 11:057, 2004.
- [27] B. Pontecorvo. Neutrino experiments and the question of leptonic-charge conservation. *Sov. Phys. JETP*, 26:984–988, 1968.

- [28] B. T. Cleveland et al. Measurement of the solar electron neutrino flux with the Homestake chlorine detector. *Astrophys. J.*, 496:505–526, 1998.
- [29] J. N. Abdurashitov et al. Measurement of the solar neutrino capture rate with gallium metal. *Phys. Rev.*, C60:055801, 1999.
- [30] W. Hampel et al. GALLEX solar neutrino observations: Results for GALLEX IV. *Phys. Lett.*, B447:127–133, 1999.
- [31] S. Fukuda et al. Solar 8B and hep Neutrino Measurements from 1258 Days of Super-Kamiokande Data. *Phys. Rev. Lett.*, 86:5651–5655, 2001.
- [32] J. P. Cravens et al. Solar neutrino measurements in Super-Kamiokande-II. *Phys. Rev.*, D78:032002, 2008.
- [33] Q. R. Ahmad et al. Measurement of the charged current interactions produced by B-8 solar neutrinos at the Sudbury Neutrino Observatory. *Phys. Rev. Lett.*, 87:071301, 2001.
- [34] S. N. Ahmed et al. Measurement of the total active B-8 solar neutrino flux at the Sudbury Neutrino Observatory with enhanced neutral current sensitivity. *Phys. Rev. Lett.*, 92:181301, 2004.
- [35] B. Aharmim et al. An Independent Measurement of the Total Active 8B Solar Neutrino Flux Using an Array of 3He Proportional Counters at the Sudbury Neutrino Observatory. *Phys. Rev. Lett.*, 101:111301, 2008.
- [36] Y. Fukuda et al. Evidence for oscillation of atmospheric neutrinos. *Phys. Rev. Lett.*, 81:1562–1567, 1998.
- [37] M. Ambrosio et al. Matter effects in upward-going muons and sterile neutrino oscillations. *Phys. Lett.*, B517:59–66, 2001.
- [38] Y. Ashie et al. A Measurement of Atmospheric Neutrino Oscillation Parameters by Super-Kamiokande I. *Phys. Rev.*, D71:112005, 2005.
- [39] M. Apollonio et al. Limits on Neutrino Oscillations from the CHOOZ Experiment. *Phys. Lett.*, B466:415–430, 1999.
- [40] M. Apollonio et al. Search for neutrino oscillations on a long base-line at the CHOOZ nuclear power station. *Eur. Phys. J.*, C27:331–374, 2003.
- [41] F. Boehm et al. Final results from the Palo Verde Neutrino Oscillation Experiment. *Phys. Rev.*, D64:112001, 2001.
- [42] K. Eguchi et al. First results from KamLAND: Evidence for reactor anti- neutrino disappearance. *Phys. Rev. Lett.*, 90:021802, 2003.

- [43] M. H. Ahn et al. Indications of Neutrino Oscillation in a 250 km Long- baseline Experiment. *Phys. Rev. Lett.*, 90:041801, 2003.
- [44] E. Aliu et al. Evidence for muon neutrino oscillation in an accelerator- based experiment. *Phys. Rev. Lett.*, 94:081802, 2005.
- [45] D. G. Michael et al. Observation of muon neutrino disappearance with the MINOS detectors and the NuMI neutrino beam. *Phys. Rev. Lett.*, 97:191801, 2006.
- [46] P. Adamson et al. Measurement of Neutrino Oscillations with the MINOS Detectors in the NuMI Beam. *Phys. Rev. Lett.*, 101:131802, 2008.
- [47] B. Pontecorvo. Mesonium and antimesonium. *Sov. Phys. JETP*, 6:429, 1957.
- [48] C. Athanassopoulos et al. Evidence for anti- $\nu/\mu \rightarrow \bar{\nu}/e$ oscillation from the LSND experiment at the Los Alamos Meson Physics Facility. *Phys. Rev. Lett.*, 77:3082–3085, 1996.
- [49] C. Athanassopoulos et al. Evidence for $\nu/\mu \rightarrow \nu/e$ neutrino oscillations from LSND. *Phys. Rev. Lett.*, 81:1774–1777, 1998.
- [50] A. Aguilar et al. Evidence for neutrino oscillations from the observation of anti- ν/e appearance in a anti- ν/μ beam. *Phys. Rev.*, D64:112007, 2001.
- [51] Ziro Maki, Masami Nakagawa, and Shoichi Sakata. Remarks on the unified model of elementary particles. *Prog. Theor. Phys.*, 28:870–880, 1962.
- [52] V. N. Gribov and B. Pontecorvo. Neutrino astronomy and lepton charge. *Phys. Lett.*, B28:493, 1969.
- [53] Leo Stodolsky. The unnecessary wavepacket. *Phys. Rev.*, D58:036006, 1998.
- [54] L. Wolfenstein. Neutrino oscillations in matter. *Phys. Rev. D*, 17(9):2369–2374, May 1978.
- [55] S. P. Mikheev and A. Yu. Smirnov. Resonance enhancement of oscillations in matter and solar neutrino spectroscopy. *Sov. J. Nucl. Phys.*, 42:913–917, 1985.
- [56] S. P. Mikheev and A. Yu. Smirnov. Neutrino oscillations in a variable-density medium and ν - bursts due to the gravitational collapse of stars. *Sov. Phys. JETP*, 64:4–7, 1986.
- [57] S. P. Mikheev and A. Yu. Smirnov. Resonant amplification of neutrino oscillations in matter and solar neutrino spectroscopy. *Nuovo Cim.*, C9:17–26, 1986.
- [58] Michele Maltoni and Thomas Schwetz. Three-flavour neutrino oscillation update and comments on possible hints for a non-zero θ_{13} . *PoS*, IDM2008:072, 2008.

- [59] T. Araki et al. Measurement of neutrino oscillation with KamLAND: Evidence of spectral distortion. *Phys. Rev. Lett.*, 94:081801, 2005.
- [60] H. L. Ge, C. Giunti, and Q. Y. Liu. Bayesian Constraints on θ_{13} from Solar and KamLAND Neutrino Data. *Phys. Rev.*, D80:053009, 2009.
- [61] Thomas Schwetz, M. A. Tortola, and Jose W. F. Valle. Three-flavour neutrino oscillation update. *New J. Phys.*, 10:113011, 2008.
- [62] Evgeny Khakimovich Akhmedov, Robert Johansson, Manfred Lindner, Tommy Ohlsson, and Thomas Schwetz. Series expansions for three-flavor neutrino oscillation probabilities in matter. *JHEP*, 04:078, 2004.
- [63] M. C. Gonzalez-Garcia and Michele Maltoni. Phenomenology with Massive Neutrinos. *Phys. Rept.*, 460:1–129, 2008.
- [64] G. L. Fogli et al. Observables sensitive to absolute neutrino masses (Addendum). *Phys. Rev.*, D78:033010, 2008.
- [65] M. C. Gonzalez-Garcia, Michele Maltoni, and Jordi Salvado. Updated global fit to three neutrino mixing: status of the hints of $\theta_{13} \neq 0$. 2010.
- [66] R. N. Mohapatra et al. Theory of neutrinos. 2004.
- [67] E. Komatsu et al. Seven-Year Wilkinson Microwave Anisotropy Probe (WMAP) Observations: Cosmological Interpretation. 2010.
- [68] Julien Lesgourgues and Sergio Pastor. Massive neutrinos and cosmology. *Phys. Rept.*, 429:307–379, 2006.
- [69] H. V. Klapdor-Kleingrothaus, A. Dietz, H. L. Harney, and I. V. Krivosheina. Evidence for Neutrinoless Double Beta Decay. *Mod. Phys. Lett.*, A16:2409–2420, 2001.
- [70] H. V. Klapdor-Kleingrothaus and I. V. Krivosheina. The evidence for the observation of $0\nu\beta\beta$ beta beta decay: The identification of $0\nu\beta\beta$ beta beta events from the full spectra. *Mod. Phys. Lett.*, A21:1547–1566, 2006.
- [71] C. Arnaboldi et al. Results from a search for the $0\nu\beta\beta$ -decay of ^{130}Te . *Phys. Rev.*, C78:035502, 2008.
- [72] Mattias Blennow, Enrique Fernandez-Martinez, Jacobo Lopez-Pavon, and Javier Menendez. Neutrinoless double beta decay in seesaw models. 2010.
- [73] C. Arnaboldi et al. CUORE: A cryogenic underground observatory for rare events. *Nucl. Instrum. Meth.*, A518:775–798, 2004.
- [74] D. Akimov et al. EXO: An advanced Enriched Xenon double-beta decay Observatory. *Nucl. Phys. Proc. Suppl.*, 138:224–226, 2005.

- [75] J. Diaz et al. The NEXT experiment. *J. Phys. Conf. Ser.*, 179:012005, 2009.
- [76] Irina Nasteva. SuperNEMO - the next generation double beta decay experiment. 2009.
- [77] Richard Gaitskell et al. White paper on the Majorana zero-neutrino double-beta decay experiment. 2003.
- [78] F. Ardellier et al. Letter of intent for double-CHOOZ: A search for the mixing angle θ_{13} . 2004.
- [79] A. Cervera et al. Golden measurements at a neutrino factory. *Nucl. Phys.*, B579:17–55, 2000.
- [80] Y. Itow et al. The JHF-Kamioka neutrino project. 2001.
- [81] D. S. Ayres et al. NOvA proposal to build a 30-kiloton off-axis detector to study neutrino oscillations in the Fermilab NuMI beamline. 2004.
- [82] P. Zucchelli. A novel concept for a anti- ν/e / ν/e neutrino factory: The beta beam. *Phys. Lett.*, B532:166–172, 2002.
- [83] J. Burguet-Castell, D. Casper, J. J. Gomez-Cadenas, P. Hernandez, and F. Sanchez. Neutrino oscillation physics with a higher gamma beta- beam. *Nucl. Phys.*, B695:217–240, 2004.
- [84] J. Burguet-Castell, D. Casper, E. Couce, J. J. Gomez-Cadenas, and P. Hernandez. Optimal beta-beam at the CERN-SPS. *Nucl. Phys.*, B725:306–326, 2005.
- [85] A. Donini and E. Fernandez-Martinez. Alternating ions in a beta-beam to solve degeneracies. *Phys. Lett.*, B641:432–439, 2006.
- [86] Sanjib Kumar Agarwalla, Sandhya Choubey, and Amitava Raychaudhuri. Neutrino mass hierarchy and θ_{13} with a magic baseline beta-beam experiment. *Nucl. Phys.*, B771:1–27, 2007.
- [87] Sanjib Kumar Agarwalla, Sandhya Choubey, and Amitava Raychaudhuri. Unraveling neutrino parameters with a magical beta-beam experiment at INO. *Nucl. Phys.*, B798:124–145, 2008.
- [88] Pilar Coloma, Andrea Donini, Enrique Fernandez-Martinez, and J. Lopez-Pavon. θ_{13} , δ and the neutrino mass hierarchy at a $\gamma = 350$ double baseline Li/B β -Beam. *JHEP*, 05:050, 2008.
- [89] <http://www.ganil.fr/eurisol/>.
- [90] S. Geer. Neutrino beams from muon storage rings: Characteristics and physics potential. *Phys. Rev.*, D57:6989–6997, 1998.

- [91] A. De Rujula, M. B. Gavela, and P. Hernandez. Neutrino oscillation physics with a neutrino factory. *Nucl. Phys.*, B547:21–38, 1999.
- [92] Steve Geer, Olga Mena, and Silvia Pascoli. A Low energy neutrino factory for large θ_{13} . *Phys. Rev.*, D75:093001, 2007.
- [93] Alan Bross et al. The multi-channel low energy neutrino factory. 2009.
- [94] J. Burguet-Castell, M. B. Gavela, J. J. Gomez-Cadenas, P. Hernandez, and Olga Mena. On the measurement of leptonic CP violation. *Nucl. Phys.*, B608:301–318, 2001.
- [95] J. Burguet-Castell and Olga Mena. Leptonic CP violation at the neutrino factory. 2001.
- [96] Hisakazu Minakata and Hiroshi Nunokawa. Exploring neutrino mixing with low energy superbeams. *JHEP*, 10:001, 2001.
- [97] V. Barger, D. Marfatia, and K. Whisnant. Breaking eight-fold degeneracies in neutrino CP violation, mixing, and mass hierarchy. *Phys. Rev.*, D65:073023, 2002.
- [98] A. Donini, D. Meloni, and S. Rigolin. Clone flow analysis for a theory inspired neutrino experiment planning. *JHEP*, 06:011, 2004.
- [99] A. Bandyopadhyay et al. Physics at a future Neutrino Factory and super-beam facility. *Rept. Prog. Phys.*, 72:106201, 2009.
- [100] IDS homepage. <https://www.ids-nf.org/wiki/FrontPage>.
- [101] Paul Langacker and David London. Mixing Between Ordinary and Exotic Fermions. *Phys. Rev.*, D38:886, 1988.
- [102] M. Czakon, J. Gluza, and M. Zralek. Nonunitary neutrino mixing matrix and CP violating neutrino oscillations. *Acta Phys. Polon.*, B32:3735–3744, 2001.
- [103] B. Bekman, J. Gluza, J. Holeczek, J. Syska, and M. Zralek. Matter effects and CP violating neutrino oscillations with non-decoupling heavy neutrinos. *Phys. Rev.*, D66:093004, 2002.
- [104] Samoil M. Bilenky and C. Giunti. Seesaw type mixing and muon-neutrino \rightarrow tau-neutrino oscillations. *Phys. Lett.*, B300:137–140, 1993.
- [105] Enrico Nardi, Esteban Roulet, and Daniele Tommasini. Limits on neutrino mixing with new heavy particles. *Phys. Lett.*, B327:319–326, 1994.
- [106] D. Tommasini, G. Barenboim, J. Bernabeu, and C. Jarlskog. Non-decoupling of Heavy Neutrinos and Lepton Flavour Violation. *Nucl. Phys.*, B444:451–467, 1995.

- [107] Sven Bergmann and Alex Kagan. Z-induced FCNCs and their effects on neutrino oscillations. *Nucl. Phys.*, B538:368–386, 1999.
- [108] Will Loinaz, Naotoshi Okamura, Tatsu Takeuchi, and L. C. R. Wijewardhana. The NuTeV anomaly, neutrino mixing, and a heavy Higgs. *Phys. Rev.*, D67:073012, 2003.
- [109] Will Loinaz, Naotoshi Okamura, Saifuddin Rayyan, Tatsu Takeuchi, and L. C. R. Wijewardhana. Quark-lepton unification and lepton flavor non- conservation from a TeV-scale seesaw neutrino mass texture. *Phys. Rev.*, D68:073001, 2003.
- [110] Will Loinaz, Naotoshi Okamura, Saifuddin Rayyan, Tatsu Takeuchi, and L. C. R. Wijewardhana. The NuTeV anomaly, lepton universality, and non-universal neutrino-gauge couplings. *Phys. Rev.*, D70:113004, 2004.
- [111] M. B. Gavela, T. Hambye, D. Hernandez, and P. Hernandez. Minimal Flavour Seesaw Models. *JHEP*, 09:038, 2009.
- [112] S. Antusch, C. Biggio, E. Fernandez-Martinez, M. B. Gavela, and J. Lopez-Pavon. Unitarity of the Leptonic Mixing Matrix. *JHEP*, 10:084, 2006.
- [113] Nima Arkani-Hamed, Savas Dimopoulos, G. R. Dvali, and John March-Russell. Neutrino masses from large extra dimensions. *Phys. Rev.*, D65:024032, 2002.
- [114] Andre De Gouvea, Gian Francesco Giudice, Alessandro Strumia, and Kazuhiro Tobe. Phenomenological implications of neutrinos in extra dimensions. *Nucl. Phys.*, B623:395–420, 2002.
- [115] E. Fernandez-Martinez, M. B. Gavela, J. Lopez-Pavon, and O. Yasuda. CP-violation from non-unitary leptonic mixing. *Phys. Lett.*, B649:427–435, 2007.
- [116] Srubabati Goswami and Toshihiko Ota. Testing non-unitarity of neutrino mixing matrices at neutrino factories. *Phys. Rev.*, D78:033012, 2008.
- [117] Guido Altarelli and Davide Meloni. CP violation in neutrino oscillations and new physics. *Nucl. Phys.*, B809:158–182, 2009.
- [118] Heiko Lacker and Andreas Menzel. Simultaneous Extraction of the Fermi constant and PMNS matrix elements in the presence of a fourth generation. 2010.
- [119] Carlo Giunti. Flavor neutrinos states. 2004.
- [120] Q. R. Ahmad et al. Measurement of day and night neutrino energy spectra at SNO and constraints on neutrino mixing parameters. *Phys. Rev. Lett.*, 89:011302, 2002.
- [121] B. Aharmim et al. Electron energy spectra, fluxes, and day-night asymmetries of B-8 solar neutrinos from the 391-day salt phase SNO data set. *Phys. Rev.*, C72:055502, 2005.

- [122] A. A. Aguilar-Arevalo et al. A Search for electron neutrino appearance at the $\Delta m^2 \sim 1\text{eV}^2$ scale. *Phys. Rev. Lett.*, 98:231801, 2007.
- [123] B. Armbruster et al. Upper limits for neutrino oscillations muon-antineutrino to electron-antineutrino from muon decay at rest. *Phys. Rev.*, D65:112001, 2002.
- [124] P. Astier et al. Final NOMAD results on $\nu/\mu \rightarrow \nu/\tau$ and $\nu/e \rightarrow \nu/\tau$ oscillations including a new search for ν/τ appearance using hadronic tau decays. *Nucl. Phys.*, B611:3–39, 2001.
- [125] Y. Declais et al. Search for neutrino oscillations at 15-meters, 40-meters, and 95-meters from a nuclear power reactor at Bugey. *Nucl. Phys.*, B434:503–534, 1995.
- [126] Hiroshi Nunokawa, Stephen J. Parke, and Renata Zukanovich Funchal. What fraction of boron-8 solar neutrinos arrive at the earth as a $\nu(2)$ mass eigenstate? *Phys. Rev.*, D74:013006, 2006.
- [127] S. Eidelman et al. Review of particle physics. *Phys. Lett.*, B592:1, 2004.
- [128] A. Pich. The Standard model of electroweak interactions. 2005.
- [129] A Combination of preliminary electroweak measurements and constraints on the standard model. 2004.
- [130] T. Petcov. *Sov. J. Nucl. Phys.*, 25:340, 1977.
- [131] Samoil M. Bilenky, S. T. Petcov, and B. Pontecorvo. Lepton mixing, $\mu \rightarrow e + \gamma$ decay and neutrino oscillations. *Phys. Lett.*, B67:309, 1977.
- [132] Ta-Pei Cheng and Ling-Fong Li. Muon Number Nonconservation in Gauge Theories. In *Coral Gables 1977, Proceedings, Deeper Pathways In High-energy Physics*, New York 1977, 659-681.
- [133] W. J. Marciano and A. I. Sanda. Exotic Decays of the Muon and Heavy Leptons in Gauge Theories. *Phys. Lett.*, B67:303, 1977.
- [134] B. W. Lee, S. Pakvasa, R. E. Shrock, and H. Sugawara. Muon and Electron Number Nonconservation in a v-a Six Quark Model. *Phys. Rev. Lett.*, 38:937, 1977.
- [135] Benjamin W. Lee and Robert E. Shrock. Natural Suppression of Symmetry Violation in Gauge Theories: Muon - Lepton and Electron Lepton Number Nonconservation. *Phys. Rev.*, D16:1444, 1977.
- [136] S. L. Glashow, J. Iliopoulos, and L. Maiani. Weak Interactions with Lepton-Hadron Symmetry. *Phys. Rev.*, D2:1285–1292, 1970.

- [137] M. L. Brooks et al. New Limit for the Family-Number Non-conserving Decay $\mu^+ \rightarrow e^+\gamma$. *Phys. Rev. Lett.*, 83:1521–1524, 1999.
- [138] Bernard Aubert et al. Search for lepton flavor violation in the decay $\tau^\pm \rightarrow e^\pm\gamma$. *Phys. Rev. Lett.*, 96:041801, 2006.
- [139] Bernard Aubert et al. Search for lepton flavor violation in the decay $\tau \rightarrow \mu\gamma$. *Phys. Rev. Lett.*, 95:041802, 2005.
- [140] Zhi zhong Xing and He Zhang. Reconstruction of the neutrino mixing matrix and leptonic unitarity triangles from long-baseline neutrino oscillations. *Phys. Lett.*, B618:131–140, 2005.
- [141] Y. Farzan and A. Yu. Smirnov. Leptonic unitarity triangle and CP-violation. *Phys. Rev.*, D65:113001, 2002.
- [142] A. Donini, D. Meloni, and P. Migliozzi. The silver channel at the Neutrino Factory. *Nucl. Phys.*, B646:321–349, 2002.
- [143] <http://meg.icepp.s.u.tokyo.ac.jp/>.
- [144] A. van der Schaaf. Muon physics at a neutrino factory. *J. Phys.*, G29:2755–2762, 2003.
- [145] A. van der Schaaf. Summary WG2 part 2: Rare muon decays. *Nucl. Instrum. Meth.*, A503:240–243, 2003.
- [146] PRIME working work. Search for the $\mu - e$ conversion process at an ultimate sensitivity of the order of 10^{18} with prism, unpublished; loi to j-parc 50-gev ps, loi-25, <http://psux1.kek.jp/jhf-np/loilist/loilist.html>.
- [147] Y. Kuno. PRISM/PRIME. *Nucl. Phys. Proc. Suppl.*, 149:376–378, 2005.
- [148] Sheldon Stone and Jon Urheim. Observation of the D/sJ(2463) and confirmation of the D/sJ*(2317). *ECONF*, C030603:MAR05, 2003.
- [149] D. Autiero et al. The synergy of the golden and silver channels at the Neutrino Factory. *Eur. Phys. J.*, C33:243–260, 2004.
- [150] Burton Richter. Conventional beams or neutrino factories: The next generation of accelerator-based neutrino experiments. 2000.
- [151] Esteban Roulet. Mikheyev-Smirnov-Wolfenstein effect with flavor-changing neutrino interactions. *Phys. Rev.*, D44:935–938, 1991.
- [152] M. M. Guzzo, A. Masiero, and S. T. Petcov. On the MSW effect with massless neutrinos and no mixing in the vacuum. *Phys. Lett.*, B260:154–160, 1991.

- [153] Yuval Grossman. Nonstandard neutrino interactions and neutrino oscillation experiments. *Phys. Lett.*, B359:141–147, 1995.
- [154] Stefan Antusch, Mattias Blennow, Enrique Fernandez-Martinez, and Jacobo Lopez-Pavon. Probing non-unitary mixing and CP-violation at a Neutrino Factory. *Phys. Rev.*, D80:033002, 2009.
- [155] K. Hayasaka et al. New search for tau \rightarrow j mu gamma and tau \rightarrow j e gamma decays at Belle. *Phys. Lett.*, B666:16–22, 2008.
- [156] Stefan Antusch, Jochen P. Baumann, and Enrique Fernandez-Martinez. Non-Standard Neutrino Interactions with Matter from Physics Beyond the Standard Model. *Nucl. Phys.*, B810:369–388, 2009.
- [157] M. C. Gonzalez-Garcia, Y. Grossman, A. Gusso, and Y. Nir. New CP violation in neutrino oscillations. *Phys. Rev.*, D64:096006, 2001.
- [158] T. Abe et al. Detectors and flux instrumentation for future neutrino facilities. *JINST*, 4:T05001, 2009.
- [159] Patrick Huber and Walter Winter. Neutrino factories and the 'magic' baseline. *Phys. Rev.*, D68:037301, 2003.
- [160] Jian Tang and Walter Winter. Physics with near detectors at a neutrino factory. *Phys. Rev.*, D80:053001, 2009.
- [161] Mattias Blennow and Enrique Fernandez-Martinez. Neutrino oscillation parameter sampling with MonteCUBES. *Comput. Phys. Commun.*, 181:227–231, 2010.
- [162] MonteCUBES homepage. <http://wwwth.mppmu.mpg.de/members/blennow/montecubes/>.
- [163] Patrick Huber, M. Lindner, and W. Winter. Simulation of long-baseline neutrino oscillation experiments with GLoBES. *Comput. Phys. Commun.*, 167:195, 2005.
- [164] Patrick Huber, Joachim Kopp, Manfred Lindner, Mark Rolinec, and Walter Winter. New features in the simulation of neutrino oscillation experiments with GLoBES 3.0. *Comput. Phys. Commun.*, 177:432–438, 2007.
- [165] Andrew Gelman and Donald B. Rubin. Inference from Iterative Simulation Using Multiple Sequences. *Statist. Sci.*, 7:457–472, 1992.
- [166] M. Maltoni, T. Schwetz, M. A. Tortola, and J. W. F. Valle. Status of global fits to neutrino oscillations. *New J. Phys.*, 6:122, 2004.
- [167] Carla Biggio, Mattias Blennow, and Enrique Fernandez-Martinez. General bounds on non-standard neutrino interactions. *JHEP*, 08:090, 2009.

- [168] A. M. Gago, H. Minakata, H. Nunokawa, S. Uchinami, and R. Zukanovich Funchal. Resolving CP Violation by Standard and Nonstandard Interactions and Parameter Degeneracy in Neutrino Oscillations. *JHEP*, 01:049, 2010.
- [169] Takashi Kikuchi, Hisakazu Minakata, and Shoichi Uchinami. Perturbation Theory of Neutrino Oscillation with Nonstandard Neutrino Interactions. *JHEP*, 03:114, 2009.
- [170] Claude Amsler and A. Masoni. The $\eta(1405)$, $\eta(1475)$, $f_1(1420)$, and $f_1(1510)$.
- [171] Precision electroweak measurements on the Z resonance. *Phys. Rept.*, 427:257, 2006.
- [172] Michel Sorel, Janet M. Conrad, and Michael Shaevitz. A combined analysis of short-baseline neutrino experiments in the (3+1) and (3+2) sterile neutrino oscillation hypotheses. *Phys. Rev.*, D70:073004, 2004.
- [173] Michele Maltoni and Thomas Schwetz. Sterile neutrino oscillations after first MiniBooNE results. *Phys. Rev.*, D76:093005, 2007.
- [174] V. Barger, D. Marfatia, and K. Whisnant. Confronting mass-varying neutrinos with MiniBooNE. *Phys. Rev.*, D73:013005, 2006.
- [175] Sergio Palomares-Ruiz, Silvia Pascoli, and Thomas Schwetz. Explaining LSND by a decaying sterile neutrino. *JHEP*, 09:048, 2005.
- [176] Andre de Gouvea and Yuval Grossman. A three-flavor, Lorentz-violating solution to the LSND anomaly. *Phys. Rev.*, D74:093008, 2006.
- [177] Thomas Schwetz. LSND versus MiniBooNE: Sterile neutrinos with energy dependent masses and mixing? *JHEP*, 02:011, 2008.
- [178] Ann E. Nelson and Jonathan Walsh. Short Baseline Neutrino Oscillations and a New Light Gauge Boson. *Phys. Rev.*, D77:033001, 2008.
- [179] Heinrich Pas, Sandip Pakvasa, and Thomas J. Weiler. Sterile - active neutrino oscillations and shortcuts in the extra dimension. *Phys. Rev.*, D72:095017, 2005.
- [180] Pierre Fayet. Supergauge Invariant Extension of the Higgs Mechanism and a Model for the electron and Its Neutrino. *Nucl. Phys.*, B90:104–124, 1975.
- [181] Pierre Fayet. Supersymmetry and Weak, Electromagnetic and Strong Interactions. *Phys. Lett.*, B64:159, 1976.
- [182] Pierre Fayet. Spontaneously Broken Supersymmetric Theories of Weak, Electromagnetic and Strong Interactions. *Phys. Lett.*, B69:489, 1977.
- [183] Hans Peter Nilles, M. Srednicki, and D. Wyler. Weak Interaction Breakdown Induced by Supergravity. *Phys. Lett.*, B120:346, 1983.

- [184] J. M. Frere, D. R. T. Jones, and S. Raby. Fermion Masses and Induction of the Weak Scale by Supergravity. *Nucl. Phys.*, B222:11, 1983.
- [185] J. P. Derendinger and Carlos A. Savoy. Quantum Effects and $SU(2) \times U(1)$ Breaking in Supergravity Gauge Theories. *Nucl. Phys.*, B237:307, 1984.
- [186] John R. Ellis, J. F. Gunion, Howard E. Haber, L. Roszkowski, and F. Zwirner. Higgs Bosons in a Nonminimal Supersymmetric Model. *Phys. Rev.*, D39:844, 1989.
- [187] Manuel Drees. Supersymmetric Models with Extended Higgs Sector. *Int. J. Mod. Phys.*, A4:3635, 1989.
- [188] Ulrich Ellwanger, Michel Rausch de Traubenberg, and Carlos A. Savoy. Particle spectrum in supersymmetric models with a gauge singlet. *Phys. Lett.*, B315:331–337, 1993.
- [189] Ulrich Ellwanger, Michel Rausch de Traubenberg, and Carlos A. Savoy. Higgs phenomenology of the supersymmetric model with a gauge singlet. *Z. Phys.*, C67:665–670, 1995.
- [190] A. Donini, M. Maltoni, D. Meloni, P. Migliozzi, and F. Terranova. 3+1 sterile neutrinos at the CNGS. *JHEP*, 12:013, 2007.
- [191] CNGS experiment. <http://proj-cngs.web.cern.ch/proj-cngs/>.
- [192] Toshihiko Ota, Joe Sato, and Nao aki Yamashita. Oscillation enhanced search for new interaction with neutrinos. *Phys. Rev.*, D65:093015, 2002.
- [193] Toshihiko Ota and Joe Sato. Can ICARUS and OPERA give information on a new physics? *Phys. Lett.*, B545:367–372, 2002.
- [194] K. Kimura, A. Takamura, and H. Yokomakura. Exact formula of probability and CP violation for neutrino oscillations in matter. *Phys. Lett.*, B537:86–94, 2002.
- [195] Keiichi Kimura, Akira Takamura, and Hidekazu Yokomakura. All you ever want to know about neutrino oscillation probabilities in constant matter. *Phys. Rev.*, D66:073005, 2002.
- [196] A. Donini and D. Meloni. The 2+2 and 3+1 four-family neutrino mixing at the neutrino factory. *Eur. Phys. J.*, C22:179–186, 2001.
- [197] A. Donini, Maurizio Lusignoli, and D. Meloni. Telling three from four neutrinos at the neutrino factory. *Nucl. Phys.*, B624:405–422, 2002.
- [198] A. Donini, M. B. Gavela, P. Hernandez, and S. Rigolin. Neutrino mixing and CP-violation. *Nucl. Phys.*, B574:23–42, 2000.

- [199] A. Donini, M. B. Gavela, P. Hernandez, and S. Rigolin. Four species neutrino oscillations at nu-factory: Sensitivity and CP-violation. *Nucl. Instrum. Meth.*, A451:58–68, 2000.
- [200] Anna Kalliomaki, Jukka Maalampi, and Morimitsu Tanimoto. Search for CP violation at a neutrino factory in a four- neutrino model. *Phys. Lett.*, B469:179–187, 1999.
- [201] Amol Dighe and Shamayita Ray. Signatures of heavy sterile neutrinos at long baseline experiments. *Phys. Rev.*, D76:113001, 2007.
- [202] Andrea Donini, Ken ichi Fuki, J. Lopez-Pavon, Davide Meloni, and Osamu Yasuda. The discovery channel at the Neutrino Factory: $\nu_\mu \rightarrow \nu_\tau$ pointing to sterile neutrinos. *JHEP*, 08:041, 2009.
- [203] Alexey Boyarsky, A. Neronov, Oleg Ruchayskiy, and M. Shaposhnikov. Constraints on sterile neutrino as a dark matter candidate from the diffuse X-ray background. *Mon. Not. Roy. Astron. Soc.*, 370:213–218, 2006.
- [204] Nobuchika Okada and Osamu Yasuda. A sterile neutrino scenario constrained by experiments and cosmology. *Int. J. Mod. Phys.*, A12:3669–3694, 1997.
- [205] Samoil M. Bilenky, C. Giunti, and W. Grimus. Neutrino mass spectrum from the results of neutrino oscillation experiments. *Eur. Phys. J.*, C1:247–253, 1998.
- [206] F. Dydak et al. A Search for Muon-neutrino Oscillations in the Δm^2 Range 0.3-eV² to 90-eV². *Phys. Lett.*, B134:281, 1984.
- [207] G. Karagiorgi et al. Leptonic CP violation studies at MiniBooNE in the (3+2) sterile neutrino oscillation hypothesis. *Phys. Rev.*, D75:013011, 2007.
- [208] Samoil M. Bilenky, C. Giunti, W. Grimus, and T. Schwetz. Four-neutrino mixing and big-bang nucleosynthesis. *Astropart. Phys.*, 11:413–428, 1999.
- [209] Robert Foot and R. R. Volkas. Studies of neutrino asymmetries generated by ordinary sterile neutrino oscillations in the early universe and implications for big bang nucleosynthesis bounds. *Phys. Rev.*, D55:5147–5176, 1997.
- [210] Marco Cirelli, Guido Marandella, Alessandro Strumia, and Francesco Vissani. Probing oscillations into sterile neutrinos with cosmology, astrophysics and experiments. *Nucl. Phys.*, B708:215–267, 2005.
- [211] A. De Rujula, Maurizio Lusignoli, L. Maiani, S. T. Petcov, and R. Petronzio. A Fresh Look at Neutrino Oscillations. *Nucl. Phys.*, B168:54, 1980.
- [212] A. M. Dziewonski and D. L. Anderson. Preliminary reference earth model. *Phys. Earth Planet. Interiors*, 25:297–356, 1981.

- [213] A. Donini, E. Fernandez-Martinez, D. Meloni, and S. Rigolin. ν/μ disappearance at the SPL, T2K-I, NO ν A and the neutrino factory. *Nucl. Phys.*, B743:41–73, 2006.
- [214] Gian Luigi Fogli and E. Lisi. Tests of three-flavor mixing in long-baseline neutrino oscillation experiments. *Phys. Rev.*, D54:3667–3670, 1996.
- [215] Osamu Yasuda. On the exact formula for neutrino oscillation probability by Kimura, Takamura and Yokomakura. 2007.
- [216] A. Broncano and Olga Mena. Corrections to the fluxes of a neutrino factory. *Eur. Phys. J.*, C29:197–206, 2003.
- [217] (Ed.) B. Autin, (Ed.) A. Blondel, and (Ed.) John R. Ellis. Prospective study of muon storage rings at CERN. CERN-99-02.
- [218] (ed.) P. Gruber et al. The study of a European Neutrino Factory complex. CERN-PS-2002-080-PP.
- [219] D. Finley and N. Holtkamp. A feasibility study of a neutrino source based on a muon storage ring. *Nucl. Instrum. Meth.*, A472:388–394, 2000.
- [220] (ed.) S. Ozaki et al. Feasibility study 2 of a muon based neutrino source. BNL-52623.
- [221] Mohammad M. Alsharoa et al. Recent progress in neutrino factory and muon collider research within the Muon collaboration. *Phys. Rev. ST Accel. Beams*, 6:081001, 2003.
- [222] M. S. Zisman. Technical design aspects of feasibility study-II. *Nucl. Instrum. Meth.*, A503:384–389, 2003.
- [223] Yoshitaka Kuno et al. A feasibility study of a neutrino factory in Japan.
- [224] Michael S. Zisman. Experimental tests of cooling: Expectations and additional needs. *PoS*, NUFACT08:079, 2008.
- [225] P. Lipari. Private communication.
- [226] Paolo Lipari, Maurizio Lusignoli, and Francesca Sartogo. The Neutrino cross-section and upward going muons. *Phys. Rev. Lett.*, 74:4384–4387, 1995.
- [227] A. Cervera-Villanueva. MIND performance and prototyping. *AIP Conf. Proc.*, 981:178–180, 2008.
- [228] A. Cervera, F. Dydak, and J. Gomez Cadenas. A large magnetic detector for the neutrino factory. *Nucl. Instrum. Meth.*, A451:123–130, 2000.

- [229] Joachim Kopp, Toshihiko Ota, and Walter Winter. Neutrino factory optimization for non-standard interactions. *Phys. Rev.*, D78:053007, 2008.
- [230] A. Bueno, Mario Campanelli, and A. Rubbia. Physics potential at a neutrino factory: Can we benefit from more than just detecting muons? *Nucl. Phys.*, B589:577–608, 2000.
- [231] Patrick Huber and Thomas Schwetz. A low energy neutrino factory with non-magnetic detectors. *Phys. Lett.*, B669:294–300, 2008.
- [232] E. Ables et al. P-875: A Long baseline neutrino oscillation experiment at Fermilab. FERMILAB-PROPOSAL-0875.
- [233] P. Huber, M. Lindner, M. Rolinec, and W. Winter. Optimization of a neutrino factory oscillation experiment. *Phys. Rev.*, D74:073003, 2006.
- [234] D. Indumathi. India-based Neutrino Observatory (INO). *Pramana*, 63:1283–1293, 2004.
- [235] Mario Campanelli, A. Bueno, and A. Rubbia. $\nu(\mu) \rightarrow \nu(\tau)$ oscillations appearance with kinematic approach at very long baselines (VLBL). *Nucl. Instrum. Meth.*, A451:176–181, 2000.
- [236] C. Fukushima et al. A thin emulsion spectrometer using a compact permanent magnet. *Nucl. Instrum. Meth.*, A592:56–62, 2008.
- [237] Davide Meloni. Solving the octant degeneracy with the Silver channel. *Phys. Lett.*, B664:279–284, 2008.
- [238] P. Migliozzi. Private communication.
- [239] Luca Scotto Lavina. Design and performance of ECC-MECC. *PoS*, NUFACT08:049, 2008.
- [240] Patrick Huber, Manfred Lindner, and Walter Winter. Superbeams versus neutrino factories. *Nucl. Phys.*, B645:3–48, 2002.
- [241] He Zhang. Sum rules of four-neutrino mixing in matter. *Mod. Phys. Lett.*, A22:1341–1348, 2007.